A genetic screen identifies novel regulators of the senescence-associated secretory phenotype

Athena Eugenia Georgilis

A thesis submitted to Imperial College London
for the degree of Doctor of Philosophy

MRC Clinical Sciences Centre
Faculty of Medicine
Imperial College London

September 2016

Statement of originality

All experiments included in this thesis are my own unless otherwise stated.

Abstract

Cellular senescence is a stable cell-cycle arrest induced by ageing or many stresses such as oncogene activation. Oncogene-Induced Senescence (OIS) is an intrinsic tumour suppressive mechanism but also has numerous extrinsic functions mediated by the senescence-associated secretory phenotype (SASP). Although the SASP attracts the immune system to clear damaged cells it can also promote cancer growth and age-associated systemic inflammation. Consequently, the SASP has been considered a potential therapeutic target. However, a better understanding of the molecular pathways regulating the complex secretome of senescent cells is necessary before designing therapeutic interventions.

In this work, we set up and carried out an siRNA screen for genes regulating the SASP during OIS. By screening siRNAs targeting 8,352 genes, 84 novel regulators of IL-8 and IL-6 were found. We further interrogated their effect on levels of $p16^{INK4a}$, $p21^{Cip1}$ and BrdU incorporation. 49 genes were found to specifically regulate the SASP without affecting other senescence features. Combining the siRNA screening system with global transcriptome profiling for 38 of these genes revealed common pathways with a potential role in regulating the SASP.

One of the candidates was the splicing factor PTBP1. PTBP1 depletion blunted the induction of several SASP factors without affecting the senescence growth arrest. The altered SASP produced upon PTBP1 depletion had distinct properties. For example, it decreased the ability to transmit senescence but retained the ability to attract natural killer cells. Mechanistically, during senescence, PTBP1 promoted exon skipping of several mRNAs involved in intracellular protein trafficking. Future work will aim at fully understanding the role of PTBP1 during senescence. Our data so far suggest the feasibility of targeting PTBP1 to specifically manipulate the SASP while maintaining the ability of inducing cell cycle arrest as a potential strategy to target inflammation-driven tumourigenesis.

Acknowledgements

For the work presented in this thesis, first and foremost I would like to thank Jesús, my supervisor, for his guidance, constructive ideas, support and opportunities to expand our research through collaboration. I am grateful for joining the Cell Proliferation group.

All the members, past and current, have contributed to make my PhD experience great and unforgettable. When I first joined the group, Juan Carlos introduced me to the field of senescence and expanded my enthusiasm about research through his devotion to science. Selina welcomed me to the group and introduced me to the daily aspects of the lab and science. Special thanks to Andrew, Joana, and Patrizia, who I shadowed and bombarded with questions but who were always helpful with a smile and patience. Thanks to past members Sadaf and Nadine for setting up techniques we all have been using. In the group, apart from good teamwork, we developed friendships that made the long lab hours fun. The brainstorming coffee breaks with Niko and Suchira and the fun news updates with my desk-buddy Luca added spice to every day lab life. I would like to also especially thank Marieke, Sharon, Ana G. and Aimee who have united the current group into a well-working fun team with their great personalities and helpful altitude.

I owe gratitude to many people outside the lab who have helped me and this experience wouldn't have been the same without them. Thank you to my fellow PhD students Anne, Paulius, Tien-chi and Angel for encouraging each other throughout. Thank you Daimona for contributing to my decision to pursue this particular PhD and being there throughout to support me. A big thanks to my best friends and flatmates Argyris, Kate, Maria and Myrto who stood by me over the past 4 years, without you guys I wouldn't have made it. Thanks to my family that supported me in whatever I chose to do. Finally, thank you to my mentors Naveenan and Richard for reassuring me that my work is on the right track and for giving me meaningful suggestions for improvement.

Table of contents

List of figures

List of tables

Abbreviations

°C	degrees centigrade
4OHT	4-Hydroxytamoxifen
53BP1	p53-binding Protein 1
AD	Alzheimer's Disease
AML	Acute Myeloid Leukemia
AON	antisense oligonucleotide
APL	Acute Promyelocytic Leukemia
ARF	Alternative Reading Frame
AS	Alternative Splicing
ATCC	American Type Culture Collection
ATM	Ataxia Telangiectasia Mutated
ATP	Adenosine Triphosphate
ATP2B4	ATPase Plasma Membrane Ca2+ Transporting 4
ATR	Ataxia Telangiectasia and Rad3 related
AUF1	AU-binding factor 1
BCA	Bicinchoninic Acid
BCL2	B-Cell CLL/Lymphoma 2
BRAF	B-Raf Proto-Oncogene, Serine/Threonine Kinase
BrdU	5-Bromo-2'-deoxyuridine
BuBR1	BUB1 Mitotic Checkpoint Serine/Threonine Kinase B
C/EBPβ	CCAAT/enhancer binding protein beta
Ca	Calcium
CAG	glycosaminoglycan
CaM	calmodulin
CaMK	Ca/calmodulin-dependent protein kinase
cAMP	cyclic adenosine monophosphate
CCL	C-C Motif Chemokine Ligand
CCN1	Cysteine Rich Angiogenic Inducer 61
CDK	Cyclin-Dependent Kinase
CDKI	CDK Inhibitor
cDNA	complementary DNA
CHK	Checkpoint Kinase
CKIα	Casein Kinase I α
CM	Conditioned Media
CMV	Cytomegalovirus
COPD	Chronic Obstructive Pulmonary Disease
CSC	Clinical Sciences Centre
CTX	Cyclophosphamide
CV	coefficient of variance
CXCR	C-X-C Motif Chemokine Receptor
DAMP	damage-associated molecular pattern
DAPI	4',6-diamidino-2-phenylindole
DAVID	Database for Annotation, Visualization, and Integrated Discovery
DCAMKL3	Doublecortin And CaM Kinase0like 3
DDR	DNA Damage Response
DMEM	Dulbecco's modified Eagle's Medium

DMSO	Dimethyl sulfoxide
DNA	Deoxyribonucleic acid
dNTP	deoxynucleoside triphosphate
DSB	Double-Strand Break
ECM	Extracellular Matrix
EDTA	Ethylenediaminetetraacetic acid
eGFP	enhanced GFP
ELISA	Enzyme-linked immunosorbent assay
EMT	Epithelial to Mesenchymal Transition
ER	Endoplasmic Reticulum
ER	Eostrogen Receptor
ESE	Exonic Splicing Enhancer
ESS	Exonic Splicing Silencer
EXOC7	Exocyst Complex Component 7
FBS	Fetal Bovine Serum
GalNAc	acetylgalactosamine
GFP	Green Fluorescent Protein
GlcNAc	acetylglucosamine
GM-CSF	Granulocyte-Macrophage Colony Stimulating Factor
GO	Gene Ontology
GPCR	G-protein coupled receptor
Gy	Gray
GRO1 or GRO-alpha	melanoma growth stimulating activity, alpha; C-X-C Motif Chemokine Ligand 1
H3K27ac	Histone 3 lysine 27 acetylation
H3K9me3	Histone 3 lysine 9 tri-methylation
HCA	High Content Analysis
HDAC	Histone Deacetylase
HDF	Human Diploid Fibroblast
HFFF2 cells	Human Foetal Foreskin Fibroblast 2 cells
HMGB1	High Mobility Group Box 1
hnRNP	heterogeneous nuclear Ribonucleoprotein
HOSE	Human Ovarian Surface Epithelial
HP1	Heterochromatin Protein 1
HRAS	Harvey Rat Sarcoma Viral Oncogene Homolog
HSC	Hepatic Stellate Cell
HSPG	Heparan sulfate proteoglycan
HTM	High-Throughput Microscopy
HTS	High-Throughput Screening
IDT	Integrated DNA Technologies
IF	Immunofluorescence
IFN	Interferon
IGF	Insulin Growth Factor
IGFBP7	Insulin Like Growth Factor Binding Protein 7
IL	Interleukin
IL-1RA	IL-1 receptor antagonist
IL6R	Interleukin 6 Receptor
IPA	Ingenuity Pathway Analysis
IPF	Idiopathic Pulmonary Fibrosis

IRES	Internal Ribosome Entry Site
ISE	Intronic Splicing Enhancer
ISS	Intronic Splicing Silencer
JAK	Janus Kinase
JMJD3	Jumonji domain containing-3, Lysine Demethylase 6B
KLF4	Kruppel-Like Factor 4
KRAS	Kirsten Rat Sarcoma Viral Oncogene Homolog
LB	Lysogeny broth
LNA	Locked Nucleic Acid
LOPAC	Library of Pharmacologically Active Compounds
MAPK	Mitogen-Activated Protein Kinase
MARK3	Microtubule Affinity Regulating Kinase 3
MATS	Multivariate Analysis of Transcript Splicing
MCS	Multiple Cloning Site
MEC	Mammary Epithelial Cell
MED23	Mediator Complex Subunit 23
MEF	Mouse Embryonic Fibroblast
MEK	Mitogen-Activated Protein Kinase Kinase
MEM	Minimum Essential Medium
MET	mesenchymal-to-epithelial transition
min	minute
miR	micro RNA
MK2 or MAPKAPK2	Mitogen-Activated Protein Kinase-Activated Protein Kinase 2
MLL1	Lysine Methyltransferase 2A
MMP	Matrix Metallopeptidase
MRC	Medical Research Council
mRNA	messenger RNA
MSD	Myelodysplastic syndrome
mTOR	Mechanistic Target Of Rapamycin
Myb	V-Myb Avian Myeloblastosis Viral Oncogene Homolog
Myc	V-Myc Avian Myelocytomatosis Viral Oncogene Homolog
NAD	Nicotinamide Adenine Dinucleotide
NADPH	NAD Phosphate Oxidase
NAV1	Neuron Navigator 1
NBS1	Nijmegen Breakage Syndrome 1
NEB	New England Biolabs
NF	Nuclear Factor
NF-κB	NF-kappa B
NFAT	Nuclear factor of activated T-cells
NGS	Next-Generation Sequencing
NK	Natural Killer
NLR	NOD-like receptors
NMD	Non-sense Mediated Decay
NOX4	NADPH Oxidase 4
NPI	Normalised percent inhibition
NRAS or v-ras	Neuroblastoma RAS Viral Oncogene Homolog
NSAID	Nonsteroidal Anti-Inflammatory Drug
nt	nucleotide
OIS	Oncogene-Induced Senescence

OSCC	oral squamous cell carcinoma
PBS	Phosphate-Buffered Saline
PBS-T	PBS-Tween
PCR	Polymerase Chain Reaction
PDGF-AA	Platelet Derived Growth Factor Subunit A
PFA	Paraformaldehyde
pH	potentia Hydrogenii
PI3K	Phosphoinositide 3-kinase inhibitor
PKA	Protein Kinase A
PKM	Pyruvate Kinase, Muscle
PLA2	Phospholipase A2
PP1	Protein Phosphatase 1
PPP3CB	Protein Phosphatase 3 Catalytic Subunit Beta
PRC	Polycomb Repressive Complex
PS	Paracrine senescence
PTBP1	Py Tract Binding Protein 1
PTEN	Phosphatase And Tensin Homolog
PTPN14	Protein Tyrosine Phosphatase, Non-Receptor Type 14
Py tract	Polypyrimidine tract
qPCR	quantitative or real-time PCR
R3HDM1	R3H Domain Containing 1
RAF	Raf-1 Proto-Oncogene, Serine/Threonine Kinase
RAGE or AGER	Receptor for Advanced Glycation End-products
RAPGEF2	Rap Guanine Nucleotide Exchange Factor 2
Rb	Retinoblastoma
RBP	RNA-binding protein
REF	reference
RNA	Ribonucleic Acid
RNA-seq	NGS of RNA
RNF6	Ring Finger Protein 6
ROS	Reactive Oxygen Species
RPKM	Read per Kilobase per Million mapped reads
rpm	revolutions per minute
RPMI	Roswell Park Memorial Institute medium
rRNA	ribosomal RNA
RT	Reverse Transcriptase
rtTA	reverse tetracycline-controlled transacivator
SA-β-Gal	Senescence-Associated β-Galactosidase
SAHF	Senescence-Associated Heterochromatin Foci
SASP	Senescence-Associate Secretory Phenotype
SDS	Sodium Dodecyl Sulphate
SDS-PAGE	SDS-Polyacrylamide Gel Electrophoresis
shRNA	short hairpin RNA
SIR	senescence-inflammatory response
siRNA	small interfering RNA
SKP	S-phase kinase-associated protein
SNP	Single-Nucleotide Polymorphism
snRNA	small nuclear RNA
snRNP	small nuclear Ribonuclear Protein

SNX14	Sorting Nexin 14
SR	serine/arginine rich
Src	V-Src Avian Sarcoma (Schmidt-Ruppin A-2) Viral
SRE	Splicing Regulatory Element
STAT	Signal Transducer And Activator Of Transcription
STX3	Syntaxin 3
T2D	Type 2 Diabetes
TASCC	TOR-autophagy spatial coupling compartment
TF	Transcription Factor
TGF	Transforming Growth Factor
TGFBR1	TGFβ Receptor 1
TGN	trans-Golgi network
TIS	Therapy-Induced Senescence
TLR	Toll-like receptors
TNFalpha or TNFα	Tumour Necrosis Factor-Alpha
TP53 or Trp53 or p53	Tumour Protein P53
TPM1	Tropomyosin 1 (Alpha)
TR	Transcriptional Regulator
TRE	Transcriptional Regulator Element
Treg	Regulatory T cell
TSO	Template-switching oligo
UPR	Unfolded Protein Response
UTR	Untranslated Region
v/v	volume per volume
VEGF	Vascular Endothelial Growth Factor
w/v	weight per volume
WNT	Wingless-Type MMTV Integration Site Family
ZFP36L1	ZFP36 ring finger protein-like 1
γH2AX	Phosphorylation of the Histone A2 Variant X
µg/µl/µM	microgram/microlitre/micromolar

Chapter 1. Introduction

1.1. Cellular senescence.

Cellular senescence is a stable cell cycle arrest programme, first described in primary human fibroblasts that had reached replicative exhaustion *in vitro* (Hayflick & Moorhead, 1961; Hayflick, 1965). Although senescent cells are unable to re-enter the cell cycle in response to mitogenic stimuli, these cells remain metabolically active. Loss of proliferative ability is accompanied by changes in gene expression, physiology and cell morphology, consistently used as principle determinants of senescence in cell culture. Specifically, senescent cells display loss of DNA synthesis, enlarged and flattened cell morphology, senescence-associated β-galactosidase (SA-β-gal) activity and accumulation of senescence-associated heterochromatin foci, SAHFs (Figure 1.1; reviewed in Kuilman et al., 2010).

Senescence was originally thought to be an intrinsic cellular mechanism. Although this might be the case for replicative senescence, it is now established that other stresses may induce an indistinguishable senescence phenotype termed stress-induced senescence or premature senescence (Kuilman et al., 2010; Serrano & Blasco, 2001). As the list of senescence types and effector pathways grows, it becomes more evident that the phenotypic markers of senescence vary depending on the context, the stimuli and the cell type (Salama et al., 2014).

1.2. Types of senescence

1.2.1. Replicative senescence

Replicative senescence was initially described by Hayflick and Moorhead (1965) as an internal mitotic clock and was later associated with telomere length regulation. Due to the 'end-replication problem' of DNA polymerase, telomeres become progressively shorter with every cell division (Olovnikov, 1973; Watson, 1972). Eventually, short telomeres are sensed as double-strand breaks (DSBs) by the DNA Damage Response (DDR) machinery leading to senescence through activation of the tumour suppressor protein p53 (d'Adda di Fagagna et al., 2003). Cell cycle arrest

due to telomere shortening can be rescued with ectopic expression of telomerase, the enzyme responsible for elongating telomeres (Bodnar et al., 1998; Harley et al.,1990; Vaziri & Benchimol, 1998).

The implementation of replicative senescence depends on the activation of both the INK4A-retinoblastoma (Rb) and the ARF-p53 tumour suppressor pathways (Ben-Porath & Weinberg, 2005; Shay et al., 1991). Both pathways are activated upon derepression of the *INK4A/ARF* locus and lead to cell cycle arrest resulting from active hypophosphorylated Rb. In brief, the hypophosphorylation of Rb is a consequence of decreased CDK4/6 activity. This is due to the accumulation of cyclin-dependent kinase inhibitors (CDKIs) during senescence. Such CDKIs include $p21^{CIP}$ resulting from p53 activation, and $p16^{INK4a}$ (Gil & Peters, 2006; Itahana et al., 2001; Narita et al., 2003; Wei et al., 2001). Activation of DDR kinases (ATM/ATR and CHK2/CHK1) also results in p21 induction by phosphorylating and activating p53 (Hirao et al., 2000). Depending on the cell type, deficiency in p53, p16 or both abrogates replicative senescence (Ben-Porath & Weinberg, 2005).

A primary example of replicative senescence is to be found in mouse embryonic fibroblasts (MEFs) that exhibit growth arrest after a very limited number of passages *in vitro*. The arrest can be prevented by changing the culturing conditions, oxygen levels or by inactivating the p53 and/or RB pathways (Dannenberg et al., 2000; Loo et al., 1987; Parrinello et al., 2003; Sage et al., 2000). However, replicative senescence in MEFs is not caused by telomere shortening but rather by oxidative stress. In particular, non-physiological oxygen conditions induce ROS production by the mitochondria resulting in a DDR (Parrinello et al., 2003; Passos et al., 2010). ROS may precede replication-associated stress and may explain how MEFs enter senescence despite retaining long telomeres, which brings us to the other type of senescence.

1.2.2. Premature senescence

In addition to telomere attrition and oxidative stress, different stresses that cause DNA damage can elicit a premature senescence response as well. Ionising radiation and other DNA damage inducing agents such as bleomycin, prompt cell cycle arrest in human fibroblasts with elevated p21, p53 and p16 (Di Leonardo et al., 1994; Robles & Adami, 1998; Rodier et al., 2011).

The most studied form of telomere-independent senescence is Oncogene-Induced Senescence (OIS), senescence induced by strong activation of oncogenes. The study of Serrano et al. in 1997 provided the first evidence for OIS whereby a constitutively active form of HRAS ($HRAS^{V12}$) was introduced into primary cells resulting in a cell cycle arrest resembling replicative senescence. Senescence induced by RAS or its downstream effectors RAF, MEK or other oncogenes (Lin et al., 1998; Zhu et al., 1998) is now considered a consequence of an initial hyperproliferation phase. An increase in usage of DNA replication origins in response to the mitotic signal leads to accumulation of genomic damage and activation of a DDR because of stalled replication forks (Bartkova et al., 2006; Di Micco et al., 2006). Uncontrolled proliferation is counteracted by activation of the tumour suppressors p16 and p53 (Lin et al., 1998; Serrano et al., 1997; Wei et al., 2001). Functional inactivation of these tumour suppressors or components of the DDR pathway can blunt senescence depending on the oncogene and cell type (Ben-Porath & Weinberg, 2005). For example, silencing of the DDR kinase ATM bypasses STAT5A-induced senescence by preventing p53 activation (Mallette et al., 2007) in human cells whereas RAS^{V12}-induced senescence in murine fibroblasts does not rely on ATM but on ARF-mediated activation of p53 (Efeyan et al., 2009).

The list of genes with the potential to induce senescence has expanded since the first report in 1997. It includes not only downstream proximal and distal effectors of RAS signaling such as CDKIs, cyclins and E2Fs but also secreted factors such as TGFβ1 or loss of tumour suppressor genes such as *PTEN* (listed in Gorgoulis & Halazonetis, 2010).

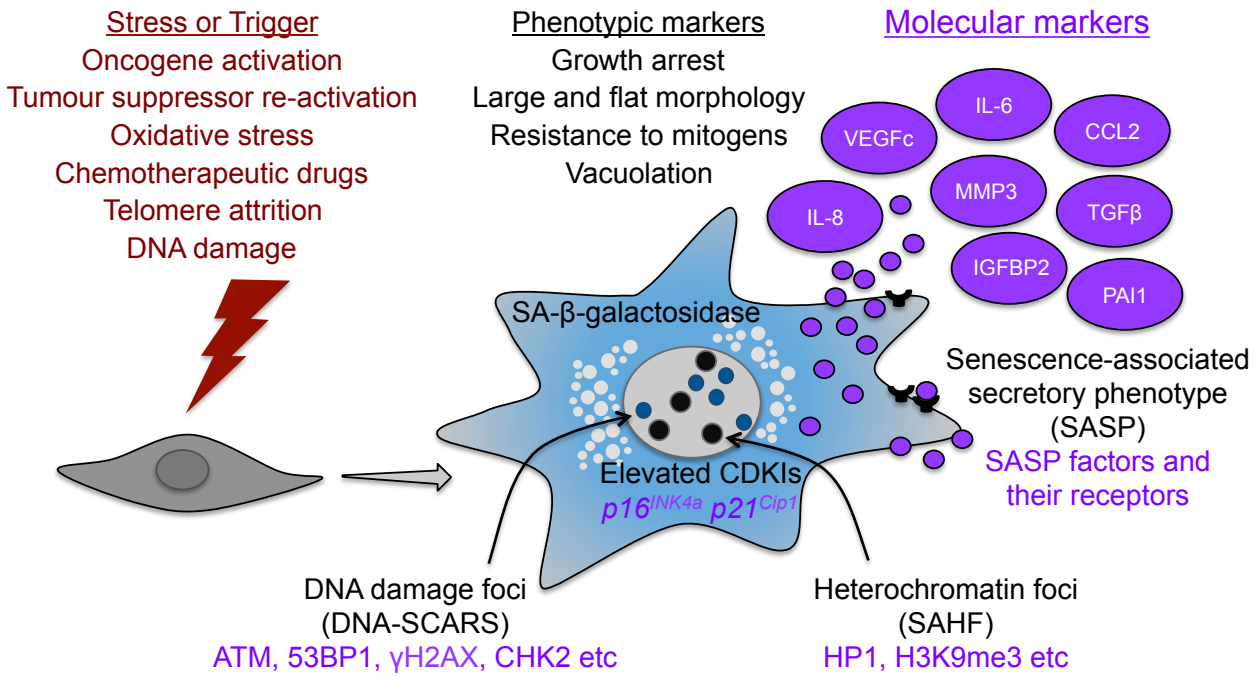

Figure 1.1. Cellular senescence.
Many different stresses may lead to a senescence-growth arrest. A number of phenotypic and molecular markers are associated with this halt. Not all traits are always present and there is no trait that is exclusive to senescence. Thus, it is imperative to use a combination of at least two markers for the identification of senescent cells. The two features most commonly used as senescence markers apart from growth arrest are $p16^{INK4a}$ and SA-β-galactosidase. $p16^{INK4a}$ is frequently used as a surrogate marker for growth arrest due to stress. SA-β-galactosidase activity is an enzymatic activity detected at sub-optimal pH 6 as senescent cells have increased lysosomal mass and is the *de facto* hallmark of senescence. (Adapted from Salama et al., 2014; Sharpless & Sherr, 2015)

1.3. Senescence *in vivo*

Cellular senescence has physiological roles with either beneficial or harmful implications on tissue homeostasis. Although senescence can prevent cancer progression by halting aberrant cell proliferation, it has also been associated with age-related diseases. A summary of the roles of senescence in the pathology of cancer and ageing will be presented here.

1.3.1. Role of senescence in cancer

Withdrawal from cell cycle in response to aberrant mitogenic stimulation is viewed as a tumour suppressive mechanism preventing potentially cancerous cells from undergoing neoplastic transformation (Campisi, 2005). However, concerns about the relevance of senescence in cancer *in vivo* were initially raised since excessively high levels of *Ras* were required in order to elicit

senescence in human cells (Deng et al., 2004) and no signs of senescence were detected in tumours arising from single copy *KRas* mutations in mice (Tuveson et al., 2004). Since then, a series of studies has provided evidence for senescence as a physiological mechanism limiting tumourigenesis *in vivo* (Collado et al., 2005; Dankort et al., 2007; Krimpenfort et al., 2001; Michaloglou et al., 2005; Sarkisian et al., 2007). A prime example is the study of Michaloglou et al. (2005) who demonstrated first *in vitro* that an activating mutation in *BRAF*, namely $BRAF^{V600E}$, induced senescence in melanocytes and then that human melanocytic nevi harbouring $BRAF^{V600E}$ displayed senescence markers. Such nevi, examples of neoplastic growth, may remain static for decades without progressing into melanoma, providing a paradigm of how senescence fits into multistep carcinogenesis. In this paradigm, malignant conversion would require additional mutations to disable senescence effectors (Krimpenfort et al., 2001). In support of this idea, mice expressing $BRAF^{V600E}$ in the lungs developed benign adenomas accompanied by senescence markers and progressed to lung tumours in the absence of the *Trp53* or *Ink4a/Arf* (Dankort et al., 2007). In a similar mouse model, Collado et al. (2005) observed senescent markers in lung adenomas driven by oncogenic RAS^{V12} but not in the corresponding malignant adenocarcinomas. It is now established that only high levels of the oncogene, e.g. RAS, lead to senescent premalignant neoplasia to prevent tumour formation (Sarkisian et al., 2007). From an evolutionary perspective, since normal levels do not activate the pathway they would not impose a high risk of cancer development. At present, there are several lines of evidence supporting the physiologic role of senescence in protection against cancer in various tissues (lung, pancreas, thymus, skin, etc) and in response to not only deregulation of oncogenes but also loss of tumour suppressor genes such as *PTEN* (reviewed and listed in Collado & Serrano, 2010). At a larger scale, Burd et al. (2013) confirmed p16 focal expression at early stages of tumourigenesis in 14 tumour models while overall p16 expression did not correlate with mortality rates.

Evidence of senescence as a feature of neoplastic lesions is not restricted to mouse models of tumourigenesis. Senescent markers have been detected in various types of human premalignant lesions but were absent in malignant stages. These include melanocytic nevi (Gray-Schopfer et al., 2006; Michaloglou et al., 2005), prostate intraepithelial neoplasias (Chen et al.,

2005), dermal neurofibromas (Courtois-Cox et al., 2006) and colon adenomas (Bartkova et al., 2006). Like apoptosis, senescence underlies the cytotoxicity induced by certain chemotherapeutic drugs (Schmitt et al., 2002; te Poele et al, 2002). Underlying mutations affecting the senescence programme may promote drug resistance hence additional knowledge is required in order to monitor treatment efficacy.

1.3.2. Role of senescence in ageing

On one hand senescence is a potent anti-cancer mechanism early in life but on the other hand it may contribute to age-related pathologies. Consequently, senescence is often considered the cellular counterpart of organismal ageing (Narita & Lowe, 2005). In this context, the net accumulation of 'dysfunctional' senescent cells may contribute to age-related tissue dysfunction. This theory is supported by the high levels of $p16^{INK4a}$ and ARF detected in tissues of aged humans and rodents respectively (Krishnamurthy et al., 2004; Ressler et al., 2006) and by the exponential increase in p16 expression during ageing of p16-luciferase reporter mice (Burd et al., 2013). Most importantly, the causal link between p16 and ageing was substantially reinforced by a study in 2011. In this study, Baker et al. showed that elimination of p16-expressing cells by drug-induced apoptosis (driven by the *INK-ATTAC* transgene) delayed the onset of tissue deficits associated with the premature ageing of BuBR1 hypomorphic mice. For example, eliminating senescent cells protected against sarcopenia, which is probably due to partial restoration of residing adult stem cells (satellite cells). Recently, exploiting a similar technique, Baker and colleagues (2016) investigated the elimination of p16-expressing cells in naturally aged mice. Indeed, some of the age-related abnormalities observed in adipose tissue, kidney, heart and cognitive function were ameliorated, which led to improved general healthspan. Still, understanding the full extent of the advantages of senescent cell elimination remains elusive because of technical limitations. Not all the senescent cells of all tissues were detected and certainly not targeted by this strategy. Nevertheless, these models have been instrumental in establishing that senescence has implications in ageing.

Senescence is consistently implicated in the diminution of the adult stem cell pool accompanying the progressive loss of tissue regeneration ability, a hallmark of ageing. Elevated p16 expression has been associated with impaired functional capacity of aged haematopoietic stem cells, neural stem cells, pancreatic islets and satellite cells, while their proliferation capacity was reinstated in a *p16*^{Ink4a} null background (Janzen et al., 2006; Krishnamurthy et al., 2006; Sousa-Victor et al., 2014). *In vitro*, overexpression of oncoproteins such as c-MYC and KLF4 is required for reprogramming of primary cells to pluripotency. The efficiency of this reaction is limited by the *INK4A/ARF* locus and p53 (Banito et al., 2009; Li et al., 2009; Utikal et al., 2009). Although these findings indicate potential targets for stem cell rejuvenation, does the benefit of increasing regenerative potential outweigh the risk of carcinogenesis? Stem cells are by nature prime targets for carcinogenesis and senescence potentially limits the incipient cancer stem cells.

The mechanisms underlying senescence may protect against cancer early in life but contribute to ageing, two antagonistically pleiotropic features. According to this view, cancer arises with advancing age as a result of the accumulating genetic aberrations eventually escaping senescence. Adding to the complexity of the link between cancer and ageing, senescent cells may provide a milieu favourable for cancer growth, a topic discussed in the next section.

1.4. Senescence secretome

One of the characteristics of cellular senescence is the diverse and multifunctional secretome that often accompanies senescent cells. Senescent cells actively secrete a mixture of soluble and insoluble factors collectively termed senescence-associated secretory phenotype (SASP). The SASP is involved in intra- and intercellular signalling.

1.4.1. Senescence-associated secretory phenotype (SASP)

The SASP is composed of proteases, growth factors, pro-inflammatory cytokines, chemokines and other signalling molecules (reviewed in Coppé et al., 2010; Kuilman & Peeper, 2009). Judith Campisi's laboratory (Coppé et al., 2008) used antibody arrays to explore the secretome of senescent cells in replicative and stress-induced senescence in human fibroblasts and epithelial

cells. This work and the mechanistic investigation of individual factors by other groups have revealed the existence of multiple factors, not always conserved across systems (depending on cell types and senescence triggers). A flavour of this complexity is given in Table 1 with examples of the better-known SASP factors, a list that is ever-growing.

The mouse models developed to track senescent cells *in vivo*, namely INK4-ATTAC and p16-3MR, by the groups of Jan van Deursen and Judith Campisi's, respectively, have aided to substantiate a physiological role for the SASP (Baker, et al., 2011, 2016; Demaria et al., 2014). In particular, high p16-expressing cells concomitantly showed higher expression of secretome components and removal of high p16-expressing cells correlated with lower expression of certain secreted factors.

Although cellular senescence is an intrinsic tumour suppressive mechanism, it also has important non-cell-autonomous functions that largely underlie the diverse role of senescent cells in pathophysiology. The onset of senescence is accompanied by changes in the composition of the extracellular matrix (ECM) with various consequences on the cellular milieu (Kuilman & Peeper, 2009). The first indication of a pathological role was the finding that senescent fibroblasts were able to promote malignant transformation of mammary epithelial cells (MECs) depending however on the state of MECs (Krtolica et al., 2001; Parrinello et al., 2005). Since then, it is increasingly recognised that the SASP has many functions either beneficial or detrimental to the organism.

Table 1. The Senescence-Associated Secretory Phenotype (SASP).

Examples of upregulated factors.			
SASP factor	**Cell type**	**Trigger**	**Study**
IL-6, IL-8 (CXCL-8)	HDF	Oncogene ($BRAF^{E600}$, MEK1, RAS^{V12})	[1] [2] [3] [4] [5]
		IR, Replicative exhaustion	[3] [4]
	Human epithelial cells	Oncogene (RAS^{V12}), IR	[3]
IL-1α	HUVEC	Replicative exhaustion	[6] [7]
	VSMC	Replicative exhaustion	[8]
	HDF	Oncogene ($BRAF^{E600}$, MEK1, RAS^{V12})	[1] [2] [4] [5]
		Replicative exhaustion	[9]
	Human epithelial cells	Oncogene (RAS^{V12}), IR	[3]
IL1-β	HDF	Oncogene ($BRAF^{E600}$, RAS^{V12})	[2] [3] [4] [5]
		IR	[3] [4]
		Replicative exhaustion	[3] [4] [9]
	Human epithelial cells	Oncogene (RAS^{V12}), IR	[3]
IL-13	HDF	Oncogene (RAS^{V12}), IR, Replicative ex	[3]
	Human epithelial cells	Oncogene (RAS^{V12}), IR	[3]
GRO-α, -β, -γ	HDF	Oncogene (MEK1, RAS^{V12})	[1] [2] [3] [4]
(CXCL-1,-2,-3)		IR, Replicative exhaustion	[3]
		Oxidative stress (H_2O_2)	[10]
	HPMC	Replicative exhaustion	[11]
	Murine hepatoblasts	Oncogene (RAS^{V12})	[12]
CXCL-4 (PF4),	HDF	Oxidative stress (H_2O_2)	[10]
CXCL-12 (SDF-1)			
CXCL-5 (ENA-78),	HDF	Oncogene (RAS^{V12})	[1]
CXCL-6 (GCP-2)	Human epithelial cells	Oncogene (RAS^{V12}), IR	[3]
CXCL-7 (NAP2)	HDF	Oncogene (MEK1, RAS^{V12})	[1]
MCP-1 (CCL-2)	HDF	Oncogene (MEK1, RAS^{V12})	[1] [2] [3]
		IR, Replicative exhaustion	[3]
		Oxidative stress (H_2O_2)	[10]
	Human epithelial cells	Oncogene (RAS^{V12}), IR	[3]
	HPMC	Replicative exhaustion	[11]
	Murine hepatoblasts	Oncogene (RAS^{V12})	[12]
MCP-2, -3 -4	HDF	IR, Replicative exhaustion	[3]
(CCL-8, -7, -13)			
CCL-20 (MIP-3a)	HDF	Oncogene (MEK1, RAS^{V12})	[1] [2] [4]
		IR, Replicative exhaustion	[3] [4]
		Oxidative stress (H_2O_2)	[10]
	Human epithelial cells	Oncogene (RAS^{V12}), IR	[3]
CSF-1	Murine hepatoblasts	Oncogene (RAS^{V12})	[12]
GM-CSF (CSF-2)	HDF	Oncogene (MEK1, RAS^{V12})	[1] [3] [4]
		IR, Replicative exhaustion	[3]
	Human epithelial cells	Oncogene (RASV12), IR	[3]

IGFBP-2	HDF	Replicative exhaustion	[13]
		Oxidative stress (H_2O_2)	[10]
	Human epithelial cells	IR	[3]
		Replicative exhaustion	[13]
IGFBP-3	HDF	Replicative exhaustion	[14]
	HUVEC	Replicative exhaustion	[13] [15]
IGFBP-4	HDF	IR, Replicative exhaustion	[3]
IGFBP-5	HDF	Replicative exhaustion	[13]
		Oxidative stress (H_2O_2)	[10]
	HUVEC	Replicative exhaustion	[13]
	Human epithelial cells	Replicative exhaustion	[13]
IGFBP-7	HDF	Oxidative stress (H_2O_2)	[10]
	Human melanocytes	Oncogene ($BRAF^{E600}$)	[16]
IGF2	HDF	Oncogene (RAS^{V12})	[4]
TGFβ1	HDF	Oncogene (RAS^{V12})	[2] [4]
	Mouse keratinocytes	Oncogene (v-RasHa)	[17]
TGFβ2	HUVEC	Replicative exhaustion	[13]
MMP2	HDF	Oxidative stress (H_2O_2)	[10]
MMP-1, -3, -10	HDF	Oncogene (RAS^{V12})	[4]
		Replicative exhaustion	[13]
TIMP-1	HDF	Oncogene (RAS^{V12})	[4]
		Oxidative stress (H_2O_2)	[10]
PAI-1	HDF	Oncogene (RAS^{V12})	[2]
		Replicative exhaustion	[18]
	MEFs	Replicative exhaustion	[18]
PAI-2	HDF	Oncogene (RAS^{V12})	[4]
uPAR	HDF	Oncogene (RAS^{V12})	[4]
	Human epithelial cells	IR,Oncogene (RAS^{V12})	[3]
uPA, tPA	HDF	Replicative exhaustion	[13]
VEGF	HDF	Oncogene (RAS^{V12})	[2] [4]
	Human epithelial cells	IR,Oncogene (RAS^{V12})	[3]
	HPMC	Replicative exhaustion	[11]
AREG	HDF	Oncogene (RAS^{V12})	[4]
		Oxidative stress (H_2O_2)	[10]
	Human epithelial cells	IR,Oncogene (RAS^{V12})	[3]
INHBA	HDF	Oncogene (RAS^{V12})	[2] [4]
HGF	HDF	Oncogene (RAS^{V12})	[4]
		Oxidative stress (H_2O_2)	[10]
FGF7	HDF	Oxidative stress (H_2O_2)	[10]

[1] Acosta et al., 2008
[2] Acosta et al., 2013
[3] Coppé et al., 2008
[4] Herranz et al., 2015
[5] Kuilman et al., 2008
[6] Garfinkel et al., 1994
[7] Maier et al, 1990
[8] Hsu et al., 1999
[9] Kumar et al., 1992
[10] Bavik et al., 2006
[11] Ksiazek et al., 2008
[12] Xue et al., 2007
[13] Shelton et al., 1999
[14] Wang et al., 1996
[15] Kim et al., 2007
[16] Wajapeyee et al., 2008
[17] Tremain et al., 2000
[18] Kortlever et al., 2006

1.4.2. Beneficial effects of the SASP

1.4.2.1. The SASP reinforces the senescence growth arrest

Accumulating evidence indicates that the SASP is in fact indispensible for execution of a senescence growth-arrest. Three studies in 2008 identified the secreted proteins IGFBP7, IL-8 and IL-6 to be necessary for the implementation and maintenance of senescence (Acosta et al., 2008; Kuilman et al., 2008; Wajapeyee et al., 2008). Wajapeyee et al. and Kuilman et al. showed that depletion of IGFBP7 and IL-6, respectively, overrode $BRAF^{V600E}$-mediated OIS in human diploid fibroblasts (HDFs) and melanocytes. These secreted proteins are reinforcing the arrest by signalling back to the cell they originate from. This autocrine activity is well evidenced by the senescence bypass observed when the corresponding receptors are knocked down. Knockdown of CXCR2, a receptor for several chemokine family members such as IL-8, or depletion of PLA2R, a receptor for several secreted phospholipase A2 enzymes (sPLA2), bypassed both replicative and stress-induced senescence (Acosta et al., 2008; Augert et al., 2009). Similar results were observed by Daniel Peeper's group when they depleted the receptor of IL-6, IL6R (Kuilman et al., 2008).

The functional connections between the SASP and growth arrest suggest there are mechanisms in place to reinforce the senescence phenotype in an autocrine manner. This is supported by links between the SASP and the tumour-suppressive role of senescence *in vivo*. High IGFBP7 levels were found in human nevi but not in melanoma (Wajapeyee al., 2008). In addition, IL-8 expression co-localised with p16 expression in the epithelium of human colon adenoma sections (Kuilman et al., 2008). Engraftment of v-Ras-expressing senescent mouse keratinocytes lacking *Smad3*, a downstream target of TGFβ, in nude mice resulted in progression from papilloma to malignant carcinoma at a high frequency (Vijayachandra et al., 2003). Similarly, ablation of TGFBR1 or inactivation of CXCR2 in a model of $KRas^{G12V}$-driven OIS in the pancreas accelerated cancer development (Acosta et al., 2013; Lesina et al., 2016). In a mouse model of *PTEN*-loss in the prostate epithelium, Andrea Alimonti's laboratory demonstrated that IL-1 receptor antagonist (IL-1RA) opposes IL-1 signaling consequently preventing senescence of proliferating epithelial cells and supporting tumour growth (Di Mitri et al., 2014). Therefore, disrupting signalling

from and to SASP may lead to defects in the senescence programme and eventually to malignant progression.

The ability of secreted proteins to induce senescence underpins the anti-proliferative effect of the SASP. Overexpression of their corresponding receptors in a wild type setting elicited a senescence response (Acosta et al., 2008; Kuilman et al., 2008). Ectopic overexpression of IGFBP7 induced senescence in breast cancer cell lines and rIGFBP7 reduced tumourigenesis in xenograft mouse models (Benatar et al., 2012; Wajapeyee et al., 2008). Interestingly, T-helper-1-cell cytokines, such as IFN-γ, limited carcinogenesis by inducing senescence in pancreatic islet cells in the absence of oncogene activation (Braumüller et al., 2013). The aforementioned results imply SASP is an inducer of senescence. The most convincing evidence came however from three studies showing that senescence was transmitted from senescent to proliferating cells in culture. This phenomenon was termed ‘paracrine senescence’ or ‘bystander senescence’ (Acosta et al., 2013; Hubackova et al., 2012; Nelson et al., 2012). Our group demonstrated that inhibition of the receptors of several SASP components such as IL-1, VEGF, TGFβ and CCL2, in the recipient cells was sufficient to partially promote the growth caused by conditioned media (CM) of senescent cells (Acosta et al., 2013). From an evolutionary point of view, paracrine senescence would limit proliferative expansion of nearby cells exposed to similar oncogenic stresses. Nevertheless, senescence propagation is somehow restricted since CM from paracrine-senescent cells was less efficient in inducing senescence in wild type cells.

1.4.2.2. The SASP contributes to several physiological processes

1.4.2.2.1 Insulin secretion

The function of senescence in physiological processes other than tumour-suppression is yet unclear. Investigating the SASP has started to shed light on this. Recently, senescence was linked to insulin secretion by β-islet pancreatic cells (Helman et al., 2016). During ageing the proliferation of these cells was reduced but their function was enhanced as they entered p16-dependent senescence and secreted more insulin in response to glucose. This is in line with a previous report showing increased expression of β-cell function genes in aged mouse cells which correlated with

an altered chromatin landscape (Avrahami et al., 2015). The authors argue that eventually the healthy balance tilts in favour of proliferating insulin-producing cells versus senescent insulin-producing cells, often leading to age-associated metabolic disease. This could be explained by the overall decrease in β-cell mass due to loss of replicative capacity or non-cell autonomous alterations in the pancreatic microenvironment.

1.4.2.2.2 Tissue repair

A substantial body of evidence indicates that the SASP acts during liver or skin injury to fine-tune tissue repair. Krizhanovsky et al. (2008) showed that upon acute liver injury the residing hepatic stellate cells (HSCs) initially proliferate and secrete pro-fibrotic proteins but shortly after they underwent senescence and secreted matrix-degrading enzymes (MMPs). Abrogating senescence in this context led to exaggerated liver fibrosis. Similarly, senescence induced by CCN1 in myofibroblasts was necessary in order to limit fibrosis in a mouse model of skin wound healing (Jun & Lau, 2010). Along these lines, PDGF-AA secreted by senescent fibroblasts or endothelial cells promoted differentiation of myofibroblasts, a key step in skin wound healing (Demaria et al., 2014). These findings strongly suggest the existence of an evolutionary pressure in favour of a SASP.

1.4.2.3. The SASP attracts immune cells

Two studies have shown that senescence occured during development of certain embryonic structures and that removal of these cells was necessary since disruption of senescence was usually compensated by apoptosis (Muñoz-Espín et al., 2013; Storer et al., 2013). The SASP contains many ligands for innate immune cells such as neutrophils, NK cells and macrophages rendering senescent cells targets for destruction. The first report on cross-talk between immunity and senescence was in p53-deficient mouse liver carcinomas driven by *Kras*. In this study, p53 restoration led to senescence *in vitro* and to clearance of senescent cells by the immune system *in vivo* due to a pro-inflammatory phenotype, resulting in tumour regression (Xue et al., 2007). This is the prototypic example of anti-tumour immunity mediated by the SASP. Immune-mediated

clearance of senescent cells depends also on the adaptive immune system since antigen-specific $CD4^+$ T lymphocytes were crucial for the clearance of premalignant senescent *Nras*^{G12V} murine hepatocytes (Kang et al., 2011). In fact, immuno-suppressed mice developed full-blown hepatocellular carcinoma. In line with this, IR-induced senescence in osteoblasts induced a SASP necessary for recruitment of NKT cells and attenuation of osteosarcomas (Kansara et al., 2013). The immunomodulatory activity of the SASP reflects an extrinsic tumour suppressive outcome of senescence probably evolved to attract immune cells to damaged tissue areas. The immune clearance of dysfunctional senescent cells is beneficial for the disrupted tissue but as the accumulation of senescent cells increases with age, it outpaces the clearance rate leading to chronic inflammation (Freund et al., 2010).

1.4.3. The detrimental effects of the SASP

1.4.3.1. The SASP promotes cancer progression

Inflammation constitutes a major risk factor for carcinogenesis (Grivennikov et al., 2010; Mantovani et al., 2008; Visser et al., 2006). Inflammatory immune cells and inflammatory mediators (chemokines and cytokines) are recurrently detected in the tumour microenvironment of human patients and experimental animal models. Inflammation may precede tumour development, as is the case with chronic inflammatory diseases such as obesity, or may follow solid malignancies arising from oncogene activation such as *MYC* and *RAS*. Regardless of the origin, the consequence is sustained proliferation and survival of malignant cells either directly or indirectly through the induction of angiogenesis (Grivennikov et al., 2010; Mantovani et al., 2008; Visser et al., 2006). Additionally, certain inflammatory mediators stimulate EMT, migration and invasion of tumour cells thereby promoting metastasis. Prolonged inflammation increases the chances that residing premalignant cells evolve to evade immune surveillance. Angiogenesis, metastasis and immune system escape are all hallmarks of cancer making inflammation an important feature of tumour biology (Hanahan & Weinberg, 2011; Mantovani et al., 2008). Many groups have explored the pro-oncogenic effects of the SASP given that it is primarily a pro-inflammatory stimulus. Various disease phenotypes have been linked to the SASP on this basis.

Several SASP factors are inflammatory mediators that have been studied in the context of cancer irrespectively of senescence and provide the basis for the concept of inflammation-driven cancer. For instance, Ras^{G12V} expression in transformed cell lines led to increased production of IL-6 and IL-8 that contributed to tumour growth and neovascularisation while targeted inhibition of IL-6 and IL-8 delayed tumourigenesis after injection into mice (Ancrile, 2007; Sparmann & Bar-Sagi, 2004, respectively). The immune cells responding to these mediators themselves may promote carcinogenesis. CXCR2 is highly expressed in tumour-associated leukocytes and CXCR2 depletion suppressed neutrophil recruitment and tumourigenesis in the skin and gut epithelia (Jamieson et al., 2012).

Multiple publications have shown that secreted factors originating from senescent cells can be misused by cancer cells. Investigators have mostly exploited functional assays in which premalignant or tumour cells are co-cultured with senescent cells or treated with senescent CM. A pioneer study was that of Krtolica et al. (2001) who demonstrated that in both types of assays, regardless of senescence inducer (DNA damage, oncogene activation, replicative exhaustion, or oxidative stress), senescent cells and their secretome were able to promote proliferation of preneoplastic and malignant epithelial cells. Various other studies have reported similar findings. Amphiregulin and Gro-alpha secreted by senescent cells promoted the growth of premalignant epithelial cells (Bavik et al., 2006; Coppé et al., 2010). CM of senescent fibroblasts stimulated EMT of human breast cancer cells and invasion of various premalignant and malignant MECs through a basement membrane (Coppé et al., 2008). The authors believe this was due to the high levels of IL-8 and IL-6 present in this media since blocking antibodies prevented analogous invasion. Some SASP factors are also angiogenic mediators like VEGF, IL-8 and CCL2. CM from senescent mesothelial cells is rich in angiogenic factors and can promote proliferation of endothelial cells (Ksiazek et al., 2008). Senescent fibroblasts compromised the differentiation potential of immortal MECs to become lactogenic and disrupted the otherwise uniform alveolar morphogenesis (Parrinello et al., 2005). Both features were partly attributed to the increased epithelial cell proliferation due to a SASP. In the same study, it was shown that MMP3 was responsible for increased branching morphogenesis observed in primary mammary organoids treated with

senescent CM. Overall, senescent cells secrete factors that disturb the mechanisms holding epithelial cell proliferation in check in part by altering the microenvironment to promote invasive and migratory phenotypes consequently entering the prodrome of cancer.

The malignant effect of the SASP has yet to be reported in naturally occurring tumours. In theory, the SASP promotes nearby mutant premalignant cells to adopt a malignant phenotype and develop into cancer as both senescent and premalignant cells accumulate with age (Campisi et al., 2011). Evidence of the detrimental functions of the SASP *in vivo* mostly comes from xenograft mouse models in which the senescent and premalignant cells are coinjected resulting in accelerated tumour growth (Krtolica et al., 2001; Liu & Hornsby, 2007; Pazolli et al., 2012). Of relevance, obesity-related inflammation of high-fat diet fed mice originates from senescent HSCs. In this context, aberrant Ras signalling can lead to hepatocellular carcinoma which was prevented by ablation of the SASP factor IL-1β (Yoshimoto et al., 2013). In a model of OIS driven by p95HER2 in breast cancer cell lines, Joaquin Arribas' group have shown that the SASP potentially promotes metastasis since partial inhibition of the secretome prevented tumour growth of metastatic cell lines at distant sites (Angelini et al., 2013; Morancho et al., 2015). Paradoxically, sustained inflammation eventually also generates resistance to an immune response, by for example Tregs, which evolved to maintain a balance and consequently tissue homeostasis. This immunosuppressive microenvironment may allow immune escape and growth of pre-malignant cells. The SASP can also contribute to the recruitment of different immune cells to the tumour microenvironment. For example, the SASP recruited myeloid-derived suppressor cells and promoted tumourigenesis in a mouse model of p27Kip1-driven senescent skin (Ruhland et al., 2016) or a mouse model of *Pten*$^{-/-}$ senescent prostatic intraepithelium (Toso et al., 2014).

1.4.3.2. The SASP is associated with age-related disease

The SASP has not only been associated with hyperplasia but also with other age-related abnormalities. The working hypothesis is that age-related inflammation, 'inflammaging', contributes to frailty and disease and the SASP is one of the sources of this chronic inflammation (Freund et al., 2010). Age-dependent increase in pro-inflammatory factors such as IL-6 was significantly

reduced upon removal of senescent cells in tissues of progeroid and naturally aged mice (Baker et al., 2011, 2016).

An emerging hypothesis is that senescent cells present in the lungs of Idiopathic Pulmonary Fibrosis (IPF) patients secrete factors responsible for ECM remodelling of alveolar spaces leading to lung stiffness and ventilator restriction (Minagawa et al., 2011). Indeed, in a model of bleomycin-induced IPF, two groups showed that genetic ablation of caveolin-1 (Shivshankar et al., 2012) or treatment with an anti-inflammatory drug (Lv et al., 2013) attenuated the senescence response, an associated SASP and consequently fibrosis. The presence of senescent cells in fat tissue with a simultaneous increase in the pro-inflammatory cytokines CCL2 and TNFalpha is thought to contribute to inflammation and insulin resistance of the two metabolic disorders obesity and type 2 diabetes (T2D) (Tchkonia et al., 2010). Indeed, inhibition of senescence and as a consequence of the accompanying SASP in murine fat tissue enhanced insulin sensitivity and glucose tolerance (Minamino et al., 2009). Consistent with this idea, although not formally linked to the SASP, high-fat diet led to β-islet cell senescence, insulin resistance and T2D (Sone & Kagawa, 2005).

Investigating the paracrine role of senescence in disease will reveal important underlying disease mechanisms. An unanticipated discovery was that removal of the senescent epithelial cells of proximal tubules improved sclerosis of the glomeruli, suggesting that secreted factors play a part in age-related kidney dysfunction (Baker et al., 2016). The list of age-related diseases in which senescent cells have been detected, and tightly linked to, is long. These include Alzheimer's Disease (AD), atherosclerosis, osteoporosis, Chronic Obstructive Pulmonary Disease (COPD) and cataracts (reveiwed in Childs et al., 2015; Muñoz-Espín & Serrano, 2014). Senescence might play a role in the pathogenesis of these diseases but most of them await *in vivo* causal confirmation. A lot of the impact on disease is credited to the chronic, sterile, inflammation imposed by a SASP (Franceschi & Campisi, 2014) but the evidence to date causally connecting the inflammatory factors to senescence *per se* is limiting.

1.4.4. The SASP is a double-edged sword

The SASP is a double-edged sword (Coppé et al., 2010) (Figure 1.2). A temporal SASP production may be beneficial in defence against cancer by signalling to the immune system to clear incipient cancer cells but also by reinforcing senescence itself. Although the SASP has been implicated in tissue repair, conversely it has been associated with age-related tissue dysfunction due to ECM remodelling via a similar mechanism. Additionally, the secretome of lingering senescent cells promote malignancy of nearby cells and promotes age-associated systemic inflammation associated with disease.

Inflammatory cytokines secreted by senescent cells can exert either pro- or anti-cancer effects on nearby cells depending on the genetic constitution of the latter. For instance, $HRAS^{V12}$ immortalised human ovarian epithelial (HOSE) cells express GRO1, which in turn induces senescence of associated stromal fibroblasts. Conversely, the production of GRO1 by the senescent stromal fibroblasts promoted ovarian cancer development (Yang et al., 2006). While the determinants of the outcome of SASP signalling are largely unknown, a commonly accepted model holds that it depends on the stage of tumour progression. Although tested in other contexts, there are examples supporting this model. IL-6 inhibited growth of melanoma cells from primary lesions whereas cells from more advanced cancer lesions or metastatic sites were resistant to IL-6 (Lu et al., 1992, 1996). TGFβ is a factor frequently associated with both tumour suppression and cancer progression by causing tumour microenvironment alterations (Massagué, 2008). An explanation for the contradictory outcomes involves dissociation of the autocrine versus paracrine TGFβ1 activity (Glick et al., 1994). The specific outcome is highly contextual, as is the pleiotropic SASP, highlighting the need for more studies in order for targeted therapy to be feasible. Nonetheless, it appears that the net effect of a SASP in advanced cancer would be tumour growth and progression.

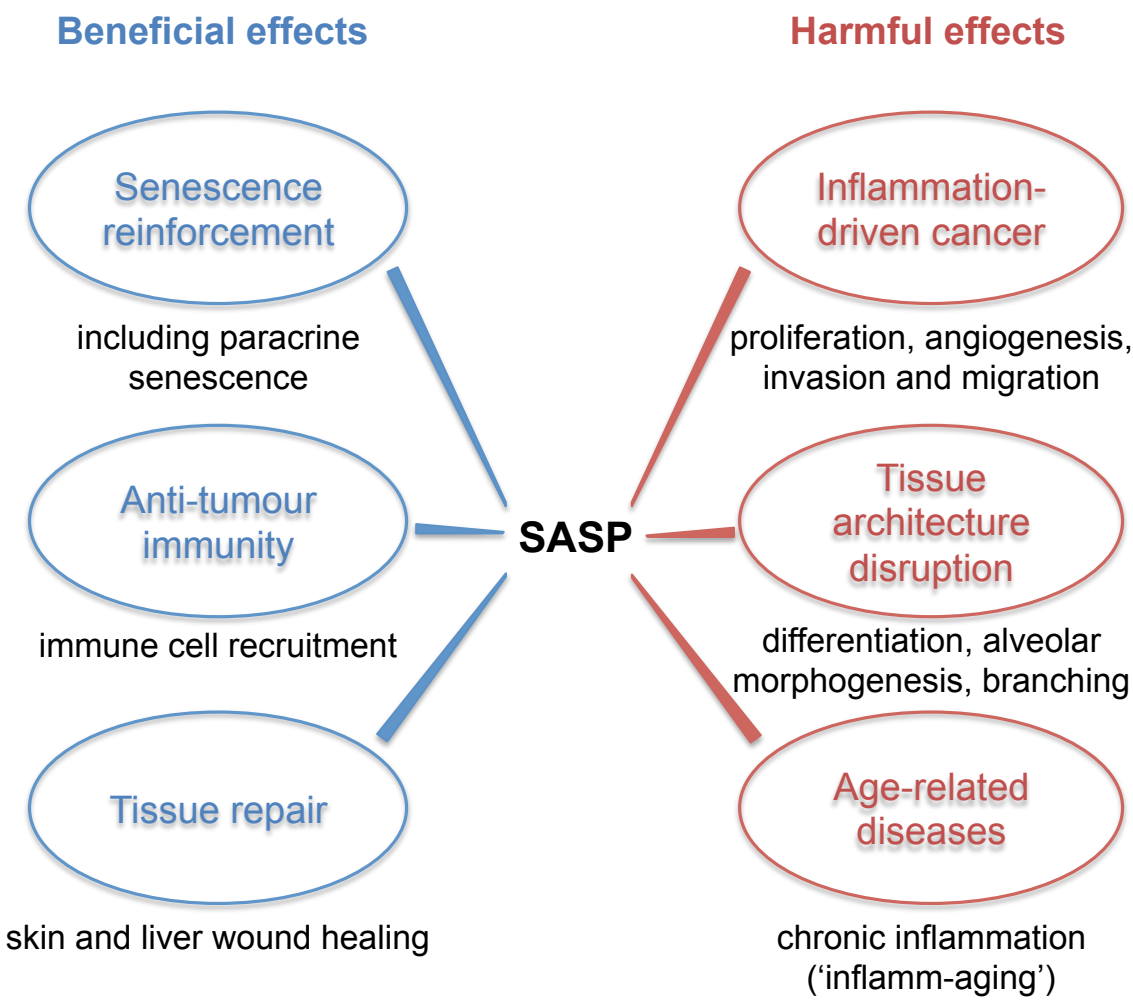

Figure 1.2. The SASP has beneficial and harmful effects on the surrounding tissue.
Senescent cells secrete a plethora of pro-inflammatory and matrix-remodelling factors that are beneficial early in life but harmful to tissue homeostasis at later stages of life. The SASP is an example of antagonistic pleiotropy.

1.5. Senescence in therapy

The tumour suppressive function of the senescence growth arrest and the SASP suggest that inducing senescence is a potential therapeutic anti-cancer strategy. In contrast, the loss of regenerative capacity due to the senescence growth arrest, and the harmful inflammation imposed by a SASP, suggests that eliminating senescent cells or suppressing the SASP can be advantageous in multiple pathologies.

1.5.1. Cooperating with senescence

Interestingly, some conventional anticancer therapies work by inducing senescence in tumour cells, a phenomenon termed Therapy-Induced Senescence (TIS). TIS arises as a result of DNA damage induced by radiation or genotoxic chemotherapy and is heterogeneously accompanied by apoptosis. Retinoic acid-arsenic trioxide is successful in treating Acute Promyelocytic Leukemia (APL) and was found to do so by inducing senescence of the leukemia-initiating cells (Ablain et al., 2014). Anticancer therapy can also cause senescence in solid tumours, with proof coming from senescence marker staining in sections of lung and breast tumours from patients who have undergone neoadjuvant chemotherapy (Roberson et al, 2005; te Poele et al., 2002). The ability of irradiation and of several cytotoxic drugs to induce senescence has been validated in culture or in xenografts using various tumour-derived cell lines reviewed and tabularised elsewhere (Ewald et al., 2010; Gewirtz et al., 2008).

Importantly, implementation of a senescence programme may determine response to cancer treatment and overall survival. To study chemoresistance, Schmitt et al. (2002) exploited an Eμ-*myc* mouse model in which overexpression of the oncogene *myc* specifically in the B-cell lineage led to lymphomas and simultaneous overexpression of anti-apoptotic *bcl2* caused apparent resistance to Cyclophosphamide (CTX) treatment. However, the authors observed instead a stable disease for an extended period of time, a phenomenon explained by the induction of senescence. Disruption of senescence by deletion of p53 or other senescence effectors led to rapid tumour growth. This report confirmed that senescence is at play in a clinically relevant context and unveiled the possibility of taking advantage of intrinsic senescence pathways to suppress tumour growth in a targeted manner.

The advantages of pro-senescence therapies are being explored by molecular or pharmacological induction of senescence in tumour cell lines or mouse tumour models (table in Pérez-Mancera et al., 2014). For instance, the CDK4/6 inhibitors LEE011 (Novartis) and Palbociclib (PD-0332991, Pfizer) induced senescence in neuroblastoma and glioblastoma cell lines respectively and suppressed xenograft tumour growth (Michaud et al., 2010; Rade et al., 2013). Palbociclib shows promising anti-tumoural activity in phase II and phase III clinical trials for

treatment of breast cancer by combinatorial therapy (Finn et al., 2015; Turner et al., 2015). Unbiased chemical screenings in search for pro-senescence compounds have revealed inhibitors of casein kinase 2 (CK2) and aurora kinase B (AURKB) as potential candidates (Kalathur et al., 2015; Sadaie et al., 2015). These studies not only open possibilities for new cancer therapeutic protocols but also help in expanding our knowledge on senescence types and mechanisms.

In addition to cancer, pro-senescence agents are potentially beneficial in other clinical contexts in which the secretory profile has an advantageous effect, for example in tissue repair after injury. In this context, administration of IL-22 or CCN1 led to senescence of HSCs and subsequently to regression of liver fibrosis (Kim et al., 2013; Kong et al., 2012).

1.5.2. Opposing senescence

Current treatment regimes have improved survival of cancer patients. However cancer survivors often suffer from premature ageing (Ness et al., 2015) with elevated $p16^{INK4a}$ levels in the skin (Marcoux et al., 2013) and severe symptoms such as heart failure (Gudmundsdottir et al., 2015; Oeffinger et al., 2006). More often than not, chemotherapy and radiotherapy also target surrounding non-neoplastic cells (bystander effect) thereby damaging healthy tissue. Collateral senescence induced by therapy, especially in cycling cells such as bone marrow, is not unexpected (Jiang et al., 2015) and as previously mentioned senescence in regenerating tissue contributes to ageing. Attempting to rejuvenate the tissue by manipulating senescence effectors could put patients at risk of secondary cancers. Selective removal of senescent cells on the other hand has been proposed as a powerful alternative strategy since results of studies by Baker et al. (2011, 2016) suggested that eliminating senescent cells could prolong cancer-free survival and improve age-associated disease.

There is growing interest in finding pharmacological agents that specifically target and kill senescent cells but not naïve cells, a class of drugs termed ‘senolytics’. The concept works on the basis that senescent cells rely on certain pathways to survive such as glucose metabolism (Dörr et al., 2013) and anti-apoptotic pathways (Chang et al., 2016; Zhu et al., 2015). In the first example, elimination of senescent lymphoma cells improved long-term survival after chemotherapy likely by

preventing the cell cycle re-entry of residing cells. In the second example, killing senescent cells improved regenerative capacity of heamatopoietic and muscle stem cells in irradiated and aged mice by increasing renewal turnover. Similarly, in a separate study targeting apoptosis regulatory pathways, elimination of senescent cells led to increased stem cell hair follicle proliferation, a tissue commonly compromised by chemotherapy (Yosef et al., 2016).

The bystander effect may also involve alterations in the tumour microenvironment and explain the short-term effectiveness of certain treatments. In this regard the secretome of senescent tumour cells determines disease progression. The SASP favours the growth and metastasis of inherently resistant clones or confers 'acquired' resistance of tumour cells to therapy. Inhibition of BRAF, or downstream kinases, showed promises for treatment of melanoma or lung adenocarcinoma and induced a senescence response accompanied by a secretome. The secretome accelerated proliferation and migration of resistant clones and resulted in tumour relapse (Obenauf et al, 2015). Sun et al. (2012) reported that chemotherapy treatment of mouse prostate neoplastic epithelium elicited a senescence response in the underlying stromal fibroblasts. One of the SASP factors associated was WNT16B, which largely accounted for cancer survival and growth following an intermittent therapeutic regime. Additionally, doxorubicin treatment caused non-malignant endothelial cells in the thymus to undergo senescence and secrete IL-6. IL-6 was responsible for the growth of lingering *Eμ-myc p19*$^{Arf-/-}$ lymphoma cells (Gilbert & Hemann, 2010; Bent et al., 2016). These scenarios theoretically could benefit from senolytic therapies but an alternative therapeutic approach would be to manipulate the SASP.

There are multiple approaches to target inflammatory diseases, for example by blocking the cytokines/chemokines and their receptors or inhibiting an upstream intracellular regulator (Dinarello, 2010). The search for novel, less toxic, compounds and methods to limit the detrimental effects of the SASP is gaining attention. Indeed, inhibition of JAK or mTOR activity blunted the SASP (Herranz et al., 2015; Laberge et al., 2015; Xu et al., 2015) and may have clinical implications since it delayed age frailty or extended lifespan in mice, respectively (Harrison et al., 2009; Xu et al., 2015). The inhibition of mTOR reduced outgrowth of the resistant melanoma cells after TIS *in vivo* (Obenauf et al., 2015). Although not in a TIS context, of importance, the mTOR

inhibitor rapamycin diminished tumour growth of cancer cells coinjected with senescent fibroblasts (Herranz et al., 2015; Laberge et al., 2015). Many other drugs are thought to exert their beneficial effects by suppressing the SASP. However, the advantages of treatment with such chemical compounds in health may not be strictly due to manipulation of senescence since causal links are still obscure.

1.5.3. Reconciling the pro- and anti-senescence demands

The net organismal consequence of senescence in tissue homeostasis depends on the temporal persistence of senescent cells. While a transient senescence response and its associated SASP can be beneficial, lingering senescent cells are thought to be detrimental. In a therapeutic context both pro-senescent and anti-senescent approaches may be of benefit and are now in the spotlight of experimental research. Induction of senescence can be used as a method to suppress the innate ability of tumours to proliferate or to enhance tissue repair processes. Blocking senescence can enhance tissue regeneration or suppress the favourable tumour microenvironment and chemoresistance.

The challenge lies in harnessing the beneficial effects while suppressing the negative ones. A possible reconciliation would be sequential treatment. The study of Xue et al. (2007) may serve as a proof of concept (see section 1.4.2.3). As Dr. Jan van Deursen reported in Science Daily "While halting cell division of these cells is important for cancer prevention, … once the 'emergency brake' has been pulled, these cells are no longer necessary." According to this model, pharmacological induction of senescence and subsequent pharmacological elimination of senescent cells would add considerably to the efficacy of cancer therapy, especially long-term when considering the pro-tumourigenic effects of the SASP. On the negative side, elimination of senescent cells can delay wound closure in aged mice (Baker et al., 2016). On the upside, suspension of senescent cell killing restored healing time to normal suggesting the constitutive senolysis would not influence normal functions if timely withdrawn.

Although senolytics are promising, new-concept, therapeutic tools and will be invaluable in understanding the function of senescent cells in age-related disease, there are a few aspects that

need disentangling. For instance, senolytics might be specific to cell type, senescence trigger and stage (Baker et al., 2016; Zhu et al., 2015; our group's unpublished data). Targeting the SASP would offer an alternative route. Despite the fact that SASP differs immensely in its composition across types, specific factors could be targeted regardless of location and origin. Inhibitors used for treating inflammatory diseases could be useful in attenuating the SASP. Examples include blockade of IL-1 and IL-6 receptor with drugs such as anakinra and tocilizumab, respectively, which are used for treatment of rheumatoid arthritis (Fleischmann, 2006; Tanaka et al., 2010). IL-6 signalling can also be blocked with JAK inhibitors, several of which are already in use for rheumatoid arthritis, renal allografts, psoriasis and myeloproliferative diseases (Galluzzo et al., 2016; Tefferi, 2013; Wojciechowski & Vincenti, 2013; Yamaoka & Tanaka, 2014), or with anti-IL-6 antibody Siltuximab, which is approved for Castleman disease (Deisseroth et al., 2015).

Searching for regulators of the SASP may be fruitful in eradicating other inflammatory diseases as well. Although senescence does not stem all age-related pathologies, inflammatory mediators might be more universal disease players. As an extrapolation of this and a word of caution, disrupting inflammatory effectors might negatively affect other cells such as immune cells or even negate essential tumour-suppresive senescence signalling, the latter being discussed in section 1.6.6.

1.6. SASP regulation

The SASP is composed of multiple inflammatory factors that mediate many of the physiological functions of senescent cells. To manipulate these functions the inflammatory factors can be specifically blocked or, alternatively, their induction can be blocked. The latter prospect underscores the necessity for dissecting the molecular regulation of the SASP. The existing knowledge on how the SASP is positively and negatively regulated (Figure 1.3), and the need for further research, will be the focus of this section.

1.6.1. Incoming senescence triggers and signals

1.6.1.1. DDR and p53

Cellular receptors of inflammatory cytokines are crucial to the robust autocrine signal amplification of the SASP (see section 1.4.2.1). Nonetheless, the senescent secretome is regulated at many levels. As expected, the trigger itself that initiates the senescence programme and the signalling that follows is strongly associated with SASP activation. The persistent DDR associated with replicative or stress-induced senescence is critical for stimulation of IL-8 and IL-6 (Rodier et al., 2009). Most of the published work specifically linked the DDR protein ATM to SASP but inactivation of other DNA damage sensing factors such as CHK2 and NBS1 also prevented SASP induction (Freund et al., 2011; Pazolli et al., 2012; Rodier et al., 2009). In support of this, induction of senescence by overexpression of $p16^{INK4a}$ and $p21^{Cip1}$, which are downstream of DNA damage, did not elicit a SASP and the associated paracrine effects (Coppé et al., 2011). Inactivation of another downstream target of the DDR, p53, rather enhanced the SASP and its tumour-promoting paracrine activities (Coppé et al., 2008). Interestingly, the p53-dependent secretome of senescent hepatocytes triggered polarisation of macrophages towards a tumour-inhibiting phenotype, which switched to a tumour-promoting phenotype when cultured with the p53-deficient proliferating counterparts (Lujambio et al., 2013). In addition, the inflammatory phenotype of intestinal epithelial cells was initially tumour-suppressive, but upon p53 inactivation promoted transformation and invasiveness (Pribluda et al., 2013). The DDR and p53 pathways clearly play an important part in the regulation of the senescence secretome. Notwithstanding, a SASP was identified in the two studies revealing developmental senescence, which is a DDR- and p53-independent response (Muñoz-Espín et al., 2013; Storer et al., 2013). This developmental SASP did not contain the DDR targets IL-8 and IL-6. Thus, multiple layers of SASP regulation exist and may reflect the various types and outcomes of senescence.

1.6.1.2. p38

The mitogen-activated protein kinase p38, herein referred to as p38 or MAPK14, is an essential part of the RAS signaling cascade and consequently OIS (Wang et al., 2002). In fact, p38 seems to be activated and is a necessary component in many other senescence types tested (Iwasa et

al., 2003). Pharmacological inhibition of p38 activity or genetic depletion of p38 transcripts prevented the induction of the majority of SASP factors in replicative-, irradiation- and oncogene-induced senescent cells (Freund et al., 2011). Over-activation of p38 led to a similar SASP and DDR inhibition was not sufficient to abolish it, further supporting the mechanistic link between p38 and SASP (Freund et al., 2011). p38 activity has been described to regulate the transcription of SASP genes through NF-κB (Freund et al., 2011) and the stability of SASP mRNAs (Alspach et al., 2014; Herranz et al., 2015), which will be discussed in later sections.

1.6.2. Transcriptional and epigenetic regulation

1.6.2.1. NF-κB and C/EBPβ

The hierarchy of the networks inducing a secretory phenotype is still unclear. Yet the transcription of several SASP genes principally depends on two transcription factors (TFs): nuclear factor-kappa B (NF-κB) and CCAAT/enhancer binding protein beta (C/EBPβ) (Acosta et al., 2008; Chien et al., 2011; Kuilman et al., 2008). NF-κB and C/EBPβ are activated and enriched in the chromatin fraction in oncogene-induced senescent cells (Chien et al., 2011; Kuilman et al., 2008). NF-κB also showed increased DNA-binding activity in replicative-, irradiation- and chemotherapy-induced senescent cells (Chien et al., 2011; Freund et al., 2011; Jing et al., 2011). Depletion of the NF-κB subunit p65 reduced expression of many pro-inflammatory SASP factors in OIS and IR-induced senescence (Chien et al., 2011). NF-κB was found to directly control transcription by binding to promoters of SASP components including IL-8, IL-6 and GM-CSF (Freund et al., 2011). C/EBPβ is on the other hand recruited specifically to the IL-6 promoter and C/EBPβ knockdown caused a collapse of the whole inflammatory network mainly due to disruption of IL-6 autocrine signaling (Kuilman et al., 2008). NF-κB and C/EBPβ are critical regulators of the SASP. In fact it seems that DDR and p38 signaling converge to NF-κB activation (Freund et al., 2011).

1.6.2.2. Chromatin modifications

There is a dynamic re-organisation of chromatin during senescence that has only just started to be understood at a functional level (Chandra et al., 2015; Shah et al., 2013). A growing body of

evidence suggests that the SASP can also be regulated by epigenetic mechanisms and chromatin remodelling. Removal of repressive marks on histones may allow access of TFs such as NF-κB to the promoters of SASP genes (Shah et al., 2013). Demethylation of lysine 27 on histone H3 by JMJD3 in glioma cell lines led to senescence-associated expression of certain cytokines, chemokines and MMPs with specific proof of demethylation on promoters of IL-8 and IL-6 (Perrigue et al., 2015). Similarly, Polycomb repressive complexes (PRC) and an HDAC NAD-dependent Sirtuin 1 (SIRT1) negatively regulate IL-6 and IL-8 transcription in normal cells by histone methylation and de-acetylation, respectively. In senescence, such chromatin repressive complexes are dissociated from the promoters (Hayakawa et al., 2015; Martin et al., 2013). Treating fibroblasts with multiple HDAC inhibitors promoted expression of SASP (Pazolli et al., 2012). In line with this, in a recent discovery Tasdemir et al. (2016) showed that the landscape of active enhancers marked with acetylated histones (H3K27ac) changes in senescence and a lot of these regulatory regions are located near SASP genes. BRD4 binds to these active super-enhancers hence controlling activation and consequently paracrine function. Histone variant exchange is another level of chromatin remodelling implicated in senescence and SASP regulation with the recent example of the variant MacroH2A1.1 being redistributed close to SASP genes promoting their transcription (Chen et al., 2015).

1.6.3. Post-transcriptional regulation of the SASP

1.6.3.1. mRNA stability

Despite the transcription of SASP genes being activated and necessary, regulating the stability of SASP mRNAs is equally important, at least for feeding the signal forward. Under normal conditions the translation of mRNAs encoding SASP factors is repressed due to molecular factors that bind to their 3' UTRs and destabilise them. Under stress, cells employ mechanisms to decrease occupancy of these factors on numerous SASP mRNAs. To date, three RNA binding factors have been linked to this function in the context of senescence, namely Nuclear Factor (NF) 90, AU-binding factor (AUF) 1, and ZFP36 ring finger protein-like (ZFP36L) 1 (Alspach et al., 2014; Herranz et al., 2015; Tominaga-Yamanaka et al., 2012). Activity of p38 is necessary for the release

of AUF1 (Tominaga-Yamanaka et al., 2012). MK2, a downstream target of the p38 kinase activity, is necessary for inactivation of ZFP36L1 (Herranz et al., 2015). This indicates that prevention of SASP mRNA degradation is, at least in part, the underlying mechanism of action of p38 on SASP induction.

1.6.3.2. Protein translation

Besides changes in the stability of mRNAs, an important post-transcriptional level of regulation is protein translation. The findings of three groups have put mTOR (mechanistic target of rapamycin) in the centre of the translation status of senescent cells. mTOR is a master regulator of protein translation and ribosome biogenesis. Narita et al. (2011) described a protein complex that supported global protein synthesis in senescence, termed the TOR-autophagy spatial coupling compartment (TASCC). In the TASCC, mTOR co-localises with autolysosomes (lysosome-autophagosome), in close proximity to the trans-Golgi network (TGN) and is necessary for a SASP. The localisation of IL-8 and IL-6 in the cytoplasm of cells is indeed often detected in a perinuclear TASCC-like structure. One possible advantage of coupling TGN with autophagy would be the accessible amino acid supply from autolysosomes supporting rapid protein turnover (Narita et al., 2011). Later, it was found that the SASP depends on mTOR indirectly because of the translation of MK2 (Herranz et al., 2015), or translation of IL-1α (Laberge et al., 2015), a SASP factor itself that is implicated in signal amplification, as described below. How regulation of the direct translation of certain SASP components may also be part of the picture is still an open field of investigation.

1.6.4. Regularion of the SASP by signal amplification

1.6.4.1. IL-1α and inflammasome

The SASP engages in feed-forward loops. Increasing evidence links receptor signalling to NF-κB and C/EBPβ activation and subsequent increase in SASP gene transcription (Acosta et al., 2008; Kuilman et al., 2008). A master regulator of the SASP positive feedback loop in response to multiple senescence stimuli is IL-1α. IL-1α activates the receptor signalling pathway of IL-1R/TLR

(Toll-like receptors), which in turn signals to NF-κB leading to IL-8 and IL-6 expression (Orjalo et al., 2009). More recently our group identified inflammasomes to be mediators of IL-1 signalling in senescence (Acosta et al., 2013).

Inflammasome signalling is briefly described here based on the reviews of Latz et al. (2013) and Schroder & Tschopp (2010). As part of innate immunity, in addition to TLRs, NOD-like receptors (NLRs) sense damage-associated molecular patterns (DAMPs) but are intracellular. A subset of NLRs, namely NLRP1, NLRP3, IPAF, and AIM2 assemble independently into a multi-molecular complex, the inflammasome, together with caspase-1. Production of IL-1α and IL-1β transcripts is a result of a primary signal usually relayed by TLRs but the proteolytic cleavage of IL-1β into its mature form is carried out by caspase-1. Many types of stresses have been described to represent the secondary signal that leads to inflammasome activation. Examples include ER stress, lysosomal destabilisation and increased ATP and ROS production, most of which also occur during senescence. IL-1β secretion in response to injury or infection causes local and systemic inflammation. Inflammasome activation and consequential IL-1 secretion has been implicated in several autoimmune and autoinflammatory diesases (examples listed in Shaw et al., 2011). Inflammasome activation is also associated with ageing as the organsim is progressively exposed to DAMPs. Not so surprisingly, the list of inflammasome-associated pathologies overlaps significantly with the emerging SASP-related pathologies. Indeed, lowering NLRP3 inflammasome delayed age-associated decline in thymic lymphopoiesis, which correlated with lower levels of T cell senescence (Youm et al., 2012). Acosta et al. (2013) demonstrated that mature IL-1β is part of the subset of SASPs responsible for propagating senescence to normal cells, an important tumour suppressive mechanism.

1.6.4.2. HMGB1

IL-1β is not the only factor secreted via the unconventional secretion pathway in senescence. HMGB1 is an Alarmin (endogenous DAMP) secreted from damaged and/or dying cells and is exploited by immune cells to amplify inflammation as part of the immune response in other contexts. Davalos et al. (2013) detected increased levels of extracellular HMGB1 in cultures of

senescent cells and found that it contributes to IL-6 upregulation by feed-forward signalling to NF-κB through membrane-bound TLR4.

1.6.4.3. p62

The autophagy and lysosome degradation pathway (section 1.6.3) have been implicated in SASP synthesis but the directionality of the relationship between autophagy and senescence is debatable. The active role of mTOR in senescence contributes to the inconsistency. In accordance with the conventional function of mTOR being an inhibitor of autophagy, some studies have shown that suppression of autophagy promotes senescence (examples in Gewirtz, 2013). Paradoxically, autophagy was necessary to counteract the ER stress and unfolded protein response (UPR) partially stemming from the high load of SASP and hence contributed to survival of senescent cells (Dörr et al., 2013). Kang et al. (2015) suggested settling with the possibility of general autophagy and selective autophagy having opposing roles. The authors came to this conclusion because a specific and normal function of p62, an autophagy adaptor, was disturbed in senescent cells. In line with this, mTOR was sequestered in the TASCC along with p62, away from ULK1 an activator of autophagy (Narita et al., 2011). Regardless of cause, the GATA4 transcription factor was no longer associated with p62 in senescence and escaped autophagy leading to increased transcription of TRAF3IP2 (Kang et al., 2015). TRAF3IP2 is necessary for transcription of SASP genes and interacts with intracellular downstream effectors of IL-1R and TLR that relay the signal of IL-1α to NF-κB, for example.

1.6.4.4. Paracrine signalling

Finally, evidence for a positive feedback loop amplifying the SASP comes from work based on paracrine senescence models. Chemical inhibition of the receptor of TGFβ1 and IL-1 prevented activation of a DDR and cellular senescence in wild type cells treated with senescent CM (Acosta et al., 2013; Hubackova et al., 2012). This was caused by reduced expression of NOX4, an NADPH oxidase, which prevented ROS production and ultimately the DDR (Hubackova et al., 2012). While a direct experimental link to regulation of NOX4 expression is missing, activation of

DDR by the SASP factors constitutes a parallel branch of SASP regulation. In the same study, it was also shown that JAK/STAT3 signalling was important for implementation of paracrine senescence. Although not in this context, IL-6/STAT3 signalling itself can lead to ROS, DDR and senescence (Kojima et al., 2012) and inhibition of JAK/STAT signalling altered the SASP of *Pten*$^{-/-}$ senescent prostate cells (Toso et al., 2014) implying that it plays a role in SASP regulation.

1.6.5. Mechanisms downmodulating the SASP

At least one microRNA (miRNA) has been implicated in negative regulation of SASP. Judith Campisi's group elegantly demonstrated that expression miR-146a/b is upregulated only in the presence of high SASP levels (Bhaumik et al., 2009). miR-146a/b inhibits transcription of IRAK1 which is an indispensible part of the IL-1R signalling cascade leading to NF-κB activation. Interestingly, the DDR in OIS that results from SASP-mediated ER stress and ROS, is necessary for macroH2A1 removal from SASP genes in an experimental setting of late-senescence with prolonged SASP signalling (Chen et al., 2015).

1.6.6. SASP regulation - an attractive therapeutic target not without risk

Given that the SASP can signal to neighbouring cells thereby affecting pathology, it has been theorised that manipulating SASP regulation is a potential route for therapeutic intervention. Indeed, the use of existing inhibitors to validate or discover (Herranz et al., 2015) new SASP regulators is a common approach. Such studies may provide an additional or alternative explanation for the anti-inflammatory or otherwise positive outcome of certain drugs used in the clinic. For instance, treatment with metformin and glucocorticoids, resulted in NF-κB inhibition, impairing the pro-inflammatory phenotype of senescent cells in culture (Laberge et al., 2012; Moiseeva et al., 2013). Rapamycin (mTOR inhibition) treatment mitigated the aggressive phenotype associated with the secretome of irradiation-induced senescent cells in murine xenografts (Herranz et al., 2015; Laberge et al., 2015). NSAIDs such as aspirin have cancer preventive properties if taken for an extended period of time during life but it is not fully understood why (Rothwell et al., 2011). The NSAID sulindac weakened the para-inflammatory, cancer-

promoting property of intestinal epithelial cells lacking p53 in a mouse model of colorectal tumour senescence (Pribluda et al., 2013).

The various pathways that activate the SASP are by nature important senescence effectors consequently rendering their therapeutic manipulation unsafe. For example, blocking the DDR would limit effectiveness of senescence induction in response to stresses, increase susceptibility to mutations, and ultimately lead to cancers. Like RAS, NF-κB has essentially pro-oncogenic functions, partially attributed to inflammation, but in the context of senescence can be tumour-suppressive. In a mouse model of B-cell malignancy with suppressed apoptosis, reducing the levels of p65 (an NF-κB subunit) left lymphoma cells resistant to chemotherapy that otherwise respond by undergoing TIS (Chien et al., 2011). This outcome is possibly due to the reduced anti-tumour immunity surrounding the lymphomas. The NF-κB-dependent inflammatory phenotype aside, inhibition of NF-κB has been shown to enhance carcinogenesis by other mechanisms. Blockade of NF-κB, either genetically in transgenic mice or by applying an inhibitor on the epidermis, gave rise to hyperplasia (Seitz et al., 1998), while over-activation prevented epithelial cell growth.

The fact that certain SASP components reinforce growth arrest adds to the risk of global SASP inhibition. A potential approach would be to specifically target the molecules most relevant to a particular pathology. However, release of inflammatory mediators is not linear but cytokines and chemokines rather exist in cascades and often act in a synergistic fashion. Interfering with one may interfere with another and eventually break down the cellular programme (Dinarello, 2010). Additional and extensive studies are necessary to navigate these overlapping cascades, to determine whether a discrepancy exists and whether this is exploitable.

An alternative strategy would be to reinforce senescence or antagonise proliferation and simultaneously impair a pathway that positively regulates the SASP. Preliminary evidence indicates that uncoupling cell proliferation and the SASP is feasible. Inhibition of mTOR confers anti-proliferative effects in addition to anti-inflammatory effects, hence the net effect of Rapamycin treatment is tumour suppression (Herranz et al., 2015; Laberge et al., 2015). Transcriptional repression of pro-proliferative cell cycle genes by MLL1 inhibition in OIS prevented the DDR and

the downstream NF-κB activity leading to lower levels of pro-tumourigenic SASP in OIS, but the growth arrest was maintained probably due to the high levels of other senescence effectors such as p16 (Capell et al., 2016). These examples provide proof for a potential approach to SASP manipulation.

The published data to date do not offer a complete picture of how the SASP is regulated. SASP-specific pathways remain to be elucidated, helped by a systematic analysis of SASP regulation.

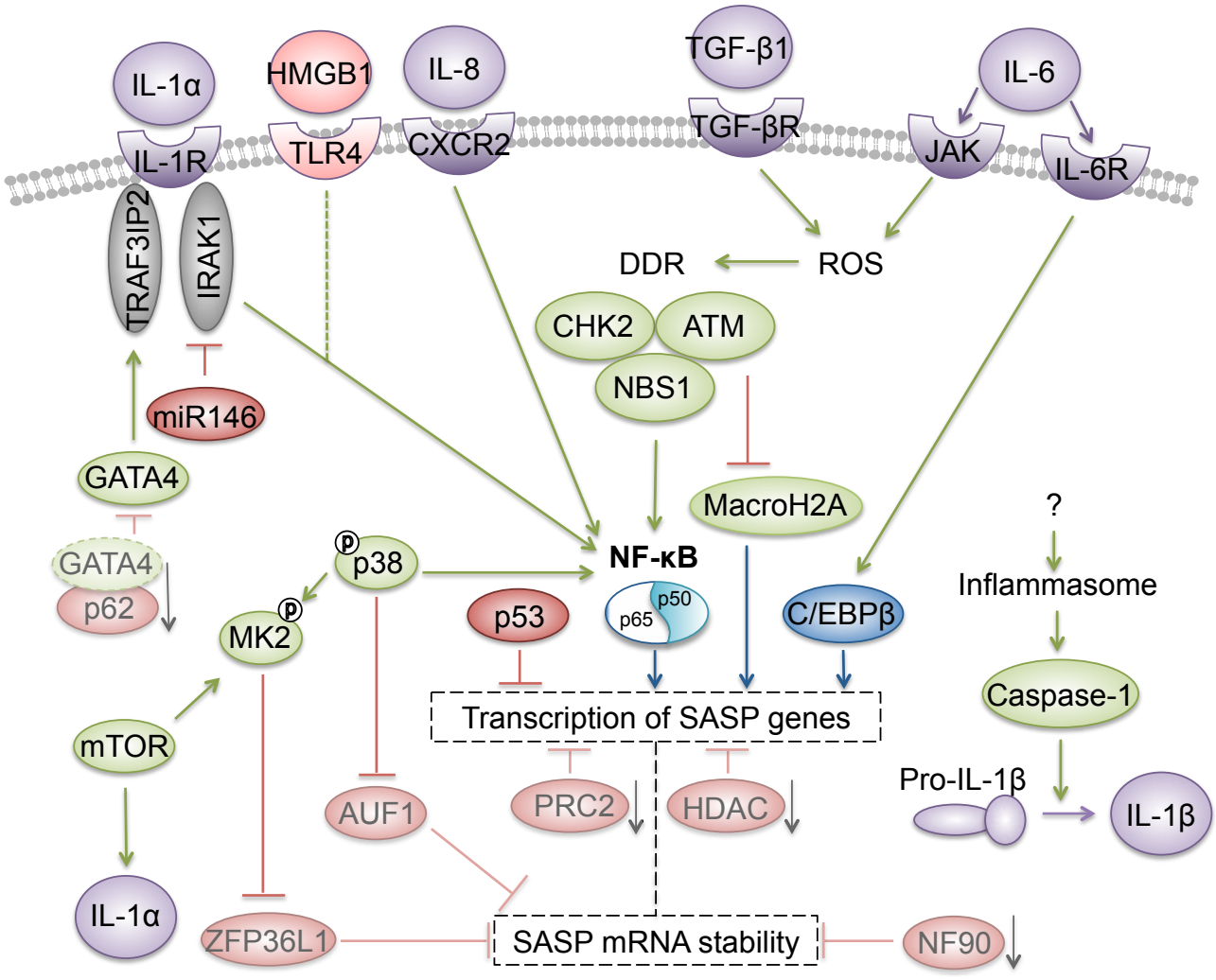

Figure 1.3. SASP regulation.
Research to date includes examples of SASP regulators acting at multiple cellular levels. At first sight NF-κB in the nucleus is the master regulator of SASP. However, signal amplification by the extracellular SASP, or other secreted molecules (e.g. HMGB1), is equally important. Incoming senescence stimuli (DDR) and the following autocrine signalling via membrane-bound receptors often result in NF-κB activation. Black arrows denote reduced levels in senescence.

1.7. RNA splicing

1.7.1. The spliceosome

One of the key post-transcriptional control mechanisms of eukaryotic gene expression is splicing of the pre-mRNA into the mature, functional mRNA. RNA splicing is the process by which introns, the intervening non-coding sequences, are excised from the pre-mRNA (primary) transcript, and exons, the coding regions, are joined together before the nascent mRNA is exported from the nucleus and translated into protein (Dvinge et al., 2016; Wahl & Lührmann, 2015).

RNA splicing is mediated by a large RNA-protein complex called the spliceosome. The spliceosome is a dynamic molecular machine that involves assembly and disassembly of its components onto the substrate in a stepwise manner and is coupled to RNA Pol II-mediated transcription. The main molecular components of the spliceosome are the small nuclear ribonuclear proteins (snRNPs) namely U1, U2, U3, U4, U5 and U6 and approximately 200 proteins. The snRNPs are 6 RNAs referred to as small nuclear RNAs (snRNAs) that are individually complexed with seven of the so-called Sm proteins for the cases of U1-5 and the LSm for the case of U6. The composition of the spliceosome changes during the splicing process and although not all stages are catalytically competent, their ordered appearance is required (Figure 1.4) (Dvinge et al., 2016; Wahl & Lührmann, 2015).

Genomic regulation of RNA splicing is necessary for the specific function of the splicing factors. In particular, splicing motifs in the pre-mRNA sequence itself guide the spliceosome and associated factors. Specific consensus nucleotide sequences flanking an intron called splice sites set the boundaries between an intron and the exons flanking that intron. Another conserved sequence of introns involved in splicing is the so-called branch point site (A) followed by a polypyrimidine tract (Py tract). These sequence characteristics are necessary for constitutive and precise splicing of exons (Figure 1.4). The splice site however that will be selected and ultimately the exon to be included in the final mRNA can vary, a phenomenon called alternative splicing (AS) (Dvinge et al., 2016; Wahl & Lührmann, 2015).

1.7.2. Alternative splicing

AS is governed by *trans*-acting splicing factors that recognise splicing regulatory elements (SREs). SREs are sequence motifs divided into 'splicing enhancers' and 'splicing silencers' present in exons (exonic: ESE and ESS) or introns (intronic: ISE and ISS) (Figure 1.5a) and are considered *cis*-regulatory elements. *Trans*-acting splicing factors are RNA-binding proteins (RBPs) categorised into two main groups, the serine/arginine rich (SR) proteins and heterogeneous nuclear ribonucleoproteins (hnRNPs). As a rule of thumb, SR proteins usually promote exon inclusion whereas hnRNPs usually promote exon skipping (Figure 1.5a). Apart from these categories, there are other identified splicing factors targeting consensus RNA motifs that regulate splicing (tabularised in Fu & Ares, 2014). The consequence of splicing factor binding within a pre-mRNA is not strictly associated to either exon repression or inclusion but is rather context-dependent. For example, the splicing factor Py Tract Binding Protein 1 (PTBP1 or hnRNP I) was initially depicted as a repressor of exon inclusion based on mini-gene construct experiments (reviewed in Spellman & Smith, 2006). Genome-wide analysis of cells lacking PTBP1 have revealed that PTBP1 is also necessary for inclusion of some constitutive exons (Xue et al., 2009; Dvinge et al., 2016; Wahl & Lührmann, 2015)

Most of the regulation of AS happens at the early stage of spliceosome assembly with splicing factors antagonising, or synergising with, the pre-spliceosome machinery in a process called exon definition (Fu & Ares, 2014). Exon definition decides the fate of an exon and/or intron hence dictates the resulting isoform of a gene. Following exon definition, different modes of AS lead to different coding sequences from the same gene, illustrated in Figure 1.5b, explaining the high protein diversity in relation to total number of genes. More than 90% of the human multi-exon protein-coding genes produce more than one different transcript (Wang et al., 2008).

The significance of tight regulation of RNA splicing is highlighted by the variety of diseases associated with altered splicing of genes or the presence of single-nucleotide polymorphisms (SNPs) in SREs whether these are splice sites, *cis*-regulatory elements, trans-acting factors or part of the main spliceosome (Scotti & Swanson, 2015). One of the earliest examples of mis-splicing in disease was that of the β-globin gene, *HBB*. An SNP forced the use of an alternative 3' ss leading

to lower levels of β-globin, the cause of β-thalassemia, probably due to non-sense mediated decay (NMD) of the resulting truncated transcript (Busslinger et al., 1981; Maquat et al., 1980). Since then, mis-splicing has been functionally linked to a multitude of muscular and neurological diseases (Scotti & Swanson, 2015).

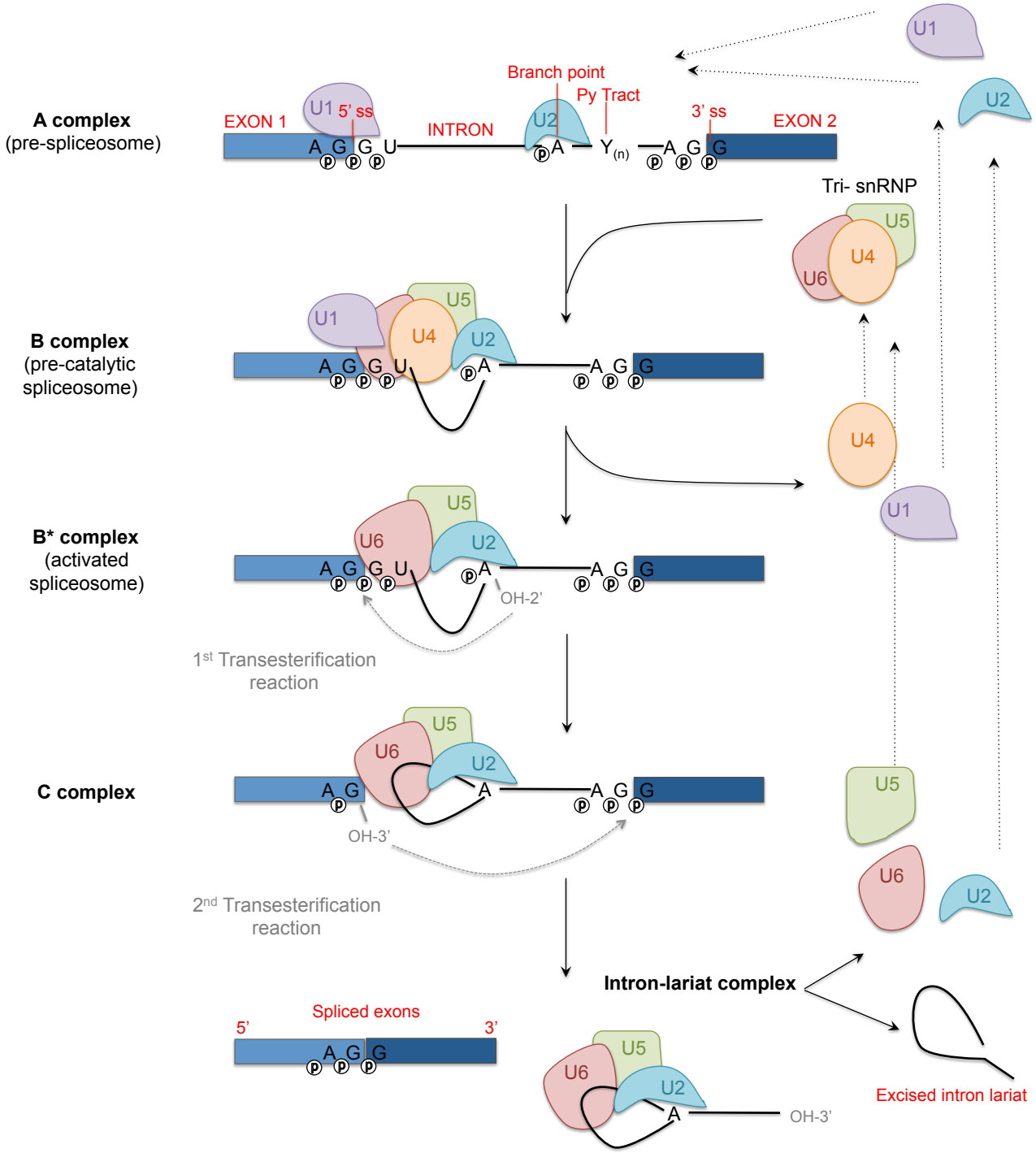

Figure 1.4. A simplified view of the splicing pathway.
Catalysis of splicing involves two successive transesterification reactions. U1 recognises the 5' splice site (ss) on the pre-mRNA and the snRNA base pairs with the pre-mRNA. The branch site is recognised by the U2 and base pairing occurs between its snRNA and the pre-mRNA excluding the A residue from the double-helical RNA formed with its OH-2' extending. The complex formed is referred to as the A complex. The A

complex is rearranged into the B complex by the joining of the tri-snRNP particle composed of the U4, U5 and U6. Breakage of the base pairing joining the U1 with the 5' splice site allows for annealing of U6 snRNA on the pre-mRNA at that site. U4 is then released from the complex allowing RNA-RNA interactions between U2 and U6. At this point, the 5' ss is cleaved and the free 5' end of the intron binds to the 2'-OH of the A branch site. Following release of U4 from the complex, the 3'-OH of the 5' exon attacks the phosphoryl group of the 3' splice site, joining the two exons. The resulting products include the spliced exon and the excised lariat intron with associated proteins. This scheme does not include any of the 200 proteins identified to form the platforms for the complexes. (Adapted from Wahl & Lührmann, 2015)

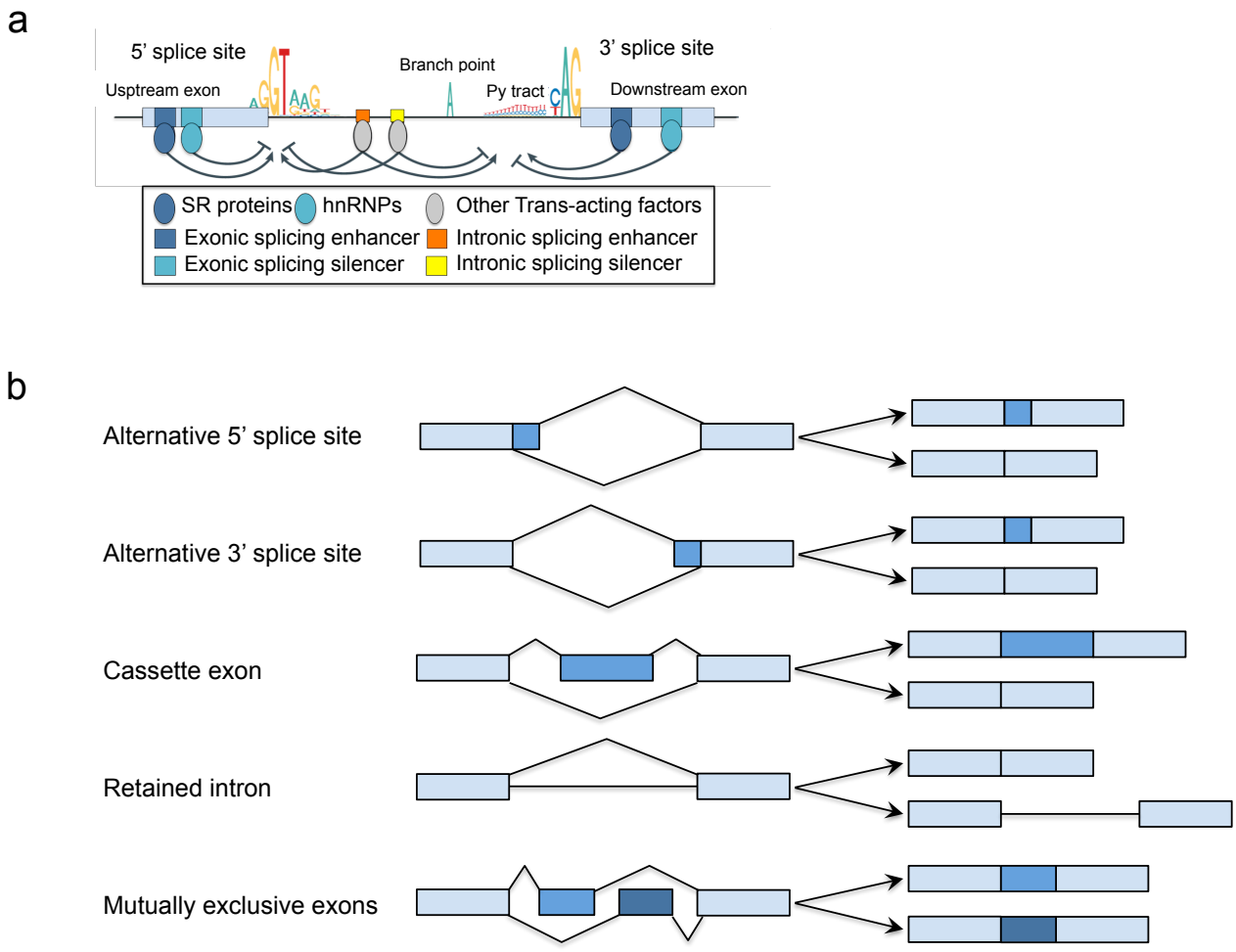

Figure 1.5. *Cis*- and *trans*-acting elements regulate alternative splicing.
a. *Cis*-regulatory elements are the two splice sites, a branch point, a poly(Y) tract and the silencers and enhancers. The height of a nucleotide reflects the frequency of the specific nucleotide at that position in the genome (hence T and not U). *Trans*-acting factors are sequestered to consensus sequences and repress or enhance the recognition of splice sites by the core spliceosome machinery. **b**. Alternative splicing exists in 5 main different modes. Parts of an exon may be skipped, a whole exon may be skipped, introns may be retained in the mature transcript, or exons may mutually exclude each other. (Adapted from Dvinge et al., 2016)

1.7.3. RNA mis-splicing in cancer, the case of PTBP1

AS is a physiological cellular mechanism whose deregulation has been implicated in the pathology of many diseases including cancer. Deregulated splicing can lead to downregulation of gene expression by nonsense-mediated decay (NMD) or to a dysfunctional truncated product or a splice variant with a different, even opposing, function. Emphasising on the latter, different transcripts with a switch in splicing are associated with all the hallmarks of oncogenesis (Figure 1.6). The critical role of specific splice isoforms in cancer is beyond the scope of this thesis but for comprehensive material the reader may refer to reviews of Liu et al., 2015 and Oltean & Bates, 2014. Whether specific splicing isoforms are universal for all types of cancer is not known and not all identified examples of splice isoforms have been scrutinised for their mechanistic role in tumour establishment and progression. Nevertheless, there is growing evidence suggesting that, firstly, mutations leading to aberrant splicing of TSGs and oncogenes can be drivers of disease (Jung et al., 2015; Okumura et al., 2011; Supek et al., 2014). Secondly, splicing factors themselves can serve as oncogenes leading to global alterations in AS (Dvinge et al., 2016). Lastly, and bridging the two models, oncogenic signalling employ deregulation of splicing factors as a means to acquire phenotypic traits of disease progression or therapy resistance, two concepts discussed below.

Cancers seem to hijack the molecular mechanisms dictating the choice of splicing as exemplified by the upregulation of specific splicing factors in cancers and the contribution of the resulting spliced transcript to disease progression. The splicing repressors hnRNPA/B and PTBP1 are expressed throughout development but not in the adult tissues studied, namely brain and muscle (Boutz & Chawla, 2007; Boutz et al., 2007; Makeyev et al., 2007). It seems that expression directly correlates with proliferation. Consistent with this, PTBP1 is overexpressed in gliomas, ovarian cancer and cancer cell lines (David et al., 2010; He et al., 2007; Jin et al., 2003). David et al. (2010) found that hnRNP A1/A2 and PTBP1 are responsible for repressing exon 9 from the adult isoform of pyruvate kinase (PKM1) and hence promoting exon 10 inclusion to form embryonic pyruvate kinase (PKM2) in undifferentiated muscle cells. PKM1 promotes oxidative phosphorylation over aerobic glycolysis. A1/A2 and PTBP1 expression correlate well with n-Myc levels in human gliomas and the A1/A2 and PTBP1-dependent switch to PKM2 in cancer cell lines

and after c-*myc* overexpression, suggest these splicing factors together contribute to the metabolic advantage of cancer cells (Warburg effect) (Figure 1.6). Indeed, Clower et al. (2010) reported that knockdown of A1/A2 and PTBP1 in a glioblastoma cell line leads to decreased production of lactic acid indicative of lower anaerobic glycolysis. In two separate studies, the contribution of PTBP1 activity to growth and migration of glioma cell lines was attributed to its regulatory role over AS of reticulon-4 (RTN4) and USP5 independently (Cheung, et al., 2009; Izaguirre et al., 2012). In the latter case, AS of PKM was not notable in the unbiased splicing analysis. This discrepancy reflects the heterogeneity of alternative splicing patterns in tumours presenting a challenge for the field if AS is to provide insight into novel therapeutic approaches (Sebestyen et al., 2015).

PTBP1 represses exon splicing of substrates whose activity has been linked to stages of malignant transformation, in one way or another. For example, PTBP1 regulates splicing of FGFR1 (Jin et al., 2003), FAS (Izquierdo et al., 2005), caspase 2 (Wang et al., 2008), ABCC1 (He et al., 2004) and c-Src (Chan & Black, 1997). The association of the splicing events with cancer progression however merits further investigation since the promising effect of inhibiting PTBP1 in cancer cells may be associated with functions other than splicing repression. PTBP1 regulates mRNA stability by binding to 3' UTR (Coles et al., 2004) and/or directly protecting from NMD (Ge et al., 2016), translation of genes by binding to IRES-Internal Ribosome Entry Site (King et al., 2010; Mitchell et al., 2005) and subcellular localisation of mRNAs (Babic et al., 2009). PTBP1 substrates are involved in many aspects of cancer, such as c-Myb (Mitchell et al., 2005) in proliferation, VEGF (Coles et al., 2004) in angiogenesis, APAF1 (Mitchell et al., 2003) in apoptosis and finally, vinculin and α-actinin-dependent focal adhesions (Babic et al., 2009) in migration. Adding to the difficulty in pinpointing the functions and targets of PTBP1 in cancer, overexpression of PTBP1 is not a common feature to all cancer cell lines and the targets for PTBP1-mediated AS depend on the context (Wang et al., 2008).

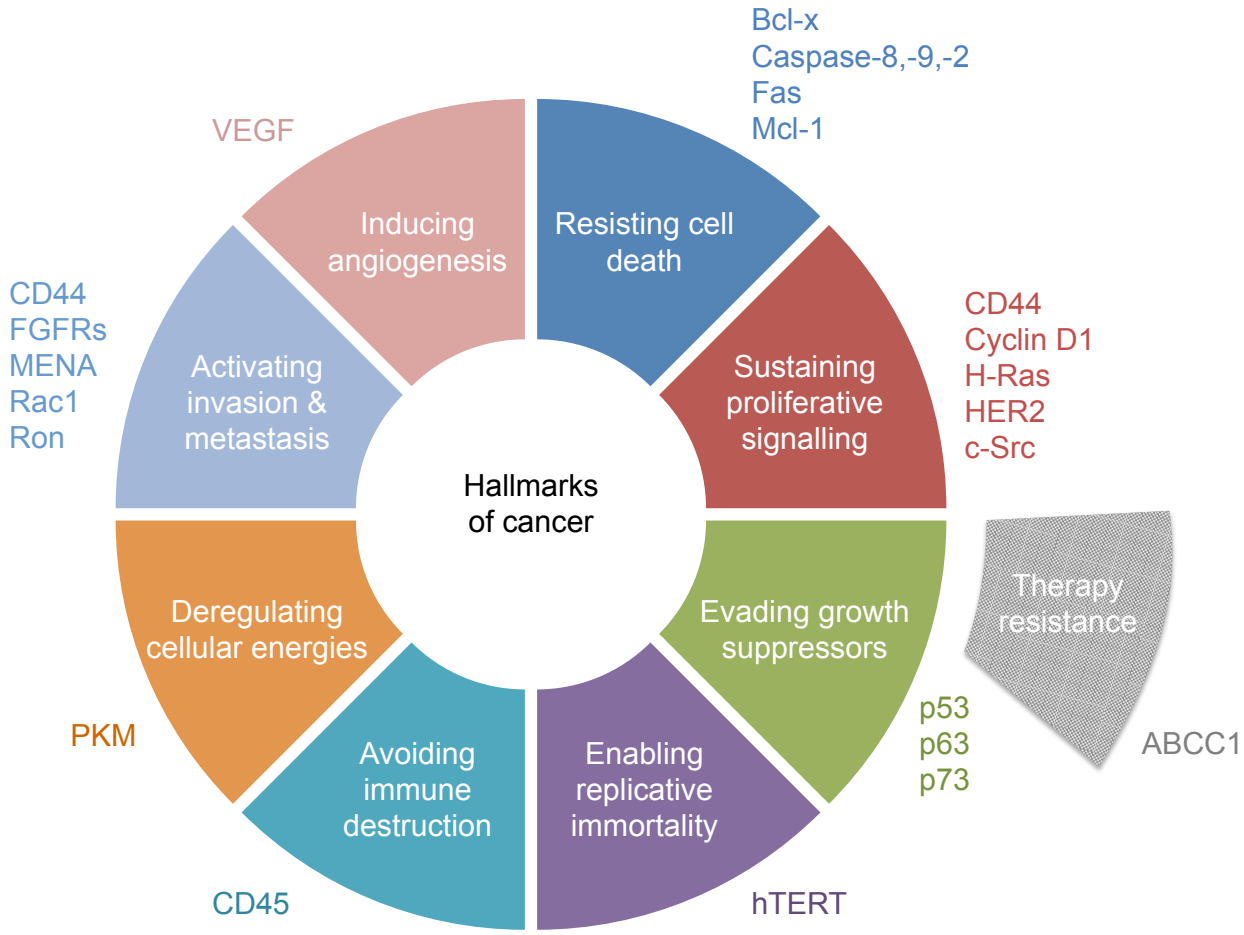

Figure 1.6. Relation between cancer hallmarks and alternative splicing.
The names of the genes whose alternatively spliced transcripts have been found to contribute to a cancer phenotype are accordingly colour-coded. (Taken and slightly adapted from Liu et al., 2015)

1.7.4. Alternative splicing in therapy

Whether PTBP1, and other splicing factors, significantly drive tumourigenesis, or are passenger markers of cancer development, remains to be determined. It was only recently confirmed *in vivo* that two spliceosomal genes have biological significance in cancer. A knock-in of mutant *Srsf2* and a transgenic of mutant *U2AF1* (U2 snRNA auxiliary factor 1) led to genome-wide alterations in splicing inclusive of targets associated with MSD (Myelodysplastic syndromes) and MSD/AML (Acute Myeloid Leukemia), respectively (Kim et al., 2015; Shirai et al., 2015). The other side of the coin is that, in MYC-driven tumours, a lot of the core spliceosomal machinery is upregulated directly or probably due to the increased demand of RNA processing of the high-turnover transcriptome of proliferating cells. This leads to global alterations in splicing fidelity and some of the affected targets, such as Mdm4, have been directly linked with cell proliferation (Bezzi et al.,

2013; Hsu et al., 2015; Koh et al., 2015). Dissociating coincidental alterations due to global changes from splicing events recurrently contributing to a cancer phenotype will be imperative if AS is to be manipulated for therapy.

The AS landscape of disease is gaining increasingly more appreciation. As a consequence, interest in developing approaches to regulate specific splicing events is growing, especially for those with the potential for therapeutic use (McClorey & Wood, 2015). Strategies employing the CRISPR-Cas9 system to induce splice switching by genome editing have been successful in improving muscular dystrophy driven by aberrant expression of *dystrophin* (Nelson et al., 2016; Tabebordbar et al., 2016; Xu et al., 2016). Alternatively, administration of two antisense oligonucleotides (AONs) to promote exon skipping, namely Eteplirsen and Drisapersen, in Duchenne muscular dystrophy patients, although promising as single agents, were shown to enhance treatment efficacy when combined with synergising compounds in a mouse model (Goemans et al., 2011; Kendall et al., 2012; Mendell et al., 2013). Current advances in such methodologies pave the way for targeted investigations into the pathogenicity of alternatively spliced variants in cancer progression.

Interestingly, the mode of action of drugs initially identified for their anti-tumour activity was later found to be splicing modulation. One of the earliest examples is FR901464 and its more recently discovered acetylated derivative, spliceostatin A (SSA), that inhibited growth of human and murine xenografts and was later found to target SF3B1, which is required for the core spliceosomeal snRNA U2 activity (Corrionero et al., 2011; Kaida et al., 2007; Nakajima et al., 1996). After these discoveries, and the possibility of splicing modulators serving as therapeutic agents, other small molecule splicing inhibitors have been designed to target spliceosomal or splicing factors in search for potential tumour suppressive actions (Salton & Misteli, 2016). Although the positive outcome is a result of gene-specific splicing alterations, the existing inhibitors target constitutive RNA splicing components. On one hand disrupting the spliceosomal machinery can be synthetically lethal since the spliceosome is a vulnerability of cancers with increased demand for RNA processing such as *myc*-driven cancers (Hsu et al., 2015). On the other hand the unspecific nature of global splicing inhibitors raise the probability of toxic side effects due to

alterations on bystander necessary splice-variants or simply because other healthy, high turn-over tissues have high demand on precise RNA processing (Eskens et al., 2013; Hong et al., 2014). Ironically, it is entirely possible that therapy resistance to certain drugs is caused by the specificity towards certain isoforms over others. A well-appreciated example of acquired resistance is the case of $BRAF^{V600E}$ melanoma to vemurafenib. Poulikakos et al. (2011) demonstrated that a shorter variant BRAF form frequently arose that escaped the drug's main mechanism of action. Broadening our knowledge on disease-associated splicing patterns or variants will provide insight into chemotherapy resistance.

Collectively, these findings highlight the prevalence of alternative splicing deregulation in cancer. The number of studies revealing cancer-associated splicing patterns increases along with the demand for specificity in splicing modulators. Still, a better understanding of the diverse molecular processes dictating AS in a context-dependent manner is needed before any application to a clinical setting is feasible.

1.7.5. Alternative splicing in senescence

From a different angle, an essential step for cancer cells is to overcome tumour suppressor programs like cellular senescence. The splicing factor SRSF3 (or SRp20) inhibits AS of *TP53* into the p53β isoform, which promotes cellular senescence. SRSF3 is downregulated in senescent cells but overexpressed in cancers suggesting an AS mechanism is at play (Jia et al., 2010; Tang et al., 2012). AS of SRSF3 is itself regulated by PTBP1 and PTBP2-dependent repression of exon 4 resulting in a more stable variant, explaining the concomitant upregulation of all three proteins in oral squamous cell carcinoma (OSCC) cells (Guo et al., 2015). Besides SRSF3, the splicing factors SRSF6 (Cohen-Eliav et al., 2013; Jensen et al., 2014) and SRSF1 (or ASF/SF2) (Karni et al., 2007) also have oncogenic properties. SRSF1 overexpression in endothelial cell senescence is counterintuitive but contributes to the senescence phenotype by regulating AS of endoglin from L- to S-endoglin which was previously shown to alter the response of TGFBR1 and was proposed to mediate vascular remodelling associated with senescence (Blanco & Bernabeu, 2011, 2012; Blanco et al., 2008). Like other oncogenes, SRSF1 overexpression is a potent senescence

stimulus in normal fibroblasts (Fregoso et al., 2013). Analogous to the multiplicity of cancer-associated PTBP1 functions, SRSF1 might mediate its effects on senescence, in parallel or stead, via mechanisms other than AS (Fregoso et al., 2013). SRSF1 can sequester the p53-repressor MDM2 away from p53 thereby inducing p53-dependent senescence.

Since cancer progression requires bypass of senescence, it might involve circumventing AS necessary to cellular senescence. Alternatively, AS observed in cancer might be reminiscent of senescence. AS in senescence is not yet widely studied and existing research is still mostly correlative. Nevertheless, preliminary evidence suggests that exploring the spliceome of senescent cells will potentially contribute to our understanding of cancer biology and consequently to development of safer therapeutic approaches.

1.8. Aims and objectives

OIS presents a barrier to tumourigenesis. The pro-inflammatory SASP can however alter the tissue microenvironment with detrimental effects to the organism such as promoting cancer progression. Elucidating SASP regulation may provide insight not only into cancer therapeutics but also into treatment of other diseases with an inflammatory phenotype. Care must be taken to not interfere with the tumour-suppressive aspect of senescence including the growth arrest and anti-tumour immunity.

The aim of this project was to identify and characterise novel regulators of the senescent secretome. The approach was to initially screen for regulators of the SASP using RNA interference (RNAi) and next to explore the mechanistic role of identified genes in SASP regulation. Specifically, the aim was to isolate SASP regulators safe to target without the risk of re-entry into the cell cycle. Finally, by focusing on one candidate, PTBP1, the intention was to address in more detail the potential functional implication of targeting PTBP1 on senescence.

Chapter 2. Materials and Methods

2.1. Plasmid amplification and generation

2.1.1. Plasmids

pLNC ER:RAS retroviral vector was used to generate inducible RAS^{G12V} cells (herein referred to as ER:RAS) and LXSN retroviral vector was used as an empty vector control. pLNC ER:RAS and LXSN were extensively used in the Cell Proliferation group hence readily available. pGIPZ lentiviral shRNA mir-30-based vectors were obtained from the library held by the MRC CSC Genomic core facility laboratory. The LT3GEPIR Tet-ON all-in-one pRRL lentiviral vector was a gift from Dr. Johannes Zuber's laboratory, Vienna, Austria. The pLenti-CMV-tight inducible vector and the pLenti-CMV-rtTA3 (reverse tetracycline controlled transactivator) plasmid were purchased from Addgene. Dr. Andrew Innes, Cell Proliferation group, had previously introduced a MCS linker in place of the eGFP by cloning. For a complete list of plasmids with associated bacterial and mammalian antibiotic selectability and short hairpin sequences used see Table A1, Table A2 and Table A3.

2.1.2. Cloning: PCR, agarose gel electrophoresis, digestion and ligation

To sub-clone the mir-30 based shRNAs from pGIPZ constructs into the LT3GEPIR construct, the mir-30 backbone was first converted to a mir-E backbone by simple PCR amplification (Fellmann et al., 2013). The protocol was provided by Dr. Johannes Zuber's laboratory. In brief, the primers miRE-Xho-short-Fw and miRE-EcoPlasmid-Rev, pGIPz plasmid template, dNTP mix (10 mM, Bioline) and all contents of the Platinum® Pfx DNA polymerase kit (Invitrogen) were all mixed according to manufacturer's instructions. For details on PCR conditions and primer sequences see Table A4 and Table A5.

To clone PTBP1 in the linker of the iCMV-tight vector, first, full-length cDNA encoding PTBP1 (NM_002819.4) was PCR amplified from pBABE-PTBP1 vector custom-synthesised by GenScript. The primers were specifically designed to include the restriction sites BstB1 and PmeI.

The primers CMVptbp1F and CMVptbp1R, pBABE plasmid template and the Platinum® PCR SuperMix High Fidelity (Invitrogen) were all mixed according to manufacturer's instructions. For details on PCR conditions and primer sequences see Table A4 and Table A5.

The PCR product was mixed with DNA loading buffer (Orange G 0.2% (w/v) in 3% glycerol (v/v)) and along with an appropriate MW range DNA ladder (NEB) was loaded on a 2% agarose (w/v) gel containing 0.5 µg/mL ethidium bromide (Sigma). Samples were resolved by size based on their electrophoretic mobility at 100 V for 30-60 min in TAE buffer (40 mM Tris and 1 mM EDTA pH 8.0 in 0.1% HAc (v/v)). The DNA was then visualised by exposing the gel to a UV using the Molecular Imager® Gel Doc™ XR+ with Image Lab™ Software (Bio-Rad). The gel band of the desired size was excised using a clean scalpel and DNA extraction from agarose and purification was performed with the QIAquick® Gel Extraction kit (Qiagen) according to manufacturer's instructions. For shRNA cloning two modifications were added to the protocol. First, after adding isopropanol to the solubilised gel band, the sample was vortexed and left to stand for 5-10 min at room temperature before continuation to the next step. Second, DNA was eluted in 30 µl of EB after a 10 min on column incubation period.

For shRNA cloning, the purified PCR product was digested with EcoRI-HF and XhoI restriction enzymes (NEB) for 3-4 hours at 37 °C. For PTBP1 cloning, the purified PCR product was digested with BstB1 and Sbf1 HF restriction enzymes (NEB) at 37 °C for 1 hour followed by 65 °C for 1 hour, due to the differential optimal activity temperatures of the two enzymes. Following digestion, on-column purification of the PCR product was carried out with the QIAquick® PCR Purification kit (Qiagen) according to manufacturer's instructions. Again, for shRNA cloning, at the final step, DNA was eluted in 30 µl of distilled water after a 10 min on column incubation period. The concentration of the purified DNA digest was estimated using a NanoDrop® ND-1000 UV-Vis spectrophotometer at an absorbance of 260 nm (A_{260}). The purified digest was ligated with 'processed vector' at an insert:target molar ration of 3:1 for shRNAs and 5:1 for PTBP1 overnight at 16 °C using T4 DNA Ligase and provided buffer (NEB) according to manufacturer's protocol. The 'processed vector' is the acceptor plasmid digested in a similar manner to the corresponding insert but followed by direct de-phosphorylation with Antarctic Phosphatase and provided buffer

(NEB) according to manufacturer's guidelines for 1 hour at 37 °C. The reaction was directly on-column purified with the QIAquick® PCR Purification kit and DNA concentration measurement was carried out as before.

2.1.3. Bacterial transformation and plasmid DNA purification

Chemically competent *E. coli* DH5α™ or One shot® TOP10 (Invitrogen) cells were thawed on ice before addition of 100 ng of plasmid DNA or ligation reaction in 50 µl of cells respectively without mixing. The competent cell/DNA mixture was incubated on ice for 30 min followed by a heat shock at 42 °C for 1 min for DH5α™ or 30 s for TOP10. The mixture was placed back on ice for a further 2-5 min, then diluted in 200 µl of SOC medium or LB broth respectively and incubated for 1 hour at 37 °C with shaking at 500 rpm. For plasmid DNA/DH5α™ mix only 10 µl was used in the next step. The transformation mixtures were spread on appropriate antibiotic-containing LB Agar plates and cultured for 16-18 hours at 37 °C.

Single DH5α™ colonies were picked, inoculated in 30 ml or 250 ml of antibiotic-containing LB broth and grown for 18 hours at 37 °C with shaking at 220 rpm. Plasmid DNA was purified using the HiSpeed® Plasmid Midi or Maxi kit (Qiagen) as per manufacturer's instructions. Plasmid DNA was eluted in 200 µl or 1 ml distilled water.

Single TOP10 colonies were picked, inoculated in 4 ml of antibiotic-containing LB broth and grown for 18 hours at 37 °C with shaking at 220 rpm. Plasmid DNA was purified using the ZR Plasmid Miniprep™ Kit (Zymo Research).

2.1.4. Verification of plasmid DNA

Verification of plasmid DNA insert was carried out by Sanger sequencing in an automated ABI3730xl DNA analyser (Applied Biosystems). Each sequencing reaction contained 600 ng of plasmid DNA, 3.2 pmol of primer and distilled water to a final volume of 10 µl. The primers are listed in Table A5. DNA sequencing was performed by the MRC CSC Genomic core facility. The provided DNA chromatogram and corresponding letter sequence were visualised using SnapGene Viewer.

2.2. Tissue Culture

2.2.1. Cell line culturing and preservation methods

IMR90 human foetal lung fibroblasts, HEK293T packaging cells and T47D breast cancer cells were obtained from the American Type Culture Collection (ATCC). 5PT squamous cell carcinoma cells were a gift from Prof. Gareth Thomas Laboratory, Southampton, U.K., originally purchased from ATCC. All four cell types were maintained in Dulbecco's modified Eagle's Medium (DMEM) from Gibco and supplemented with 10% (v/v) Fetal Bovine Serum (FBS) (Sigma) and 1% 100x antibiotic-antimycotic solution (Gibco), hereafter referred to as 'complete media'. Detachment of adherent cultures from culture plates was achieved by treatment with trypsin (Gibco). The stock of inducible IMR90 ER:RAS cells was generated by retroviral infection of IMR90 cells with pLNC-ER:RAS, a vector expressing a constitutively active form of RAS (RAS^{G12V}) fused to the ligand binding domain of the oestrogen receptor. To activate the exogenous receptor and induce cellular senescence, IMR90 ER:RAS cells were treated with 100 nM 4-Hydroxytamoxifen (4OHT) (Sigma) reconstituted in DMSO 1 day after plating (Acosta et al., 2008).

Cell viability and cell number were determined by microcapillary flow cytometry using Guava ViaCount® reagent (Millipore), Guava EasyCyte™ (Millipore) and the attached software guavaSoft, enabling gating of only viable cells and excluding debris and dead cells from final concentration. For optimal cell measurements, a concentration of 200 to 500 particles per µl was obtained by appropriate dilution in ViaCount® reagent. For primary cell cultures, IMR90 and IMR90 ER:RAS, experiments were performed using cells strictly of passage 12 to 15.

The NK92 lymphoma natural killer cell line was a gift from Dr. Valery Krizhanovsky's laboratory, Rehovot, Israel, originally purchased from ATCC. NK92 cells were maintained in medium from 500 ml Minimum Essential Medium (MEM) Alpha (Gibco) supplemented with 65 ml FBS (Sigma), 65 ml Horse serum (Gibco), 5 ml Penicillin-streptomycin (Gibco), 0.6 ml Inositol (Acros Organics) 0.2 M filter sterilised, 0.6 ml Folic Acid (Sigma) 0.02 M prepared in 0.1 M $NaHCO_3$ and filter sterilised and 4.1 µl 2-Mercaptoethanol (Gibco). 0.2 µm pore size cellulose acetate membranes (Gilson) were used for filter sterilisation. For transwell migration assays, NK92 cells were cultured in medium from 500 ml Roswell Park Memorial Institute medium (RPMI) 1640

(Gibco), 2.75 ml FBS (Sigma), 5.5 ml Penicillin-streptomycin (Gibco), 5.5 ml L-Glutamine (Gibco), 5.5 ml Sodium Pyruvate (Gibco) and 5.5 ml MEM Non-Essential Amino Acids (Gibco).

For cryopreservation, IMR90, IMR90 ER:RAS, HEK293T and T47D cells were suspended in 10% DMSO whereas 5PT and NK92 were suspended in 50% DMSO. Cells at a concentration ranging from 1 to $4x10^6$ cells per CryoTube™ (Nunc) were cooled to -80 °C at a rate of 1 °C per min using the Nalgene® Mr Frosty container 5 days before being transferred to liquid nitrogen tanks for long-term storage. Thawing of cells was achieved by rapid warming in a 37 °C water bath, subsequent removal of DMSO by centrifugation and resuspension of cell pellet in appropriate culture media. Thawing was performed at least 48 hours prior to any experiments. All cell cultures were maintained in a humid incubator at 37 °C and 5% CO_2.

2.2.2. Retrovirus and lentivirus production and infection

HEK293T cells were used for virus packaging. The transfection mix for one expression plasmid contained 1 mL of DMEM, 20 µg of retroviral plasmid or 10 µg of lentiviral plasmid, 7.5 µg of gag-pol (Clontech) or psPax2 (Addgene) respectively, 2.5 µg of pVSV-G (Clontech) and 80 µL of linear 25 kDa linear polyethylenimine (PEI; 1 mg/ml (w/v), Polysciences). The mix was vortexed and left to stand for 30 min before being added drop-wise to each 10 cm plate of 80-90% confluent HEK293T cells. Transfection efficiency was assessed the next day by visual inspection of expression of fluorescent reporter genes using the Olympus CKX41 inverted fluorescence microscope. 24 hours after transfection the media of transduced cells were replaced with fresh media (6 mL per plate) and target IMR90 or IMR90 ER:RAS were seeded at 10^6 cells per 10 cm plate. The next day, viral supernatant was collected, filtered through 0.45 µm pore-sized acetate filters (VWR International) and added 4 µg/ml of polybrene.

For retroviral infection, the target IMR90 cells were incubated with 6 ml of virus titre 3 times for 4 hours with the final round being replaced with fresh complete medium. For single vector lentiviral infection, the viral supernatant was diluted in fresh medium 1:4 to minimise cytotoxicity and the target IMR90 ER:RAS cells were infected once with 6 ml for 4 hours before changing to normal culture media. For double vector lentiviral infection, i.e. iCMV-tight and rtTA, after a 1:4

dilution, the two virus titres were mixed at a 1:1 ratio and target IMR90 cells were treated only once with 12 ml for 4 hours. Three days after infection the cells were split. For an estimation of infection efficiency the percentage of cells positive for GFP or mCherry was measured by flow cell cytometry using Guava EasyCyte™ (Millipore). The cells infected with retrovirus were grown in neomycin for an extra 5-7 days in order to select against uninfected cells. The cells infected with lentivirus were grown in puromycin for 3-4 days or hygromycin for 5-7 days or in combination in order to select against uninfected cells. Antibiotic selection was judged to be successful when an uninfected control plate had died. For details on antibiotic providers and working concentration see Table A1.

2.3. Conditioned Media (CM)

2.3.1. CM generation and processing

0.6 or 1.2x10^6 IMR90 ER:RAS proliferating or IMR90 ER:RAS pre-senescent cells respectively were seeded in a 10 cm dish for each condition. The next day the media were replaced with fresh complete media supplemented with neomycin and puromycin at maintenance concentrations (half the selection concentration) and where appropriate, 4OHT. For paracrine senescence assays, the media were replaced 3 days later (3rd day) with DMEM (Gibco) supplemented with 0.5% (v/v) FBS (Sigma) and 1% 100x antibiotic-antimycotic solution (Gibco). 4 days later, ensuring each 10 cm dish contained confluent but alive cells, the CM were collected and initially centrifuged at 1000 rpm to remove cellular debris. The CM were then filtered through a 0.2 μm pore size cellulose acetate membrane (Gilson) into a new tube, aliquoted and stored at -20 °C short-term or -80 °C long-term. This media is referred to as 'CM' hereafter.

For proteomics analysis of the secretome (section 2.10.2.3) or for assaying the chemoattractant properties of the secretome (section 2.3.3), before replacement to appropriate media on the 3rd day, the cells were washed 3 times with pre-warmed PBS. After that, the cells were cultured for another 3 days in high glucose, no glutamine, no phenol red DMEM (Gibco) supplemented with L-Glutamine (Gibco), no FBS and where appropriate, 4OHT. On the 6th day, the conditioned media were collected and centrifuged at 2,500 rpm for 15 min at 4 °C to remove

cellular debris. The supernatant was then filtered through a 0.2 μm pore size cellulose acetate membrane (Gilson) into a new tube and then concentrated by ultracentrifugation using the Vivaspin 20 5kDa MWCO columns (GE Healthcare) about 100 times. At this point, the protein concentration was determined using the Pierce™ BCA Protein Assay Kit (Thermo Scientific) in a 96-well plate following manufacturer's guidelines. For accurate protein measurement a 4X dilution of the sample was required and each diluted sample was represented twice on the plate. The absorbance reading was taken at 562 nm (A_{595}) in a SpectraMAX340PC (Molecular Devices) microplate reader. Protein concentration was then estimated according to a calibration curve obtained from the absorbance values of the dilution series of the kit's standard protein control. The dilutions were freshly prepared in the appropriate culturing media. Following measurement, the samples were adjusted to equal concentrations using the appropriate culturing media with 1.625 μg/μl being the minimum concentration, snap frozen and stored in aliquots at -80 °C. Hereafter these samples are referred to as 'Concentrated CM'.

2.3.2. Induction of paracrine senescence

$2x10^3$ or $3x10^4$ IMR90 cells per well were seeded in 96-well plates or 6-well plates respectively. Two days later, the media were replaced with CM previously thawed and mixed with DMEM supplemented with 40% (v/v) FBS (Sigma) in a 3:1 ratio. For immunofluorescence analysis, the cells were fixed as per section 2.10.1. For SA-β-gal assay, the media was replaced 4 days later with fresh CM media adjusted to 10% (v/v) FBS as before and subsequently treated as per section 2.8.1.

2.3.3. NK cell assay

To assess the chemoattractant properties of the secretome, migration of NK92 cells was assayed according to Valery Krizhanovsky's laboratory protocol with adjustments. NK92 cells were starved for 4 hours in RPMI 1640 (Gibco) supplemented as previously described but lacking FBS. The Concentrated CM was diluted in FBS-containing RPMI 1640 to a final concentration of 162 ng/μl. 600 μl of that was added to the bottom chamber of a 6.5mm Transwell® apparatus with an 8.0 μm Pore Polycarbonate Membrane Insert (SLS). 200 μl containing $2.5x10^5$ NK92 cells were added to

the upper chamber. The cells in the Transwell® apparatus were incubated for 18 hours before the number of cells at the bottom chamber were counted like before for at least 1 min per sample.

2.4. Transfection of siRNA

siRNAs were purchased from Qiagen lyophilised either in a Flexitube® or spotted in Flexiplates®, i.e. predispensed in 96-well tissue culture plates ideal for high-throughput screening (HTS) experiments. Lyophilised siRNAs were reconstituted with RNAse-free water to a concentration of 1 μM. For HTS, in order to minimise manual handling and improve accuracy, the Flexiplate siRNA solutions were reconstituted using a 96-well multichannel (Liquidator™; Mettler Toledo) and further aliquoted to daughter 96-well plates using the Laboratory Automation Workstation Biomek® NX^P (Beckman Coulter). A list of siRNAs used is given in Table A6.

For immunofluorescence analysis, 1.5-2x10^3 IMR90 and IMR90 ER:RAS cells or 6x10^3 senescent IMR90 ER:RAS cells in suspension (100 μl) were reverse transfected with siRNAs on a well of a 96-well plate. The suspension media was DMEM supplemented with 10% FBS but not with antibiotic-antimycotic. The transfection mix for each sample well contained 0.1 μL DharmaFECT™ 1 (GE Healthcare), unless otherwise specified, in 17.5 μL plain DMEM mixed with 3.6 μL siRNA 30 min prior to cell seeding. 18 hours after transfection, allowing ample time for target cells to adhere, the media were replaced with fresh complete media, containing 4OHT only when appropriate. A fluorescent siRNA (siGLO, Thermo Scientific) was used to visualise transfection efficiency. Media was changed every 3 or 4 days and the cells were fixed at the specified time-point with 4% PFA (w/v) for 1 hour. For HTS, all steps were performed using the 96-well multichannel.

For mRNA analysis, 8x10^4 IMR90 and IMR90 ER:RAS cells or 2x10^5 senescent IMR90 ER:RAS cells in suspension (2 mL) were instead reverse transfected on a well of a 6-well plate. The procedure was identical but scaled up 20 times. The cells were harvested at the specified time-point by washing with PBS once, then scraping in 0.8 ml TRIzol® RNA isolation reagent (Ambion) per well followed by storage in -80 °C for future use.

2.5. AON design and transfection

Dr. Dave Wee Keng Boon, IHPC, Singapore, rationally designed AONs for exon skipping by using a computational algorithm accounting for 3 variables: 1) avoiding co-transcriptional secondary structures that would block AON binding accessibility, 2) including regions with ESE motifs that normally direct exon inclusion, areas ideal for masking, and 3) restricting target length to approximately 20nt hence enhancing binding specificity and thermodynamics (Pramono et al., 2012; Wee et al., 2008). All the designed AONs were synthesised by IDT as single-stranded 2'-*O*-methyl modified phosphorothioate oligoribonucleotides.

Forward transfection of AONs was carried out as per siRNA transfection with the only difference being the addition of transfection mix on adhered cultures plated 3 or 4 days in advance.

2.6. Chemical inhibitors

1.5-2x10^3 or 8x10^4 IMR90 ER:RAS cells were seeded in a well of a 96-well plate or a 6-well plate respectively. The following day, allowing ample time for target cells to adhere, the media were replaced with fresh complete media with 4OHT only when appropriate. For a 'standard' timeline, the media also contained the chemical compound at the indicated concentrations. For a 'post-senescence induction' timeline, the media containing the chemical compound was added 5 days after 4OHT induction. Drug-containing media was refreshed every 2 days by media change to prevent additive effects. For immunofluorescence analysis, the cells were fixed at the specified time-point with 4% PFA (w/v) for 1 hour. For HTS, all steps were performed using the 96-well multichannel. For mRNA analysis, 8x10^4 IMR90 ER:RAS cells were harvested at the specified time-point by washing with PBS once, then scraping in 0.8 ml TRIzol® RNA isolation reagent (Ambion) per well followed by storage in -80 °C for future use.

The chemical compounds were reconstituted in DMSO and stored as per manufacturer's guidelines. A list of compounds and suppliers is given in Table A7.

2.7. Growth assays

2.7.1. Colony formation assays

For colony formation assays, 10^4 or $1.5x10^4$ cells per well were seeded in 6-well dishes. Cell cultures were maintained for 10-14 days by replenishing with complete media, in the absence or presence of 4OHT, every 3-4 days. Upon colony formation or confluence, cells were fixed with 0.5% glutaraldehyde (w/v) (Sigma) in PBS for 1 hour. The plates were air dried before being simultaneously stained with 0.2% crystal violet (w/v) (Sigma) for 1 hour. Stained plates were imaged using an HP Scanjet4850 photo scanner. Crystal violet was quantified by extraction with 10% acetic acid (v/v) for 5-10 min followed by an absorbance reading at 595 nm (A_{595}) in a SpectraMAX340PC (Molecular Devices) microplate reader. Absorbance values were then normalised to a control (referred to as 'REF' in figures).

2.7.2. 5-Bromo-2'-deoxyuridine (BrdU) incorporation

$1.5x10^3$ or $2x10^3$ cells per well were seeded in 96-well plates in triplicate and allowed to adhere overnight. Cells were incubated with 10 μM 5-Bromo-2'-deoxyuridine (BrdU) 16-18 hours prior to the desired analysis time-point at which point cells were fixed with 4% PFA (w/v) for 1 hour. The fixative was removed by washing 3 times with PBS. For immunofluorescence initially the cells were permeabilised with 0.2% Triton® X-100 (v/v) (Sigma) in PBS for 10 min followed by 3 washes with PBS. To avoid non-specific antibody binding, the cells were incubated for 30 min with blocking solution containing 1% BSA (w/v) (Sigma) and 0.4% fish gelatin (v/v) (Sigma) in PBS. Next, cells were treated with mouse anti-BrdU and 0.5 U/μl DNAse (Sigma) in the presence of 1 mM $MgCl_2$ in blocking solution for 30 min. Cells were then washed 3 times with PBS before incubation with secondary antibody Alexa Fluor 594® goat anti-mouse suspended in blocking solution for 40 min. For antibody lists, suppliers and dilutions refer to Table A8. Following 2 washes with PBS, cells were incubated with 1 μg/ml DAPI (Sigma) for 20 min. After this final step, cells were washed at least 3 times with PBS. All incubations were performed with gentle agitation. Cells were stored in PBS at 4 °C for future analysis. The IN Cell Analyzer 2000 automated high-throughput fluorescent

microscope (GE Healthcare) and the IN Cell Investigator (attached software) was used for image acquisition and quantification of DAPI and BrdU positive cells as described in section 2.10.1.2.

2.8. Senescence-associated β-galactosidase assay (SA-β-gal)

2.8.1. Cytochemical method

$3x10^4$ IMR90 or IMR90 ER:RAS cells per well were plated in 6-well dishes, allowed to adhere overnight and treated with appropriate media. 9 days later, cells were fixed with 0.5% glutaraldehyde (w/v) (Sigma) in PBS for 10-15 min. Fixed cells were washed with 1 mM $MgCl_2$ in PBS (pH 6.0) 2-3 times and then incubated with X-Gal staining solution (1 mg/mL X-Gal, Thermo Scientific, 5 mM $K_3[Fe(CN)_6]$ and 5 mM $K_4[Fe(CN)_6]$) for 16-18 hours at 37 °C with gentle agitation. The cells were washed with distilled water and stored at 4 °C for future analysis. Bright field images of cells were taken using the DP20 digital camera attached to the Olympus CKX41 inverted light microscope. The percentage of SA-β-gal positive cells was estimated by counting at least 200 cells per replicate sample facilitated by the 'point picker' tool of ImageJ software.

2.8.2. Fluorescence method

$1.5x10^3$ or $2x10^3$ IMR90 ER:RAS cells per well were plated in 96-well dishes, allowed to adhere overnight and treated with complete media in the presence or absence of 4OHT. 9 days later, the cells were incubated with fresh complete medium containing 9*H*-(1,3-Dichloro-9,9-Dimethylacridin-2-One-7-yl) β-D-Galactopyranoside (DDAOG, Molecular Probes™) for 2 hours. The cells were then fixed with 4% PFA (w/v) for 10-15 min. The fixative was removed by washing 3 times with PBS. Cells were subsequently stained with 1 µg/ml DAPI (Sigma) for 10 min and washed at least 3 times with PBS. Fluorescence was imaged and quantified using the In Cell 2000 automated high-throughput fluorescent microscope (GE Healthcare) and the IN Cell Investigator (attached software) as described in section 2.10.1.2. The percentage of SA-β-gal positive cells was estimated by counting at least 1,000 cells per replicate sample.

2.9. RNA expression analysis

2.9.1. Total RNA extraction and purification

For total RNA extraction and processing, 0.8-2x10^5 cells were plated in 10 cm dishes or in a well of 6-well plates and cultured in the presence or absence of 4OHT for the specified duration. On collection day, the cells were washed with PBS, scraped off in the presence of 0.8 ml TRIzol® RNA isolation reagent (Ambion) per sample plate or well, vortexed and frozen at -80 °C to facilitate homogenisation of the lysate. Once thawed, 150 µl of Chloroform (Sigma) were added and samples were vortexed for 15 s and centrifuged at 15,000 rpm at 4 °C for a minimum of 30 min. After the phase separation step, the top clear RNA-containing phase was transferred to a new tube carefully without disrupting the DNA-containing interphase. Total RNA was then purified using the RNAeasy® Mini Kit (Qiagen) from step 2 onwards according to manufacturer's protocol. At the final step, the RNA was eluted in 30-40 µl of RNAse-free water and the concentration was measured using a NanoDrop® ND-1000 UV-Vis spectrophotometer at an absorbance of 260 nm (A_{260}). For measurement of expression of specific genes, the appropriate amount was transferred to a fresh PCR tube for cDNA synthesis to be performed on the same day. The remaining RNA was stored at -80 °C.

2.9.2. Large-scale gene expression profiling of 12 samples

Prior to library preparation for deep sequencing, the purity and integrity of RNA samples was assessed using the Agilent 2100 Bioanalyser and Agilent RNA 6000 Nano Kit following manufacturer's instructions. The attached 2100 Expert Software provided a bioanalyzer trace. A satisfactory RNA quality was assumed only when the trace included two peaks corresponding to the 18S and 28S rRNA, with a ratio of approximately 1:2, and an RNA Integrity Number (RIN) of approximately 10, with 8 being minimum acceptable (Figure 2.1).

cDNA library preparation and Next-Generation Sequencing (NGS) of RNA (RNA-seq) was performed by the MRC CSC Core Genomic facility. In brief, a cDNA library from 12 samples was prepared using the TruSeq Stranded mRNA LT Sample Prep kit (Illumina) following manufacturer's protocol (LS). The cDNA library was then hybridised to the flowcell of the Illumina HiSeq® 2500

and sequenced. The library was run on 3 separate lanes in order to achieve good coverage depth of approximately $12x10^7$ reads per sample. The sequencing data were processed by the instrument's attached Real Time Analysis (RTA) software application, version 1.17.21.3. Reads were then generated, de-multiplexed by sample of origin according to index and aligned to human genome hg19 with CASAVA 1.8.2. Data processing with R packages was performed by Thomas Carroll and Gopuraja Dharmalingham, MRC CSC Computing and Bioinformatics facility.

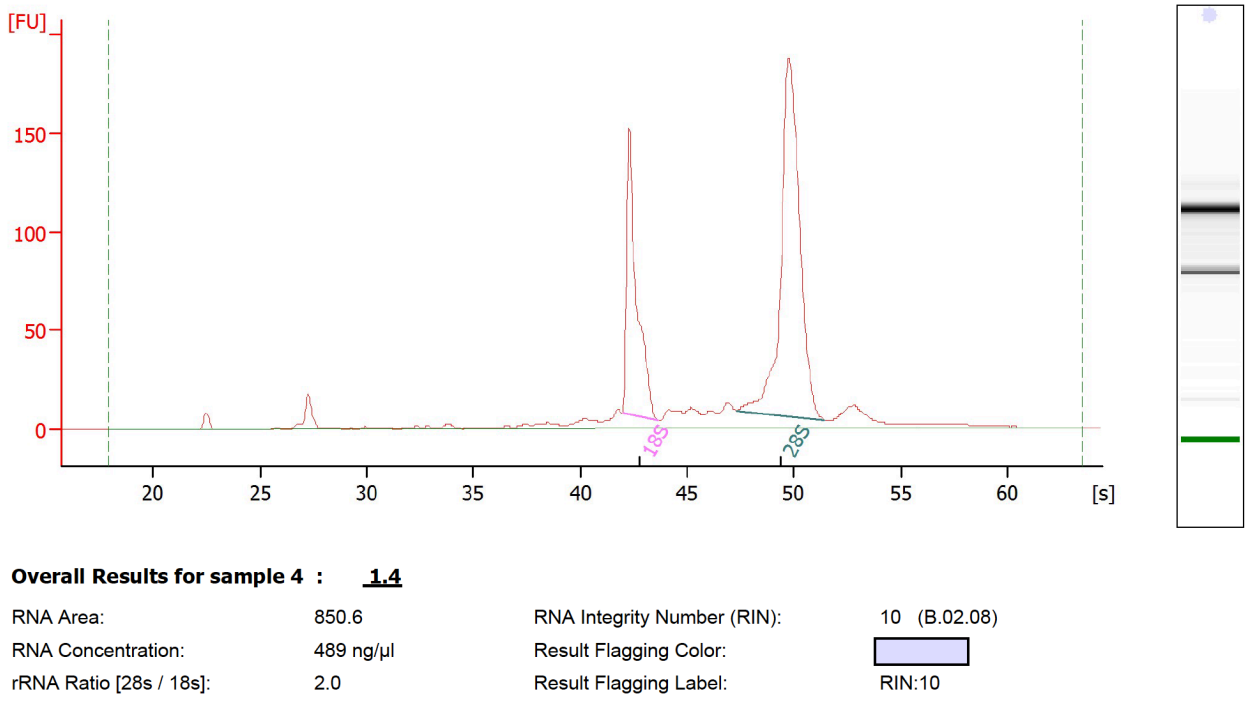

Figure 2.1. Bioanalyzer trace of purified RNA in preparation for RNA-seq.
A representative example of good quality RNA with a profile of two peaks of rRNA at a ratio of 2 and a RIN of 10.

2.9.3. Complementary DNA (cDNA) synthesis

1-5 µg of RNA (consistent amount throughout samples per experiment) was mixed with 1 µl of 50 ng/µl Random Primers (Invitrogen), 1 µl of 10 mM dNTP mix (10 mM, Bioline) and RNAse-free water to a final volume of 11 µl. The mix was heated at 65 °C for 5 min and quickly brought down to 4 °C. cDNA generation was carried out using the SuperScript® II Reverse Transcriptase (RT) kit (Invitrogen). In detail, 4 µl of 5X First-Strand buffer, 2 µl of 0.1 M DTT and 1 µl of 200 U/µl of SuperScript® II RT were added to the mix and subjected to the following conditions: 10 min at 25 °C, 50 min at 42 °C and 15 min at 70 °C on a Dyad® Peltier Thermal cycler (Bio-Rad). For

subsequent quantitative RT-PCR, the samples were then diluted to 10 ng/µl (according to the initial RNA concentration) and stored at -20 °C. For subsequent alternative splicing analysis, the samples were diluted to 50 ng/µl (according to the initial RNA concentration) and stored at -20 °C.

2.9.4. Quantitative RT-PCR (RT-qPCR)

RT-qPCR reactions were performed using the CFX96™ Real-Time PCR Detection system (Bio-Rad). 5 µl of cDNA was mixed with 4 µl of distilled water, 0.5 µl of each primer (10 µM) and 10 µl of SYBR® Green PCR Master Mix (Applied Biosystems) in a well of a Hard-Shell® PCR 96-well plate with thin-wall white wells (Bio-Rad). Each RT-qPCR reaction for each sample was duplicated in side-by-side wells. The plate was then loaded on the C1000™ Thermal Cycler (Bio-Rad) and applied the following cycling conditions: 2 min at 52 °C (step 1), 5 min at 95 °C (step 2), 30 s at 95 °C (step 3), 30 s at 60 °C (step 4), 15 s at 72 °C (step 5), after which fluorescence was read and step 3-5 was repeated 39 more times. To calculate gene expression ('relative mRNA levels') the ΔΔCT method was applied to the resulting CT (Cycle Threshold) values of the exponential amplification phase. For this method, the CT values of Ribosomal protein S14 (RPS14) were used as the normaliser, and the untreated sample, usually denoted 'REF', as relative control. Specifically, relative mRNA levels = $2^{-\Delta\Delta CT}$, where $\Delta\Delta CT = \Delta CT_{treated} - \Delta CT_{REF}$ and $\Delta CT = CT_{target\ gene} - CT_{RPS14}$.

The primers were designed using PrimerBank or Primer-BLAST to span exon-exon junctions, or to flank an intron of > 1 kb in size, to anneal to all transcript variants of a the gene of interest, and to generate a PCR product of no more than 150 bp. For a list of RT-qPCR primers used refer to Table A9.

2.9.5. Alternative Splicing analysis

Global alternative splicing analysis was done by Thomas Carroll, MRC CSC Computing and Bioinformatics facility. Briefly, Multivariate Analysis of Transcript Splicing (MATS) on R was employed to catalogue the 5 common AS events (Figure 1.5) changing across different sample groups. The source-code is freely available at http://rnaseq-mats.sourceforge.net. This method first assigns an AS type to each expressed sequence. Second, it calculates the exon inclusion level

which is also called 'percent spliced in' or Ψ (Figure 2.2). Third, the output is the exon inclusion level difference between the means of paired replicates of a sample and a reference sample (ΔPSI). Finally, a likelihood-ratio statistical test is applied to identify the events with an exon inclusion level difference between two samples larger than a user-defined cut-off, in our case 20% splicing change. Hence, the null and alternative hypothesis is user-defined and the MATS output is the significance of an AS event rather than a list of transcripts that are alternatively spliced (Liu, et al, 2014).

To validate alternative splicing of a specific transcript by PCR, the primers were specifically designed to anneal to flanking exons of the alternatively spliced exon. cDNA, primers and Platinum® PCR SuperMix High Fidelity (Invitrogen) were all mixed at concentrations according to manufacturer's instructions. For details on PCR conditions and primer sequences see Table A4 and Table A5. The PCR product was then size-resolved using Agilent 2100 Bioanalyzer and Agilent High Sensitivity DNA Analysis Kit following manufacturer's instructions and the bands were visualised using the 2100 Expert Software. In any given sample, PSI was calculated by the given concentration of the larger product (included exon) relative to the sum of concentrations of both products.

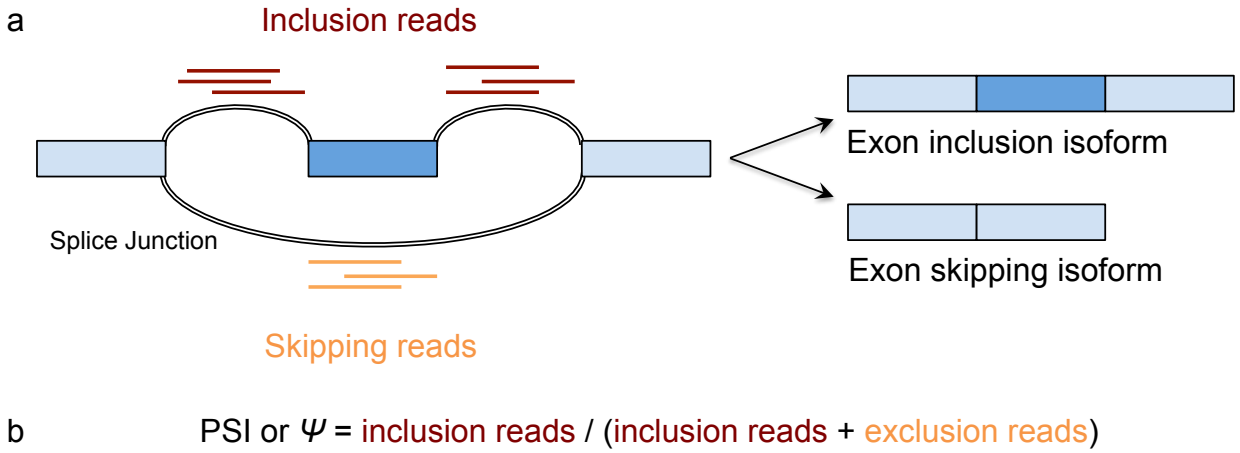

Figure 2.2. Schematic diagram of the exon inclusion level estimation.
a. Exon skipping is used as an example to illustrate alignment of reads on splice junctions to be used for AS analysis. **b**. Calculation of exon inclusion level.

2.9.6. Large-scale gene expression profiling of 272 samples

For analysis of the transcriptome of more than 12 samples pooled into one library, a different extraction and library preparation method was adopted. The method is called Smart-seq2 (Figure 2.3) and was originally designed to perform RNA-seq from single cells taking into account the need for efficient amplification of the limited starting RNA material. This method additionally takes into account the large number of samples needed if the heterogeneity within a cell population is to be inferred. However, this technique is not restricted to single cell analysis. The 96-well plate format consequently lends itself for preparation of large numbers of samples for RNA-seq in other experimental settings.

siRNA transfection of $2x10^3$ cells per well onto 96-well plates was done as per section 2.4 with sole difference at the time-point of analysis the cells were washed 3 times with ice-cold PBS and stored at -80 °C. On the first day of cDNA library preparation, the cells of each well were lysed with 50 µl of lysis buffer containing 2 U/µl recombinant rRNasin® ribonuclease inhibitor (Promega) and 0.2% Triton® X-100 (v/v) in Nuclease-Free Water (Ambion). 2 µl of lysate from each well were transferred into a new Hard-Shell® PCR 96-well plate with thin-wall clear wells (Bio-Rad). Each sample was mixed with 0.1 µl of 100 µM Oligo-dTV30, 1 µl of 10mM dNTP mix (Bioline) and 0.9 µl of Nuclease-Free Water (Ambion) to a final volume of 4 µl. After that, the very detailed procedure of Smart-seq2 provided by (Picelli et al., 2014) was exactly followed from step 6 to 33. The only adaptation lying in the PCR preamplification, step 12, whereby 2 µl of first-strand reaction was used instead of 10 with the remaining volume adjusted with Nuclease-free water and the number of PCR cycles chosen was 10. For indexing of several samples before pooling (step 32), the Nextera XT Index Kit for 96 Indexes (FC-131-1002) was used which allows for 384 different combinations of dual indexing. After Nextera PCR, step 33, 2 µl of each sample were pooled in one tube. The final PCR purification was performed according to 'Using C1 to Generate Single-Cell cDNA Libraries for mRNA Sequencing Protocol' (PN 100-7168) following all the steps of the section 'Pool and Clean Up the Library' onwards. The quality check of the cDNA library and concentration measurement was performed according to Picelli et al. (2014).

A 50-bp single-end sequencing of the library was performed by the MRC CSC Genomic core facility on an Illumina HiSeq® 2500. The sample was run on 4 lanes ensuring a coverage depth of $2.5x10^6$ reads per sample in over 80% of the samples; coverage fairly adequate for total and SASP gene expression analysis (Figure 2.4). The sequencing data were processed by the instrument's attached Real Time Analysis (RTA) software application, version 1.17.21.3. Reads were then generated, de-multiplexed by sample of origin according to index combination and aligned to human genome hg19 with CASAVA 1.8.2. Hierarchical clustering of samples and GO analysis of arising clusters was done by Thomas Carroll, MRC CSC Computing and Bioinformatics facility.

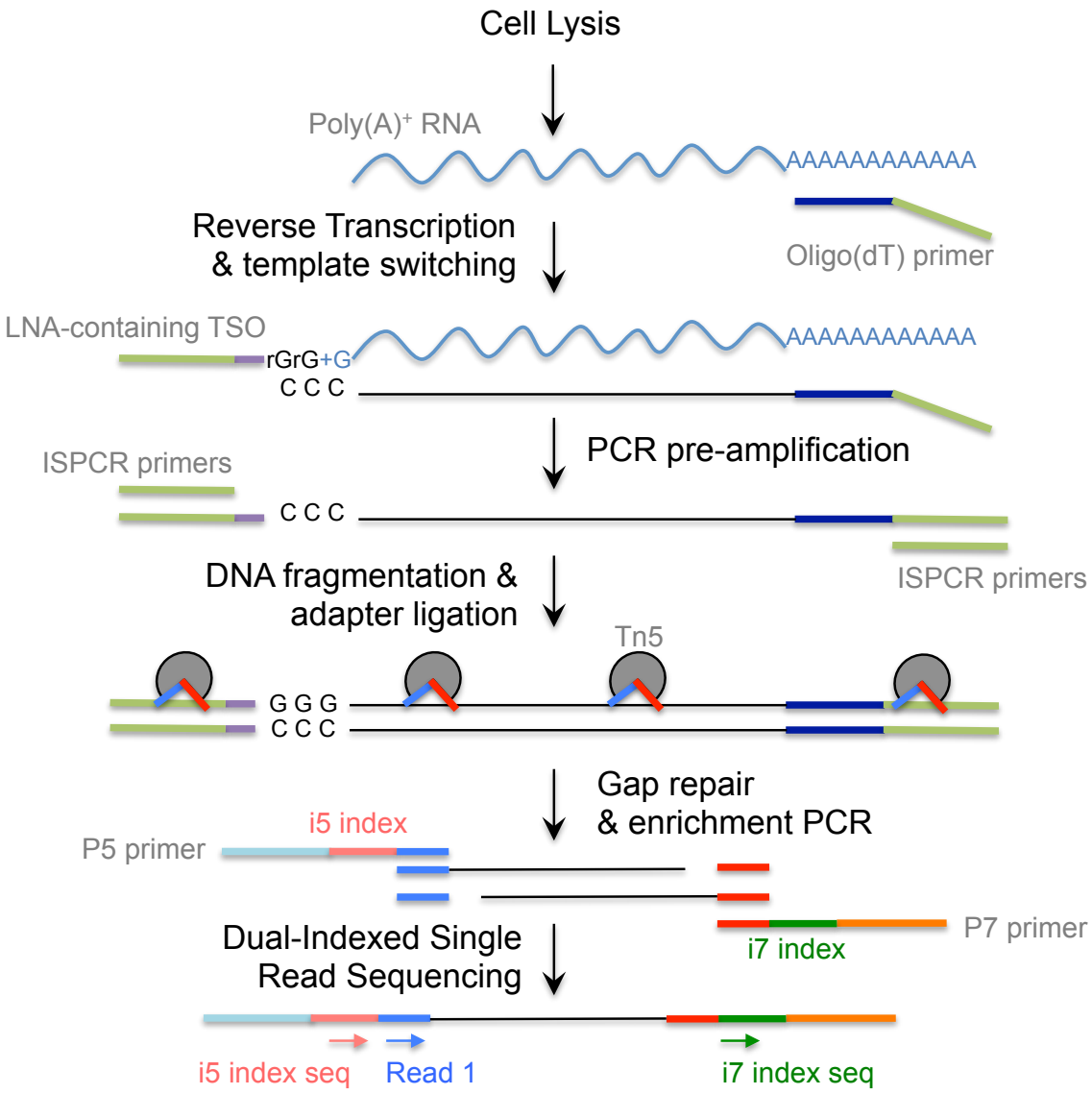

Figure 2.3. Outline of Smart-seq2 protocol.
Following cell lysis and priming of the RT reaction with oligo-dT oligonucleotides, RT takes place coupled to introduction of an artificial sequence to the 5' end of every cDNA transcript aided by a reaction called 'template switching'. Template-switching oligos (TSOs) are stretches of oligonucleotides that carry the artificial sequence but also riboguanosines that anneal to the extra 2-5 nucleotide 3' overhang of the cDNA produced by the RT enzyme. In smart-seq2, the TSOs contain a locked nucleic acid (LNA) at the final base of their 3' end (light blue), which binds strongly to the untemplated 3' end of the cDNA. The LNA-containing TSO can now serve as the new template and the RT enzyme can continue to transcribe into the additional sequence. This sequence (light green) is identical to the sequence introduced at the 3' end with the oligo(dT) primer. Hence, the subsequent PCR pre-amplification step needs a single primer. For deep-sequencing library construction, the average size required is 300-800bp. Fragmentation of the amplified cDNA is carried out using a hyperactive derivative of the transposase Tn5. Use of Tn5 allows simultaneous ligation of additional oligonucleotides flanking each fragment, which are complementary to part of the indexing primers of the next step. In the final step, the gaps are repaired simultaneous to enrichment PCR, which serves not only to amplify the product but also to index each sample with a combination of two unique 6 bp sequences (indices) followed by the deep-sequencing adapters. After pooling the barcoded samples, dual-indexed single read sequencing can be performed. (Adapted from Picelli et al., 2014).

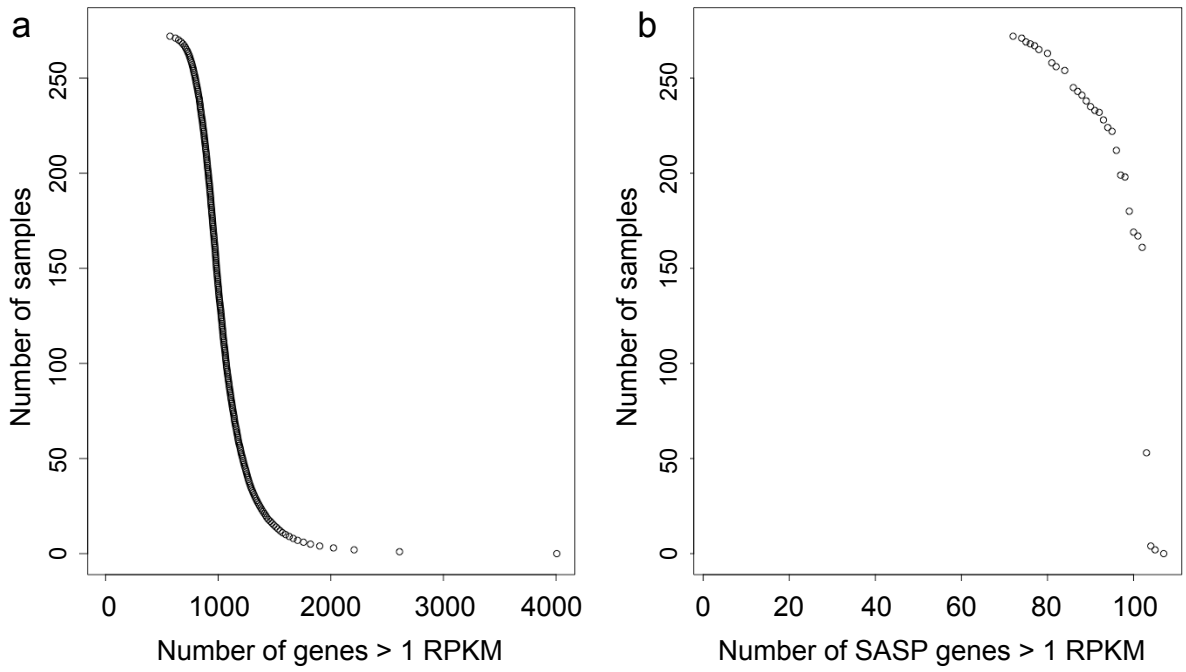

Figure 2.4. Number of genes detected from RNA-seq of a pool of 272 samples.
Plots showing the minimum number of samples in which the indicated number of genes was detected (a) throughout the human genome or (b) within a previously defined SASP gene list (Acosta et al., 2013). The read counts were normalised to Read per Kilobase per Million mapped reads (RPKM) to account for gene length and sequencing depth of each sample.

2.10. Protein expression analysis

2.10.1. Quantitative Immunofluorescence (IF)

2.10.1.1. Staining

$1.5x10^3$ or $2x10^3$ cells per well were seeded in 96-well plates in triplicate and allowed to adhere overnight. The cells were then grown in complete media in the presence or absence of 4OHT. At the desired analysis time-point cells were fixed with 4% PFA (w/v) for 1 hour. The fixative was removed by washing 3 times with PBS. For immunofluorescence initially the cells were permeabilised with 0.2% Triton® X-100 (v/v) (Sigma) in PBS for 10 min followed by 3 washes with PBS. To avoid non-specific antibody binding, the cells were incubated for 30 min with blocking solution containing 1% BSA (w/v) (Sigma) and 0.4% fish gelatin (v/v) (Sigma) in PBS. Next, cells were treated with primary antibody diluted in blocking solution for 40 min. Cells were then washed 3 times with PBS before incubation with secondary antibody Alexa Fluor® 488 and/or 594 suspended in blocking solution for 40 min. For antibody lists, suppliers and dilutions used refer to Table A8. Following 2 washes with PBS, cells were incubated with 1 µg/ml DAPI (Sigma) for 10 min. After this final step, cells were washed at least 3 times with PBS. All incubations were performed with gentle agitation. Cells were stored in PBS at 4 °C for future analysis.

2.10.1.2. High Content Analysis (HCA) coupled to High-Throuput Microscopy (HTM)

IF imaging was carried out using the automated high-throughput fluorescent microscope IN Cell Analyzer 2000 (GE Healthcare) with a 20x objective with the exception of DNA damage foci analysis which required a 40x objective. Fluorescent images were acquired for each of the fluorophores as required using built-in wavelength settings ('DAPI' for DAPI, 'FITC' for AlexaFluor® 488 FITC, 'Texas Red' for AlexaFluor® 594 and 'Cy5' for DDAOG). Multiple fields within a well were acquired in order to include a minimum of 1,000 cells per sample-well. For HTS, multiple 96-well plates were sequentially loaded on the microscope platform and removed after each complete acquisition by an automatic plate loader composed of the KiNEDx™ Robotic Arm (PAA) and the attached software application Overlord™ (PAA).

HCA of the images were processed using the IN Cell Investigator 2.7.3 software (Figure 2.5). DAPI served as a nuclear mask hence allowed for segmentation of cells with a Top-Hat method. To detect cytoplasmic staining, a collar of 7-9 μm around DAPI was applied. Nuclear IF in the reference wavelength, i.e. all the other wavelengths apart from DAPI, was quantitated as an average of pixel intensity (grey scale) within the specified nuclear area. Cytoplasmic IF in the reference wavelength was quantitated as a coefficient of variance (CV) of the pixel intensities within the collar area. Nuclear foci IF in the reference wavelength was quantified as *n* number of foci per nucleus or else per cell. A threshold for positive cells was assigned above the average intensity of unstained or negative control sample (Figure 2.5) unless otherwise specified.

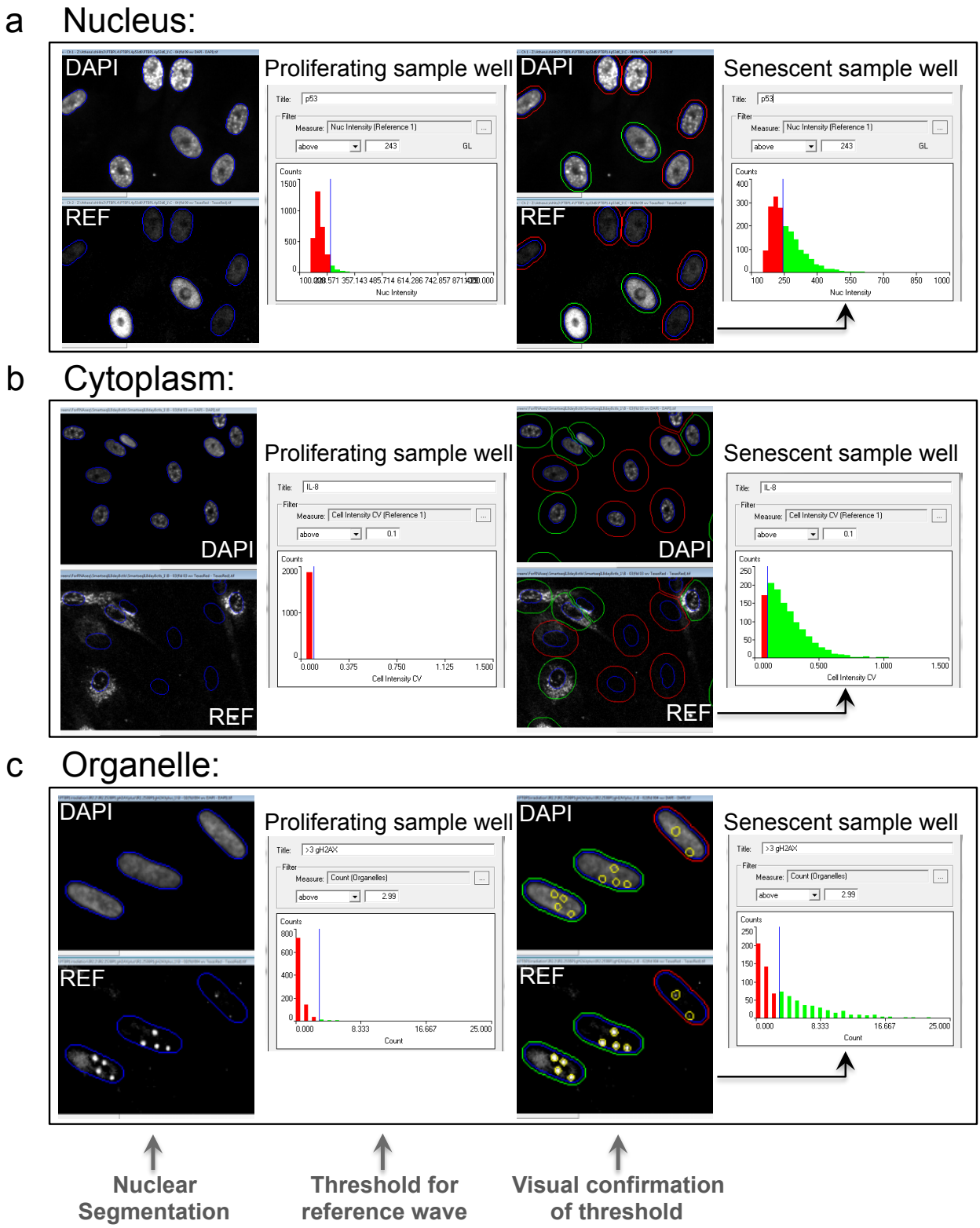

Figure 2.5. High Content Analysis with In Cell Investigator 2.7.3.
Cell segmentation is based on the DAPI wavelength. The analysis of the marker of interest is customised depending on localisation and pattern visualised in the reference (REF) wavelength. The staining is (a) nuclear or (b) cytoplasmic or (c) presents nuclear foci. To distinguish between cells with high expression levels (green) from those with low (red), a threshold is placed on the following measures: (a) mean nuclear intensity levels, (b) cell intensity CV or (c) number of discrete foci per cell. The threshold is based on the frequency distribution (histograms) of the specified measure in a control sample that exemplifies background levels.

2.10.2. Immunoblot

2.10.2.1. Cell lysis and protein extraction

2-3x10^5 cells were seeded in 10 cm dishes and allowed to adhere overnight. The cells were then grown in complete media in the presence or absence of 4OHT. At the desired analysis time-point cells were first washed in ice-cold PBS, then scraped off and pelleted by centrifugation at 1000 rpm for 5 min. To achieve whole cell lysis, the cell pellets were resuspended in RIPA buffer (80 mM Tris pH 8.0, 150 mM NaCl, 1% Triton® X-100, 0.5% Na-Doc, 0.1% SDS, 1mM EDTA) supplemented with 1 tablet of phosphatase and 1 tablet of protease inhibitors (Roche) per 10 ml RIPA. Lysis was performed on ice for 20 min with occasional vortexing or on a rotating wheel at 4 °C, followed by very brief sonication in Vibra-Cell™ (Sonics) when necessary for proper homogenisation. The samples were then centrifuged at 15,000 rpm at 4 °C for 10 min and the protein-containing supernatant was harvested while the DNA-containing pellet discarded. Quantification of protein content was carried out using the *DC*™ Protein Assay (Bio-Rad) in a 96-well plate following manufacturer's guidelines. Usually the samples were diluted 2X for accurate protein measurement and each diluted sample was represented twice on the plate. The absorbance reading was taken at 595 nm (A_{595}) in a SpectraMAX340PC (Molecular Devices) microplate reader. Protein concentration was then estimated according to a calibration curve obtained from the absorbance values of the dilution series of a standard protein control (containing BSA). The dilutions were freshly prepared in the same lysis buffer each time. The samples were adjusted to equal concentrations using RIPA buffer and diluted in 5X Laemmli Sample Buffer. To prepare 10 ml of 5X Laemmli Sample buffer the following were mixed: 875 µl of 1 M Tris-HCl pH 6.8, 4.5 ml Glycerol, 2.5 ml of 20% SDS, 125 µl of 1% Bromophenol Blue, 1.250 ml β-mercaptoethanol and distilled water. Laemmli containing protein samples were then heated at 95 °C for 5 min before storage at -20 °C for future use.

2.10.2.2. SDS-PAGE and Western Blot

The adjusted protein samples were thawed and heated at 95 °C for 5 min before being loaded along with a Precision Plus Protein™ Standards ladder (Bio-Rad) on a precast Mini-PROTEAN®

TGX™ Gel (Bio-Rad). The proteins were separated by size by electrophoresis in Tris-Glycine buffer (25 mM Tris, 192 mM Glycine, 0.1% SDS (w/v)) at 100 V until the control ladder showed appropriate band separation. The proteins were then transferred from the SDS-PAGE gel onto a 0.2 µm Nitrocellulose Membrane (Bio-Rad) at 100 V for 1 hour in Transfer buffer (25 mM Tris, 192 mM Glycine, 20% methanol). Prior to blocking and blotting of the membrane, efficient protein transfer was confirmed visually by staining with Ponceau S (Sigma) for 10 s and washed with distilled water twice briefly. Blocking of the membrane to prevent unspecific binding was done in 5% skim milk (w/v) (Sigma) diluted in PBS-T (0.1% Tween® 20 (v/v) (Sigma) in PBS) for 1 hour with gentle agitation. The membrane was then incubated (overnight) at 4 °C with primary antibody diluted in blocking solution containing either 5% milk (w/v) (Sigma) or 5% BSA (w/v) (Sigma) in PBS-T according to manufacturer's instructions. The following day the membrane was washed 3 times for 5 min with PBS-T followed by incubation for 1 hour with Horseradish Peroxidase (HRP)-conjugated secondary antibody diluted in blocking solution. For a list of antibodies, suppliers and dilutions used refer to Table A8. The membrane was then washed 3 times with PBS-T before being probed with an Amersham™ Enhanced Chemiluminescence (ECL™) Western Blotting Detection reagent (GE Healthcare). Detection of ECL was carried out using an automatic film processor (Photon Imaging Systems) after exposure of the membrane to a chemiluminescence film Amersham Hyperfilm™ ECL (GE Healthcare).

2.10.2.3. Mass Spectrometry

Mass spectrometry of the Concentrated CM was performed by Peter Faull and Alex Montoya, MRC CSC Proteomics core facility, as previously described by Herranz et al., 2015 (under 'Secretome characterisation'). Raw files were analysed by the facility using Maxquant version 1.5.3.8. Protein sequences were reversed to provide a decoy database that enabled a protein and peptide false discovery rate of 1%. Protein quantification information was produced using the label-free quantification ('LFQ') algorithm to enable direct comparison of protein intensity between samples. The clustering analysis was carried out by Gopuraja Dharmalingham, MRC CSC Computing and Bioinformatics facility.

2.10.2.4. Enzyme-linked immunosorbent assay (ELISA)

To detect and quantify substances in the Concentrated CM, Quantikine® ELISAs (R&D Systems) were used following the manufacturer's instructions. The samples were diluted 1,000X and each diluted sample was represented twice on the plate. The absorbance reading was taken at 450 nm (A_{595}) in a SpectraMAX340PC (Molecular Devices) microplate reader. Protein concentration was then estimated according to a calibration curve obtained from the absorbance values of a dilution series of the supplied standard protein control.

Chapter 3. Screening for regulators of the SASP

3.1. Introduction

Robust cellular models recapitulating senescence *in vitro* have been exploited for the identification of important senescence-associated molecular pathways. An established technique for verifying the function of a gene in senescence has been the experimental depletion of the gene resulting in bypass of the growth arrest. In this manner, loss-of-function screens in senescence models have been used to discover new regulators of OIS (Acosta et al., 2008; Bishop et al., 2010; Ewald et al., 2009; Herranz et al., 2015; Lahtela et al., 2013). The results of these screens have greatly expanded our knowledge of senescence effectors and pathways.

The primary aim of this project was to identify novel regulators of the senescence secretome. Here, a large-scale siRNA library served as the platform for finding new pathways regulating the SASP in a cellular model of OIS.

3.2. A cellular model to study OIS

To study OIS our group utilises the established inducible IMR90 ER:RAS system (Acosta et al., 2013). The H-*Ras*^{G12V} had previously been fused to a mutant form of the ligand-binding domain of the oestrogen receptor (ER) (Tarutani et al., 2003). Ectopic expression of the mutant *Ras* gene is hence responsive to 4-hydroxytamoxifen (4OHT) but not endogenous oestrogen. Here, IMR90 primary fetal lung fibroblasts were stably infected with the pLNC-ER:RAS and pLXSN retroviral vectors to produce IMR90 ER:RAS and vector cells. IMR90 ER:RAS cells treated with 4OHT show a characteristic senescence phenotype. Specifically, they display a change in cell morphology with an enlarged cytoplasm (Figure 3.1a) and growth arrest as evaluated by colony formation assays and a decreased percentage of cells incorporating BrdU compared to untreated cells (Figure 3.1b and c). These cells exhibit upregulation of the tumour suppressors p16^{Ink4a}, p21^{Cip1} and p53 and elicit a DNA damage response (Figure 3.1c). Ultimately, 4OHT-treated IMR90 ER:RAS cells present a substantial increase in the levels of the SASP factors IL-8 and IL-6 (Figure 3.1d) in

addition to high SA-β-gal activity (Figure 3.1e). The assessment of a combination of such senescence-associated markers is required for reliable identification and characterisation of senescent cells. This is achieved rapidly, in a highly quantitative and qualitative manner, using the In Cell Analyzer high throughput microscopy (HTM) and subsequent high content analysis (HCA) (described in Chapter 2). Thus, the IMR90 ER:RAS model recapitulates OIS and coupled to high throughput techniques lends itself to the study of senescence and the SASP.

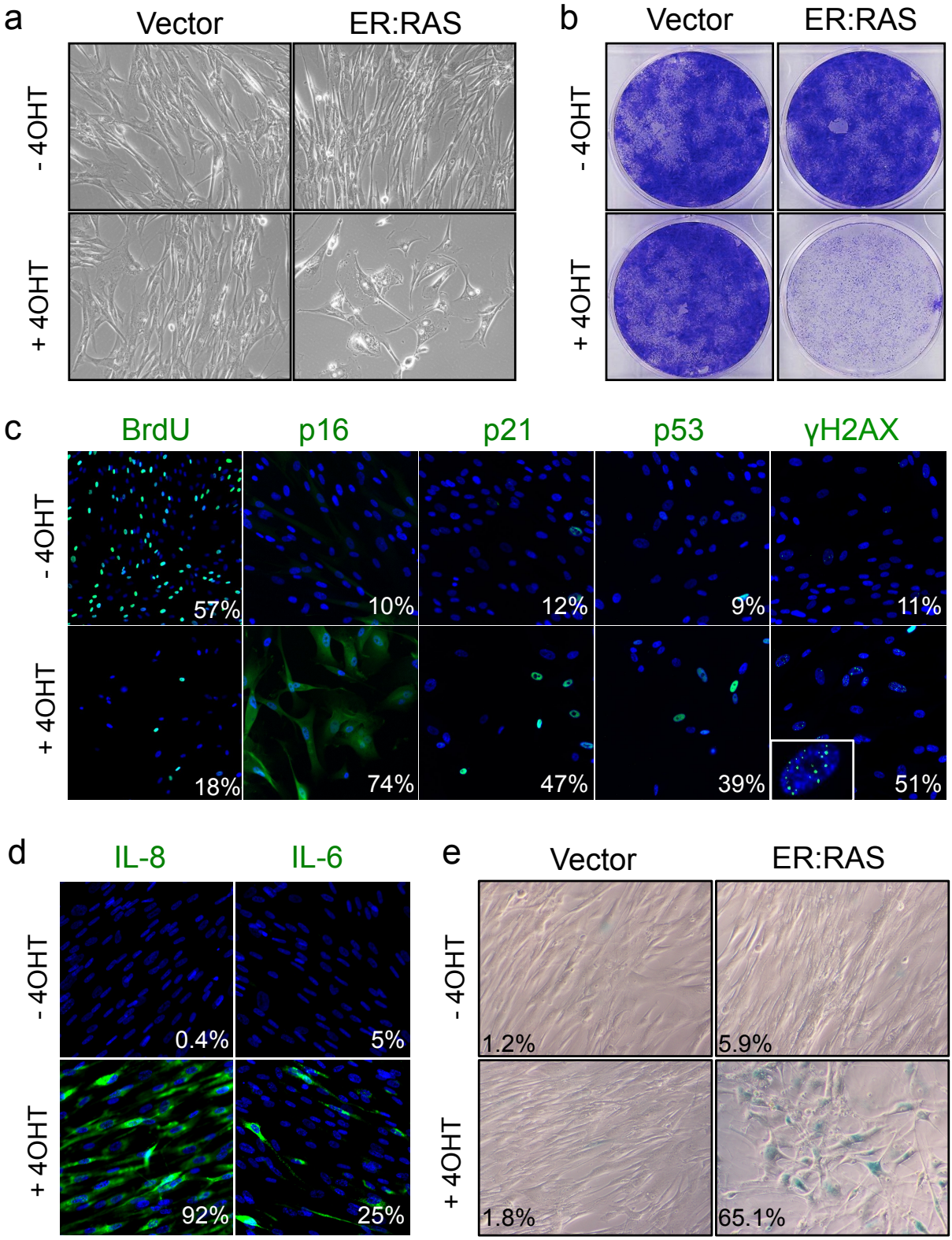

Figure 3.1. Induction of senescence upon conditional expression of oncogenic RAS.
(a) Bright field microphotographs showing the effect of oncogenic RAS activation on the cell morphology of IMR90 cells. (b) Crystal-violet stained plates of cells infected with the indicated vectors and fixed 14 days following 4OHT treatment. (c and d) Percentage of cells staining positive for the indicated senescence markers 6 and 8 days after 4OHT respectively. Representative images that were used for quantification of IF are shown. (e) SA-β-gal staining of cells fixed 8 days following 4OHT. The numbers are mean values of three replicate wells of a representative experiment of OIS.

3.3. Set-up of the siRNA screen for SASP regulators in IMR90 ER:RAS cells

Our group holds libraries of siRNAs targeting the Human Druggable Genome, Kinases, Phosphatases and G-protein coupled receptors (GPCRs) (Qiagen). The siRNAs are arranged in 96-well plates; a format that lends itself to HCA by the available automated HTM system. The aim was to use these siRNA library subsets to identify novel regulators of the SASP in the highly controlled IMR90 ER:RAS inducible model of OIS.

Prior to conducting a screen, the appropriate readouts must be determined and assay conditions must be optimised. Previous members of the group have shown that senescent cells produce a plethora of secreted factors as part of the SASP (Acosta et al., 2013). Hence, we tested antibodies for IF detection of various secreted proteins (Figure 3.2a and b), in order to identify the most appropriate readouts. IL-8 and IL-6 were chosen on the basis of the specificity of the antibodies and equally importantly based on their induction levels compared to untreated or vector cells. The expression of IL-8 and IL-6 was temporally upregulated as expected from a self-amplifying stimulus (Figure 3.2c).

Next, the transfection conditions were optimised by transfecting the cells with control siRNAs targeting the senescence effectors p16 and p53 with different transfection reagents at different concentrations. 0.1μL of DharmaFECT™ 1 resulted in the highest level of knockdown of the targets compared to mock (water) or scramble transfected cells undergoing OIS (Figure 3.3a and b). To identify positive controls for a SASP screen, i.e. siRNAs preventing induction of the SASP, the cells were transfected with a customised siRNA 96-well plate (Qiagen) including multiple siRNAs per gene targeting 17 genes shown to be involved in SASP regulation in published reports or the group's unpublished data. The production of IL-8 and IL-6 after 4OHT induction of OIS was assessed by quantitative IF at time-points corresponding to an expected increase in comparison to untreated IMR90 ER:RAS cells (Figure 3.2c). We grouped the siRNAs consistently resulting in lower percentage of IL-8 and IL-6 positive cells in at least two of the three time-points in relation to the scramble transfected cells (Figure 3.3c). This information has allowed us to select siRNAs against three genes as positive controls for our screening; namely p65 (a subunit of NF-κB), C/EBPβ and p38 or else MAPK14. The three candidate siRNAs were able to knockdown their

corresponding targets and to reduce the levels of other SASP components in addition to the two readouts, although not all at the same extent (Figure 3.4). This finding suggests by using this screening method it is feasible to identify factors whose regulatory activity is not just restricted to IL-8 and IL-6, but also to other SASP components.

The use of appropriate positive controls serves to further optimise the screening conditions Although siRNA-mediated reduction of the positive controls was sustained until 6 days post-induction of senescence (Figure 3.4a), siRNAs offer only a transient experimental means to a knockdown. However, 6 days post-induction of senescence was not optimal to detect the SASP by IF in IMR90 ER:RAS cells (Figure 3.2c). The levels of SASP in siRNA scramble transfected cells were heterogeneous at 7 days post-induction (Figure 3.3c). On the other hand, 8 days post-induction of senescence resulted in stable IL-8 and IL-6 levels that were consistently lower in the positive control siRNA transfected cells in comparison to 10 days post-induction (Figure 3.5a and b). Finally, taking a closer look into the single-cell intensity values of this time-point led to reassessment of the quantification method (Figure 3.5c). The percentage used to quantitate the IF of senescence markers is the result of a cut-off that excludes background or noise intensity (described in chapter 2). Nevertheless, this method does not fully account for differences in the distribution of intensities per sample. By changing the threshold and grouping the cells that express high levels of IL-6 and IL-8, better differences between positive and scramble controls were obtained (Figure 3.5c), therefore providing a higher dynamic range for the screen. Consequently, detection of siRNAs reinforcing IL-8 and IL-6 expression was made possible with the example of siRNA targeting p16 (Figure 3.5c). The revised quantification method was used for further analyses of IL-8 hereafter.

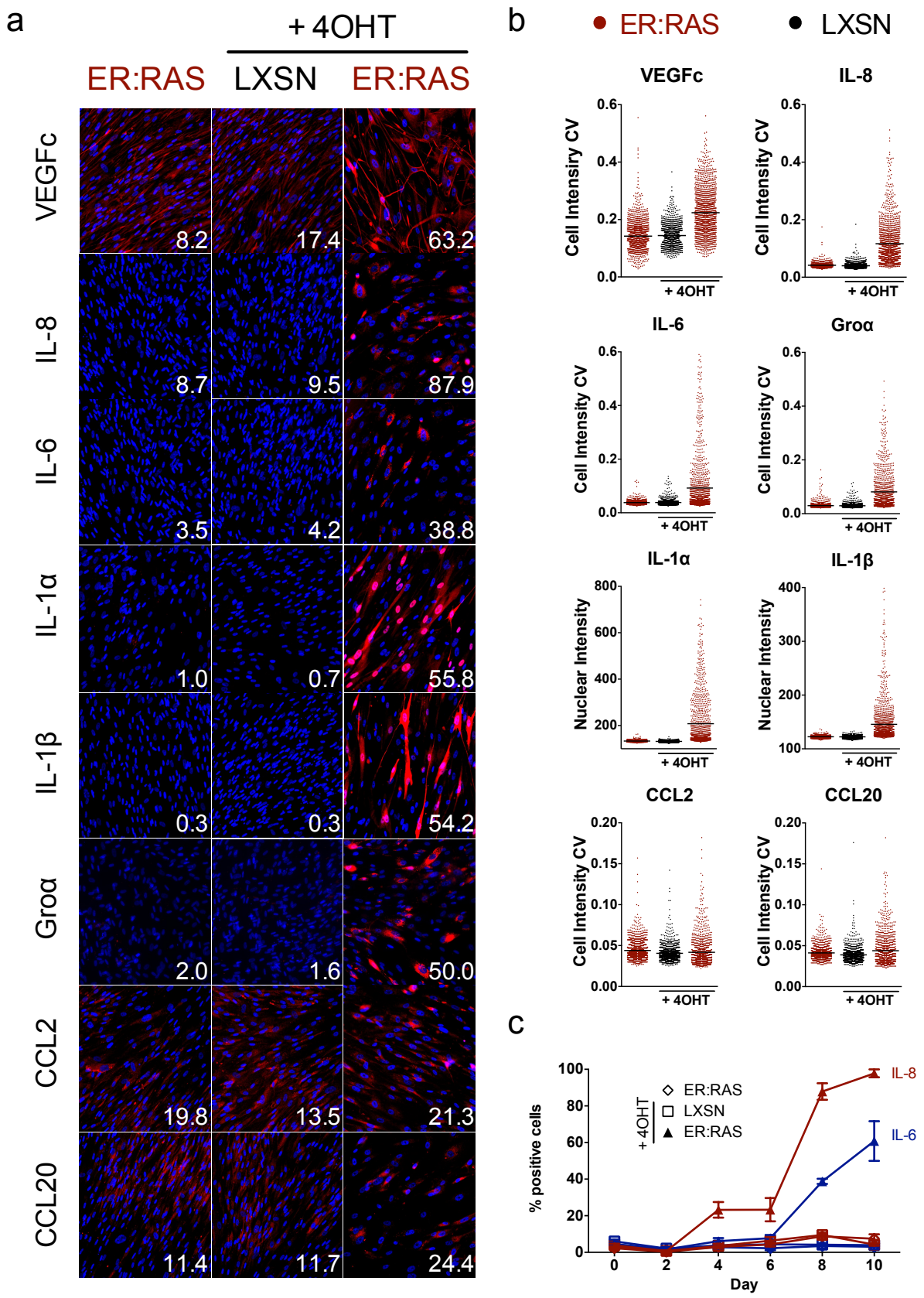

Figure 3.2. IL-8 and IL-6 are appropriate readouts for a SASP screen based on IF.
IL-8, Gro-alpha and IL-6 antibodies show specific cytoplasmic localisation and higher induction after 4OHT treatment in comparison to other antibodies. To avoid any expected overlap in mode of regulation, Gro-alpha was discarded as an option since its gene located on the same locus as IL-8. (a) Representative IF images

of the indicated SASP markers (red staining) co-stained with DAPI (blue staining) in IMR90 vector or IMR90 ER:RAS cells treated with 4OHT for 8 days. Percentage of cells positive for the indicated marker for each sample is given at the bottom right of each image and is a mean of three replicate wells of a single experiment. (b) Distribution of single cell intensities of each marker within each sample from (a). (c) IL-8 and IL-6 levels increase in a temporal fashion as measured by quantitative IF. Day 0 = day of induction. Time-course shows mean values with SD from three replicate wells of a single experiment.

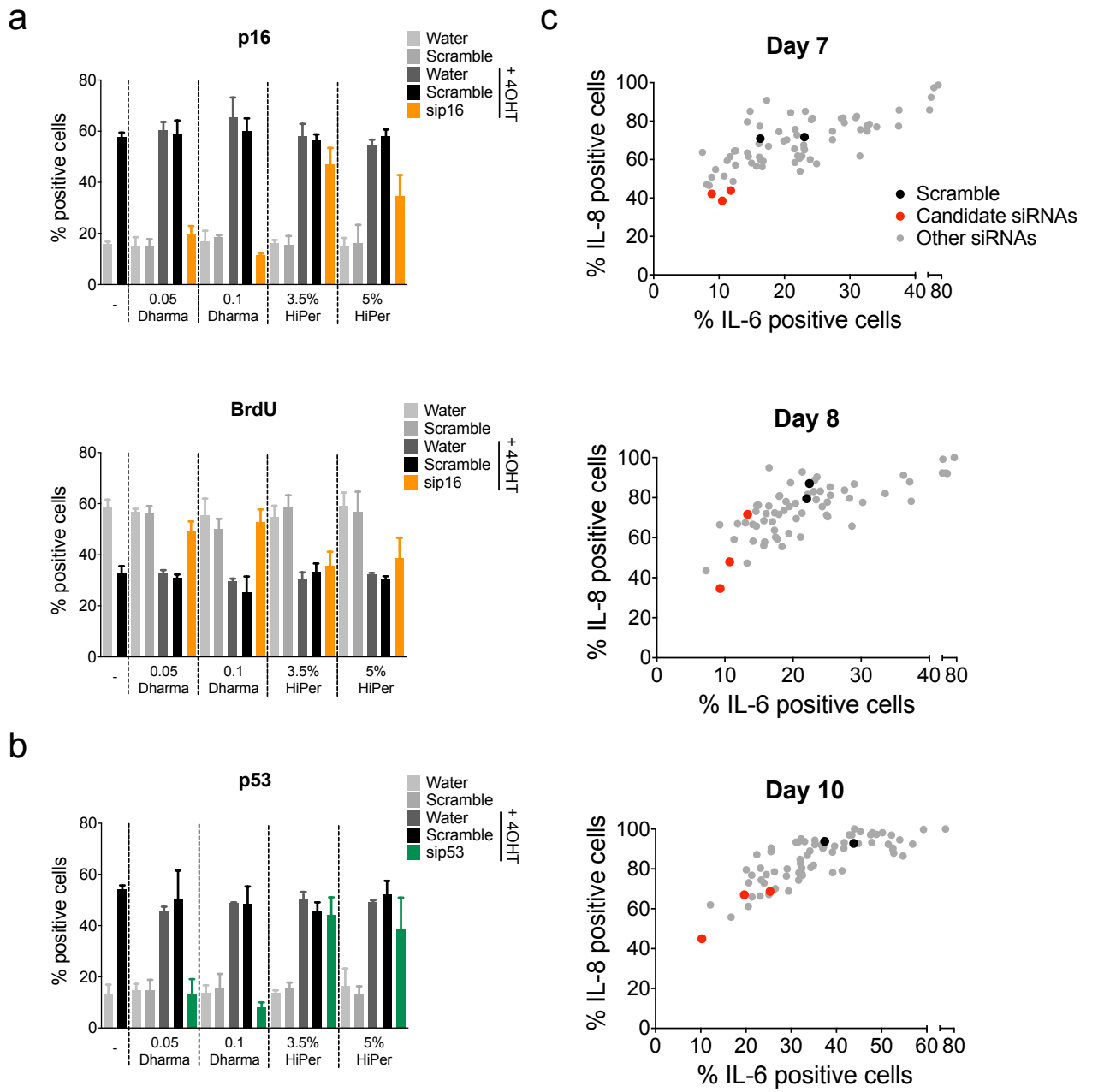

Figure 3.3. Optimising siRNA transfection and identifying positive controls.
(a and b) IMR90 ER:RAS cells were transfected with water, scramble siRNA or an siRNA targeting p16 or p53 respectively. The transfection mix contained the indicated µl of DharmaFECT™ 1 (GE Healthcare) or percentage (v/v) of HiPerfect (Qiagen) in the transfection mix for each well of a 96-well plate. The indicated samples were induced the next day with 4OHT. (a) The knockdown of p16 and growth rescue over scramble samples were detected 4 days post-senescence induction by quantitative IF of p16 and BrdU respectively. (b) The knockdown of p53 was confirmed 6 days post-senescence induction by quantitative IF of p53. (c) IMR90 ER:RAS cells were reverse transfected on a custom-designed siRNA plate, induced with 4OHT the

next day and fixed at the indicated time-points. The two screen readouts were quantified and plotted against each other to show candidate control siRNAs that consistently resulted in lower levels of both IL-8 and IL-6. For (a) and (b) the bars are mean values with SD from three experiments. For (c) each dot is the mean of two experiments performed simultaneously.

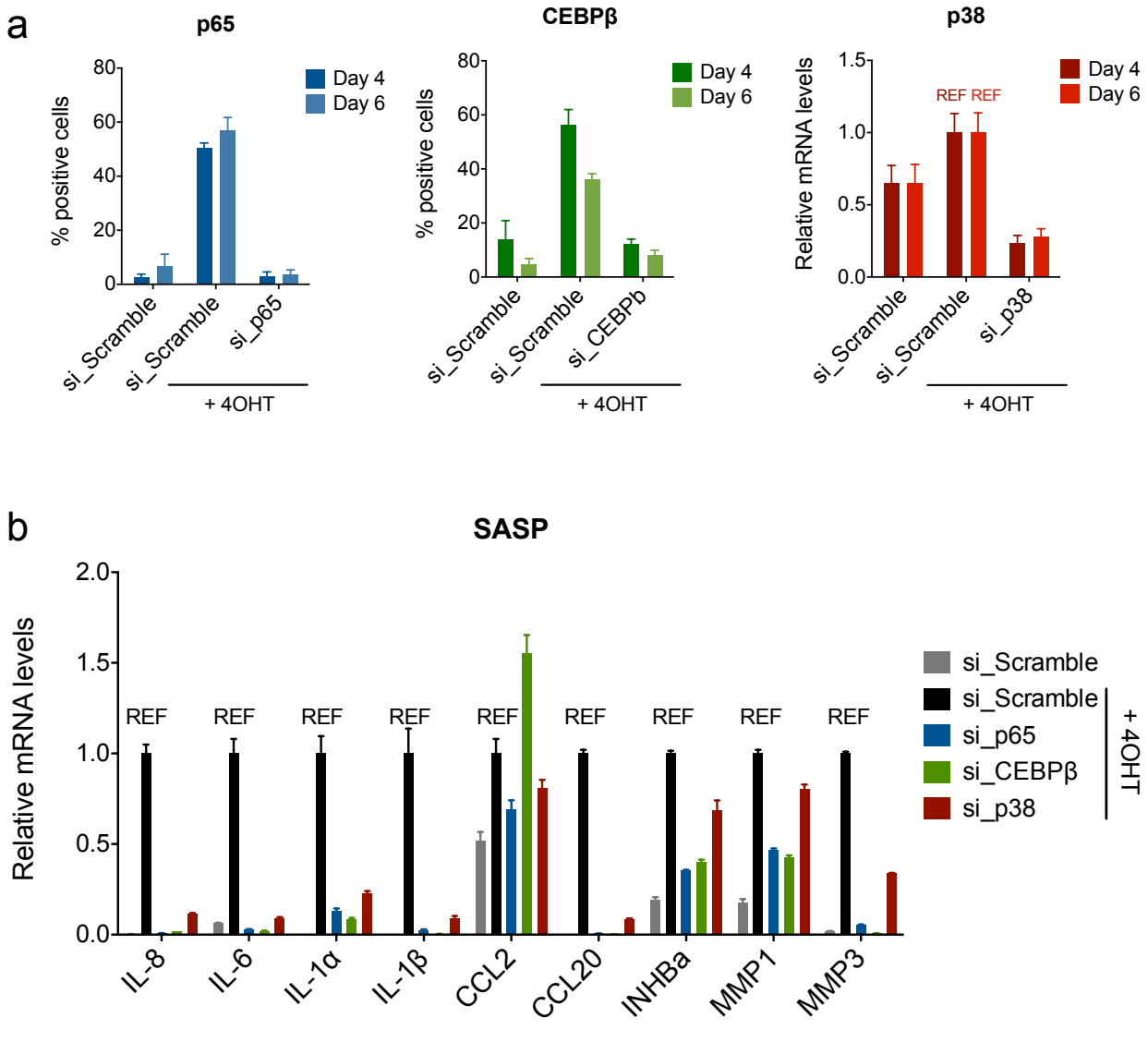

Figure 3.4. Ablation of p65, CEBPβ and p38 impairs SASP gene transcription.
IMR90 ER:RAS cells were transfected with scramble siRNA and siRNAs targeting p65 (RELA), C/EBPβ and p38 (MAPK14). (a) The knockdown of the respective targets was confirmed 4 and 6 days post-senescence induction by quantitative IF or RT-qPCR. (b) Transcription of the indicated SASP genes was impaired, albeit heterogeneously, as assessed 5 days post-senescence induction by RT-qPCR. Bars represent mean values with SD of three experiments performed simultaneously.

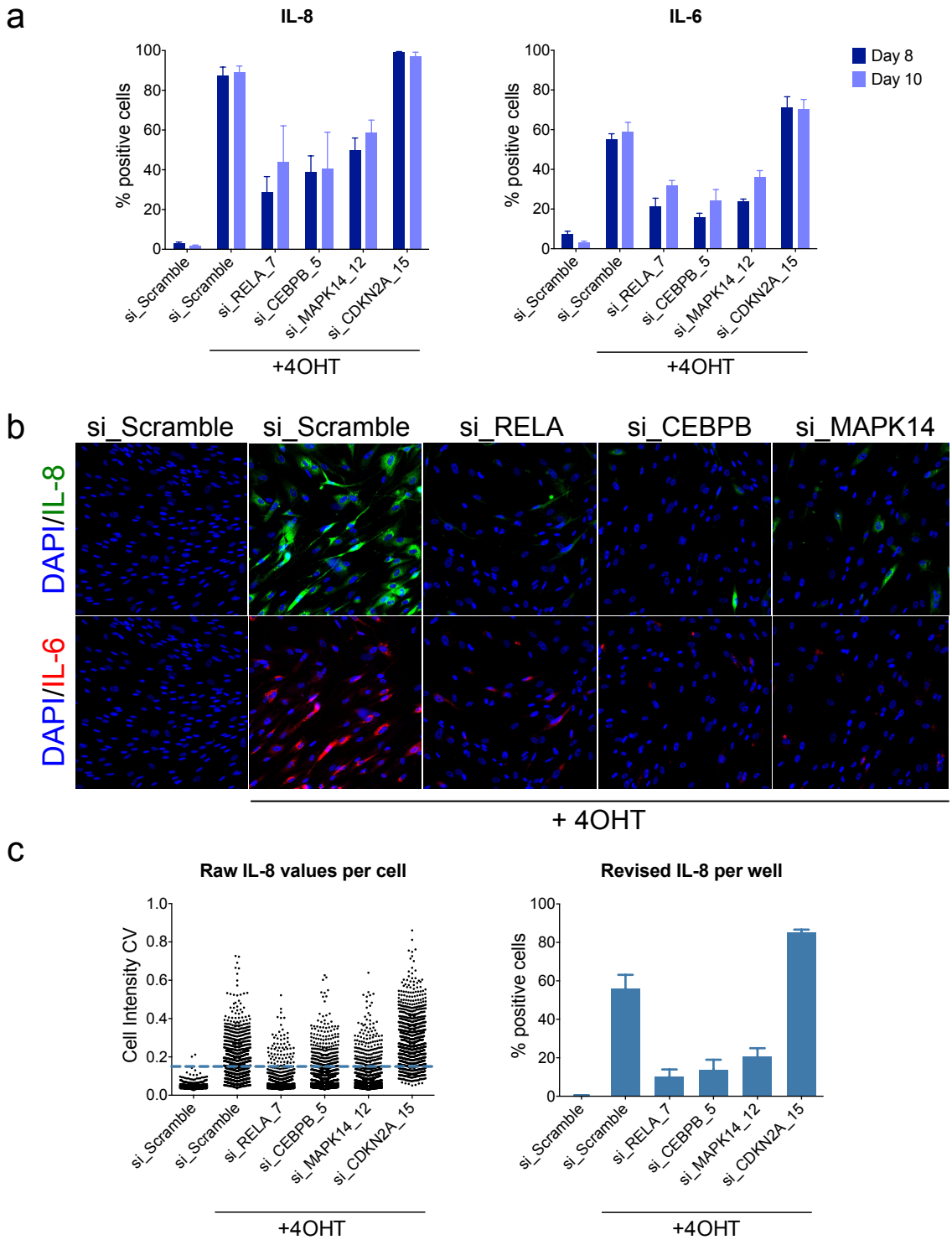

Figure 3.5. siRNA mediated knockdown of senescence regulators alters IL-8 and IL-6 IF levels providing the basis for a SASP screen.

(a) IL-8 and IL-6-positive cells, 8, or 10 days post-induction of senescence in cells transfected with scramble or control siRNAs. The siRNA targeting p16 (CDKN2A) was also tested which resulted in a slight increase in IL-6 levels. Bars represent mean values with SD of three experiments performed simultaneously. (b) Representative IF images of the indicated SASP markers showing loss of signal intensity with knockdown of SASP regulators. (c) Left panel shows single-cell intensity values of IL-8, 8 days post-induction of senescence. Blue line denotes new cut-off for quantification resulting in the revised IL-8 percentage shown in the right panel. The decrease in IL-8 with positive controls and increase with si_CDKN2A were pronounced after readjustment of the threshold.

3.4. A large-scale siRNA screen identified novel SASP regulators

Having set-up the screening conditions, a large-scale siRNA screen was then carried out to identify novel SASP regulators (Figure 3.6). The available siRNA libraries contained a pool of 2 siRNAs per gene spotted in each well of a 96-well plate. The outermost columns of wells were free of samples allowing space for the addition of external negative (scramble) and positive (siRNAs targeting p65, C/EBPβ, p38 or p16) controls. To better monitor positional effects, a variety of scramble negative controls were used and were spotted with positive controls alternately. A 96-well plate format high-throughput screen can suffer from unintended differences originating from intra- and inter-plate variability. The initial readout of the screen was the percentages of cells positive for IL-6 staining and high IL-8 staining. However, to accurately identify siRNAs preventing SASP induction, a plate normalisation method was applied. Each sample was normalised in relation to the rest of the samples within the same 96-well plate. Specifically, each sample in each plate was assigned a B-score (described in Malo et al, 2006), which allows for data normalisation avoiding confounding variables across plates for example those arising from lengthy staining procedures (Figure 3.7a and b). By taking into account the offset of the column and row in which each sample is located the B-score also reduces within-plate positional-related bias for example corrects for an artefact termed ‘plate-edge effect’. High-Throughput Screening (HTS) is subject to adversities in procedural efficiency due to the high load of manual handling. To minimise random error further, each siRNA sample was screened under the same experimental conditions three times.

To verify successful normalisation, the independent B-scores from all samples from all plates were combined resulting in a normal distribution (Figure 3.7c). In such a normal distribution the majority of the samples including external and internal scramble controls lied along the midpoint. On the other hand, samples with high or low SASP cluster at the respective tails as did the external positive controls. To further evaluate the quality of the analysis method, potential upstream transcriptional regulators (TRs) were searched for using the Ingenuity Pathway Analysis (IPA®) portal. Indeed, certain genes whose siRNAs showed low IL-8 B-score directly correlated to inhibition of known SASP TRs such as NF-κB and IL-1, but also of other inflammation-related

upstream regulators such as lipopolysaccharide and TNFalpha (Figure 3.8a and b). Equally, drug-induced inhibition of PI3K an activator of the SASP enhancer mTOR, or activation of EZH2, a subunit of the SASP epigenetic repressor PRC2, are associated with genes belonging to the low IL-8 B-score set (Figure 3.8a).

The unbiased identification of biological functions relevant to SASP regulation ensured validity of the screening and analysis method hence allowed for progression to hit shortlisting. To select the strong candidate SASP regulators, and to minimise the chance of selecting false-positives, we applied a cut-off farther than the intersection point of negative and positive controls. In particular, the cut-off was the B-score equal to 2 SD above or below the mean B-score of negative (scramble) controls to select siRNA pools reinforcing (si_Reinforcers) or repressing (si_Repressors) the SASP respectively (Figure 3.9a). As an informal probability rule, only the samples that scored at least 2 out of 3 replicates were shortlisted. The hits were further grouped into those represented in both IL-8 and IL-6 shortlists (Figure 3.9) with a final of 96 SASP-reinforcing siRNAs and 125 SASP-repressing siRNAs.

Prior to undertaking any further characterisation of candidate SASP regulators, as is customary, a secondary siRNA screen for the repressors was performed to rule out any hits selected due to siRNA off-target effects. To this end, the original siRNA pool was deconvoluted in addition to two separate siRNAs making a total of 4 siRNAs per gene that were screened for SASP induction with similar settings to the primary screen. Despite the deliberate exclusion of outermost plate wells to prevent positional effects, the plate-to-plate variability must still be taken into consideration. The B-score was however not a suitable plate normalisation method since it assumes that most compounds are inactive not the case for a biased secondary screen. Therefore, a control-based method was employed namely normalised percent inhibition (NPI) in which each sample is normalised in relation to positive and negative controls within the plate under investigation. Phenotype confirmation was accepted when an siRNA sample with a mean of three NPI replicate values was significantly lower than an arbitrary threshold in both screen readouts. To ensure siRNA target specificity only the genes represented by more than 2 siRNAs were carried forward. Overall, in spite of the absence of an error rate probability-based statistical model for the

hit identification process of the primary screen, 67.2% of the genes whose knockdown reduced SASP levels were independently verified by a distinct scoring system in a secondary screen.

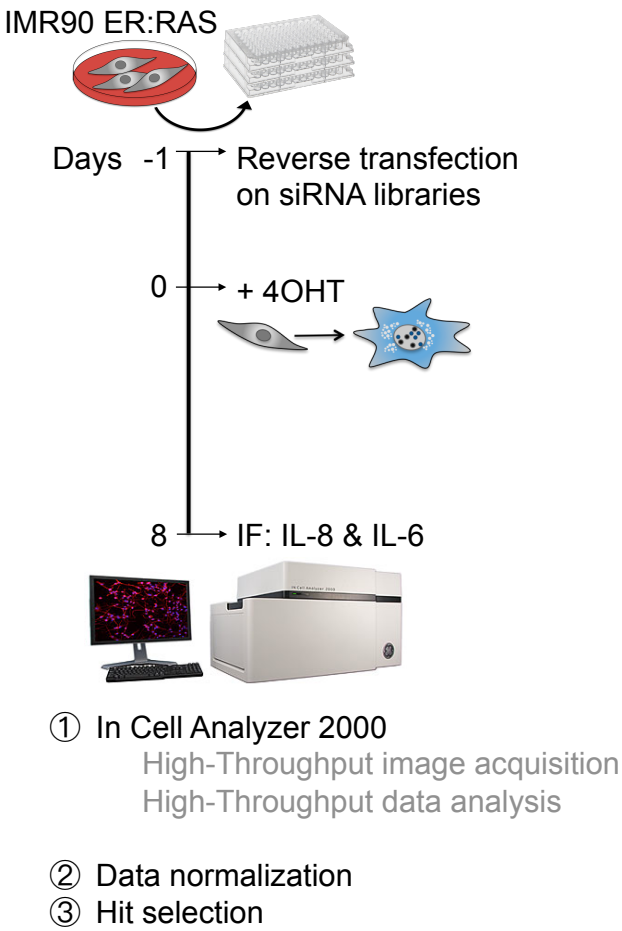

Figure 3.6. SASP siRNA screen workflow.
IMR90 ER:RAS cells were reverse transfected onto 96-well plate siRNA library collections targeting the Human Druggable Genome, Kinases, Phosphatases and GPCRs. The following day the cells were treated with 4OHT to initiate Ras-induced senescence and 8 days later were fixed and stained for IL-8 and IL-6 IF analysis. Rapid image acquisition and quantification was achieved by the HTM system IN Cell Analyzer 2000. All data were normalised by B-score using the freely available online software found at http://web-cellhts2.dkfz.de/cellHTS-java/cellHTS2/ (Pelz et al, 2010). Selection of hits was performed as described in the text.

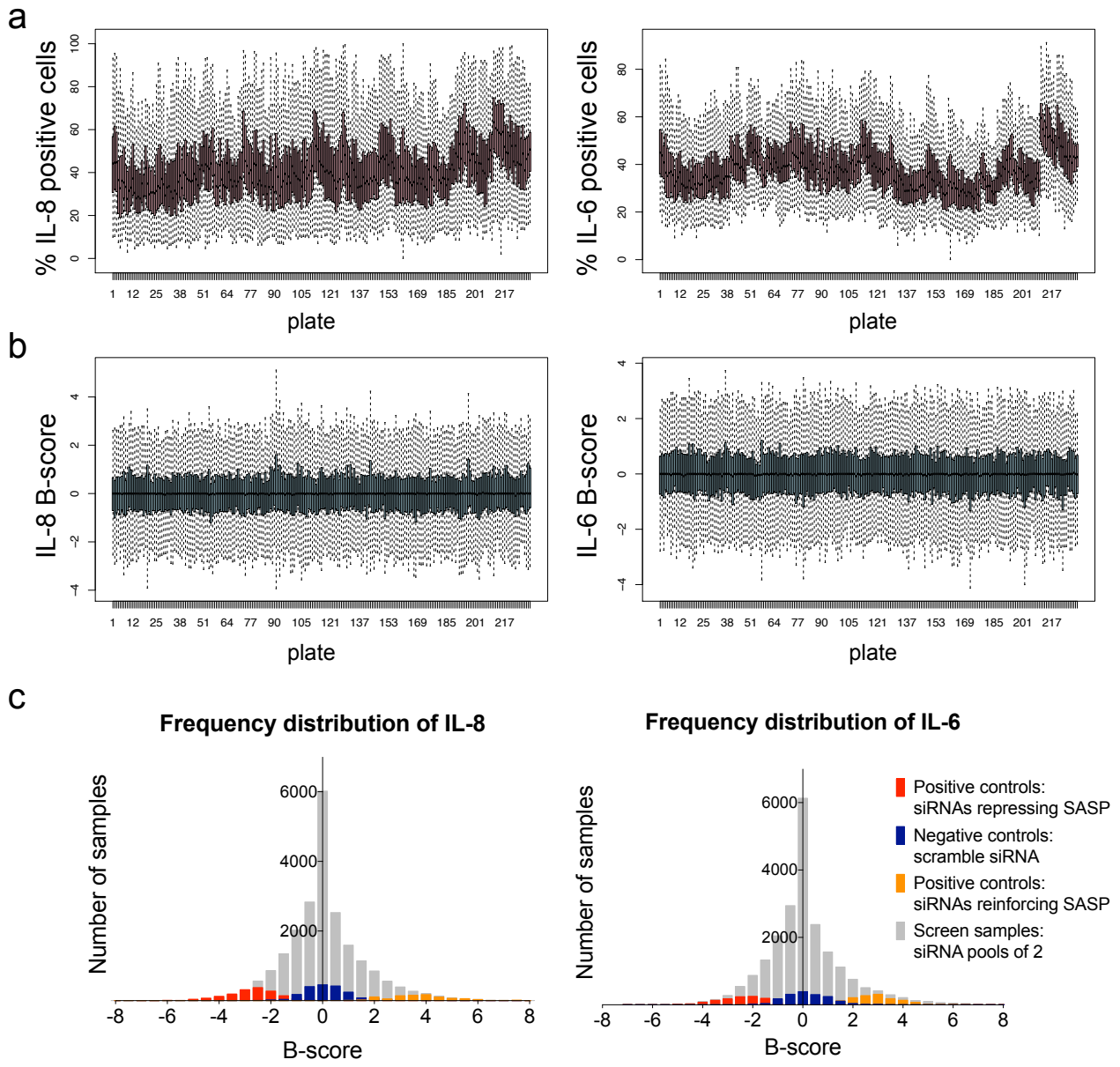

Figure 3.7. siRNA screen data normalisation by B-score.
(a) HCA of IL-8 and IL-6 IF resulted in a percentage of positive cells, the distribution of which within each screen plate is shown as a single box-and-whisker. (b) Inter-plate variability was improved after B-score normalisation of the percentage values as demonstrated by the better alignment of the box-and-whiskers. For (a) and (b) each screen plate is represented three times corresponding to experimental replicates. (c) Combining all the B-scores across plates revealed a normal distribution of the screen samples with the positive and negative external controls segmented as intended. This observation is indicative of a successful adjustment of inter- but also intra-plate variability even more so because the external controls were particularly prone to undesirable positional effects (plate-edge effect).

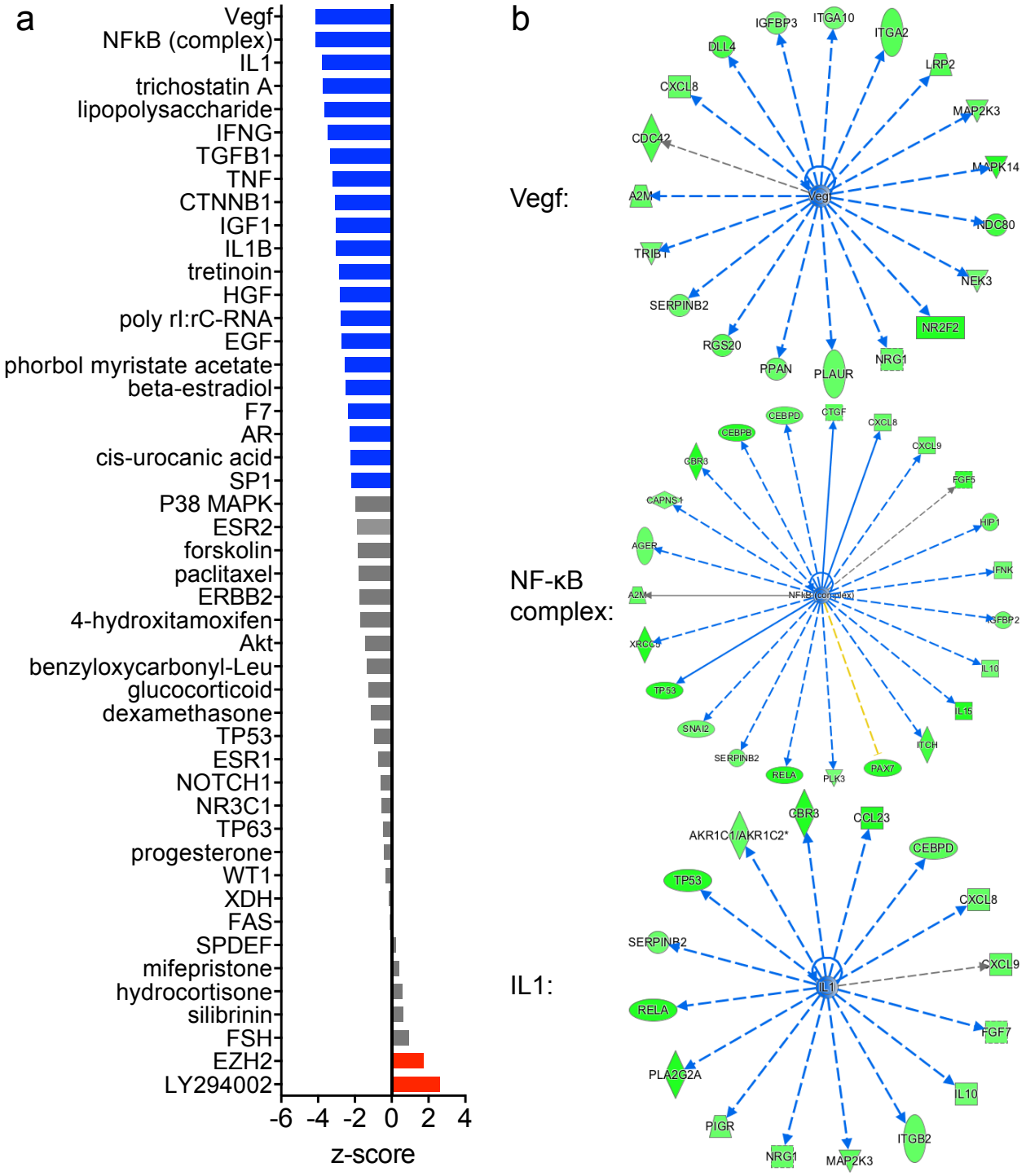

Figure 3.8. Conceptual quality control of the primary siRNA screen for IL-8 regulators.
From the three replicates of IL-8 B-scores, the second lowest for each sample siRNA was chosen for the Ingenuity Upstream Regulator Analysis in IPA®. (a) The z-score is the predicted inhibition (blue) or activation (red) state of a transcriptional regulator (TR) based on the direction of the observed differential regulation of a gene in the user's dataset. In this case, the direction is the reduction of IL-8 with siRNA against a gene. By default, a Fisher's Exact Test is calculated to determine a statistically significant overlap between the user's dataset and that of the predefined set stored in the Ingenuity® Knowledge Base for the particular TR. Here, only the TRs with an overlap p-value of < 0.01 are depicted. (b) Network visualisation of the top three most reliably inhibited TRs (blue) and their targets presenting low expression levels (green) thereby predicting the implication of Vegf, NF-κB complex and IL-1 signaling in IL-8 induction.

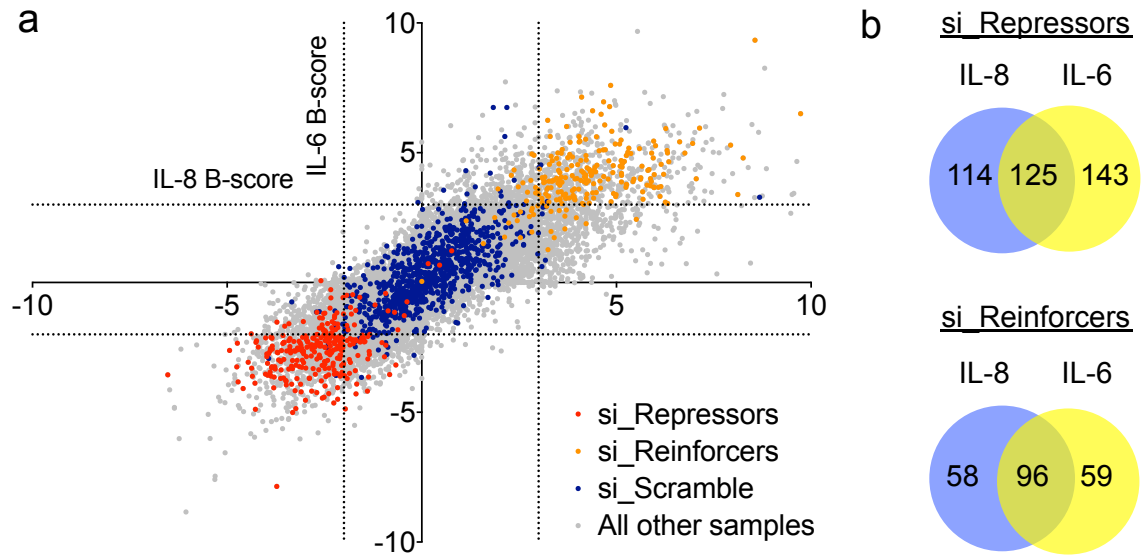

Figure 3.9. Selection of hits from the primary SASP siRNA screen.
(a) Scatter dot plot of normalised IL-8 versus normalised IL-6 values for each individual replicate sample. The dotted lines indicate the cut-offs of ±2 SD of negative scramble controls. Specifically, siRNA pools were called hits if surpassed a B-score of - 2 or + 3 more than two times in both readouts. All hit replicate samples are colour-coded displaying also the replicate sample that did not pass the filter. (b) Venn diagrams showing the number of siRNA pools passing the filter from each direction and the overlap between IL-8 and IL-6.

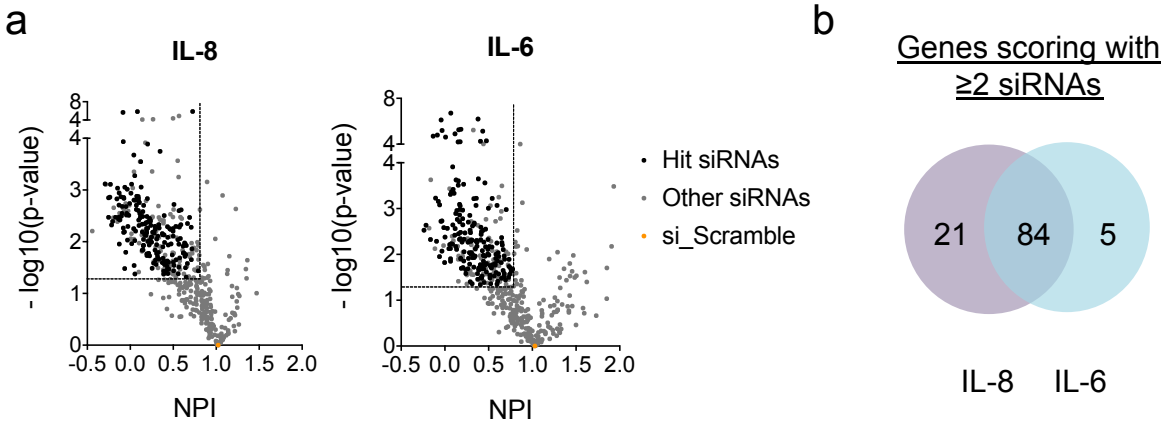

Figure 3.10. Secondary siRNA screen confirms reduced SASP in 84 of 125 target genes.
The Normalised percent inhibition (NPI) reflects the IL-8 (a) or IL-6 (b) percentage positive values in a sample siRNA subtracted from the mean of negative controls divided by the difference between the means of positive and negative controls. To obtain a p-value, three replicate NPI values of each sample siRNA were compared to all scramble siRNA values by t-test. (a) The NPI and p-value thresholds are depicted by dotted lines. Only the siRNAs targeting genes of (b) are colour-coded as 'Hit siRNAs'. (b) 84 genes were represented by ≥2 siRNAs with an IL-8 and IL-6 NPI < 0.8 and a p-value of ≤ 0.05.

3.5. Clustering analysis identified a group of genes regulating SASP but not growth arrest

Given that the molecular pathways resulting in senescence growth arrest and a SASP are intertwined, it is possible that the identified candidates not only regulate the SASP but also senescence. To dissociate the candidate genes regulating the SASP from those regulating senescence altogether, we assessed how the siRNAs identified in the screen affect senescence by evaluating different readouts using IF. These included upregulation of p16 and p21 and the loss of BrdU incorporation. The screening settings remained the same (Figure 3.6) but the library of siRNAs comprising the secondary SASP screen was used as a platform and the cells were fixed 5 days after induction of senescence following an 18 hour BrdU pulse. IF staining for p16, p21 and BrdU was carried out and was analysed by HTM and data normalised as previously described. Here, the B-score was chosen as a plate normalisation method since, analogous to the primary screen, the majority of the genes being screened had no predictable bias towards any of the readouts. Indeed, the scramble negative controls had a B-score of near 0 for all three readouts. Having earlier tested and confirmed the siRNA experimental conditions by targeting the two key senescence effectors p16 and p53 (Figure 3.3), these suitably served as the positive controls of the screen (Figure 3.11a). The siRNA targeting p16 (sip16) resulted in a low p16 B-score but high BrdU B-score confirming the target knockdown, growth arrest bypass and overall feasibility of detecting regulators of senescence. Similarly, the siRNA targeting p53 (sip53) resulted in low p21 B-score, indicating lower p53 activity since p21 is a downstream target, and high BrdU B-score demonstrating the growth advantage.

To identify the SASP-repressing siRNAs that specifically regulate the SASP, the measurements of siRNAs with a mean IL-8 NPI score below 0.7 were isolated and subsequently categorised according to p16, p21 and BrdU levels. A desirable variance across categories was achieved when 4 groups were assumed but progressively diminished with further categorisation (Figure 3.11b). Therefore, Thomas Carroll (MRC CSC Computing and Bioinformatics facility) divided the siRNAs into 4 clusters based on their similarity to the cluster mean, a method termed *k*-means clustering (Figure 3.11c). A cluster of siRNAs (Cluster 1) grouped with the scramble controls, i.e. no change in p16, p21 or BrdU levels. Cluster 2 and 4 displayed reduced p16 levels

or p21 levels concomitantly with increase in BrdU indicative of senescence bypass. Finally, cluster 3 represented siRNAs boosting p21 levels and exaggerating loss of BrdU incorporation suggesting reinforcement of senescence. To eliminate genes that were separated due to siRNA off-target effects, we focused only on genes represented by multiple siRNAs within the same cluster. Cluster 1 contained the majority of genes having multiple siRNAs falling into the same category (Figure 3.12).

Impairing the expression of important senescence regulators would hinder harmful inflammation but at the expense of losing a powerful tumour-suppressive mechanism. The clustering analysis therefore enabled exclusion of such genes from the shortlist of SASP regulators. At this stage the shortlist included 49 genes that seem to regulate IL-6 and IL-8 without interfering with the senescence growth arrest.

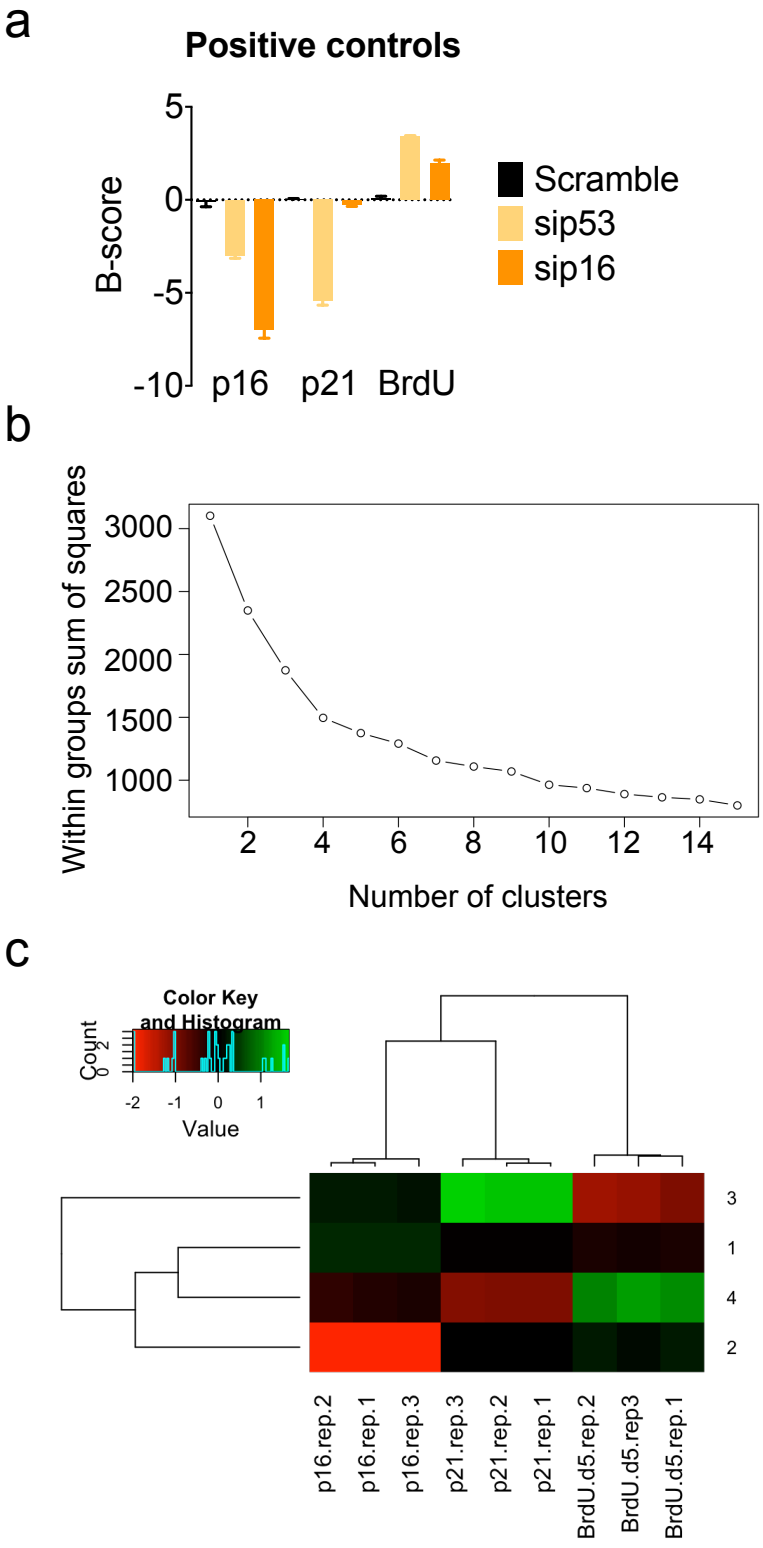

Figure 3.11. Workflow for the categorisation of siRNAs repressing the SASP.
The library of SASP-repressing siRNAs was screened for the three senescence readouts: upregulation of p16, p21 and BrdU loss and the percentage positive values were normalised by B-score. (a) The direction of B-scores corresponding to positive controls was as expected. (b) As a measure of variance, the sum of squares within groups decreased with a decreasing set number of clusters. (c) *k*-means clustering into 4 clusters sub-classified SASP-repressing siRNAs that reinforce (cluster 3), maintain (cluster 1) or bypass (cluster 2 and 4) the senescence phenotype.

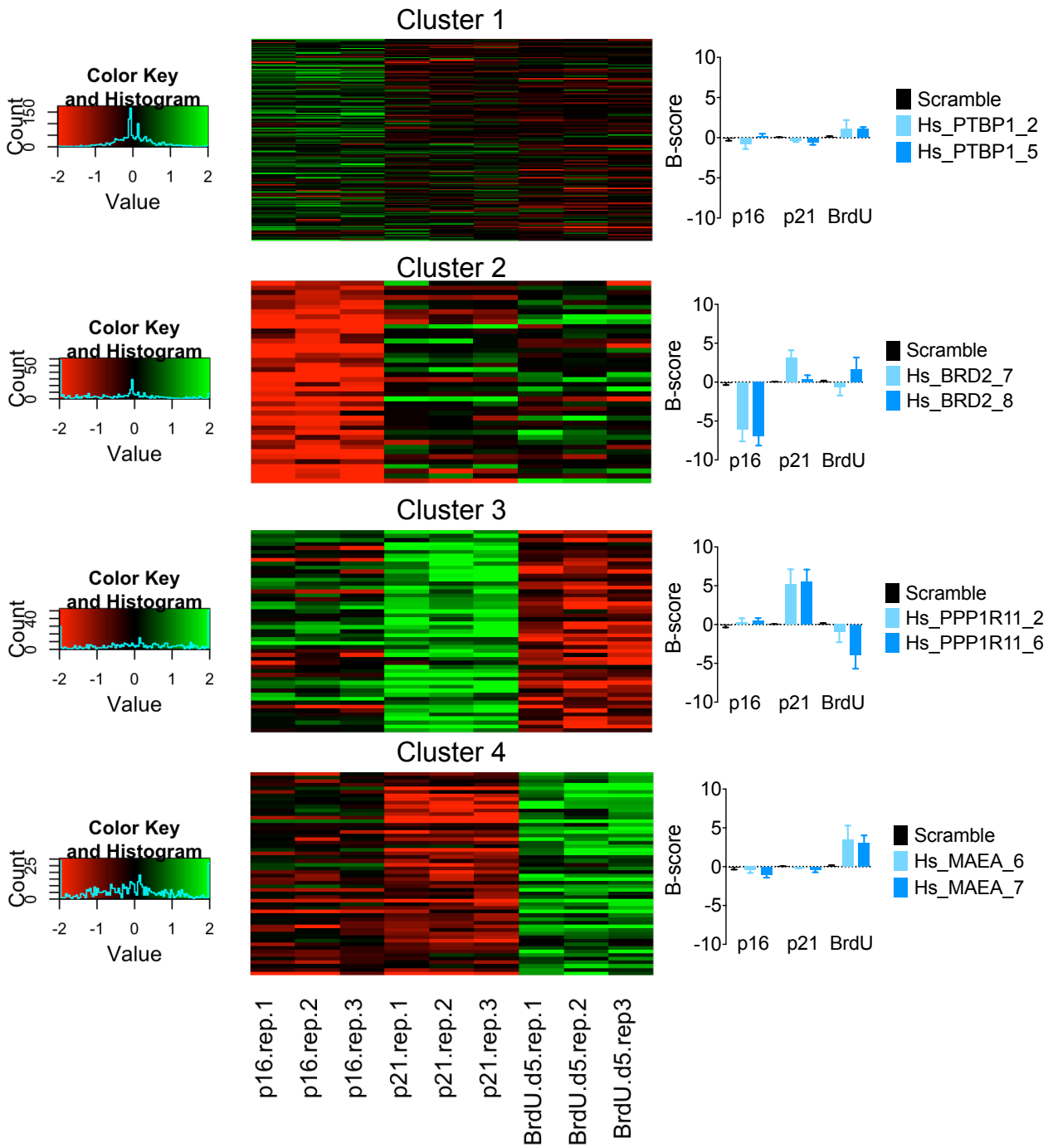

Figure 3.12. SASP-repressing siRNAs fell into 4 senescence-associated categories.
Heat-maps of the 4 clusters showing B-score expression of the indicated measure for each replicate experiment. Each line of a heat-map reflects the measures from one siRNA from a list of siRNA samples that had previously reduced IL-8 expression. Next to each cluster are the B-scores of an example gene represented by more than 2 independent siRNAs in that cluster.

3.6. Exploring the nature of the novel SASP regulators

To explore the mechanism of action of the novel SASP regulators, two approaches were undertaken. Firstly, to dissect whether the master SASP regulator NF-κB is a downstream target, we tested the effect of knocking down the hit genes in a paracrine senescence model. Secondly, we measured global transcriptional changes upon knockdown in OIS in an unbiased manner to detect possible novel, universal, molecular mechanisms of SASP regulation.

3.6.1. Effect on paracrine senescence

The transcription of many SASP genes depends on the transcription factor NF-κB and on the autocrine signaling conferred by the SASP factors themselves further reinforcing NF-κB activity (Figure 1.3). Paracrine senescence recapitulates these two SASP-specific phenomena. By exposing proliferating IMR90 cells to media conditioned by senescent cells, media that is rich in inflammatory factors, NF-κB is activated translocating to the nucleus. Shuttling of NF-κB from the cytoplasm to the nucleus is detectable by IF within the first hour (Figure 3.13a). The cells respond by initiating a senescence-like response, characterised by cell cycle arrest, upregulation of the CDKI p21, flattened morphology, increased SA-β-gal activity and, of high relevance, expression of SASP factors (Figure 3.13b and c; Acosta et al., 2013). Induction of a SASP can be efficiently monitored by IF as early as 1 day after addition of CM to proliferating IMR90 cells (Figure 3.14a and b). High levels of IL-8 and IL-6 are maintained throughout at least 4 days and knocking down the NF-κB subunit p65 abolishes it. On the other hand, C/EBPβ does not seem to play a major part in regulating the SASP in this setting as the siRNA against it did not alter IL-8 nor IL-6 levels (Figure 3.14b).

Since this cellular system of paracrine senescence is NF-κB-driven, the hypothesis entailed it would specifically serve to provide insight into the mechanism of action of the SASP-repressing siRNAs. Therefore, IMR90 cells were transfected with the library of siRNAs comprising the secondary SASP screen and IL-8 and IL-6 were analysed as before but only 2 days after paracrine senescence induction (Figure 3.14a). We had determined that we could detect a reduction in SASP at this time-point (Figure 3.14b) and hence it was chosen due to its proximity to time of

transfection therefore minimising variation due to a merely transient knockdown. To normalise the data of the readout-biased paracrine senescence screen, we used the control-based method of NPI. The IL-8 and IL-6 NPI values of the paracrine senescence screen had little correlation to those of the OIS screen (Figure 3.14c). Nevertheless, 17 genes of 125 presented an NPI of < 0.7 with > 2 siRNAs in both readouts and screens. One of these genes was PPP1CB, encoding a catalytic subunit of Protein Phosphatase 1. Mitsuhashi et al. (2008) showed drug-mediated inhibition of PP1 with Tautomycetin suppresses NF-κB activity by targeting the upstream activator IKK complex in HEK293T cells. Another one of the common hit genes was AGER, or else RAGE (Receptor for Advanced Glycation End-products) a gene encoding a receptor for HMGB1 in immune cells culminating in NF-κB-mediated cytokine release (Klune et al., 2008). HMGB1 was in fact shown by Judith Campisi's group to contribute to NF-κB induction in a senescence context but through a different receptor, TLR4. These two findings provide conviction for the appropriateness of this screening method in identifying SASP regulators directly regulating NF-κB or acting via the autocrine loop (Davalos et al., 2013).

The paracrine senescence screen was not fruitful in illuminating the mechanism of action of the majority of OIS SASP-repressing siRNAs. Only 6 genes of the 49 SASP-specific regulators of cluster 1 were present in the shortlist. Although paracrine sensing of the SASP and integrating the signal via NF-κB resembles autocrine regulation, it does not rule out the possibility that distinct upstream mechanisms exist between OIS and paracrine senescence.

Only a fraction of the SASP regulatory mechanisms in OIS can be captured by the paracrine senescence method. Therefore, a more in-depth analysis was next undertaken to elucidate possible underlying causes of SASP reduction in OIS following knockdown of the cluster 1 genes.

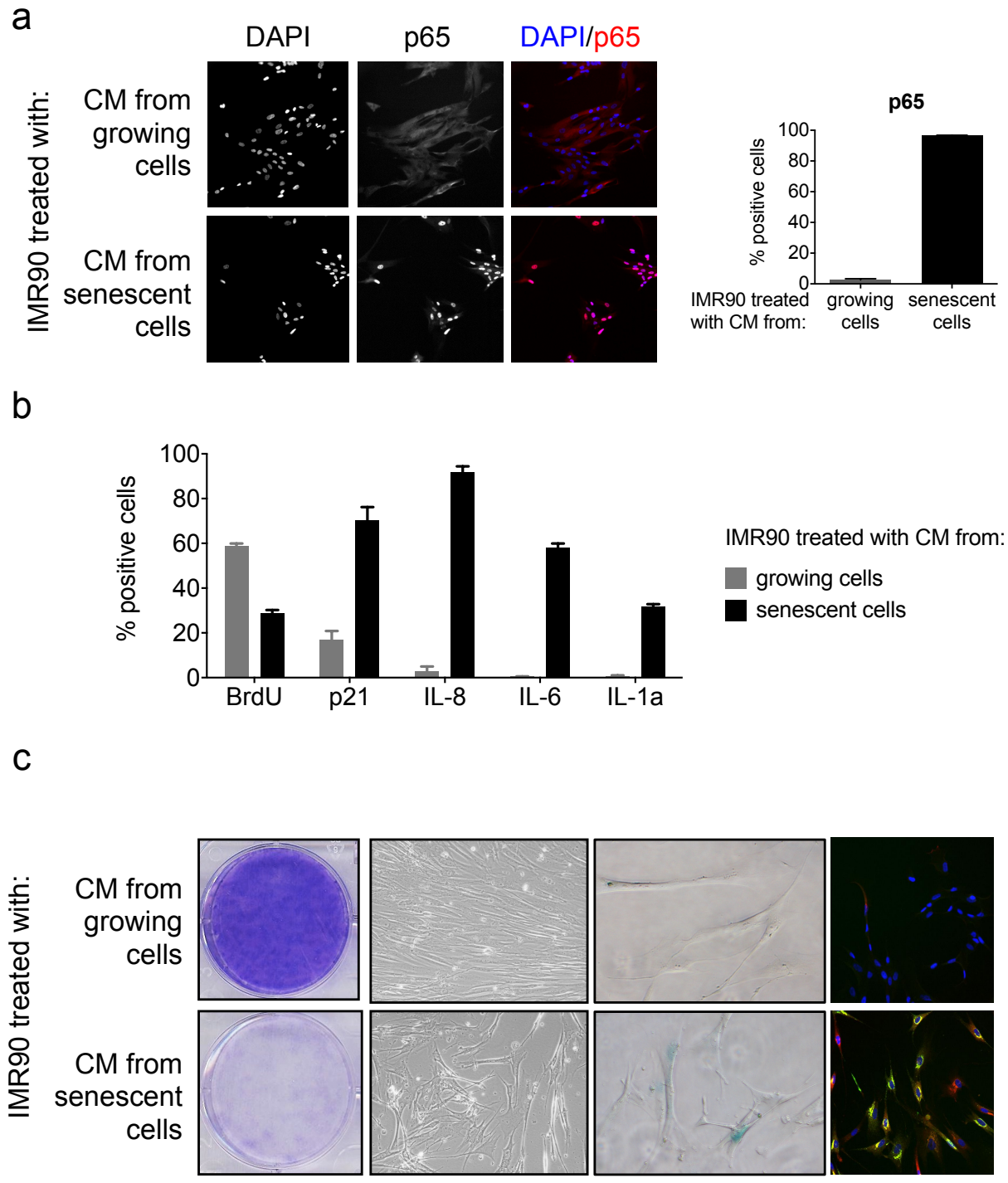

Figure 3.13. Induction of paracrine senescence upon exposure to senescent CM.
(a) IF imaging of p65 cytoplasmic-to-nuclear translocation induced only with senescent CM and not media conditioned by growing cells. Percentage of cells staining positive for nuclear p65 is shown on the right. (b) Percentage of cells staining positive for the indicated senescence markers 3 days after induction with CM. (c) Crystal-violet stained plates, bright field microphotographs and SA-β-gal staining of cells treated with CM for 8 days. Final panel on the right shows representative images of SASP IF of (b). The numbers for all are mean values of three replicate wells of a representative experiment.

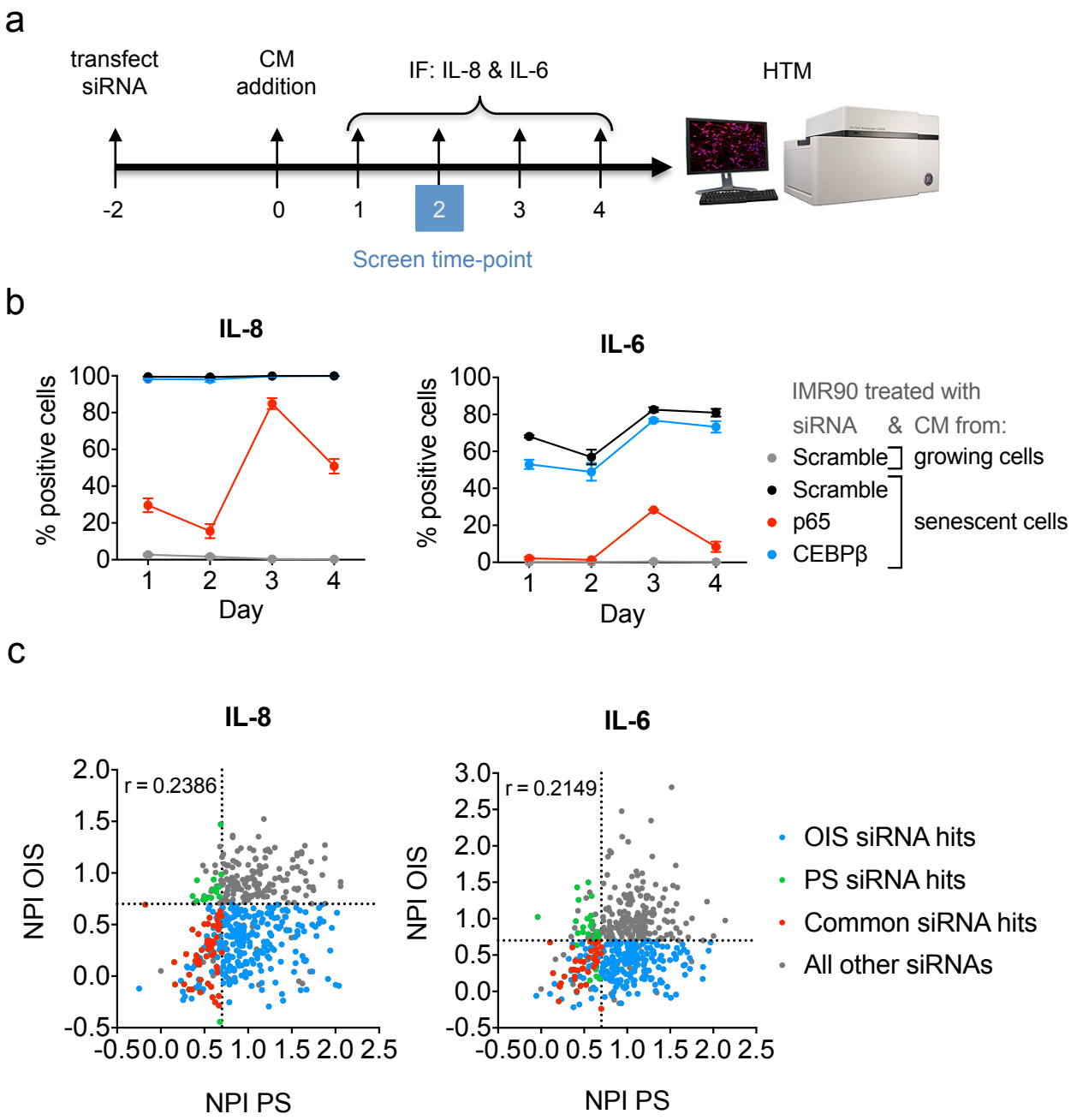

Figure 3.14. Outline of paracrine senescence siRNA screen set-up and results.
(a) Experimental timeline of the screen set-up and time-point chosen for execution of the screen. (b) High IL-8 and IL-6 levels are maintained throughout the examined time-points as measured by quantitative IF. SASP induction relies on NF-κB (p65) but not on C/EBPβ as assayed by the reduction or absence thereof with respective siRNA treatment. Time-course shows mean values with SD from three replicate wells of a single experiment. (c) Secondary screen of SASP-repressing siRNAs revealed a small group of siRNAs hindering SASP induction with < 0.7 NPI (dotted lines) in both OIS and PS shown in red. Each NPI value is a mean of three experiments. However, there was no direct linear association between the two screens as shown by the low Pearson correlation coefficient (r).

3.6.2. Categorisation according to global transcriptional changes

To investigate mechanisms by which the identified candidates regulate the SASP, possibly irrespective of senescence growth arrest, we performed global gene expression analysis of cells transfected with cluster 1 SASP-specific regulator siRNAs. This approach was feasible through an adaptation of a sample preparation method originally designed for deep sequencing of multiple samples with low starting material. This method is termed smart-seq2 (described in section 2.9.6). The cluster 1 genes comprised of 49 genes as previously mentioned but was narrowed down to 38 on the basis of lowest SASP detection in the secondary SASP siRNA screen. To monitor off-target effects 2 siRNAs of 4 were chosen resulting in 76 samples. Finally, control samples included proliferating cells and senescent cells transduced with scramble siRNA or siRNAs targeting p16, p53, p65, CEBPβ and p38. Each sample was replicated three times mounting to 249 samples. The experimental settings remained the same as the siRNA screens but the cells were not assessed by IF and were instead processed for mRNA isolation and sequencing library preparation (Figure 3.15).

To identify possible mechanisms regulating the SASP, the SASP-specific regulators were sub-categorised by unsupervised hierarchical clustering based on the altered gene expression profiles upon knockdown (Figure 3.16). 6 groups of genes seemed to be the main drivers of this categorisation. To further understand the distinct biological processes affected across samples, gene ontology enrichment analysis was carried out for each of the 6 groups, named A-F (Figure 3.16, 3.17 and 3.18).

Knockdown of a number of genes such as DCAMKL3 resulted in upregulation of group A genes involved in ion homeostasis (Figure 3.17A) a lot of which encode transmembrane transporters (Figure 3.18A) in line with cellular and subcellular ion exchange regulation. This enrichment was not observed in neither senescent scramble transfected controls nor their proliferating counterparts presenting possibly a separate synthetic branch of regulation. On the other hand, high levels of group A genes correlated with high levels of group D genes which is a group enriched in mitotic cell cycle genes. Although group D genes were relatively upregulated in proliferating controls and downregulated in senescent controls as expected, they were particularly

increased in samples with high group A gene levels. A closer look into the molecular function of group D genes pointed to NADH dehydrogenase activity, again relating to ion exchange.

Interestingly, a group of genes termed F is involved in cell division (Figure 3.17F) but seems to be involved in chromosome organisation during DNA replication (Figure 3.18F) separating it from the mitosis-related genes of group D (Figure 3.16). Senescence-associated downregulation of group F genes in comparison to proliferating samples was maintained in the majority of samples indicating growth arrest whereas upregulation in sip16 and sip53 samples indicated bypass.

Group C genes, showing upregulation upon senescence, associated with GO annotations of immune system response (Figure 3.17C) and extracellular compartment localisation (Figure 3.18C). Given that immune system genes overlap with SASP genes, group C possibly reflects the screen readout. However, the great variation across samples observed in the gene expression levels within this group suggests differential SASP gene expression, a phenomenon worth exploring in the future.

Group B gene expression was impaired in several samples of SASP-specific siRNAs such as siRNAs targeting SKP1A. Group B genes were found to be involved in carbohydrate metabolism and glycosylation processes (Figure 3.17B) and were highly expressed upon senescence (Figure 3.16B). These processes constitute a gene regulatory mechanism via addition of post-translation modifications to proteins as they are being processed from the ER to Golgi through to final destination, consistent with the subcellular localisation of group B gene products (Figure 3.18B). Although glycoprotein biosynthesis is a process worth investigating in search for SASP manipulation methods, knockdown of certain SASP-specific genes paradoxically resulted in increased group B gene levels. Noteworthy is the fact that the majority of these SASP-specific genes such as RNF6 when knocked down displayed particular reduction of genes involved in protein translation (Figure 3.17E) and specifically of genes encoding ribosomal subunits (Figure 3.18E).

Overall, we have presented here a method for coupling global gene expression profiling to an siRNA screen. Identification of universal mechanisms altered by SASP-repressing siRNAs underscores the potential to find further targets for SASP manipulation.

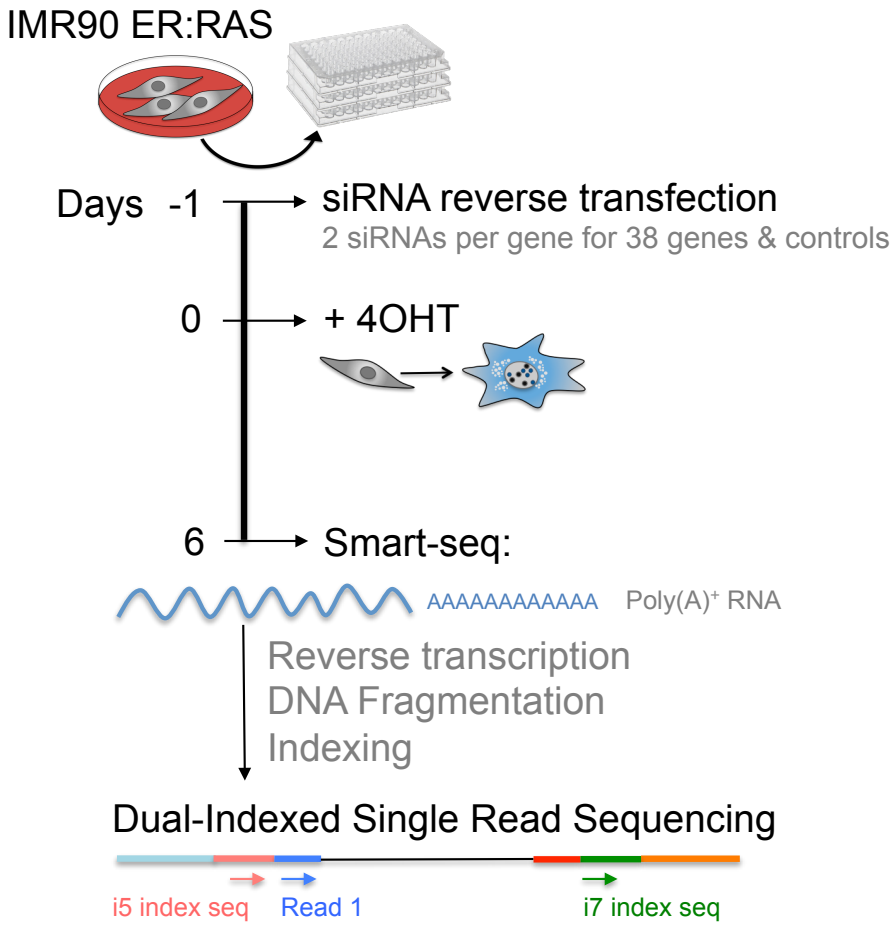

Figure 3.15. Workflow of global gene expression profiling of SASP-specific regulators.
A cDNA library of 249 samples was prepared and subsequently sequenced. The 249 samples originated from the IMR90 ER:RAS cells transfected with siRNAs targeting the SASP-specific regulators and known senescence regulators, three independent times.

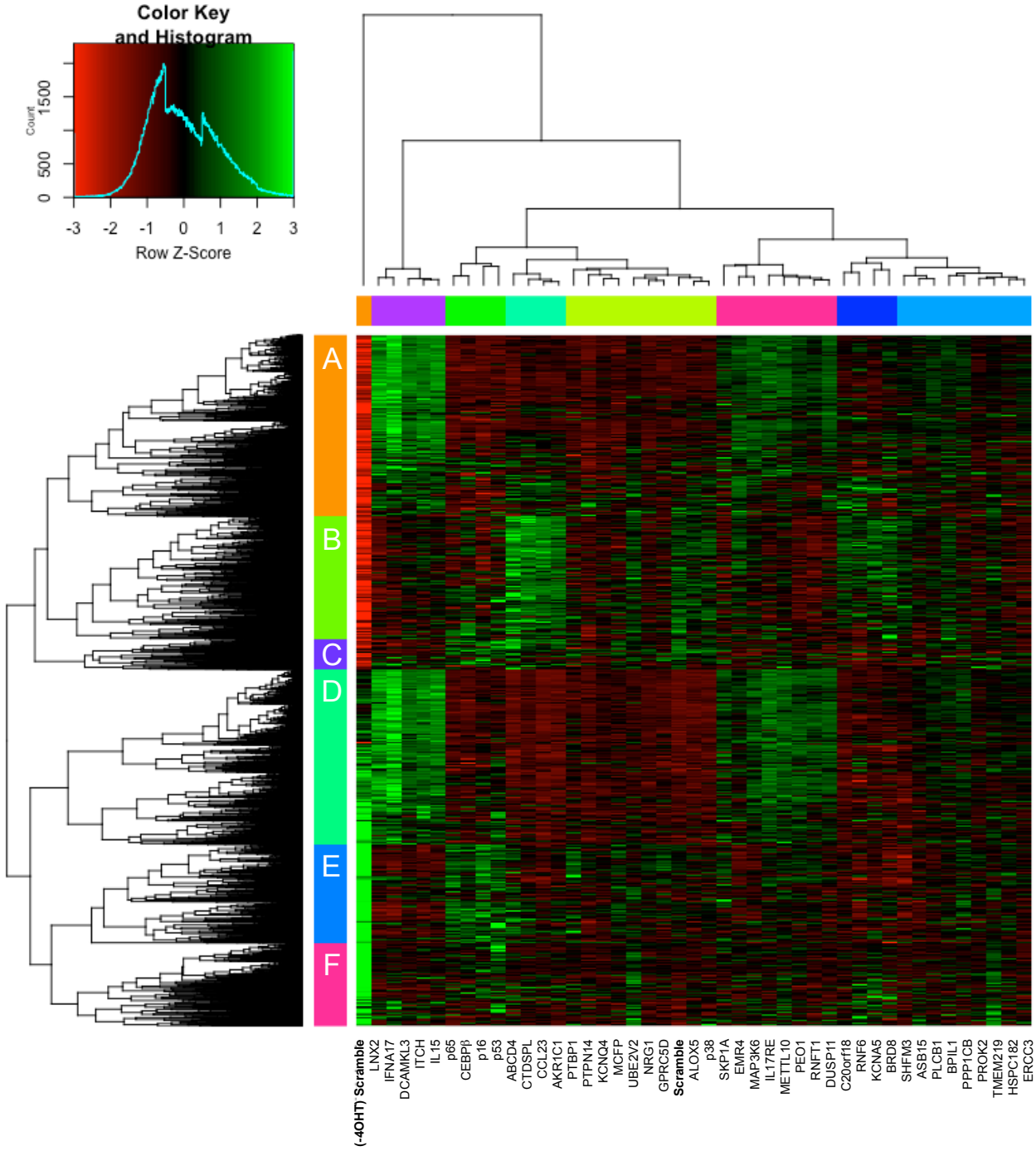

Figure 3.16. SASP-specific regulators were categorised based on alterations in gene expression. Heat-map showing altered transcription of genes (row) falling into 6 groups (A-F) which drive clustering of samples after knockdown of the indicated SASP-specific regulator (column). Each heat-map cell is the mean expression level of a gene across three experimental replicates and 2 separate siRNAs against the indicated target. Each value is colour-coded in relation to all the values of that gene (row). All samples were induced with 4OHT unless accompanied by (-4OHT).

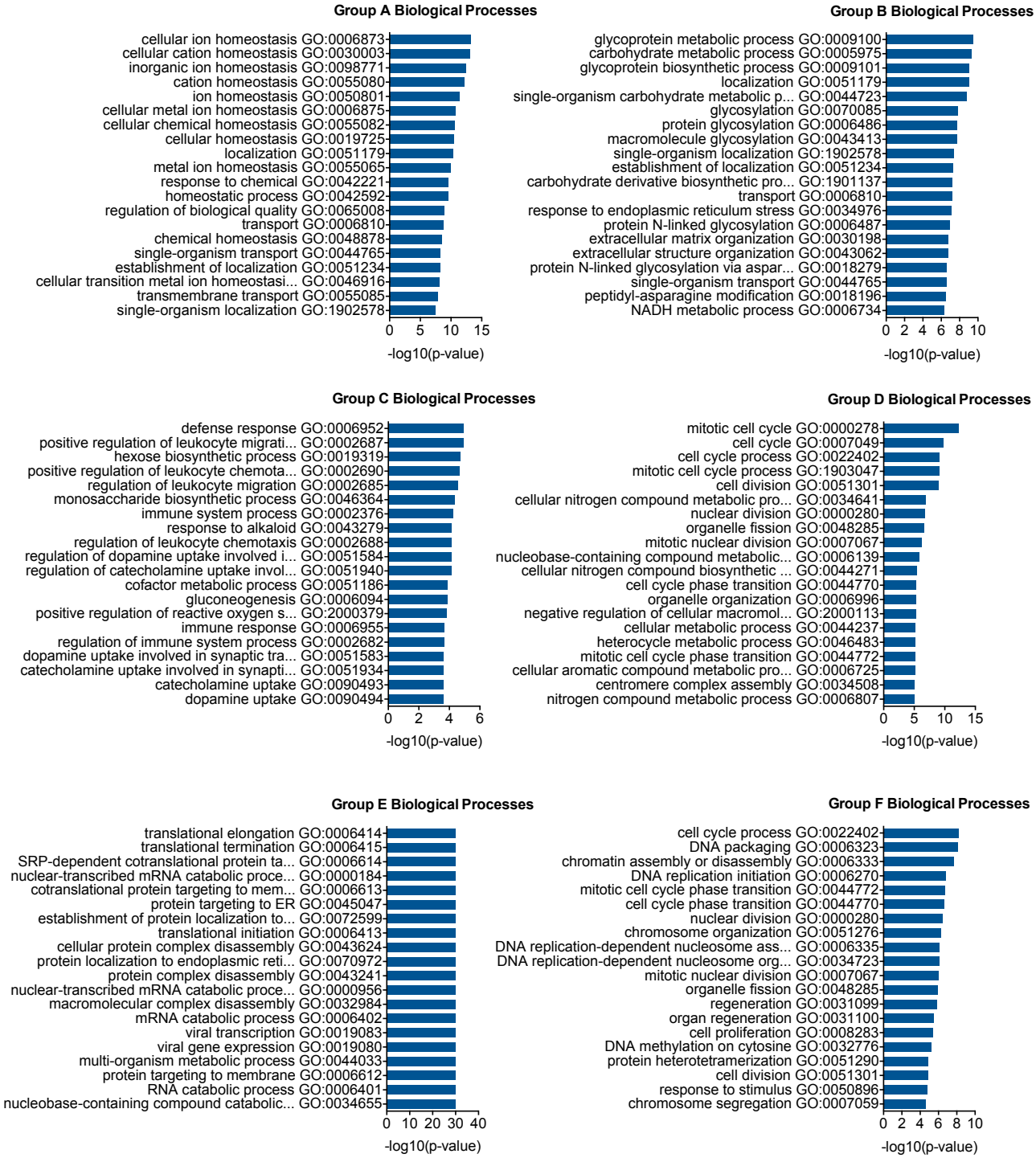

Figure 3.17. Biological processes of differentially expressed genes in response to knockdown of candidate SASP-specific regulators.

Top 20 GO terms with p-value < 0.05 for each of the 6 differentially expressed gene groups.

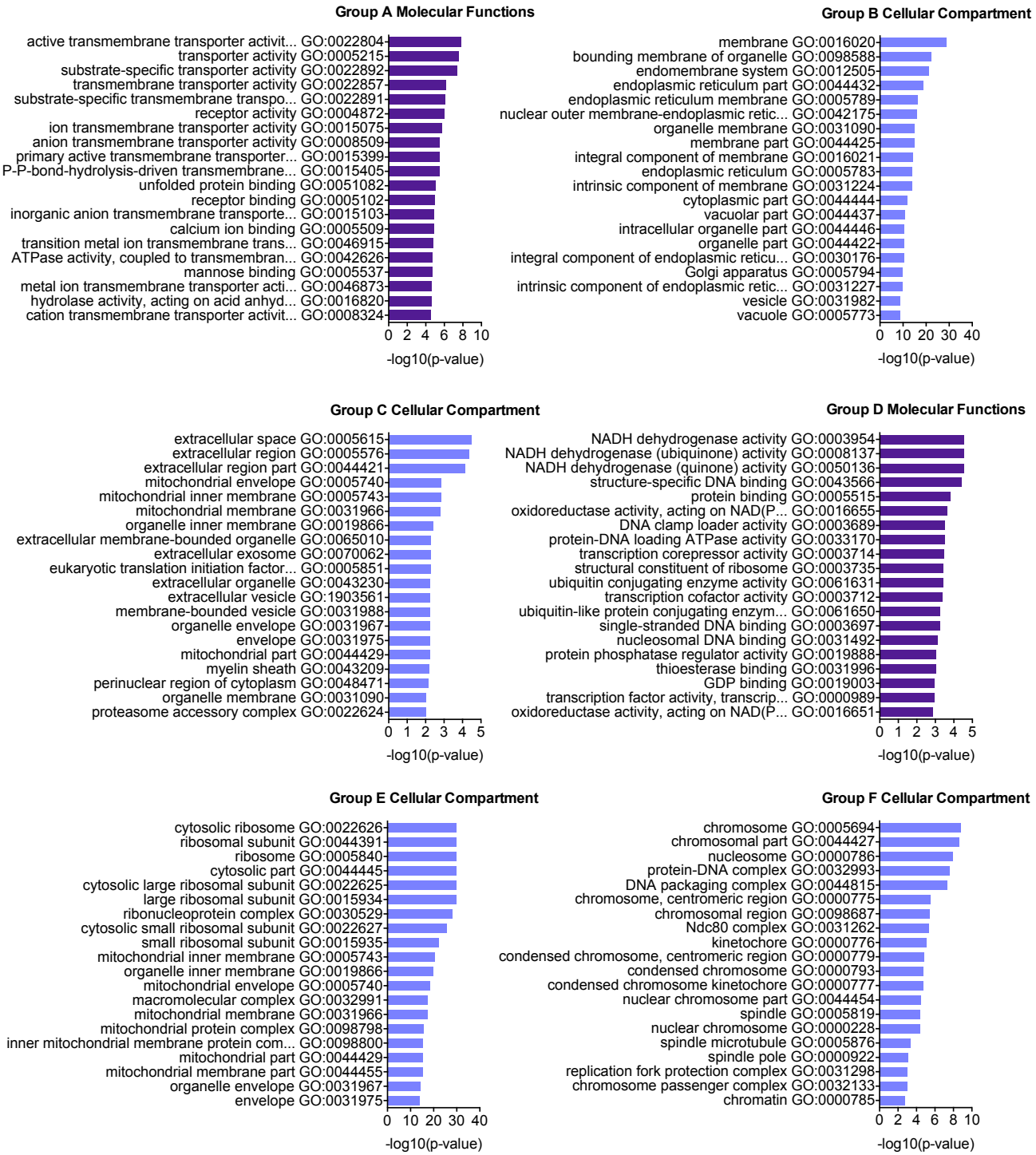

Figure 3.18. Cellular compartments or molecular functions of differentially expressed genes in response to knockdown of candidate SASP-specific regulators.
Top 20 GO terms with p-value < 0.05 for each of the 6 differentially expressed gene groups.

3.7. Identifying chemical inhibitors to repress the SASP

The aim of this project was to identify molecular factors that regulate the SASP. From an academic point of view, the siRNA screens coupled to deep sequencing have opened new routes for exploring SASP regulation. From a therapeutic point of view, the objective was to explore the possibility of impairing the inflammatory phenotype of senescent cells without affecting the tumour-suppressive growth arrest. 49 genes were found to be potential targets for achieving this result. 6 of these were found to be either the main target or a close relative of the targets of an existing chemical inhibitor. 5 of these were able to inhibit IL-8 and IL-6 but did not bypass the proliferation arrest as assessed by BrdU incorporation mirroring the phenotype of cells treated with an inhibitor of mTOR called Torin (Figure 3.19a-c). On the other hand, as expected, treatment with a potent inhibitor of MEK signaling called PD98059 bypassed senescence altogether since a reduction in SASP was accompanied by increase of BrdU incorporation similar to proliferating counterparts. The phenotype of Ras-induced cells treated with one of the compounds, JQ1, which targets bromodomain-containing proteins, was recapitulated by Tasdemir et al. (2016) providing further confirmation for the validity of the screening approaches.

In a therapeutic setting, the chemical compounds impairing a SASP but maintaining a growth arrest are appealing. However, the inflammatory phenotype will be already established at the time of disease detection and treatment initiation. Therefore, the SASP-repressing drugs were tested for their ability to reduce an established SASP by treating cells already 5 days into senescence (Figure 3.19d), a time at which a substantial increase in several SASP factors was detected (Figure 3.4b). Only one of the compounds, BW-B whose target is 5-lipoxygenase was able to reduce the SASP in the post-senescence induction setting (Figure 3.19e). Another compound targeting 5-lipoxygenase called Zileuton also reduced IL-8 and IL-6 in this setting confirming the specificity of the target (Figure 3.19e).

To identify additional compounds able to reduce established inflammation driven by the SASP, a more direct and unbiased approach was undertaken. To this end, IMR90 ER:RAS cells were induced to undergo senescence for 5 days at which time they were treated with a Library of Pharmacologically Active Compounds (LOPAC; Sigma; 10μM) which was manually distributed to

fit a 96-well plate format. The effect of the compound treatment on IL-8 and IL-6 levels was assessed. Like previously, to minimise false positives and negatives due to procedural inefficiencies each plate was screened under the same experimental conditions three times. Due to the smaller dynamic range of intensity values across samples, a threshold for distinguishing positive cells from negative cells was deemed too restrictive. Therefore, the readout of this screen was the raw pixel cell intensity values of IL-8 and IL-6 IF staining (Figure 3.20a). Following B-score normalisation of IL-8 and IL-6 intensity values (Figure 3.20b), taking into consideration the visual positive skewness of the data (Figure 3.20c), an arbitrary cut-off of B-score – 2.5 or + 10 was applied to select inhibitors or enhancers of the SASP respectively. Samples with low cell numbers were eliminated. Additionally, only compounds represented at least two times of three, and scoring for both screen readouts, were shortlisted, concluding to 17 inhibitors and 5 enhancers of IL-8 and IL-6. Indomethacin and acetylsalicylic acid are two known anti-inflammatory drugs shortlisted in the SASP inhibitors confirming the robustness of the screening and analysis method.

A secondary, validation screen was performed by assessing SASP levels following treatment with shortlisted compounds simultaneous to induction of senescence or 5 days after induction of senescence to recapitulate the primary screen (Figure 3.19d). 4 chemical compounds significantly enhanced both IL-6 and IL-8 levels whether the cells were already senescent at the time of treatment or not (Figure 3.21a and b). Their mechanism of action is inhibition of phosphodiesterase 3 or 4, or activation of adenylate cyclase. 12 chemical compounds significantly reduced IL-6 and IL-8 levels of senescent cells or significantly prevented full induction of these when treatment was initiated simultaneous to senescence induction (Figure 3.21a and b). Some of the SASP inhibitors belong to groups of tricyclic antidepressants or glucocorticoids or are antagonists of receptors of dopamine, histamine or serotonin. Surprisingly, indomethacin and acetylsalicylic acid did not pass the strict criteria of the secondary screen indicating the experimental setting was too limiting and permitted false negatives. Nevertheless, all 4 drugs enhancing the SASP target parts of adenosine metabolism suggesting cAMP has a role in regulating inflammation. On the other hand, 12 FDA approved chemical compounds seem to be

strong inhibitors of high IL-6 and IL-8 maintenance with immediate potential for anti-inflammatory use.

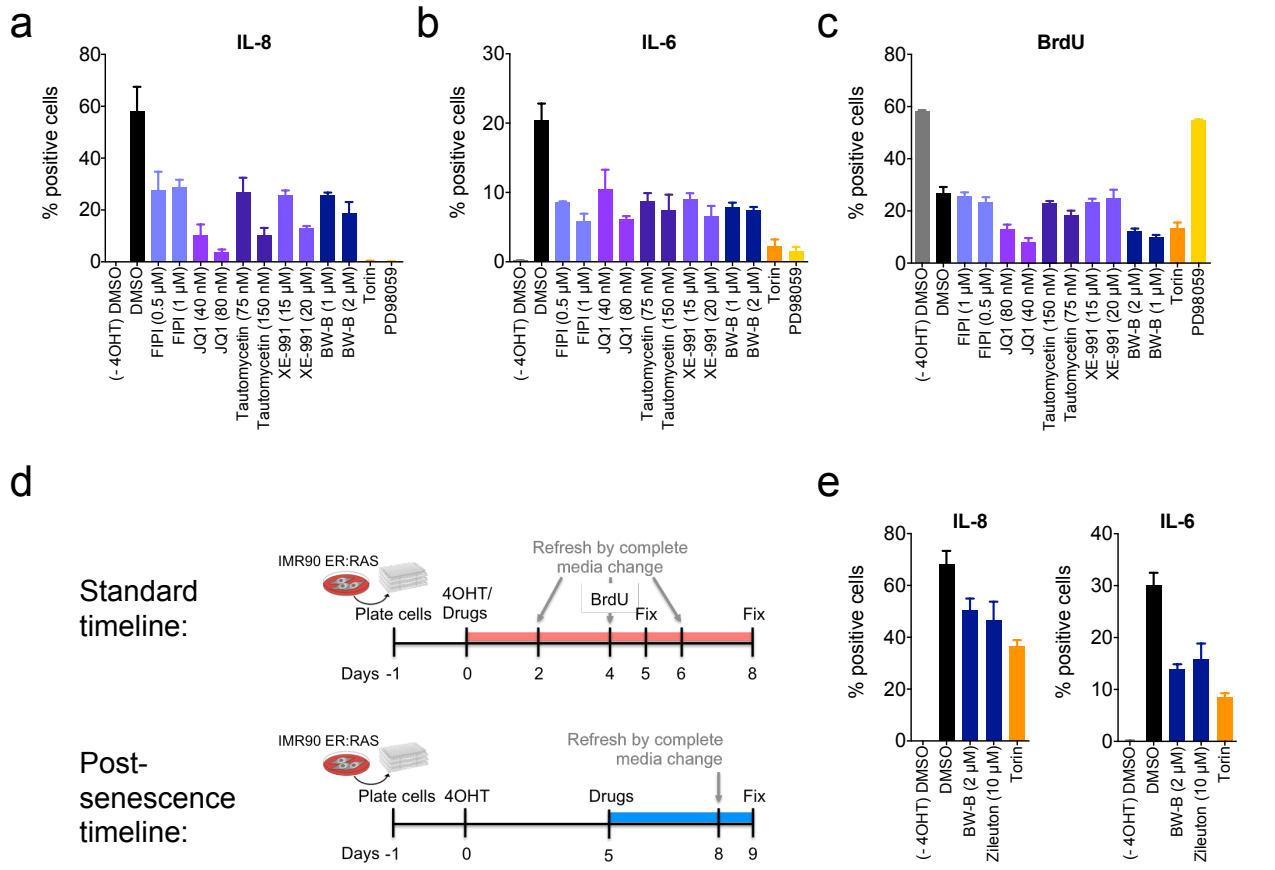

Figure 3.19. 5 compounds prevent full induction of the SASP but only 1 compound reduces an established SASP.

Percentage of cells staining positive for the indicated senescence markers 8 (a and b) or 5 (c) days after induction of senescence with 4OHT according to the standard experimental timeline shown in (d). The cells were treated with DMSO or with two different concentrations of compounds targeting Phospholipase D (FIPI), BET bromodomain (JQ1), Protein phosphatase 1 (Tautomycetin), Kv7 voltage-gated potassium channels (XE 991) and 5-lipoxygenase (BW-B). As a control, the cells were treated with inhibitors of mTOR (Torin) and MEK (PD98059). (e) Percentage of cells staining positive for the indicated SASP markers 9 days after induction of senescence with 4OHT according to the post-senescence experimental timeline shown in (d). The cells were treated with DMSO, or with two inhibitors of 5-lipoxygenase (BW-B and Zileuton) at the specified concentration and an inhibitor of mTOR (Torin). All samples were induced with 4OHT unless accompanied by (- 4OHT). The numbers for all are mean values with SD of three replicate wells of a single experiment.

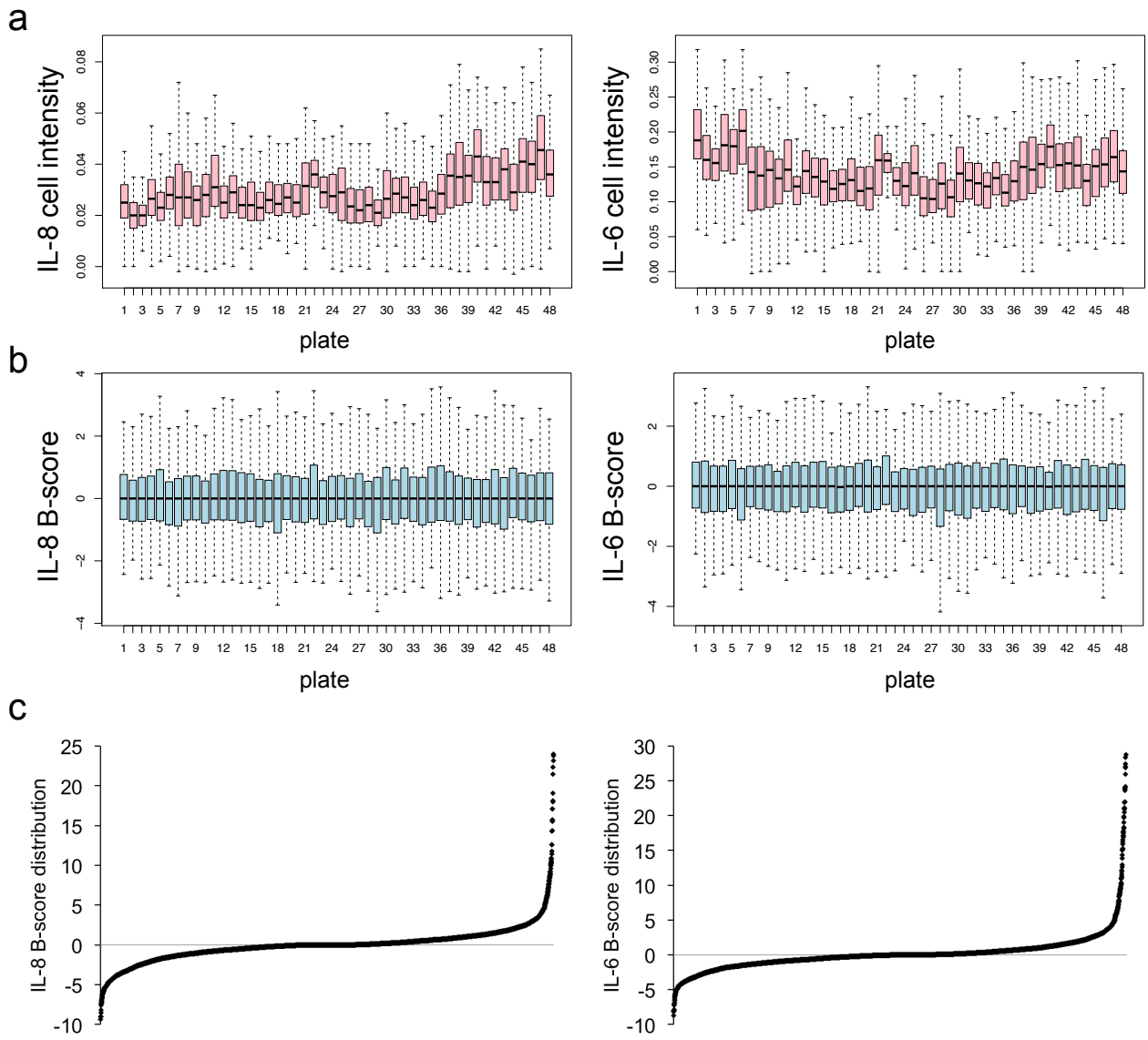

Figure 3.20. Compound screen data normalisation by B-score.
(a) HCA of IL-8 and IL-6 IF resulted in an intensity value for each cell, the distribution of which within each screen plate is shown as a single box-and-whisker. (b) Inter-plate variability was improved after B-score normalisation of the percentage values as demonstrated by the better alignment of the box-and-whiskers. For (a) and (b) each screen plate is represented three times corresponding to experimental replicates. (c) Combining all the B-scores across plates revealed a normal distribution with positive skewness of the screen samples.

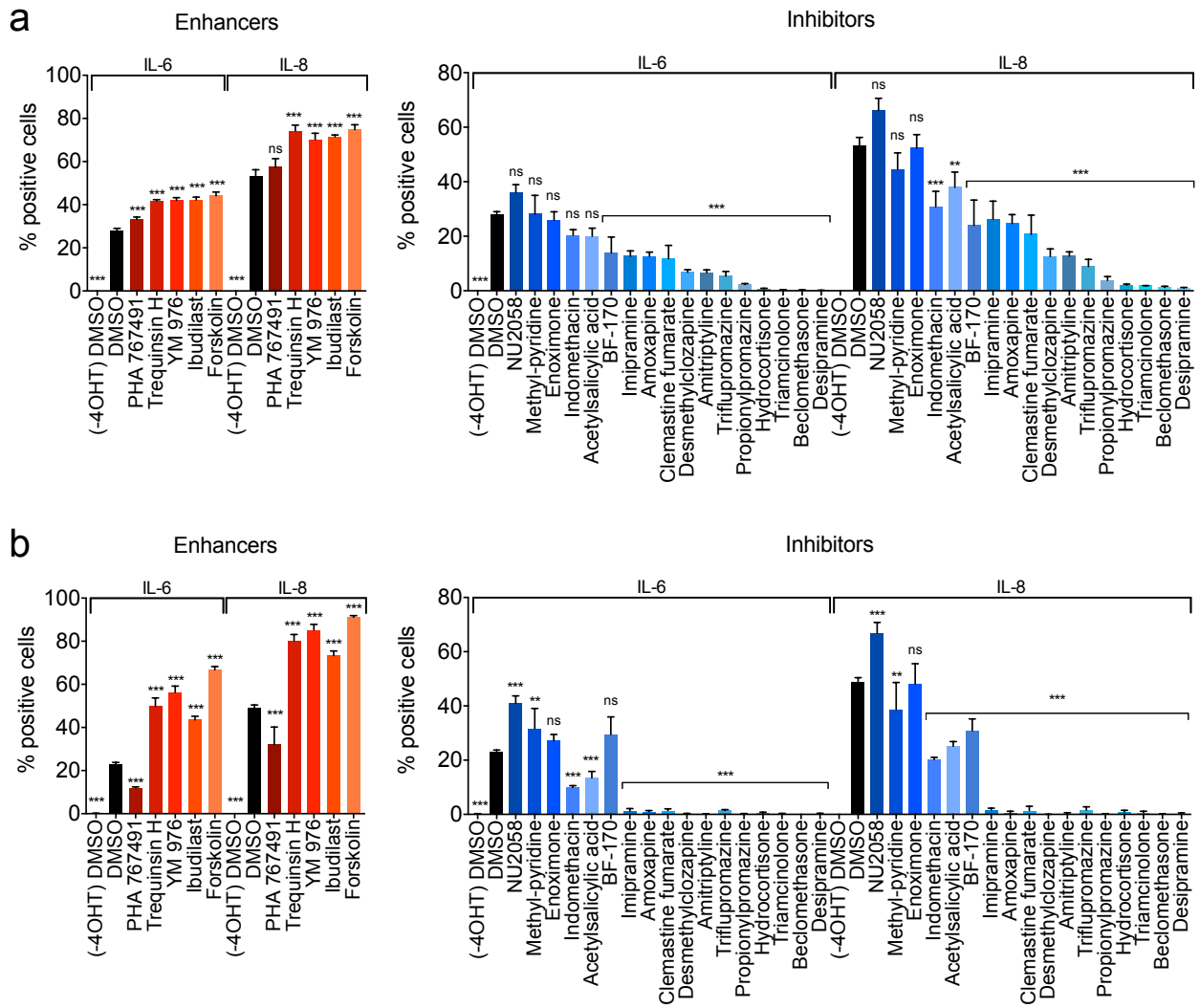

Figure 3.21. 4 drugs enhanced the SASP and 12 drugs inhibited and prevented SASP induction.
(a) IMR90 ER:RAS cells were induced to undergo senescence with 4OHT and 5 days later were treated with the indicated drugs at 1 μM (left panel) or 10 μM (right panel). The percentage of IL-6 or IL-8 positive cells was assayed after 4 days by IF coupled to HTM. (b) IMR90 ER:RAS cells were induced to undergo senescence with 4OHT and treated with the indicated drugs at 1 μM (left panel) or 10 μM (right panel). The percentage of IL-6 or IL-8 positive cells was assayed after 8 days by IF coupled to HTM. (a and b) All samples were induced with 4OHT unless accompanied by (-4OHT). Bars are mean values with SD of three experiments performed simultaneously. One-way ANOVA, Dunnett's test, comparing the mean of each sample to DMSO control was carried out to test significance of difference. ns = not significant, ** = $p < 0.01$, *** = $p < 0.001$.

3.8. Summary

To summarise, a large-scale siRNA screen identified novel SASP regulators in OIS (Figure 3.22). A few of these are necessary for implementation of the SASP in paracrine senescence as well. Clustering analysis based on other senescence markers allowed for separation of candidate genes into senescence regulators and SASP-specific regulators. Global gene expression profiling of senescent cells lacking the SASP-specific regulators revealed alterations in various functional gene groups. Certain SASP-specific regulators were targeted with chemical inhibitors, which, similar to siRNAs, prevented full induction of the SASP. However, only 1 was able to repress an established SASP. Finally, by screening a library of available chemical inhibitors for SASP regulators in OIS, 12 chemical inhibitors were identified with potential to repress an established SASP.

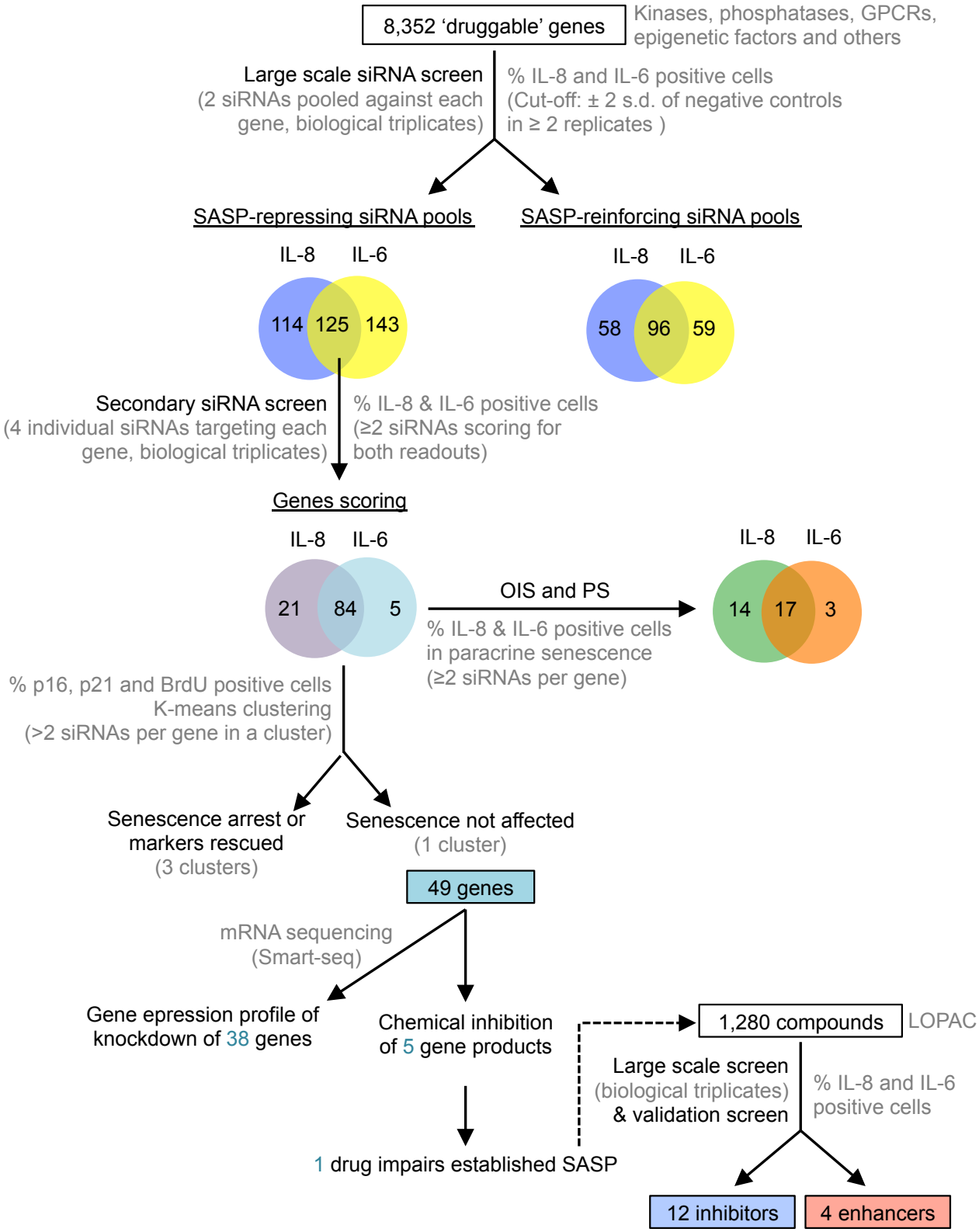

Figure 3.22. Summary of SASP screens.

Chapter 4. The splicing factor PTBP1 is a regulator of the SASP

4.1. PTBP1 regulates IL-8 and IL-6 transcription.

The siRNA system for exploring senescence and SASP was robust in identifying 49 novel specific regulators of the SASP that did not affect the senescence growth arrest. To induce a stable knockdown, IMR90 ER:RAS cells were infected with vectors expressing shRNAs targeting several of these factors. In particular, to rapidly discard false positives, 11 of the SASP-specific regulator genes were each targeted by introduction of a pool of 4 pGIPZ-based shRNAs into IMR90 ER:RAS cells. The 11 genes encode factors that belong to a variety of functional categories including chromatin remodeler, ubiquitin ligase, protein phosphatase, splicing factor and membrane receptor among others. After induction of senescence with 4OHT, growth arrest was evaluated by BrdU incorporation and relative expression levels of the gene in question and of IL-8 and IL-6 was assessed in relation to empty vector infected cells. Loss of BrdU incorporation upon 4OHT treatment remained unaltered indicative of a stable growth arrest while shRNA of the tumour suppressor p53 resulted in an increased number of cells incorporating BrdU implying efficiency of the proliferation assay (Figure 4.1a). A 60% expression knockdown of 10 gene targets and 50% of 1 gene target was achieved and 3 of the targets, namely PTPN14, PTBP1 and SKP1A dramatically and consistently reduced IL-8 and IL-6 transcription (Figure 4.1b-d). The absence or milder reduction in SASP transcription by the knockdown of the other 8 genes could be explained by the inherently different methodology compared to that of original detection with siRNAs.

PTBP1 is a protein implicated in alternative splicing and was one of the 3 genes whose expression is necessary for SASP induction as demonstrated by siRNA- but also shRNA-mediated knockdown. A increase in IF intensity of PTBP1 was observed in 4OHT-induced senescent cells in relation to 4OHT-untreated IMR90 ER:RAS cells. Quantification of this by HTM and HCA showed a temporal induction of PTBP1, which was prevented by expression of the 4 pGIPZ-based shRNAs separately (Figure 4.2a and b). Knockdown of PTBP1 using 4 different shRNAs did not prevent entry into cell cycle arrest as shown by the gradual loss of BrdU incorporation after 4OHT

treatment at a similar rate to the cells infected with an empty vector (Figure 4.2c). In addition, PTBP1 knockdown did not overcome the senescence growth arrest contrary to that observed in cells infected with shRNA against p53 (Figure 4.2c and d). On the other hand, IL-8 production decreased upon PTBP1 knockdown (Figure 4.2e). These observations collectively confirm that the phenotype of cells lacking PTBP1 was not a false positive of the siRNA screen or a result of off-target effects since it was recapitulated by 4 individual shRNAs. For further experiments, the second and third best shRNAs were employed to knock down PTBP1 and study senescence and SASP regulation.

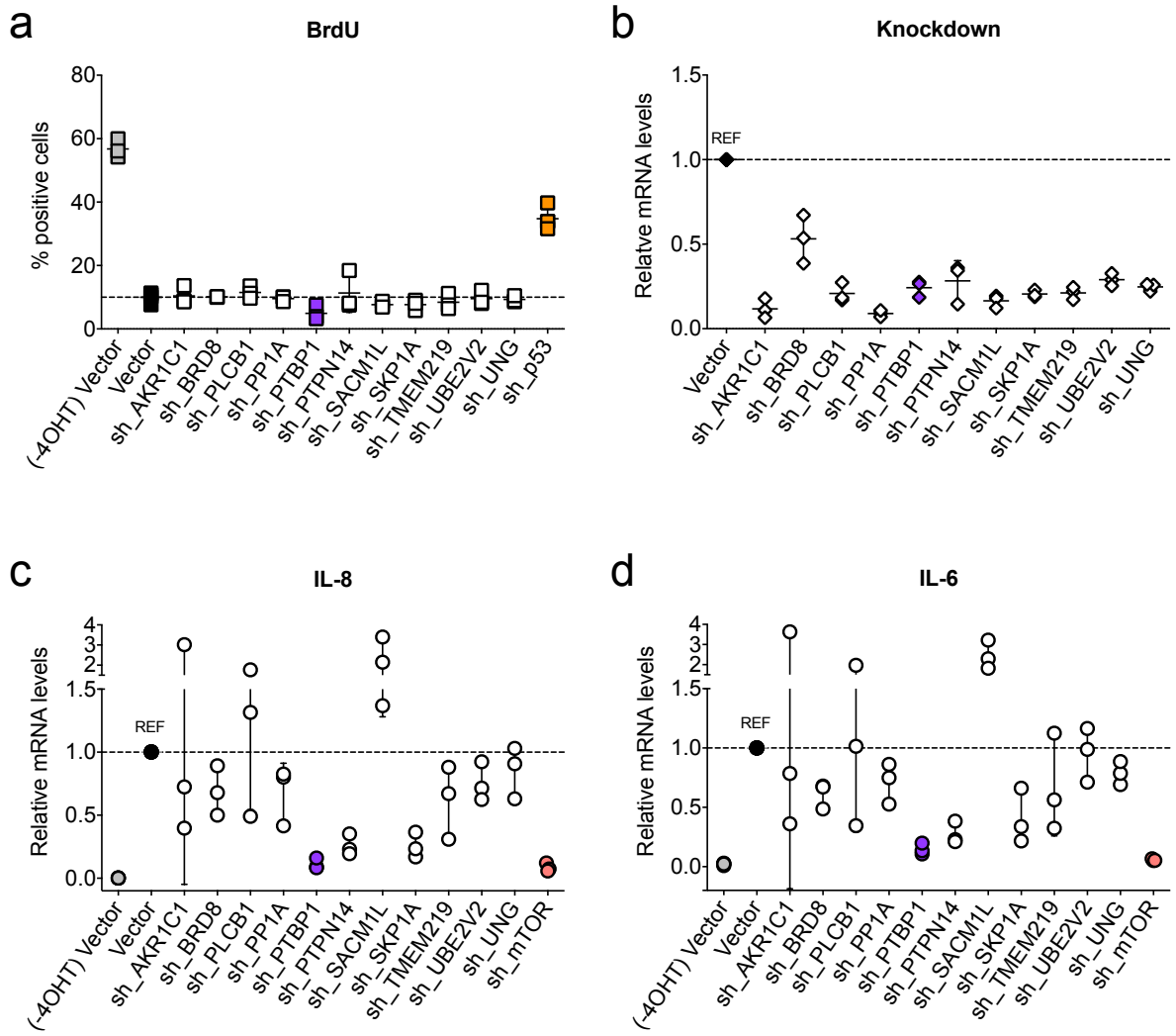

Figure 4.1. Retesting of candidate SASP regulators by shRNA-mediated knockdown.
IMR90 ER:RAS cells were stably infected with an empty pGIPZ vector (Vector) or pools of 4 pGIPZ vectors containing different shRNAs against the indicated genes. After antibiotic selection of cells with stable integration of the vector, the cells were induced with 4OHT. (a) BrdU incorporation was assayed 6 days later by IF coupled to HTM. (b-d) Expression levels of each gene or IL-8 and IL-6 were measured by qRT-PCR 6

days after 4OHT induction. Each point represents the value obtained from each of the 3 independent experiments with vertical lines showing the SD. All samples were treated with 4OHT unless accompanied by (- 4OHT).

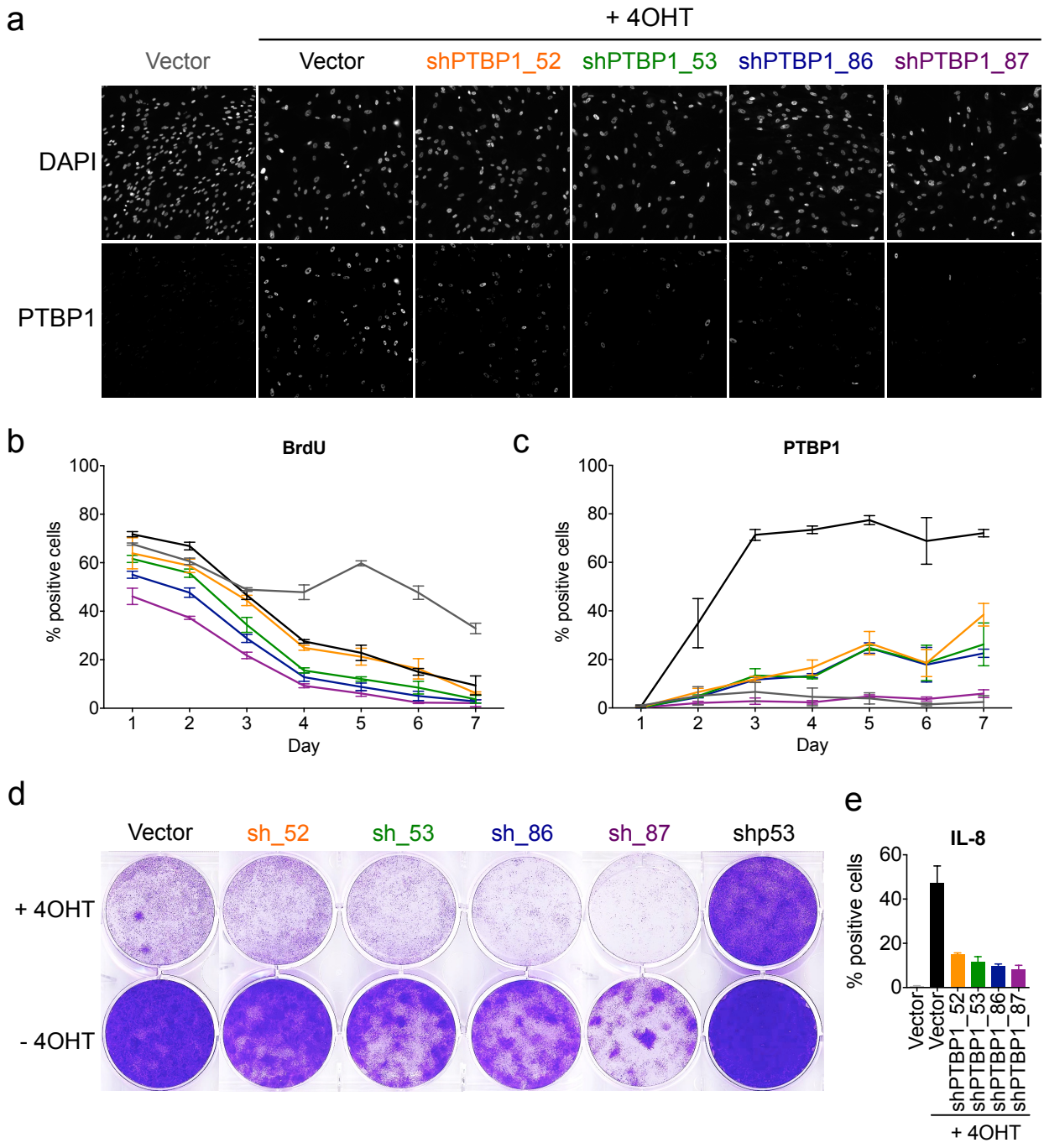

Figure 4.2. Knockdown of PTBP1 with multiple shRNAs does not affect growth arrest but blunts IL-8 induction.

(a) Representative IF images of PTBP1 staining 6 days after 4OHT addition. (b and c) Quantification of PTBP1 and BrdU IF by HTM coupled to HCA at the indicated times after 4OHT treatment. Colour coding based on (a). (d) Crystal-violet stained plates of cells infected with the indicated vectors and fixed 12 days following 4OHT treatment. (e) Percentage of cells staining positive for IL-8 8 days after 4OHT. The numbers are mean values of three replicate wells of a single experiment.

4.2. PTBP1 regulates the SASP but not other senescence phenotypes

To further confirm and examine how PTBP1 affects senescence, other senescence markers were studied and transcription of a variety of SASP factors was assessed upon knockdown of PTBP1 with two of the verified shRNAs. Loss of BrdU incorporation, upregulation of p16, p21, p53, and the senescence-associated DNA damage response were all unaffected by PTBP1 knockdown as opposed to the relative reversal observed in cells expressing shp53 (Figure 4.3a and b). A further confirmation of senescence maintenance in spite of PTBP1 knockdown was achieved by detecting increased SA-β-gal activity in all the senescence conditions in contrast to cells infected with shRNA targeting mTOR, which served as an assay positive control (Figure 4.3c). On the other hand, transcription of the shRNA target, PTBP1, and the majority of SASP factors tested including different Interleukins and MMPs, was impaired upon PTBP1 knockdown mediated by both shRNAs (Figure 4.3d). Interestingly, CCL2 transcription was not affected by PTBP1 knockdown.

Knockdown of PTBP1 slowed down slightly the proliferation of normal cells but the cells did not stop proliferating and there was no upregulation of SA-β-gal activity (Figure 4.2d and Figure 4.4). To determine whether the impact on cell growth was partly responsible for the inhibition of SASP induction, the effect of PTBP1 loss after establishment of senescence and a SASP was investigated. To this end, IMR90 ER:RAS cells already 5 days into senescence, expressing high levels of IL-8 and IL-6 (Figure 3.4b), were reverse transfected with the two best siRNAs targeting PTBP1 from the secondary SASP siRNA screen. The following day, corresponding to 6 days after senescence induction, induction of senescence markers p16 and p21 was confirmed and as well as stable PTBP1 levels (Figure 4.5a). The knockdown of PTBP1 transcripts was validated after 4 days (Figure 4.5b) at which point a reduction of IL-8 and IL-6 transcription was also observed (Figure 4.5b). 2 days later a substantial reduction in IL-8 and IL-6 protein levels was also detected (Figure 4.5c and d). To confirm this result, IMR90 ER:RAS cells were infected with the two shRNAs coupled to GFP in the pRRL vector. The shRNA expression is induced by the release of a transactivator upon doxycycline treatment. Although doxycycline treatment was initiated 5 days after induction of senescence with 4OHT, high levels of PTBP1 were still detectable on the 6th day similar to the post-induction of senescence setting with siRNAs (Figure 4.6a). Partial knockdown of

PTBP1 upon doxycycline induction was observed on the 12th day corresponding to only a partial induction of GFP expression (Figure 4.6b-d). Nevertheless, a reduction in IL-8 and IL-6 transcription was achieved. The suboptimal expression of shRNAs in this system was only observed in cells induced to undergo senescence since non-senescent samples expressed GFP after doxycycline treatment. In spite of such discrepancies, the results confirm those of the siRNA-mediated knockdown suggesting PTBP1 is necessary for maintenance of a SASP.

To understand how general the role of PTBP1 in senescence is, we studied how PTBP1 depletion affected irradiation-induced senescence. In particular, HFFF2 cells, a different fibroblast strain, were infected with two shRNAs against PTBP1 and irradiated to induce senescence. The growth arrest of PTBP1-depleted cells, as assessed by colony formation assays and BrdU incorporation, was similar to vector infected cells and was accompanied by a DDR (Figure 4.7a-c), whereas increased transcription of IL-8 and IL-6 was prevented (Figure 4.7d). Next, we infected IMR90 cells with iCMV-tight vector to allow for the conditional expression of ectopic PTBP1 in a doxycycline dose-response manner. An increase in transcription of IL-8 was observed but not CCL2 (Figure 4.8) in accordance with PTBP1-regulation of the SASP in OIS (Figure 4.3d). However, ectopic expression of PTBP1 eventually resulted in cell death hence this system did not allow for further experimentation. Overall, PTBP1 seems to directly regulate the SASP but not other senescence phenotypes.

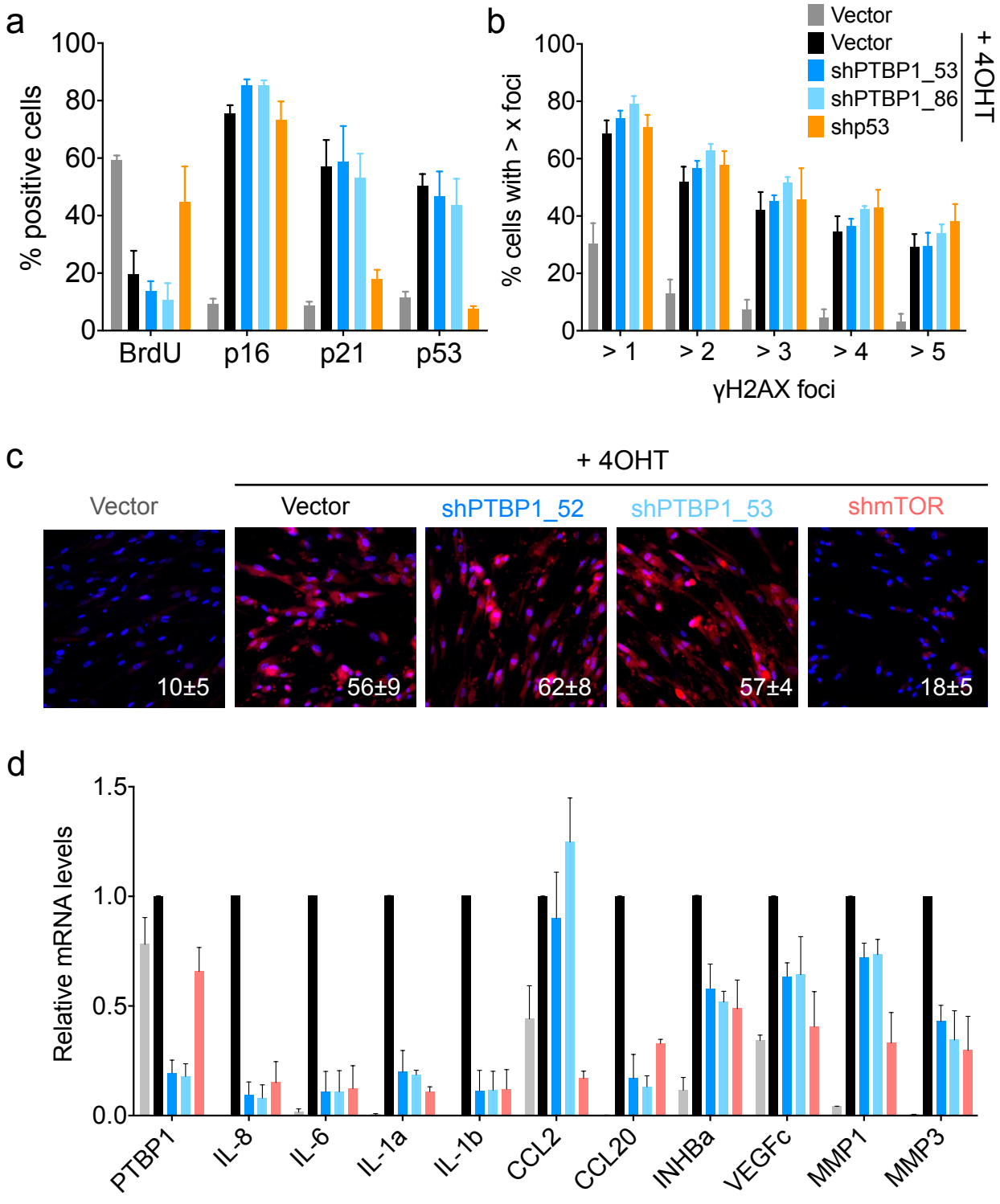

Figure 4.3. Loss of PTBP1 inhibits transcription of multiple SASP factors but not other senescence phenotypes.

(a and b) Percentage of cells staining positive by IF coupled to HTM for the indicated senescence phenotypes 6 days after 4OHT induction. (c) Percentage of cells positive for the fluorescent marker of β-galactosidase activity 9 days after 4OHT induction. (d) Transcription of PTBP1 and the indicated SASP genes was impaired, apart from CCL2, as assessed 6 days post-senescence induction by RT-qPCR. Bars or numbers represent mean values with SD of three experiments.

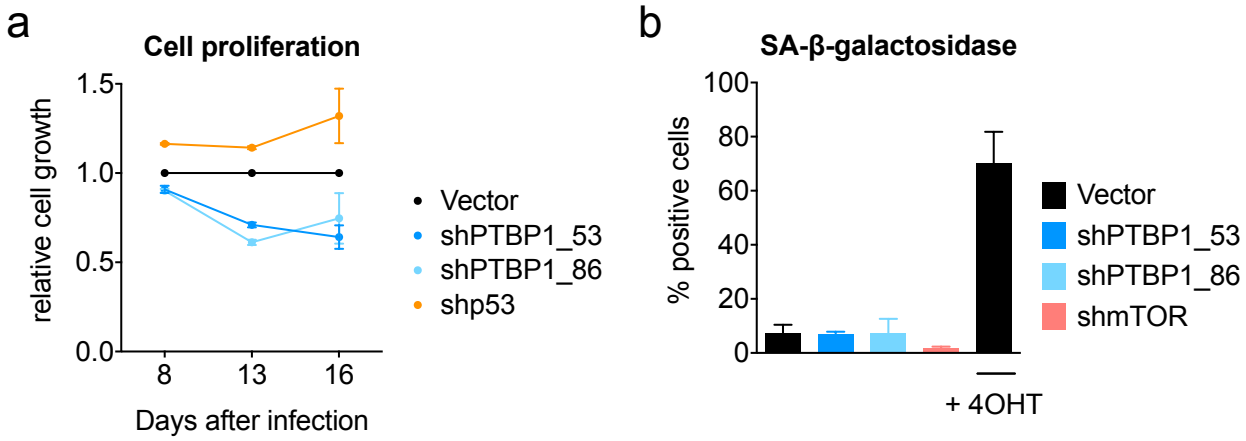

Figure 4.4. PTBP1 knockdown slows down cell proliferation.
IMR90 ER:RAS cells were stably infected with an empty pGIPZ vector (Vector) or pGIPZ vectors containing shRNAs against the indicated genes. For the purpose of these tests, the cells were not induced to undergo senescence unless otherwise specified by + 4OHT serving as a control. (a) Cell proliferation was assessed by BrdU incorporation 8 or 13 days after infection and by colony formation assays 16 days after infection. The results are plotted in relation to empty vector infected cells. (b) Percentage of cells positive for the fluorescent marker of β-galactosidase activity 16 days after infection corresponding to 9 days after 4OHT induction of the positive control. Values represent mean values with SD of two experiments for measurements taken 8 or 13 days after infection and three experiments for measurements taken 16 days after infection.

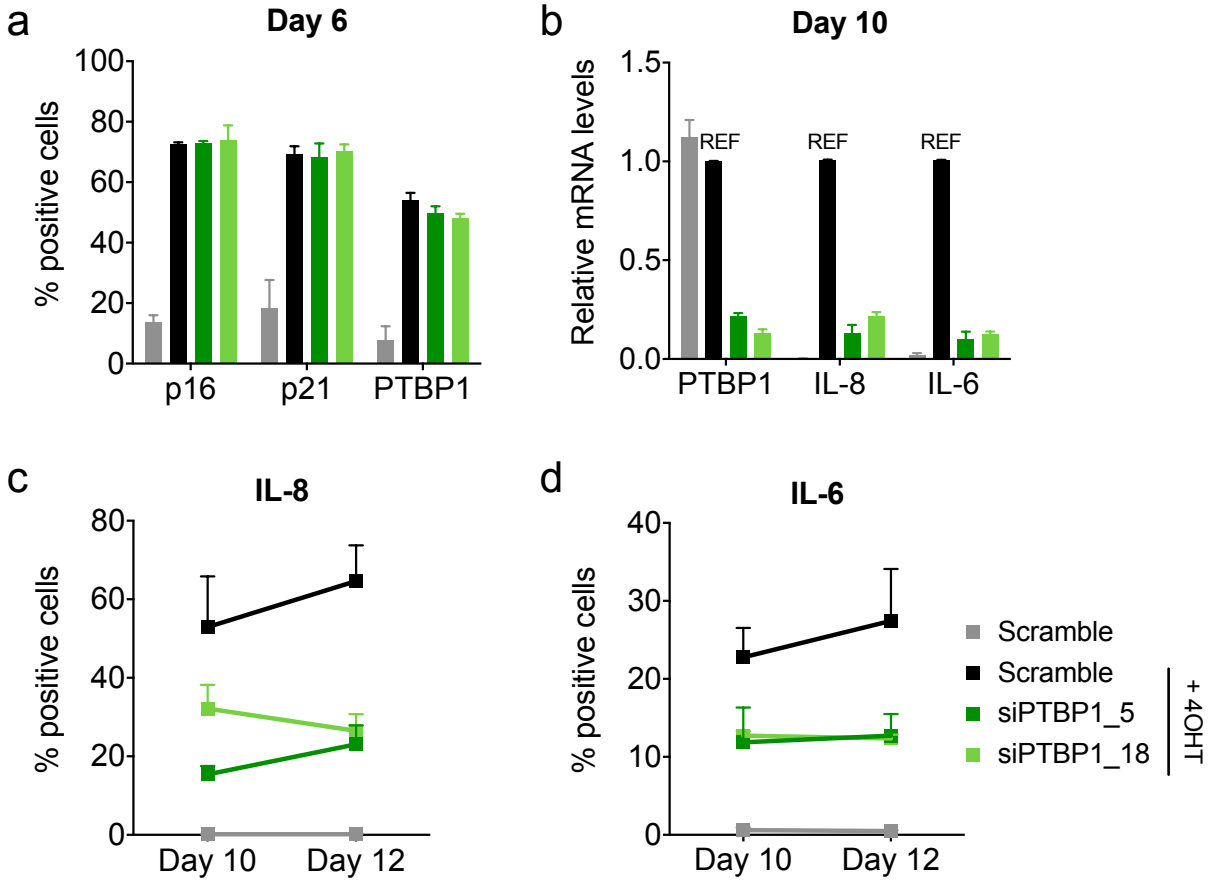

Figure 4.5. PTBP1 is necessary for SASP maintenance.
IMR90 ER:RAS cells were transfected with the indicated siRNAs 5 days after 4OHT-induction of senescence. (a) 1 day later, upregulation of the senescence markers p16 and p21 and of PTBP1 was confirmed by quantitative IF coupled to HTM. (b) Knockdown of transcription of the siRNA target and indicated SASP factors was assessed by qRT-PCR after 5 days corresponding to the 10th day after 4OHT-induction of senescence. (c and d) The percentage of cells staining positive for IL-8 and IL-6 levels was obtained by quantitative IF coupled to HTM on the 10th and 12th day of senescence. The bars or dots are mean values and SD of three experiments.

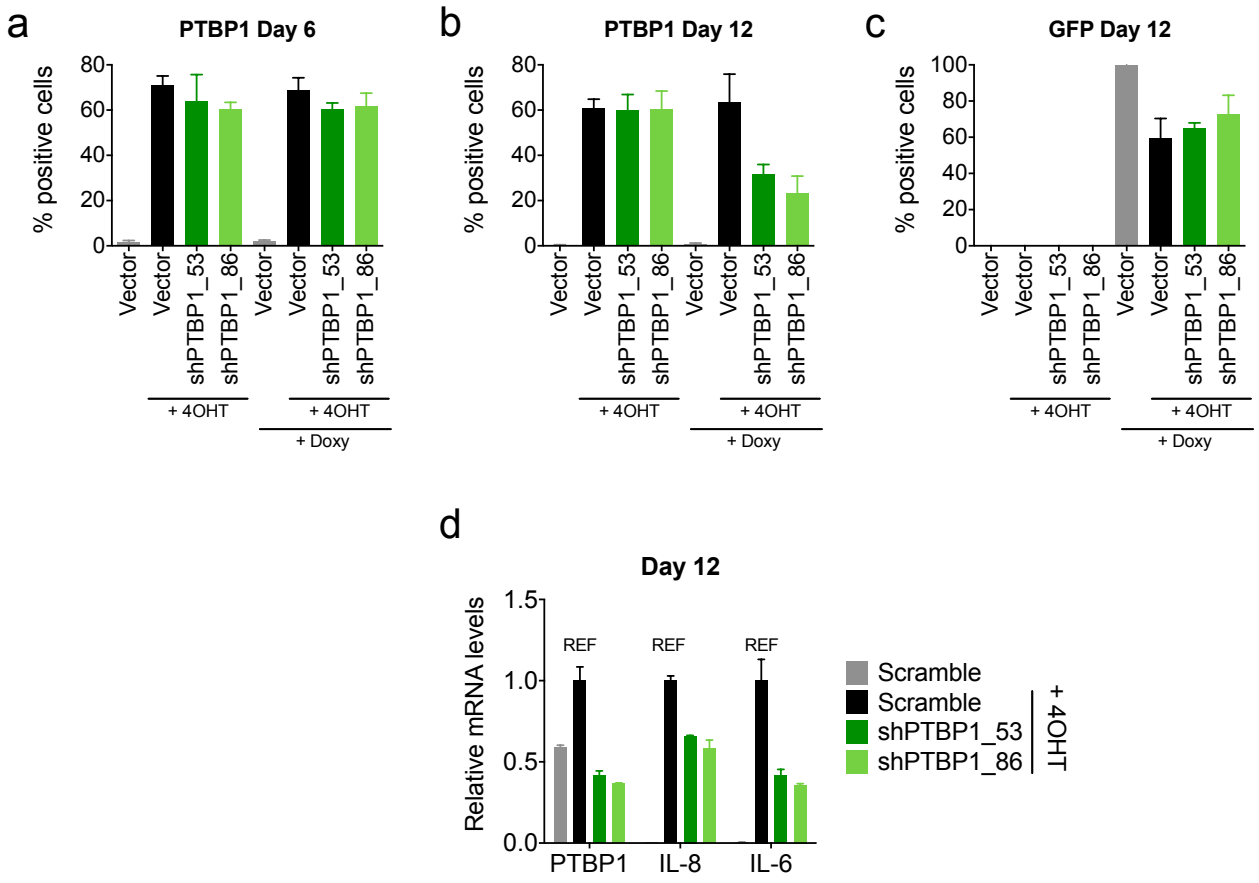

Figure 4.6. PTBP1 is necessary for maintenance of the SASP.
IMR90 ER:RAS cells were stably infected with shRNAs against PTBP1 whose expression is responsive to doxycycline (Doxy) and can be monitored via GFP expression. Doxycycline treatment at a concentration of 2 µg/ml was initiated 5 days after 4OHT-induction of senescence. (a-c) 1 day or 7 days later the percentage of cells staining positive for PTBP1 and GFP were quantified by HCA of IF. (d) Transcription of the siRNA target and indicated SASP factors was assessed by qRT-PCR after 7 days corresponding to the 12th day after 4OHT-induction of senescence. The bars are mean values and SD of three replicate wells of a single experiment.

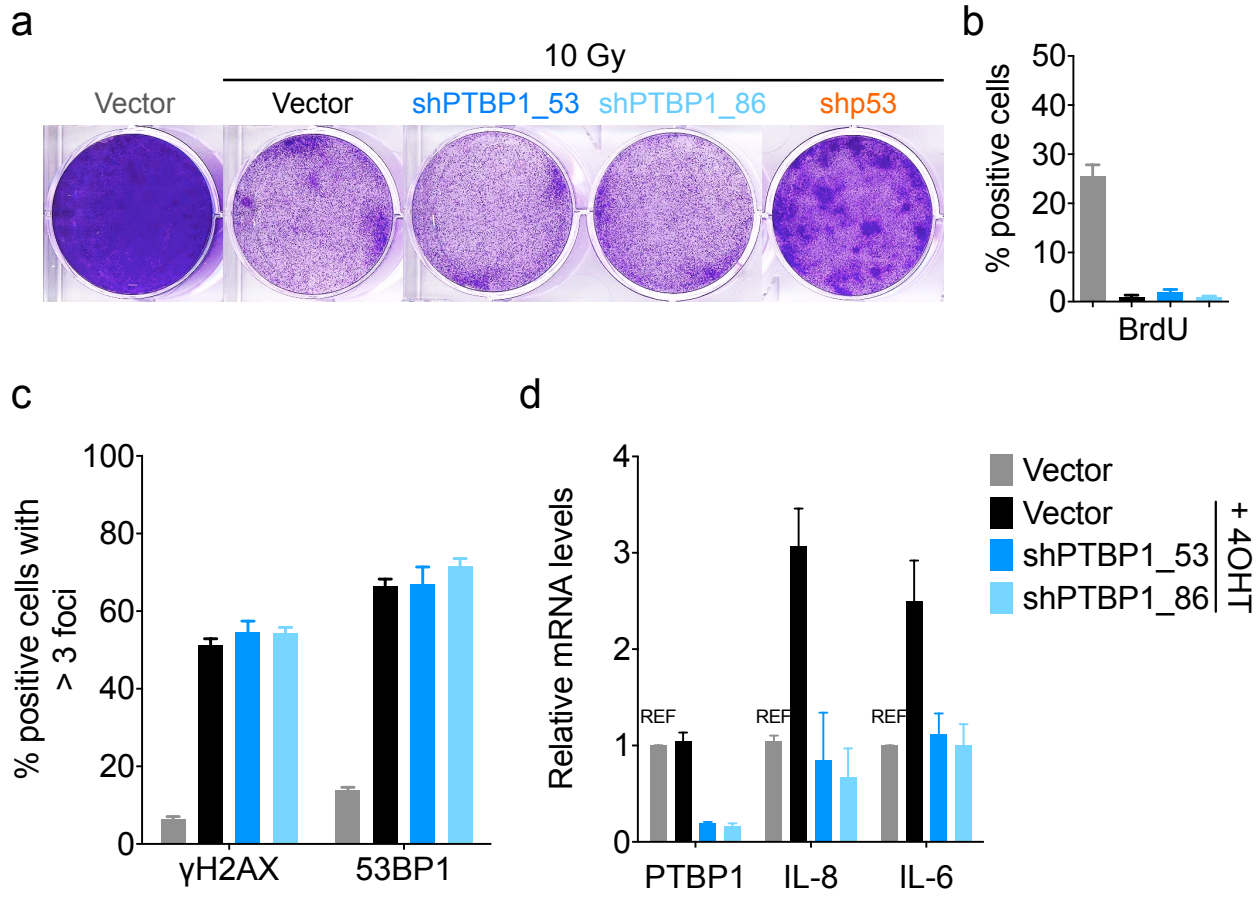

Figure 4.7. PTBP1 is necessary for SASP induction in irradiation-induced senescence.
HFFF2 cells were stably infected with pGIPZ-based shRNAs targeting PTBP1 and were irradiated with 10 Gy. (a) Crystal-violet stained plates of cells infected with the indicated vectors and fixed 14 days following irradiation. (b and c) Percentage of cells staining positive for BrdU and DDR markers 5 days after irradiation. (e) Transcription of the indicated genes 9 days after irradiation. The numbers are mean values and SD of three experiments performed simultaneously.

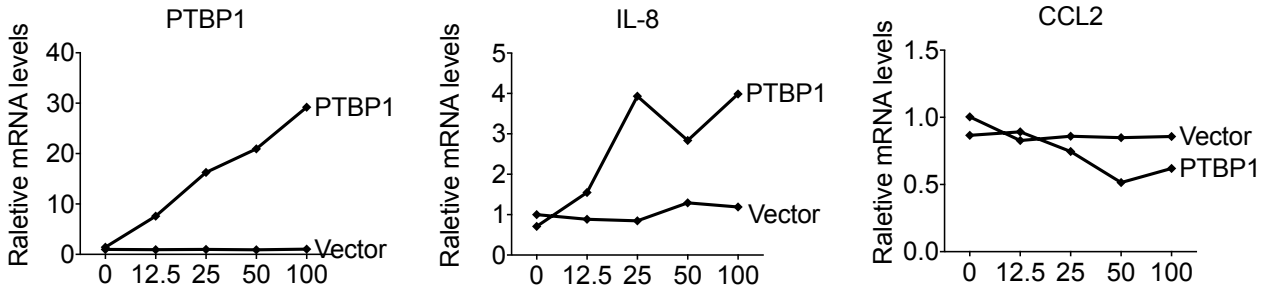

Figure 4.8. Ectopic expression of PTBP1 induced IL-8 transcription.
Increasing concentration of doxycycline (x-axis in ng/ml) respectively induces PTBP1 transcription in relation to the cells infected with an empty vector. Increase in transcription of the target IL-8 but not of CCL2 was also confirmed. Transcription was assessed by qRT-PCR 2 days following initiation of treatment.

4.3. PTBP1 regulates a subset of the SASP

To catalogue the SASP factors specifically regulated by PTBP1, a global and unbiased approach was undertaken. We used label-free mass spectrometry (MS) to analyse the secreted factors present in the media conditioned by growing cells, 4OHT-induced senescent cells or cells 4OHT-induced but lacking PTBP1 or mTOR via shRNA-mediated knockdown. Following global identification of factors, a list of SASP components was generated by applying a filter to include factors common to a published list produced by other members of our group who employed a similar technique (Acosta et al., 2013; Herranz et al., 2015). A visual representation of the differential levels of the SASP factors detected across conditions suggested that from the 55 upregulated factors upon senescence, the production of 22 of those commonly depends on PTBP1 and mTOR including chemokines, interleukins, MMPs, IGFBPs and others (Figure 4.9a). On the other hand, there were 6 SASP factors solely downregulated as a result of mTOR knockdown and 13 uniquely downregulated as a result of PTBP1 knockdown (Figure 4.9b).

To examine the functional implications of a differential SASP caused by loss of PTBP1 or loss of mTOR, two assays were performed. Initially, the ability to induce SASP production and paracrine senescence was investigated. IMR90 cells were treated with CM from proliferating cells, 4OHT-induced senescent cells, senescent cells depleted of PTBP1 using two shRNAs and senescent cells depleted of mTOR. The induction of paracrine senescence observed in cells treated with CM from senescent cells was partially repressed in cells treated with CM from the knockdown senescent cells. Specifically, CM originating from PTBP1 and mTOR knockdown conditions was not sufficient to induce a comparable loss of BrdU incorporation or upregulation of the SASP components IL-8 and IL-6, of the CDKI p21 and the DDR signified by γH2AX (Figure 4.10). Although *in vitro* paracrine senescence was previously found to depend on TGFβ and CCL2 (Acosta et al., 2013), these two factors were differentially regulated by PTBP1 and mTOR. TGFβ secretion was negatively affected by the absence of PTBP1 and CCL2 secretion was negatively affected by mTOR but not reciprocally (Figure 4.9a). Either both factors are very important or the presence of other factors, commonly regulated by PTBP1 and mTOR, are equally necessary for transmitting senescence to normal cells.

CCL2 is an important mediator of senescent cell clearance through the attraction of immune cells such as NK cells (Iannello et al., 2013; Xue et al., 2007). To test the ability of the remaining SASP, still rich in CCL2 after PTBP1 loss, to mediate such an important function, the chemotaxis of NK92 cells was explored. CM collected from the different cells were placed at the bottom of a chamber and the migration of NK92 cells from the top and through a membrane was recorded (Figure 4.11a). The migration of NK92 cells towards CM generated by PTBP1-knockdown senescent cells was equivalent to that in response to vector senescent CM (Figure 4.11b). Conversely, CM generated by mTOR-knockdown senescent cells did not retain the full ability to cause migration. This finding is in line with the important role of CCL2 in attracting immune cells but does not preclude the possibility that other factors are also key players. Also, this finding does not ensure that CCL2-mediated NK cell recruitment will be sufficient to kill senescent cells *in vivo*. Overall, these findings point to the possibility of targeting SASP regulators to exploit the different functions that senescent cells exert on the microenvironment.

a

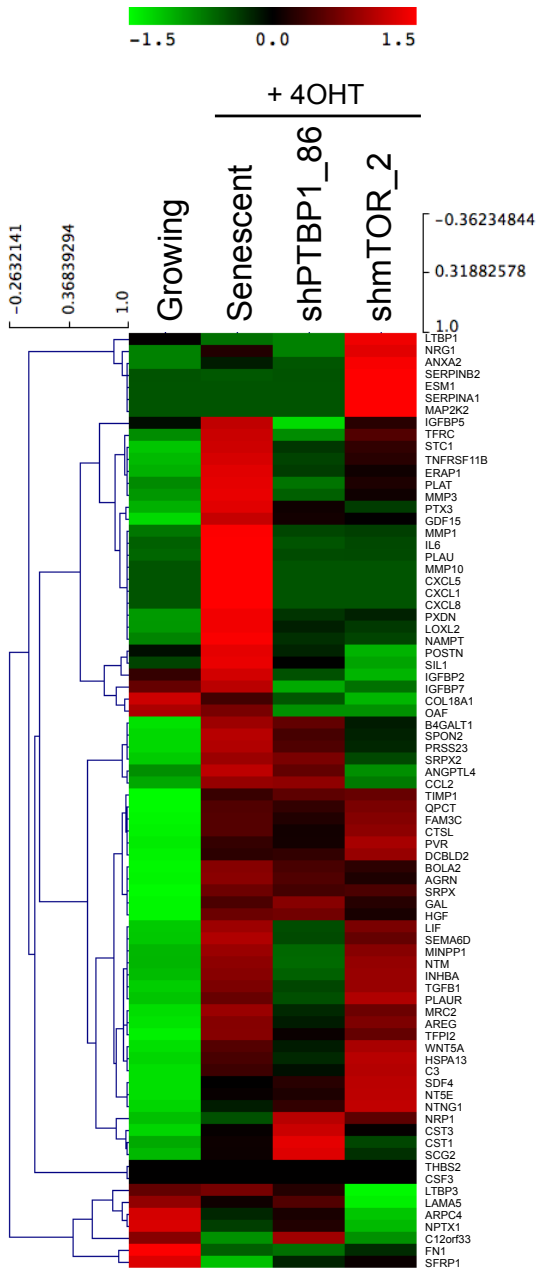

b

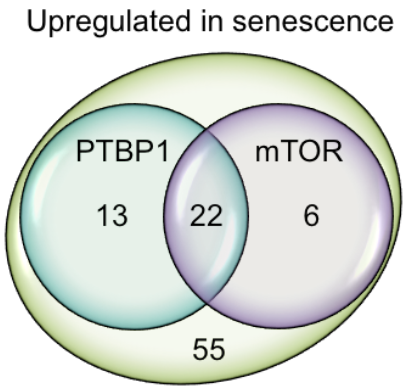

Figure 4.9. PTBP1 and mTOR differentially regulate the SASP.

(a) Unsupervised hierarchical clustering of the differential secretion of the enlisted SASP factors shown as a mean of three replicate experiments. The value of each factor is normalised to the overall peptide count detected within that sample. (b) Overlap of SASPs that depend on PTBP1 and mTOR.

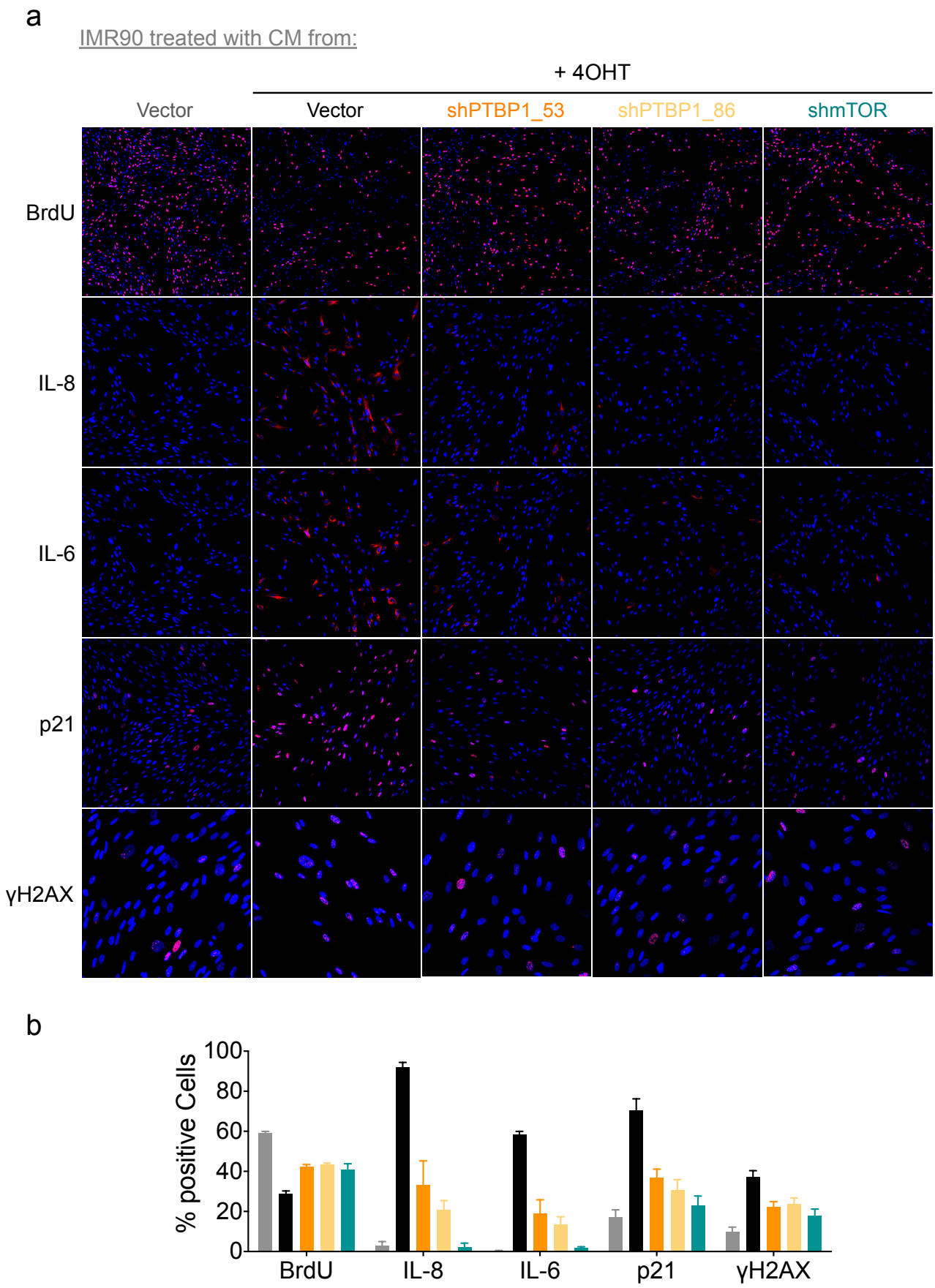

Figure 4.10. PTBP1 and mTOR regulate the secreted factors responsible for paracrine senescence.

(a) Representative IF images of the indicated markers expressed by IMR90 cells treated for 3-4 days with media conditioned by the specified senescent states. (b) Percentage of cells staining positive for the senescence markers as quantified by IF coupled to HTM. Colour coding as per (a). Bars of BrdU, IL-8 and IL-6 represent mean values and SD of three experiments and bars of p21 and γH2AX represent mean values with SD of two experiments. Each replicate experiment corresponds to independent generation of CM.

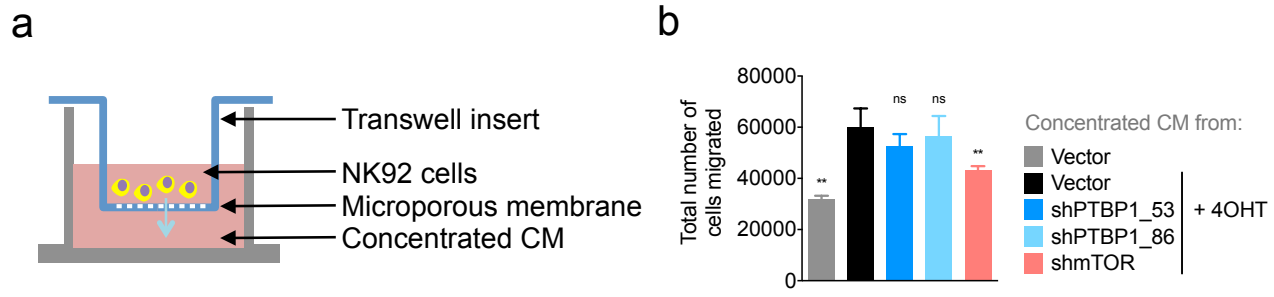

Figure 4.11. The SASP from PTBP1-deficient cells is sufficient to attract NK92 cells
(a) Abstract of the experimental setting. (b) Number of cells migrated towards the lower chamber after 18 hours as counted using the Guava flow cytometry system. Bars are mean values with SD of three experiments. Each replicate experiment corresponds to independent generation of CM. One-way ANOVA, Dunnett's test, comparing the mean of each sample to 'Vector + 4OHT' was carried out to test significance of difference. ns = not significant, ** = $p < 0.01$.

4.4. PTBP1-mediated AS during senescence regulates the SASP

Senescent cells do not show an increase in the levels of PTBP1 expression (Figure 4.3d) or production (Figure 4.12a) but exhibit higher nuclear PTBP1 levels as detected by IF (Figure 4.2a). This suggests a change in localisation and possibly a functional role of PTBP1 in the nucleus. In the absence of PTBP1 cells are able to undergo senescence but show an altered SASP. To investigate how PTBP1 regulates the SASP, first the levels and activation of known SASP regulators were tested. The total levels of the downstream Ras effectors MAPKAPK2 and p38 remained unchanged in cells lacking PTBP1 so did the activation of MAPKAPK2 by phosphorylation and stabilisation of ZFP36L1 (Figure 4.12a). The upregulation of the important SASP inducer C/EBPβ is easily monitored by IF but was again not significantly altered by PTBP1 knockdown, whereas p53 knockdown resulted in lower C/EBPβ levels in relation to vector senescent cells (Figure 4.12c). To examine NF-κB activation, IMR90 cells were stably infected with a lentivirus vector containing NF-κB transcriptional response elements (TRE) fused to GFP (a kind gift from Prof. Andrei Gudkov; Natarajan et al., 2014). The cells were treated with TNFα to induce activation of NF-κB. GFP expression was measured by HTM and HCA over time showing activation of the reporter within 2 hours (Figure 4.13) and was detected in the majority of the cell population within 8 hours. GFP expression progressively decreased in the next few days possibly due to dilution of infected cells because of inability to select against uninfected cells using antibiotics. Nevertheless, this cellular system served to monitor NF-κB activity showing siRNA-mediated knockdown of the NF-κB subunit p65 prevented GFP induction whereas knockdown of PTBP1 did not significantly alter the kinetics of NF-κB activity (Figure 4.13b).

PTBP1 regulates AS of mRNAs. To investigate AS events resulting from PTBP1 loss, we performed global mRNA sequencing of IMR90 ER:RAS cells proliferating, senescent or senescent but PTBP1-deficient via two separate shRNAs. Each condition was replicated 3 times. First, we confirmed that the spliceosome machinery is all in all not affected transcriptionally, by examining the differential expression of a list of genes corresponding to core and non-core spliceosomal factors (Figure 14) (Agafonov et al., 2011; Hegele et al., 2012). One striking difference was the increased expression of PTBP2 upon PTBP1 knockdown (Figure 4.14b). The upregulation of

PTBP2 confirmed that PTBP1-specific alterations in gene expression were detectable. It has previously been shown that the presence of PTBP1 promotes degradation of PTBP2 mRNA by NMD hence in the absence of PTBP1 stabilisation of PTBP2 mRNA is expected (Spellman et al., 2007).

Given that general splicing is not affected by loss of PTBP1, Thomas Carroll (MRC CSC Computing and Bioinformatics facility) employed the Multivariate Analysis of Transcript Splicing (MATS) method to catalogue the alternative splicing events altered by 20% across the different conditions. From the 5 possible alternative splicing events, namely skipped exon (SE), retained intron (RI), mutually exclusive exon (MXE), alternative 5' (A5 SS) or 3' splice site (A3 SS), the majority of changes were observed in the list of whole exon inclusion or skipping (SE) upon PTBP1 knockdown in both shRNA conditions (Figure 4.15a). Taking a closer look at the direction of exon splicing, more than 60% of exon events in senescence exceeded the 20% loss of inclusion signifying an increase in exon skipping (Figure 4.15b). On the other hand, more than 57% of exon events in PTBP1-deficient senescent cells denoted exon inclusion. These observations are in line with the published role of PTBP1 on promoting exon skipping.

The exon events that significantly changed upon PTBP1 depletion by at least 20% in relation to senescence were shortlisted. Certain exon events were induced solely upon PTBP1 knockdown and showed no change in senescent cells compared to proliferating cells. Exon events belonging to this category and changing more than 40% were shortlisted as well (Figure 4.15c). 31 genes contained an exon that was skipped upon senescence but included in the absence of PTBP1 while 4 genes contained an exon that was included upon senescence but skipped in the absence of PTBP1. 4 genes contained an exon whose inclusion was enhanced upon PTBP1 knockdown. The additional genes that were shortlisted from the 40% change exons upon PTBP1 loss were: 42 genes showing exon inclusion and 19 genes showing exon exclusion. Certain genes such as TPM1 were represented by multiple exons showing inclusion and exclusion reversal. Functional gene clustering analysis using the online portal DAVID revealed that many of these genes encode proteins involved in intracellular transport and localisation (Figure 4.16).

To determine whether there is an alternatively spliced gene or group of genes that is responsible for the altered SASP after PTBP1 loss, a screen approach was taken. The siRNA screening approach for SASP regulators was recapitulated using a library of 4 siRNAs per gene targeting the 95 shortlisted PTBP1-alternatively spliced candidates identified from mRNA profiling. The readouts were again IL-8 and IL-6 and the normalisation method employed was the control-based NPI. An arbitrary cut-off of below 0.4 and above 1.2 NPI was chosen to group the genes altering both IL-8 and IL-6 in relation to scramble siRNA-transfected cells with multiple siRNAs (Figure 4.17a). 53 genes were selected in this manner and 13 were further shortlisted on the basis of adequate cell survival, implication in protein localisation and transport, and lowest or highest NPI accordingly with all the siRNAs. From the 13 genes, the alternative splicing of 10 of them was verified by PCR amplification of cDNA using primers annealing to regions flanking the exon of interest. The PCR product was separated by gel electrophoresis and the percentage of the longer fragment i.e. an exon 'spliced in', within both isoform possibilities was calculated (Figure 4.17b). In 9 of 10 confirmed cases, the longer fragment predominated indicating exon inclusion in both PTBP1 shRNA infected cells in comparison to empty vector senescent cells. One of them induced exon skipping in line with the direction predicted by the MATS analysis.

Finally, to rule out any genes regulating the SASP regardless of isoform and strengthen the causal link between PTBP1 and a particular AS event in senescence, a phenotype rescue experiment was performed. Following transfection of a previously confirmed siRNA targeting PTBP1, the IMR90 ER:RAS cells were induced to undergo senescence and transfected with antisense oligonucleotides (AONs) to enforce skipping of an exon otherwise being included upon PTBP1 knockdown. The levels of IL-8 and IL-6 were measured showing that reversal of multiple independent AS events partially rescued the downregulation caused by PTBP1. 2 of the 5 most consistent exon skipping events that rescued the PTBP1-dependent phenotype were splicing of EXOC7 and SNX14. AON-induced exon skipping in those two genes was validated by PCR amplification of cDNA (Figure 4.19). Overall, we found that PTBP1 promotes exon skipping of several genes encoding proteins involved in intracellular molecular transport such as EXOC7 and SNX14. Specific isoforms of these are necessary for IL-8 and IL-6 induction during senescence.

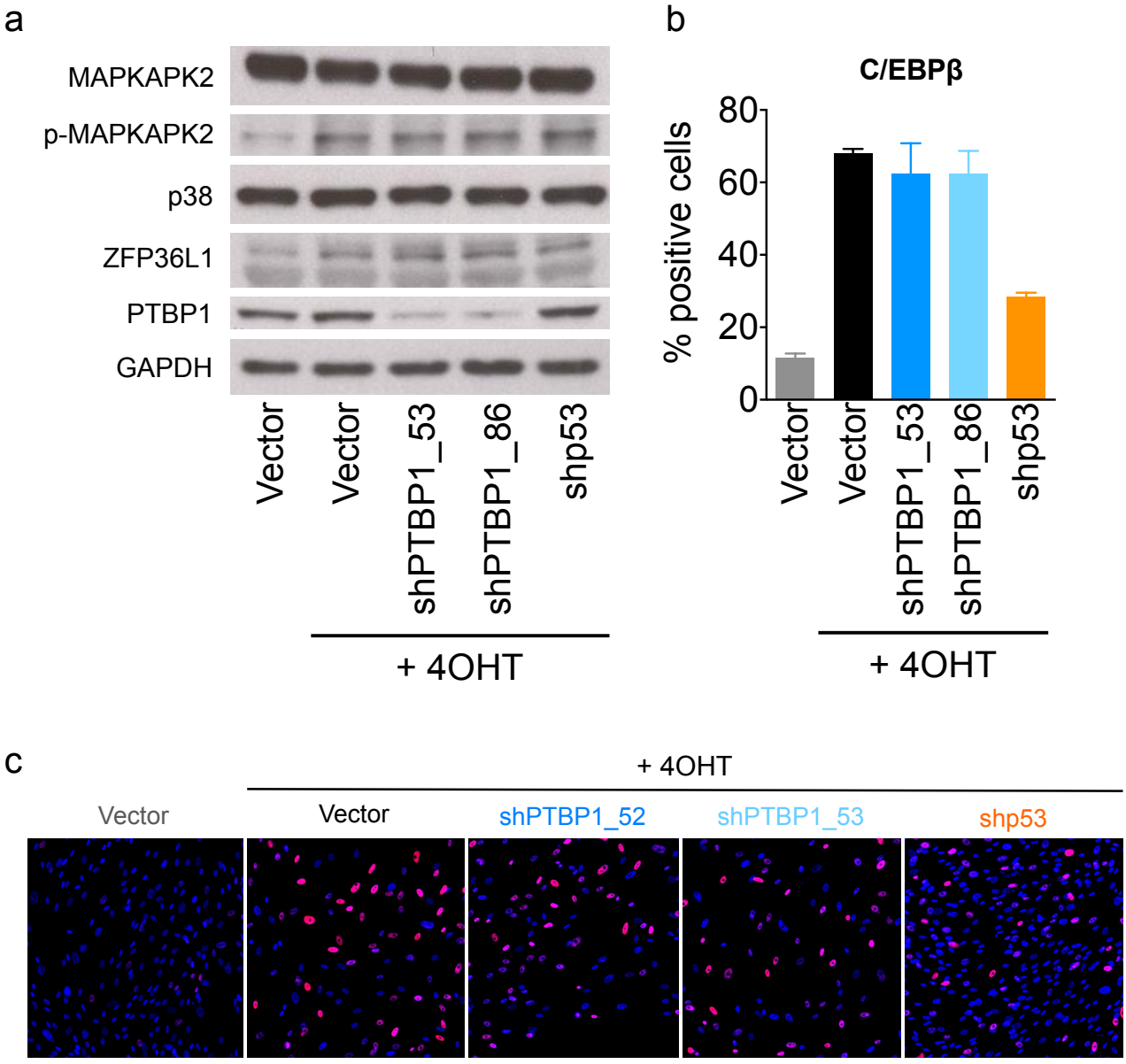

Figure 4.12. PTBP1 does not affect known SASP regulators.
IMR90 ER:RAS cells were stably infected with an empty pGIPZ vector (Vector) or pGIPZ vectors containing shRNAs against PTBP1 and p53. (a) Immunoblots of total cell lysates 6 days following 4OHT induction of senescence. GAPDH was tested as an indicator of sample concentration variability. (b) Percentage of cells staining positive for C/EBPβ as quantified by IF coupled to HTM. Bars show mean values with SD of three replicate wells of a single experiment. (c) Representative IF images of C/EBPβ staining used for quantificiation in (b).

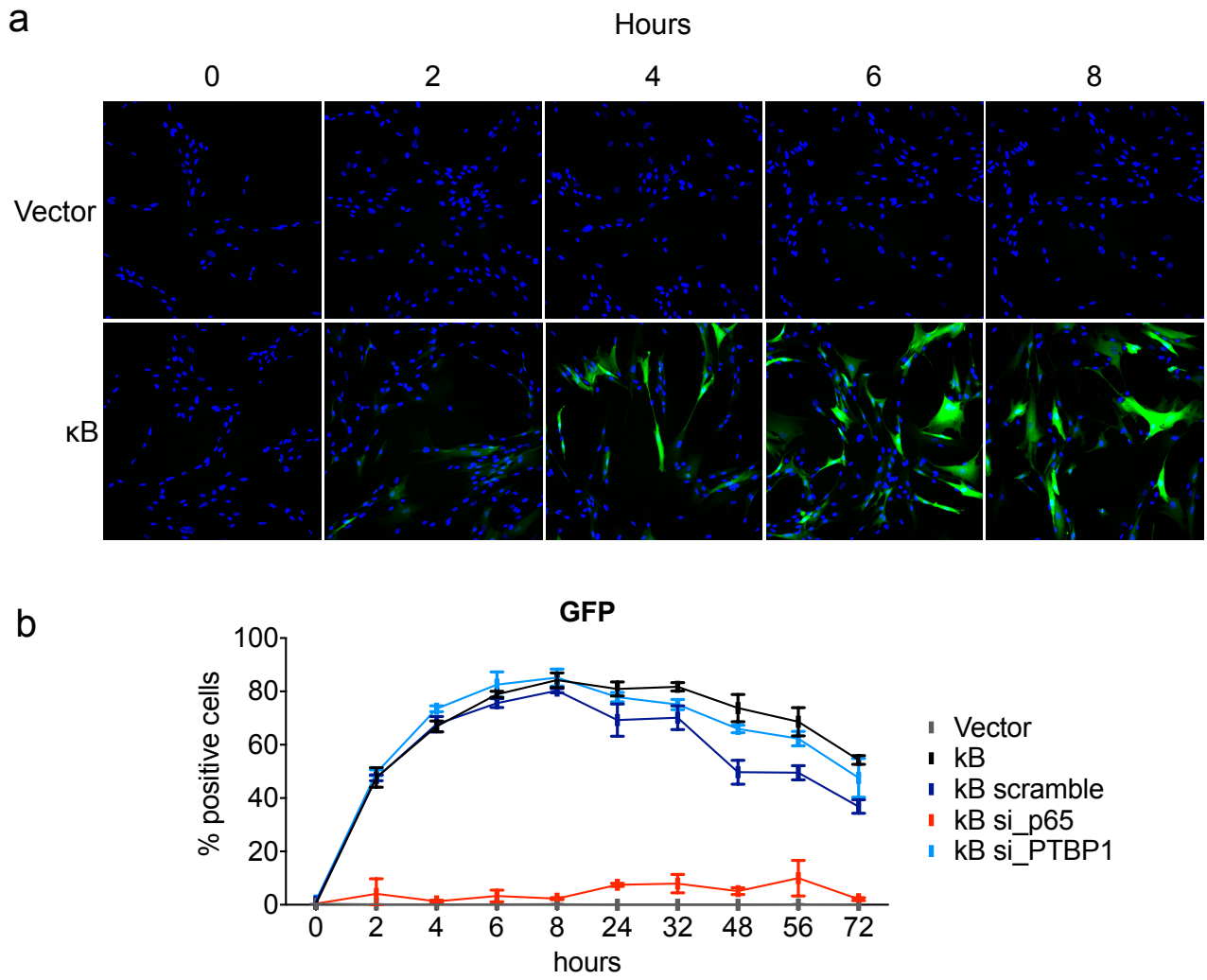

Figure 4.13. PTBP1 does not regulate NF-κB activity directly.
IMR90 cells were stably infected with pRTR-mCMV-copGFP (denoted as Vector) or pRTR-NF-κB-mCMV-copGFP (denoted as κB). 3 days later the cells were plated on 96-well plates and 3 days after induced with 50 ng/ml of TNFα. GFP expression was measured by IF imaging with the InCell HTM system over time. (a) Representative IF images of the first day of TNFα treatment to confirm efficiency of detection. (b) 3 days prior to TNFα treatment initiation, the infected cells were transfected with siRNAs targeting the indicated genes. Graph shows kinetics of GFP expression with time = 0 being time of TNFα addition. The values are mean and SD of two independent experiments up to time = 8 hours from which point values are mean and SD of three replicate wells of a single experiment.

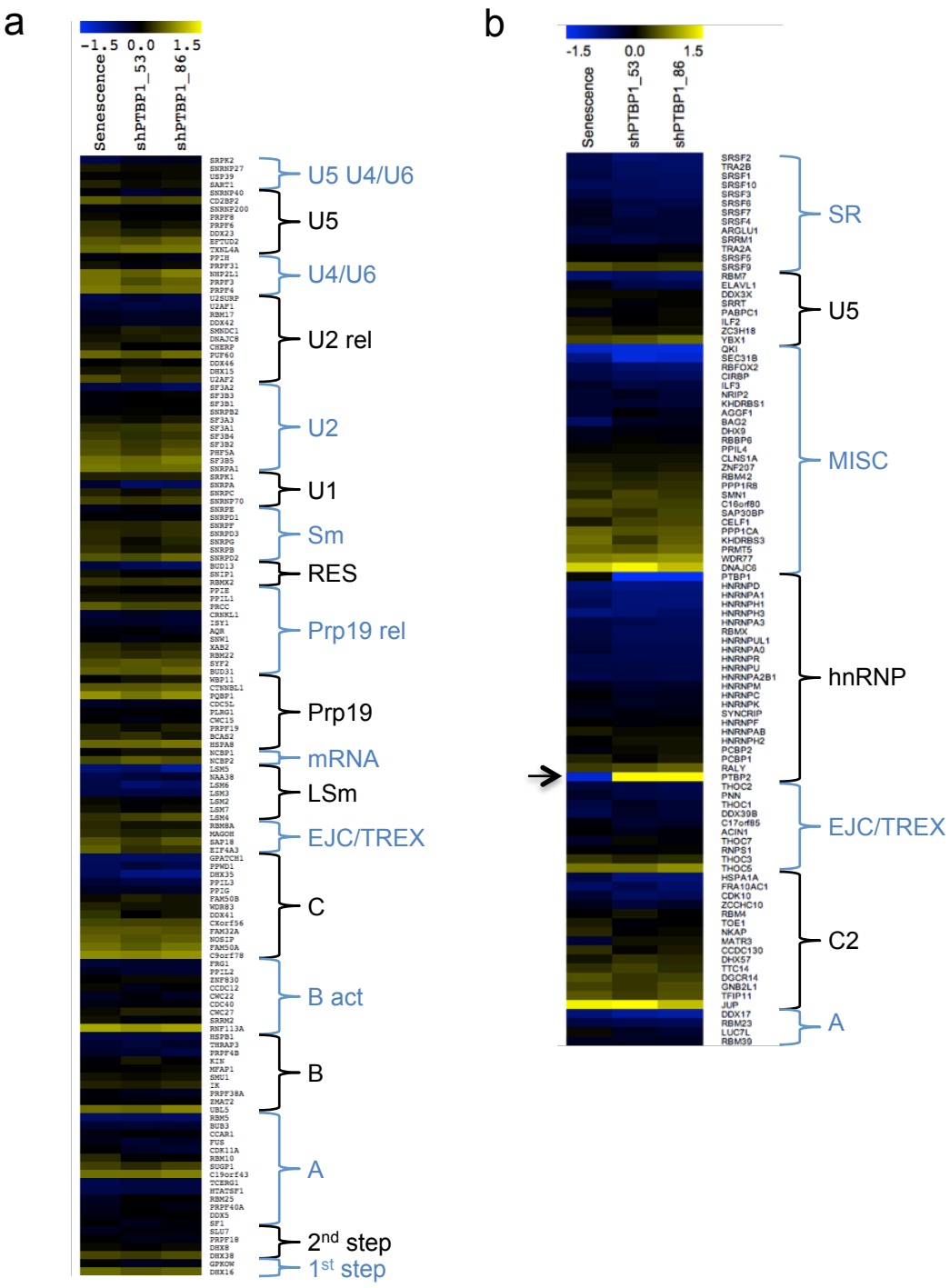

Figure 4.14. Ablation of PTBP1 does not alter the expression of components of the spliceosome. IMR90 ER:RAS cells were stably infected with an empty pGIPZ vector or pGIPZ vectors containing shRNAs against PTBP1 and were induced to undergo senescence with 4OHT. 5 days later global mRNA profiling was performed. Heat-maps showing log2 differential expression of core (a) and non-core (b) spliceosome genes in each sample compared to proliferating vector cells. In (b), the arrow indicates expression of PTBP2.

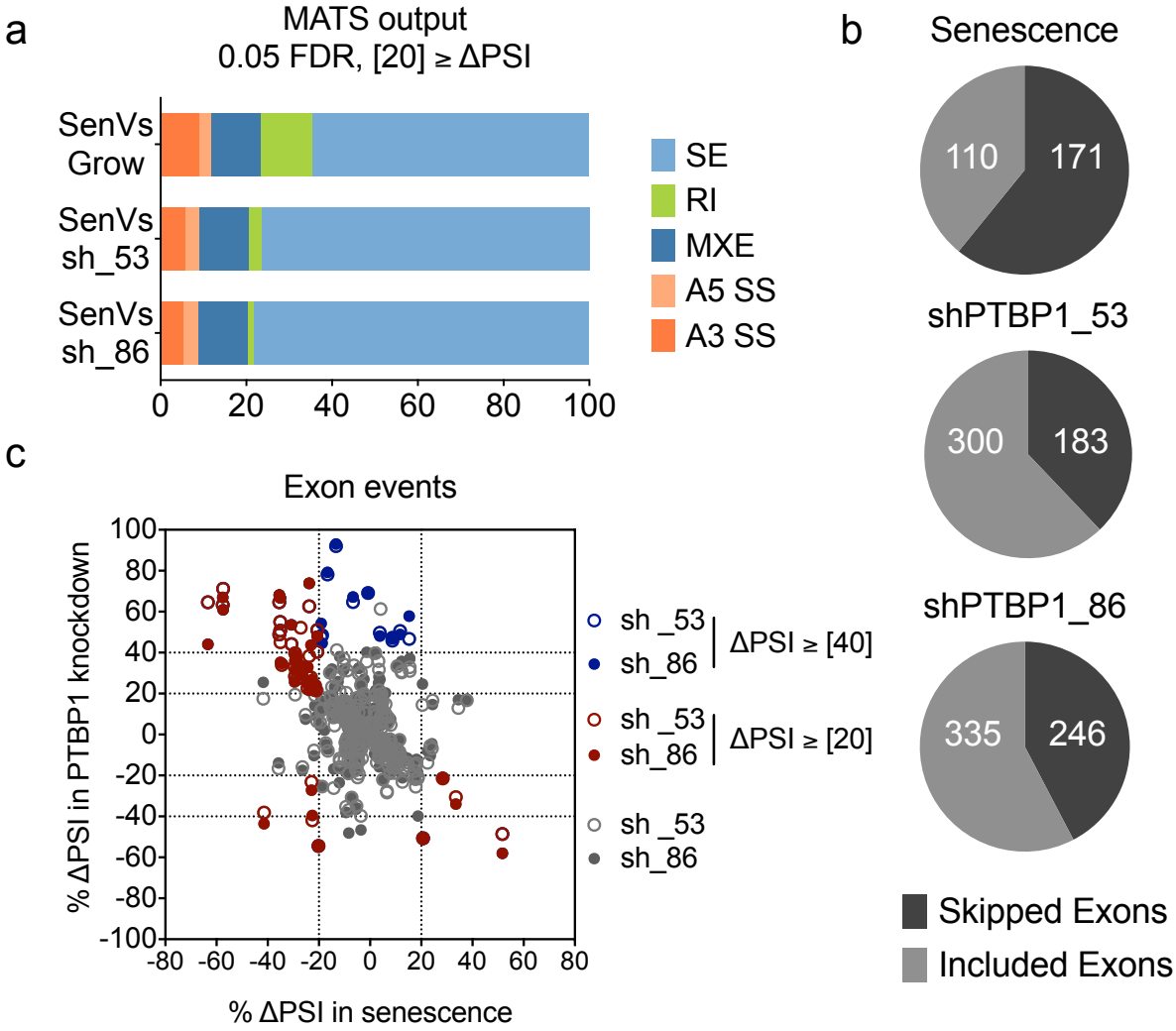

Figure 4.15. PTBP1 regulates AS during senescence.
IMR90 ER:RAS cells were stably infected with an empty pGIPZ vector or pGIPZ vectors containing shRNAs against PTBP1 and were induced to undergo senescence with 4OHT for samples 'Sen', 'sh_53' and 'sh_86' respectively. 5 days later global mRNA profiling was performed and MATS analysis. (a) The total number of each AS event in each sample compared ('Vs') to another is plotted as a percentage within all 5 AS events. For abbreviations of AS events refer to text. (b) Number of exons within the SE group of (a). (c) ΔPSI cut-offs used for shortlisting AS events changing due to loss of PTBP1. For explanation of ΔPSI refer to Figure 2.2.

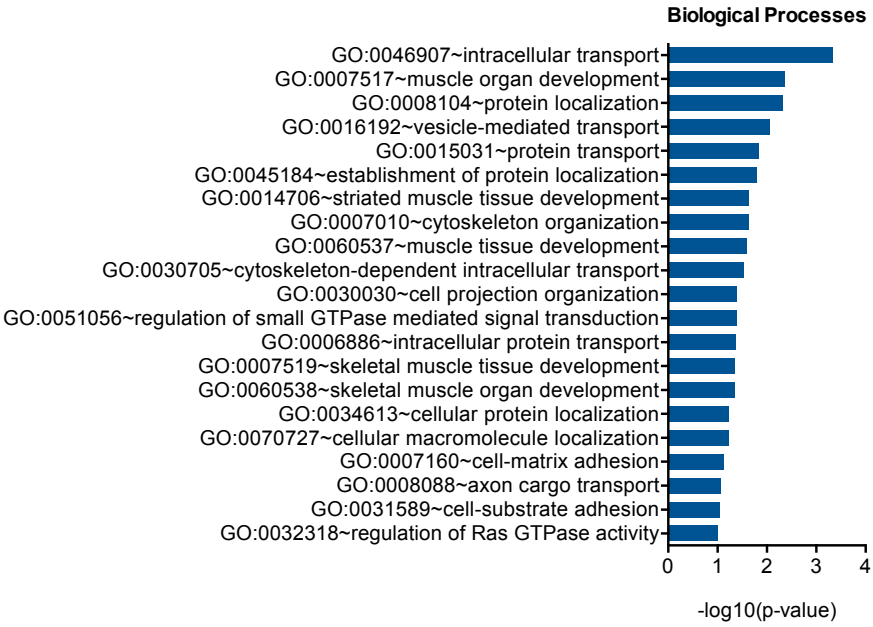

Figure 4.16. Many PTBP1-dependent AS events occur in genes that fall into intracellular transport categories.

GO term analysis of 95 genes having exons with substantially different splicing levels after PTBP1 loss. The online Bioinformatics database DAVID was used.

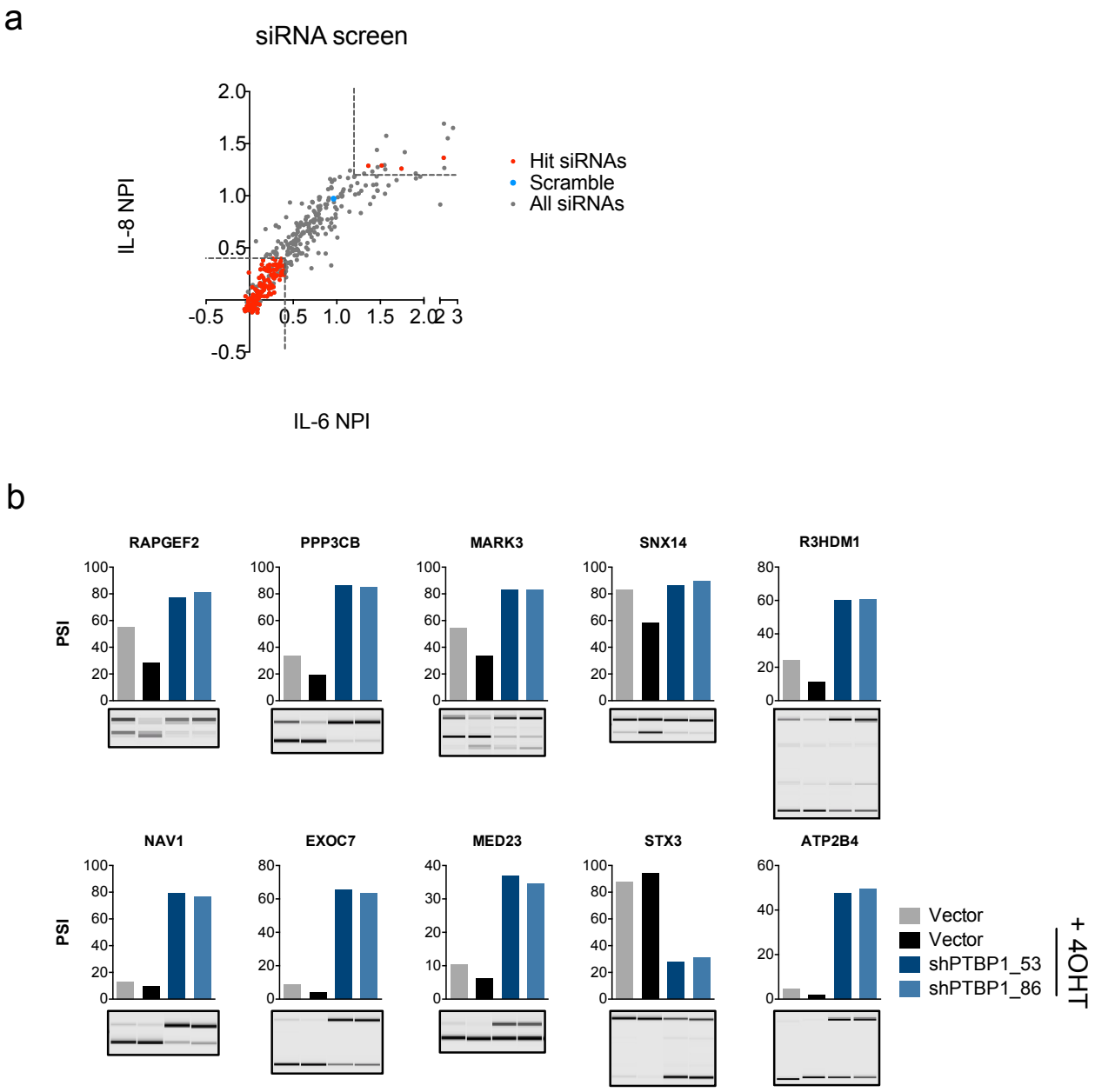

Figure 4.17. Shortlisting and confirming PTBP1-dependent AS events affecting SASP expression. (a) IMR90 ER:RAS cells were reverse transfected onto 96-well plate siRNA library collections targeting the 95 PTBP1-alternatively spliced genes with 4 siRNAs against each. The following day the cells were treated with 4OHT to initiate Ras-induced senescence and 8 days later were fixed and stained for IL-8 and IL-6 IF analysis. Rapid image acquisition and quantification was achieved by the HTM system IN Cell Analyzer 2000. All data were normalised by NPI. Dotted lines show cut-offs for selection of hits as described in the text. Hit siRNAs represent siRNAs targeting genes scoring with more than 2 siRNAs in both readouts. (b) IMR90 ER:RAS cells were stably infected with an empty pGIPZ vector or pGIPZ vectors containing shRNAs against PTBP1 and were induced with 4OHT. 6 days later RNA was retrotranscribed and AS was analysed by PCR amplification followed by Bioanalyzer gel analysis. PSI = Percent Spliced In.

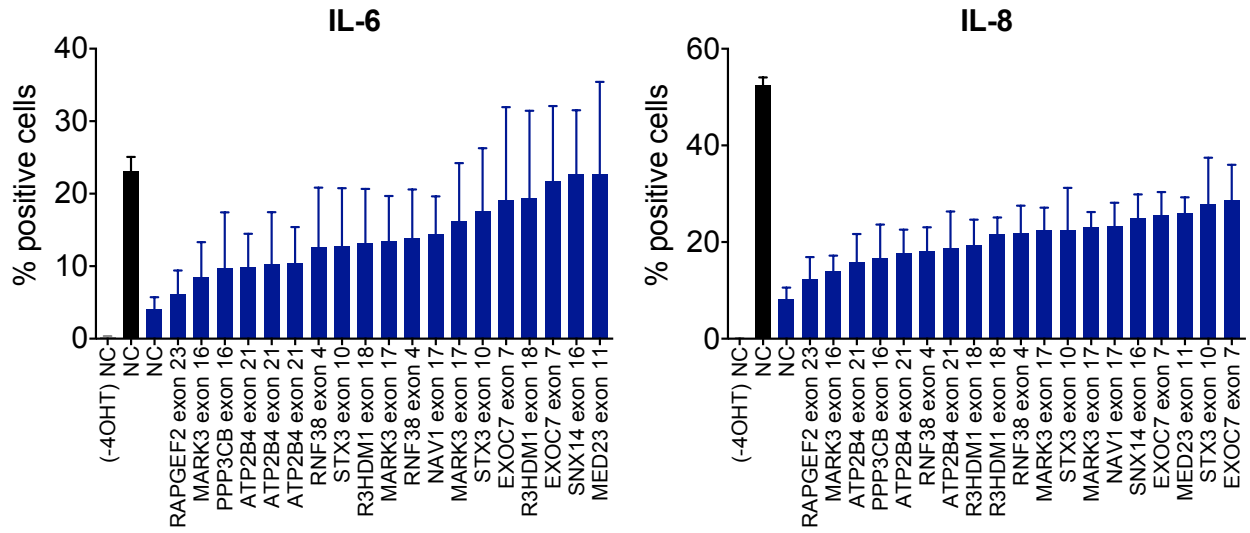

Figure 4.18. Antisense oligonucleotides rescues SASP induction in the absence of PTBP1.
IMR90 ER:RAS cells were reverse transfected with scramble siRNA (black bars) or siRNA against PTBP1 (blue bars), next day 4OHT-induced unless shown by (-4OHT) and 2 days later transfected with a Non-Targeting AON (NC) or AONs targeting the indicated exons. 8 days later the cells were fixed and analysed for IL-6 (left) and IL-8 (right) by IF coupled to HTM. Bars represent mean values with SD of four experiments.

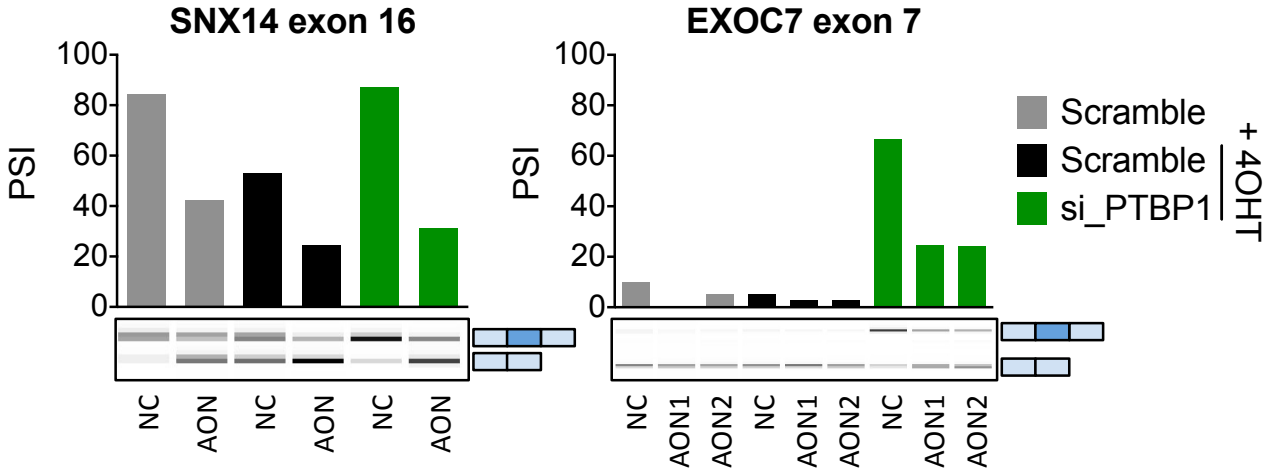

Figure 4.19. AONs induce exon skipping in the genes SNX14 and EXOC7.
IMR90 ER:RAS cells were reverse transfected with scramble siRNA or siRNA against PTBP1 next day 4OHT-induced and 2 days later transfected with a Non-Targeting AON (NC) or AONs targeting the indicated exons. After 2 days, total RNA was retrotranscribed into cDNA, PCR amplified with primers flanking the exon of interest and finally run on a gel on the Bioanalyzer. PSI = Percent Spliced In.

Chapter 5. Discussion

5.1. A loss-of-function screen identified regulators of senescence and the SASP

RNAi- and compound-based screens have been widely used to unveil the functional and causal role of genes in cancer and more specifically in senescence (Acosta et al., 2008; Berns et al., 2004; Bishop et al., 2010; Ewald et al., 2009; Herranz et al., 2015; Lahtela et al., 2013). Loss-of-function by RNAi-mediated suppression of gene expression utilises either an shRNA or an siRNA, both of which rely on the endogenous miRNA biogenesis pathway employed by cells to silence genes (Rao et al., 2009). The former type (2^{nd} generation shRNAs) confers constitutive expression of a secondary hairpin structure, which is processed by Dicer before being incorporated into the RISC complex, whereas the latter (siRNA) constitutes a transient introduction of an anti-sense oligonucleotide ready to enter RISC.

Here, to search for novel SASP regulators, we used a library of synthetic siRNAs spotted in single wells targeting the human druggable genome. The screen readout was the expression of IL-8 and IL-6 in the IMR90 ER:RAS model of OIS. The conditions of the siRNA screen were set and optimised with the aid of siRNAs targeting known regulators of senescence, p53 and p16, and known regulators of IL-8 and IL-6, specifically NF-κB, C/EBPβ and p38. These positive controls served to determine not only the experimental conditions but also to improve how we quantified the immunofluorescence results. The screen was performed in an automated manner with available multichannel pipettes and robotics where possible to minimise extraneous variation due to lengthy procedures and manual handling. The large-scale single-well assay was acquired and analysed using a high throughput microscope. Following the acquisition of immunofluorescence images and conversion to the readout of percentage of positive cells, the B-score normalisation method was used and was confirmed to be appropriate by the analogous distribution of the positive controls.

Pathway analysis of the IL-8 B-scores confirmed expected upstream positive regulators such as IL-1 and NF-κB itself. A strong association with the HDAC inhibitor trichostatin A was also found supporting previous findings suggesting that HDAC inhibitors can enhance SASP gene

expression (Pazolli et al., 2012). Lipopolysaccharide (LPS) was also in the top of the list and is known to induce secretion of pro-inflammatory cytokines (Lu et al., 2008). Interestingly, *CTNNB1*, which encodes β-catenin, was also predicted to be an upstream regulator of IL-8. Beta-catenin is an intracellular transducer of Wnt signaling, which has been found to initiate a transcription programme that promotes cancer. Wnt signaling is important for the self-renewal of the intestinal epithelium and its hyperactivation leads to colorectal cancer. Ablation of Casein Kinase Iα (CKIα) in the intestinal epithelium led to stabilisation of β-catenin but did not result in gastrointestinal tumours unless this was accompanied by additional stresses such as inactivating p53 mutations (Elyada et al., 2011). Pribluda et al. (2013) showed that loss of CKiα was associated with senescence and a senescence-inflammatory response termed SIR, which shared only a few secretory factors with the SASP. Those included IL-1α and the CXCR2 ligands CXCL-1 and CXCL-5. Another indication that Wnt signaling may contribute to SASP induction comes from a paracrine-driven tumour model. Pituitary progenitor cells that express sox2 were able to differentiate into various lineages. Aberrant activation of β-catenin in clusters of sox2+ cells led to pituitary tumours which unexpectedly did not originate from the β-catenin+ cells but resided in the vicinity (Andoniadou et al., 2013). Expression of WNT ligands such as WNT5A was detected in the β-catenin+ and sox2+ cells. WNT5A was one of the factors secreted by the IMR90 ER:RAS cells following induction of senescence with 4OHT (Herranz et al., 2015).

It is possible that the initial secretion of certain SASP components leads to expression of a larger set of the SASP in an autocrine or paracrine manner as part of the signal amplification loop, similar to what has been previously shown for IL-8 or IL-6 (section 1.6.4). This could be the case for β-catenin signaling or VEGF and TGFB1, which were also part of the upstream regulators of IL-8 identified using IPA. On the other hand, secretion of factors like WNT, VEGF or TGFB1 could be necessary for establishment of senescence hence disruption of downstream signaling pathways would prevent senescence and concomitant IL-8 production. IFN-γ and TNF, that are also amongst the upstream IL-8 regulators, have been shown to induce senescence in cancer as part of the T-helper-1-cell anti-tumour immunity (Braumüller et al, 2013).

The identification of known regulators of senescence and the SASP in the screen provided conceptual confirmation for the screening method. Alas, the RNAi screening method used here has limitations. First, introduction of a double stranded (ds) RNA molecule like an siRNA resembles a microbial infection and can hence evoke an immune response. Since the screen readouts were immunity genes, it is possible that part of the induction observed was due to siRNA transfection and consequently variation in the transfection efficiency could have resulted in lower readout detection without real biological significance. Secondly, in such a large-scale experiment, the knockdown of the target genes cannot be confirmed. Lastly, the altered phenotype may be the result of an unwanted siRNA off-target effect, that is, targeted-knockdown of a gene other than the gene intended. To address those issues, one of the common solutions is to perform a secondary screen with multiple individual siRNAs targeting the same gene and recording reproducibility of the original phenotype. Using 4 siRNAs per gene spotted in individual wells, the original assay was repeated for the top 125 hit genes whose knockdown resulted in SASP repression. The reduced IL-8 and IL-6 levels were reproduced with at least 2 separate siRNAs targeting 84 genes.

The siRNA screen identified 84 positive regulators of the SASP. However, at this stage we didn't know whether the function of these genes might have implications in senescence implementation hence not specific to the regulation of the SASP. Alternatively, their inhibition might pose the risk of bypassing the tumour-suppressive growth arrest. To dissociate the SASP from growth arrest we interrogated the effect that those siRNAs had on other senescence markers. This approach revealed 49 genes whose inhibition did not affect the induction of the important senescence effectors p16 and p21 or subsequent cell cycle arrest.

By antagonising proliferation and inhibiting the SASP, the tumour suppressive cell cycle arrest can be maintained but the potential deleterious effects of a pro-inflammatory SASP can be excluded. Two examples of this phenotype have already been described upon inhibition of mTOR and MLL1 (Herranz et al., 2015; Capell et al., 2016). Antagonising proliferation could also mean reinforcing or inducing a growth arrest. Mimicking p16 activity by inhibiting CDK4/6 with Palbociclib induced senescence and showed promising anti-cancer results (Michaud et al., 2010; Rader et al., 2013). Overexpression of p16 alone did not induce a SASP (Coppé et al., 2011) and siRNA- and

shRNA-mediated p16 knockdown in the IMR90 ER:RAS system reinforced SASP production (our data). Together these observations suggest that Palbociclib used as a pro-senescent agent would probably not cause a pro-inflammatory response that could otherwise have negative pathophysiological effects. For example, treatment with Palbociclib induced senescence of proximal tubule epithelial cells and ameliorated the acute kidney injury caused by a postischemic inflammatory environment (DiRocco et al., 2014). This observation implies that one of the sources of the pro-inflammatory environment is senescent cells. This is in agreement with the recent finding that age-related glomerulosclerosis was improved after removal of senescent cells from the proximal tubules possibly thanks to disruption of the paracrine signaling of secreted factors (Baker et al., 2016).

One of the 49 genes identified in the screen, whose siRNA-mediated depletion lowered IL-8 and IL-6 without affecting the growth arrest, was S-Phase Kinase-Associated Protein 1 (SKP1). SKP1 is part of the SKP1/Cul1/F-box (SCF) complex. An inhibitor of Skp2-SCF complex, MLN4924, triggered senescence and suppressed tumour growth in various mouse models and has entered Phase I clinical trials (Nawrocki et al., 2012). MLN4924 has also been found to inhibit NF-κB signaling, which could explain the target's ability to regulate the SASP.

5.2. Investigating mechanisms relevant to SASP regulation

5.2.1. Effect of candidate genes on paracrine senescence

Among the candidate genes, there were also genes encoding receptors such as IL-17RE and TMEM219 (or IGFBP-3R). As aforementioned, disruption of SASP signal amplification is a plausible mechanism by which the novel SASP regulators may act and often receptor signaling pathways converge to NF-κB activation. Therefore, we reasoned that by investigating the ability of the candidate siRNAs to inhibit the SASP in a model of paracrine senescence would provide insight into which genes are possibly involved in these two processes. This screen identified genes that have been previously linked with receptor signaling in senescence (e.g. RAGE; Davalos, et al., 2013; Klune et al., 2008) or NF-κB regulation (e.g. PPP1CB; Mitsuhashi et al., 2008). However, the majority of the 48 genes assayed did not score in this setting. For instance SKP1, which has been

linked to NK-κB, was not identified in the paracrine screen. This is possibly due to differences between OIS and paracrine senescence. A more direct way of determining whether the mechanism of action of these genes is via regulating NF-κB would be to either use expression of an NF-κB pathway effector as our screen readout, or use TNF as a trigger instead of CM of senescent cells.

5.2.2. Transcriptome profiling

To investigate how the identified candidates regulate the SASP, RNA sequencing was performed to analyse the global transcriptome of senescent cells transfected with siRNAs targeting 38 of the 49 novel SASP regulators (Figure 3.16). This approach enabled the coupling of deep mRNA sequencing to a loss-of-function screen. The vast amount of data produced by this method remains to be fully scrutinised. Preliminary analysis involved sample clustering based on global gene expression changes and GO analysis of the cluster profiles. In this manner, we were able to identify common features across sample clusters changing in comparison to the scramble transfected counterparts. A few of these characteristics will be discussed in this section.

5.2.2.1. Glycosylation

A group of genes that was found to be frequently downregulated in SASP-repressing siRNA samples belonged to the general category of carbohydrate metabolism and glycosylation (section 3.6.2, Figure 3.16). The expression of this group of genes increased during senescence suggesting their gene products play role in senescence. The downregulation did not seem to be a secondary phenotype to reduced cytokine activity since it was not observed across all samples.

Glycosylation is a post-translational regulatory mechanism that involves the enzymatic glycosidic linkage of saccharides to proteins, lipids or other saccharides to make up the glycome (Pinho & Reis, 2015). The glycosylation status can alter the function or binding capacity of a substrate thereby increasing molecular heterogeneity. The glycome is extremely diverse. The glycan structures can be characterised based on the linkage anchoring the monosaccharides to the polypeptide chain, which can be nitrogen- or oxygen-based (*N*- or O-glycans). Another category involves glycosaminoglycans (CAG), which are repeating units of acidic disaccharides

making linear polymers. Glycosylation patterns can be specific to the protein, the site and cell-type and contribute to phenotypes, hence it is not so surprising to find altered glycans expression during oncogenic transformation (Pinho & Reis, 2015).

Changes in glycosylation have been previously reported in cancer and ageing underscoring a possible role of glycosylation in controlling senescence and the SASP. Alterations in glycosylation may stem from changes in the transcriptional levels of glycosyltransferases. Several reports have provided substantial associations between high-grade metastatic tumours and glycosylation changes due to differential corresponding enzyme levels (Pinho & Reis, 2015). The focus of this section however will be on literature supporting a link between glycosylation and senescence- or SASP-relevant proteins

Branching of *N*-linked acetylglucosamine (GlcNAc) is mediated by the enzyme GnT-V encoded by the *Mgat5* gene. The RAS-RAF-MAPK signaling pathway regulates MGAT5 expression. In the absence of MGAT5, mouse mammary tumour growth and metastasis was reduced (Granovsky et al., 2000). In addition, colon adenoma size was reduced and was associated with decreased ability of colon cancer stem cells to self-renew due to aberrant Wnt/β-catenin signaling possibly resulting from altered *N*-linked branching of the Wnt receptor (Guo et al., 2014). In tumour cells, MGAT5 was shown to stabilise membrane-bound growth factor receptors such as FGF by preventing their endocytosis-mediated internalisation (Partridge, 2004).

N-linked acetylgalactosamine (GalNAc) modifications by sialylation can be regulated by the enzyme ST6GALNAC1. Expression of ST6GALNAC1 in gastric cancer cells was necessary for expression of the insulin growth factor 1 (IGF-1) (Tamura et al., 2016). IGF-1, like β-catenin, was predicted to be one of the regulators of IL-8 activation by IPA analysis of the screen.

O-linked GlcNAc levels of a prostate cancer cell line positively correlated with VEGF and MMP-2 and -9 expression (Lynch et al., 2012). Heparan sulfate proteoglycans (HSPGs) contain CAGs and can modulate cytokines, chemokines and growth factors by binding and regulating their interactions, solubility and proteolysis (Sarrazin et al., 2011). HSPGs can also modulate growth factor receptor activity such as that of hepatocyte growth factor (HGF), TGFβ and VEGF.

In addition to secreted factors and their receptors, known SASP regulators can be affected by glycosylation. Ramakrishnan et al. (2013) showed how *O*-GlcNAcylation contributes to activation of the NF-κB subunit RelA in lymphoma cells. The Notch receptor can also be modulated by glycosylation. The receptor of Notch is modified by *N*-glycans and *O*-glycans and these can affect interactions with its ligands (Haines & Irvine, 2003; Takeuchi & Haltiwanger, 2014). Very recently, Hoare et al. (2016) demonstrated that fluctuations in Notch activity during senescence control the temporal expression of the pro-inflammatory SASP factors. In particular, this control was mainly over 'lateral induction' of senescence via the Notch ligand Jagged.

Regulation by glycosylation has been implicated in cancer and affects various SASP-related pathways, which may provide cues as to how the SASP is regulated. Vice versa, understanding the senescent glycome may help decipher the underlying molecular mechanisms in action and consequently to unravel the biological significance of glycosylation.

5.2.2.2. Ion homeostasis

A group of genes that was found upregulated in some SASP-repressing siRNA samples belonged to the general category of ion homeostasis (section 3.6.2, Figure 3.16). The expression of this gene group was relatively unchanged when comparing senescent to proliferating cells. The intracellular ion concentrations and gradients are important for several physiological processes. The ion flow is controlled by electrical gradients driven by sodium (Na^+) and potassium (K^+) channels that lie on membranes. One of the key signaling ions is calcium (Ca^{2+}). Ca^{2+} level alterations can regulate various cancer hallmarks including proliferation (Bose et al., 2015). High expression of ion homeostasis genes was observed in the samples showing elevated expression of mitotic genes. This may indicate that these two gene groups are co-dependent. Alterations in ion levels may also reflect a synthetic mechanism by which the SASP is reduced, as this would not occur during normal mitosis.

Changes in intracellular Ca^{2+} levels due to reduced cation channel expression have been shown to regulate nuclear translocation of the Nuclear factor of activated T-cells (NFAT) via the upstream calcium sensor calmodulin (CaM) (Weber et al., 2010). Expression of immune-response

genes such as IL-2 is activated by NFAT (Im & Rao, 2004). Disruption of calcium influx can affect RAS signaling and NF-κB activation (Yamamoto et al., 2008). These observations, depending on the context, could explain why ion homeostasis may be of relevance to the study of SASP regulation.

5.2.2.3. Immune response genes

One of the 6 gene groups driving the clustering of SASP-repressing siRNA samples was enriched in immune system response genes (section 3.6.2, Figure 3.16). Although this gene group may reflect the screen readout, the expression across different samples was variable. There was no clear expression direction within or across samples. This could be due to the small number of genes present in this group or could also indicate the possibility of differential regulation of the various components of the SASP. Further analysis of SASP expression is needed to examine this hypothesis. In support of this, two of the hit SASP-repressing siRNAs target Notch modulators, specifically LNX2 and ITCH (Camps et al., 2013; Qiu et al., 2000; Zhou et al., 2015). Notch activity in DNA-damage and Ras-induced senescence inhibits expression of the pro-inflammatory SASP factors, like IL-8 and IL-6, but not others like TGFβ (Hoare et al., 2016). Future analysis will include investigating differences in expression of Notch-dependent SASP factors across SASP-repressing siRNA samples.

The SASP is composed by a multitude of cytokines, chemokines and growth factors, hence lends itself nicely to the study of differential regulation of immune response genes. However, the functions accosiated with the SASP vary across factors and may also depend on the context and tissue type. Therefore, elucidation of the highly contextual nature of such factors is as important as investigating the differential regulatory mechanisms if such findings are to be of clinical use.

5.2.3. Identifying chemical inhibitors that regulate the SASP

From an academic point of view, it is interesting to explore the mechanism of action of the novel SASP regulators in an unbiased global manner. In cancer therapy, considering the detrimental net effect of the SASP, the direct use of the information obtained from our screen could be beneficial.

In this regard, of particular interest were the genes whose knockdown regulates the SASP but does not affect other senescence-related phenotypes. 5 available inhibitors targeting products of the genes identified in the screen, or related gene family member, recapitulated the effect of the corresponding siRNAs. Phenotype confirmation by an alternative approach (using chemical inhibitors) served to validate further the functional specificity of the candidate genes.

Using drugs to inhibit the SASP could also be directly applicable to clinical use. Inflammation that governs advanced tumours is harmful but cannot always be prevented. Therefore, we reasoned that the ability of drugs to repress a full-blown established SASP would confer an additional advantage and can be experimentally tested. To this end, we treated senescent cells already expressing a SASP with the 5 chemical inhibitors. Only one compound was able to diminish IL-8 and IL-6 in this experimental setting. Similar results were obtained using a separate inhibitor, Zileuton, targeting the same protein, which is 5-lipoxygenase. Zileuton is used for asthma treatment but was also recently shown to prevent neutrophil accumulation and consequent lung metastasis in a mouse mammary tumour model (Wculek & Malanchi, 2015).

The association between the candidate SASP repressor Zileuton and cancer provided confidence in the model used for the study of repression of an established SASP. To expand these results, we searched for additional drugs able to reduce high levels of IL-8 and IL-6 by screening the 1280 inhibitors of the LOPAC. The normalisation and dynamic range of the drug screen results were not ideal. Nevertheless, the majority of the drugs re-tested as a result of arbitrary hit selection criteria showed significant reinforcement or repression of the SASP readouts, validating the screen result.

4 compounds were found to reinforce IL-8 and IL-6 expression. According to the defined function of these compounds, an increase in intracellular cAMP is expected after treatment. These compounds either inhibit phosphodiesterases, which function to decrease intracellular cAMP levels, or have been found to increase cAMP levels in the case of forskolin. Paradoxically, phosphodiesterase inhibitors and forskolin are used as anti-inflammatory drugs (Barnes, 2013; Dinarello, 2010). However, both PDE4 inhibitors and forskolin have been shown to cause severe health side effects. The discrepancy in our findings and published literature is indicative of a

potential risk in using these compounds or, could reflect the limitations of our cellular system to study inflammation reinforcement. Interestingly, Pattabiraman et al. (2016) demonstrated that increased levels of PKA following treatment with forskolin induced a mesenchymal-to-epithelial transition (MET). The morphology of the senescent cells treated with all 4 SASP enhancers did indeed resemble that of epithelial according to visual inspection (not shown). There is a possibility that the observed increase in SASP was an artefact of MET.

In the drug screen, we identified 12 compounds that repressed IL-8 and IL-6 during OIS. These included 3 glucocorticoids which have previously been shown to affect NF-κB-induced SASP factors (Laberge et al., 2012). Although the 12 compounds reduced the SASP, their effect on senescence and specifically growth arrest is yet to be examined. Lowering NF-κB activity and the SASP may lead to senescence bypass and run the risk of unwanted aberrant proliferation and cancer. One of the tested inhibitors, Tautomycetin, which inhibits PPP1CB, has been found to regulate NF-κB but did not bypass proliferation arrest in our IMR90 ER:RAS system (Mitsuhashi et al., 2008). This does not preclude however that Tautomycetin can affect other pathwyas and as a result prevent bypass or reinforce an arrest, or that the amplitude of NF-κB activity is the critical determinant of cell proliferation status. Prior to any further use of the SASP-repressing compounds, induction of senescence effectors and growth arrest must be confirmed.

The number of mouse models used for studying the paracrine action of senescent cells in cancer development and chemoresistance is increasing. Future work should involve testing the efficacy of the candidate drugs in preventing inflammation-driven cancer in such settings. The LOPAC drugs are already used in the clinic for the treatment of various diseases. Direct use of SASP-repressing compounds will hence be rapidly applicable as the appropriate dosage and corresponding side-effects have been previously determined.

5.3. The splicing factor PTBP1 regulates the SASP

Our RNAi screen revealed 49 novel specific regulators of the SASP that do not affect the growth arrest. PTBP1 was one of the strongest candidates consistently presenting a lower SASP following

knockdown regardless of RNAi methodology. Therefore, we took a closer look at how PTBP1 regulates senescence and the SASP.

5.3.1. PTBP1 in senescence

Although the total transcriptional or protein levels of PTBP1 do not change in senescent cells, we observed a specific increase in nuclear PTBP1 using IF. This observation suggests that PTBP1 plays a role in the nucleus of senescent cells, which would fit the model of the previously described functions for PTBP1 such as mRNA splicing that occurs primarily in the nucleus. An increase in nuclear detection by IF upon senescence could either be due to activation resulting from complex formation or due to PTBP1 nuclear accumulation resulting from translocation. Cytoplasmic re-localisation of PTBP1 can be induced by phosphorylation of its nuclear export signal by PKA (Knoch et al., 2006; Ma et al., 2007; Xie et al., 2003). PKA is activated by high cAMP levels. Forskolin is a known inducer of cAMP and Forskolin treatment has been shown to cause nucleo-cytoplasmic shuttling of PTBP1 in PC12 cells by Ma et al. (2007) upon neurite growth stimulalion but not in PC12 by Xie et al. (2003) or in INS-1 cells by Knoch et al. (2006). This discrepancy is possibly due to differences in methodologies or cellular systems and types. The anti-inflammatory role of forskolin could fit with forskolin-induced PKA-dependent export of PTBP1 from the nucleus and a lower SASP. However, we observed an increase in SASP after forskolin treatment further underscoring the possibility of cell type and system specificity. Indeed, changes in cAMP levels and PKA activity have tissue-specific effects (Vossler et al., 1997). it would be interesting to determine whether the nuclear accumulation of PTBP1 in senescence is regulated by PKA by preventing PKA-dependent phosphorylation of PTBP1 by mutagenesis of the specific sites.

5.3.2. PTBP1 is a potential target for repressing the SASP without affecting the senescence growth arrest

Regardless of whether PTBP1 was activated in OIS, PTBP1 was necessary for the induction of several SASP genes. On the other hand, in the absence of PTBP1, IMR90 ER:RAS cells were still able to respond to the senescence-inducing stimulus (4OHT) by upregulating CDKIs and arresting

proliferation. This was the case also when the senescence stimulus was DNA damage by irradiation, an *in vitro* setting representing a separate senescence type. Overall, loss of PTBP1 did not prevent induction of the favourable tumour-suppressive cell cycle arrest.

The DDR observed during OIS results from an initial boost in proliferation caused by activation of an oncogene like *Ras*. Therefore, blunting proliferation might result in a delay or diminution of the senescence onset and accompanied SASP. We observed a slow decrease in the proliferation of wild type cells lacking PTBP1, consistent with published results in other cell lines (Wang et al., 2008). Hence, we aimed to determine whether this was responsible for the observed reduction in SASP in OIS. This did not seem to be the case since PTBP1 knockdown via siRNAs and shRNAs in senescent cells was also able to decrease an established SASP.

Our efforts to overexpress full length PTBP1 in wild type IMR90 cells, although incomplete due to technical limitations, resulted in an increase in IL-8 expression but not CCL2. This discrepancy was an indication of specificity and not artefact since CCL2 was one of the SASP factors whose expression was unaffected by loss of PTBP1 in OIS. Induction of IL-8 expression following ectopic PTBP1 expression could support an active role of PTBP1 in SASP production.

PTBP1 seems to be a regulator of SASP induction independently of effects on proliferation and is necessary for the maintenance of the SASP. From a therapeutic point of view, being able to control established inflammation by targeting PTBP1 without hindering senescence would be preferable.

5.3.3. PTBP1 regulates a subset of the SASP

The secretome of Ras-induced senescent cells is composed of many factors (Table 1). Depending on the context, the SASP can promote a deleterious cancer growth or beneficial anti-tumour immunity. The complex composition of the SASP makes it difficult to pinpoint which factor contributes to which function. In addition, not all previously identified regulators were systematically linked to each SASP component. Recent studies using high-throughput analysis of the SASP composition following genetic manipulation of a SASP regulator have uncovered that the SASP

components are differentially regulated and this can be linked to the various functions of senescent cells (Herranz et al., 2015; Hoare et al., 2016).

The unbiased proteomic characterisation of the senescent secretome in the absence of PTBP1 or mTOR revealed an overlap but also a difference in the SASP factors being affected. The differential regulation of the SASP by mTOR and PTBP1 was also reflected in the differences seen in the two functional assays performed. The secretome commonly regulated by mTOR and PTBP1 was necessary for paracrine induction of senescence. On the other hand, the mTOR-dependent secretome was necessary for attraction of NK cells but PTBP1 did not regulate factors, such as CCL2, that play important roles in immune cell migration.

It is unclear which specific SASP factor or group of factors is responsible for each of the variable paracrine effects on nearby wild type or cancer cells. Therefore, as differential regulation of the SASP is identifiable and measurable, it could be exploited to better define the contextual functions of the SASP.

It would be interesting to explore how the differential regulation of the SASP reflects on different *in vivo* phenotypes. The attraction and function of NK cells could be measured in a model of tumour cell senescence upon rescue of p53. In that model, tumour regression following p53 rescue was found to be predominantly due to NK cells (Xue et al., 2007). For another model of senescent cell clearance that depends more strongly on T-cells, a possible option is NRas-induced senescence in the liver following hydrodynamic injection of transposons. This has been frequently used for this purpose by others and our group (Herranz et al., 2015; Hoare et al., 2016; Kang et al., 2011; Tasdemir et al., 2016). Since immune cells tend to work in cascades, it will however be difficult to dissociate the specific function of different types of immune cells using these models.

The significance of reducing the PTBP1-dependent pro-inflammatory arm of the SASP could be also tested in senescent cell xenograft models of SASP-driven tumour growth. Mouse engraftment of cancer cells with senescent cells leads to exacerbated tumour growth compared to cancer cells co-injected with normal cells (Herranz et al., 2015; Laberge et al., 2015). Knockdown of PTBP1 in the senescent cells to be co-injected and measurement of resulting tumour growth, hopefully to be reduced, would confirm that depletion of PTBP1 could abolish the detrimental

effects of the SASP. Previously, members of our group explored the antagonistic effect of rapamycin on the tumourigenic properties of the SASP (Herranz,et al., 2015). Assays *in vitro* for assessment of PTBP1-dependent alterations in the SASP's ability to induce EMT, cancer cell migration and invasion are currently underway.

In summary, PTBP1 regulates specifically a subset of the SASP in OIS. This subset contains several harmful pro-inflammatory factors but not CCL2, an immune cell chemoattractant. The functional implications and applicability of altering the PTBP1-regulated SASP *in vivo* must be determined. Nevertheless, these findings suggest there is a possibility, by identifying and targeting different regulators, to differentially affect the SASP ultimately aiming to harness the good aspects of the SASP while suppressing the negative ones.

5.3.4. PTBP1-dependent mRNA splicing during senescence affects the SASP

To understand the mechanism by which PTBP1 regulates the SASP, we first examined possible links between PTBP1 and previously identified SASP regulators, such as NF-κB and C/EBPβ. This was not however the case. The next step involved exploring the putative function of PTBP1 in the context of senescence and the SASP.

PTBP1 is multifunctional with described roles in IRES-driven translation and mRNA stability via 3'UTR binding (Coles et al., 2004; Ge et al., 2016; Mitchell et al., 2005). These are possible mechanisms of PTBP1 action unexplored in the work presented here. On the other hand, we focused on the most studied, canonical function of PTBP1, which is its role in AS of mRNAs. To study how PTBP1 regulates AS during senescence, we performed global mRNA sequencing of senescent cells and senescent cells in the absence of PTBP1.

Even though PTBP1 is not a basal splicing factor, initially, we sought to ensure that general constitutive splicing is not substantially affected by PTBP1. Since the expression of spliceosome genes had not been formerly evaluated upon senescence, a comparison was drawn between senescent cells and proliferating cells. Small changes were observed in the expression of spliceosomal genes belonging to various steps of the spliceosome pathway and their differential expression patterns remained overall unchanged following PTBP1 knockdown.

MATS analysis of mRNA splicing from global RNA-seq showed changes in AS patterns belonging to all 5 possible splicing events, i.e. skipped exon (SE), retained intron (RI), mutually exclusive exon (MXE), alternative 5' (A5 SS) or 3' splice site (A3 SS) (Figure 1.5). In line with the known exon skipping function of PTBP1, in its absence, the number of altered exon inclusion events increased when compared to exon skipping or other AS events. Very few examples including TPM1 and ATP2B4 have been previously associated with PTBP1 splicing activity (Izaguirre et al., 2012; Xue et al., 2009). The majority of putative PTBP1-dependent exon skipping events were notably absent from our gene list. This may be due to the different methods of splicing analysis employed or because splicing patterns can be tissue-specific (Izaguirre et al., 2012; Liu et al., 2014; Wang et al., 2008).

Although surely not all AS events were captured by our analysis, using RT coupled to PCR we confirmed 10 splicing events of the 13 that were tested. The PTBP1-dependent AS events did not always correlate with reversal of a senescence-associated isoform to a wild type isoform. In particular, certain isoforms were unchanged upon senescence and AS occurred solely upon PTBP1 knockdown. This does not exclude the possibility that a certain isoform of a gene product is essential for SASP induction. Similarly, although PTBP1 upregulation in senescence is unclear, its function was necessary for SASP induction.

It is unlikely that all splicing alterations observed account for the SASP reduction following PTBP1 knockdown. To isolate events that are causally linked to the SASP, we followed a two-step approach. As a first step, the effect on the SASP after knockdown of the alternatively spliced products was tested. The genes that contributed to a SASP in a negative or positive way were selected for the second assay. The second assay involved a phenotype rescue experiment by which each splicing event was reverted in senescent cells lacking PTBP1 with the use of AONs. The readout measure was SASP induction as per usual. This approach aimed at reinforcing the link between PTBP1-driven splicing and SASP induction. Splicing reversal of the majority of the targets was capable of rescuing SASP reduction. It is likely that many of the targets work in a cooperative manner to control an essential pathway in SASP regulation. All in all, using this two-step approach, certain AS events were causally linked to PTBP1 and the SASP. However, further

analysis is required to reinforce this link. For example, a search for the presence of consensus polypyrimidine binding motifs on the mRNA targets. In addition, RNA pull-down with PTBP1-specific antibodies could be pursued.

A significant amount of the PTBP1 alternatively spliced targets encode products involved in intracellular protein transport according to a functional annotation analysis. In immunoprecipitation experiments by others, PTBP1 has also been found associated with transcripts that relate to GO terms of 'intracellular protein transport' and 'vesicle-mediated transport' (Gama-Carvalho et al., 2006). The most consistent SASP-associated splicing events here were those of SNX14 and EXOC7, which belong to these functional categories. Future work will involve deciphering any changes in intracellular transport machinery and mechanisms such as Golgi, membrane exocytosis or even endocytosis. Blockade of secretion of SASP components would interfere with the autocrine loop of SASP amplification. Alternatively, loss of membrane receptor recycling by endocytosis can be a mechanism of interfering with the SASP autocrine loop. EXOC7 is part of the exocyst complex, which has been associated with both secretion and endocytosis (Takahashi et al., 2012; Wu & Guo, 2015). Such underlying molecular mechanisms would explain the reduction in SASP activation in paracrine senescence observed in cells lacking PTBP1.

5.4. Summary and concluding remarks

OIS is a mechanism that blocks tumourigenesis by preventing the aberrant proliferation of cells with oncogenic mutations. Senescent cells secrete a plethora of factors with functions that can be beneficial or detrimental depending on the context. The pro-inflammatory SASP can promote cancer growth but can also attract the immune system to clear damaged cells thereby maintaining tissue homeostasis.

Blockade of SASP factors or manipulating SASP regulation is a potential route for therapeutic intervention. When targeting SASP regulation, care must be taken to not interfere with the tumour-suppressive aspect of senescence including the growth arrest and anti-tumour immunity. Our group recently identified mTOR as a master regulator of the SASP (Herranz et al., 2015). Although inhibition of mTOR with Rapamycin could be used to avoid detrimental effects of

the SASP, it also blunts its tumour-suppressive effects and compromises the immune system. Therefore, a systematic search for novel regulators of the SASP is needed.

Loss-of-function screens have greatly expanded our knowledge of molecular pathways involved in senescence and the SASP. Here, an siRNA screening system for SASP regulators in OIS was developed. By combining siRNA screens and global transcriptome profiling, we identified novel regulators of the SASP that alter the expression of genes whose products are involved in glycosylation and ion homeostasis, fields worth exploring in the future. Since the SASP is a pro-inflammatory phenotype there is potential for extrapolating these results to other diseases. Of particular benefit for cancer therapy, many genes were shown to be potential targets whose depletion resulted in SASP repression without running the risk of re-entry into the cell cycle. In addition, a few of these genes could be pharmacologically inhibited with existing chemical compounds resulting in a similar phenotype. Having set up a SASP screen, using the LOPAC as a template, we were able to expand the list of available chemical compounds repressing the SASP.

In an siRNA screen, we found a novel regulator of the SASP, the splicing factor PTBP1. Apart from PTBP1 being an attractive therapeutic target, finding this novel regulator implicated that alternative splicing can also be a process regulating the SASP.

The senescence growth arrest does not depend on PTBP1 expression. In addition, only a subset of the SASP is regulated by PTBP1 and is partially different to the one regulated by mTOR. This had implications on the two assays performed to study the function of the SASP resulting in different phenotypes. Our data suggest that it is possible, targeting part of the SASP, to maintain the good aspects and abolish the harmful ones while maintaining the ability to undergo senescence growth arrest. These findings await *in vivo* confirmation.

The splicing of genes depends on PTBP1 during senescence and this is at least in part how PTBP1 regulates the SASP. Many of the genes whose splicing is regulated by PTBP1 control intracellular protein trafficking. Pending experiments aim at fully understanding the function of PTBP1, which can result in finding more specific splicing substrates that could be targeted to treat cancer and other diseases with an inflammatory phenotype.

References

Ablain, J., Rice, K., Soilihi, H., de Reynies, A., et al. (2014) Activation of a promyelocytic leukemia-tumor protein 53 axis underlies acute promyelocytic leukemia cure. *Nature Medicine*. 20 (2), 167–174.

Acosta, J.C., Banito, A., Wuestefeld, T., Georgilis, A., et al. (2013) A complex secretory program orchestrated by the inflammasome controls paracrine senescence. *Nature Cell Biology*. 15 (8), 978–990.

Acosta, J.C., O'Loghlen, A., Banito, A., Guijarro, M. V, et al. (2008) Chemokine signaling via the CXCR2 receptor reinforces senescence. *Cell*. 133 (6), 1006–1018.

Agafonov, D.E., Deckert, J., Wolf, E., Odenwälder, P., et al. (2011) Semiquantitative proteomic analysis of the human spliceosome via a novel two-dimensional gel electrophoresis method. *Molecular and Cellular Biology*. 31 (13), 2667–2682.

Alspach, E., Flanagan, K.C., Luo, X., Ruhland, M.K., et al. (2014) P38MAPK plays a crucial role in stromal-mediated tumorigenesis. *Cancer Discovery*. 4 (6), 716–729.

Ancrile, B., Lim, K.H. & Counter, C.M. (2007) Oncogenic Ras-induced secretion of IL6 is required for tumorigenesis. *Genes & Development*. 21 (14), 1714–1719.

Andoniadou, C.L., Matsushima, D., Mousavy Gharavy, S.N., Signore, M., et al. (2013) Sox2+ stem/progenitor cells in the adult mouse pituitary support organ homeostasis and have tumor-inducing potential. *Cell Stem Cell*. 13 (4), 433–445.

Angelini, P.D., Zacarias Fluck, M.F., Pedersen, K., Parra-Palau, J.L., et al. (2013) Constitutive HER2 signaling promotes breast cancer metastasis through cellular senescence. *Cancer Research*. 73 (1), 450–458.

Augert, A., Payré, C., de Launoit, Y., Gil, J., et al. (2009) The M-type receptor PLA2R regulates senescence through the p53 pathway. *EMBO reports*. 10 (3), 271–277.

Avrahami, D., Li, C., Schu, D., Kaestner, K.H., et al. (2015) Aging-Dependent Demethylation of Regulatory Elements Correlates with Chromatin State and Improved b Cell Function Aging-Dependent Demethylation of Regulatory Elements Correlates with Chromatin State and Improved b Cell Function. *Cell Metabolism*. 22 (4), 619–632.

Babic, I., Sharma, S. & Black, D.L. (2009) A role for polypyrimidine tract binding protein in the establishment of focal adhesions. *Molecular and Cellular Biology*. 29 (20), 5564–5577.

Baker, D.J., Childs, B.G., Durik, M., Wijers, M.E., et al. (2016) Naturally occurring p16 Ink4a - positive cells shorten healthy lifespan. *Nature*. 530 (7589), 1–5.

Baker, D.J., Wijshake, T., Tchkonia, T., LeBrasseur, N.K., et al. (2011) Clearance of p16Ink4a-positive senescent cells delays ageing-associated disorders. *Nature*. 479 (7372), 232–236.

Banito, A., Rashid, S.T., Acosta, J.C., Li, S., et al. (2009) Senescence impairs successful

reprogramming to pluripotent stem cells. *Genes & Development*. 23 (18), 2134–2139.

Barnes, P.J. (2013) New anti-inflammatory targets for chronic obstructive pulmonary disease. *Nature Reviews Drug Discovery*. 12 (7), 543–559.

Bartkova, J., Rezaei, N., Liontos, M., Karakaidos, P., et al. (2006) Oncogene-induced senescence is part of the tumorigenesis barrier imposed by DNA damage checkpoints. *Nature*. 444 (7119), 633–637.

Bavik, C., Coleman, I., Dean, J.P., Knudsen, B., et al. (2006) The gene expression program of prostate fibroblast senescence modulates neoplastic epithelial cell proliferation through paracrine mechanisms. *Cancer research*. 66 (2), 794–802.

Ben-Porath, I. & Weinberg, R.A. (2005) The signals and pathways activating cellular senescence. *The International Journal of Biochemistry & Cell Biology*. 37 (5), 961–976.

Benatar, T., Yang, W., Amemiya, Y., Evdokimova, V., et al. (2012) IGFBP7 reduces breast tumor growth by induction of senescence and apoptosis pathways. *Breast cancer research and treatment*. 133 (2), 563–573.

Bent, E.H., Gilbert, L.A. & Hemann, M.T. (2016) A senescence secretory switch mediated by PI3K/AKT/mTOR activation controls chemoprotective endothelial secretory responses. *Genes & Development*. 30 (16), 1811–1821.

Berns, K., Hijmans, E.M., Mullenders, J., Brummelkamp, T.R., et al. (2004) A large-scale RNAi screen in human cells identifies new components of the p53 pathway. *Nature*. 428 (6981), 431–437.

Bezzi, M., Teo, S.X., Muller, J., Mok, W.C., et al. (2013) Regulation of constitutive and alternative splicing by PRMT5 reveals a role for Mdm4 pre-mRNA in sensing defects in the spliceosomal machinery. *Genes & Development*. 27 (17), 1903–1916.

Bhaumik, D., Scott, G.K., Schokrpur, S., Hiruyeh, et al. (2009) MicroRNAs miR-146a/b negatively modulate the senescence - associated inflammatory mediators IL-6 and IL-8. *Aging*. 1 (4), 402–411.

Bishop, C.L., Bergin, A.M.H., Fessart, D., Borgdorff, V., et al. (2010) Primary cilium-dependent and -independent hedgehog signaling inhibits p16INK4A. *Molecular Cell*. 40 (4), 533–547.

Blanco, F.J. & Bernabeu, C. (2011) Alternative splicing factor or splicing factor-2 plays a key role in intron retention of the endoglin gene during endothelial senescence. *Aging Cell*. 10 (5), 896–907.

Blanco, F.J. & Bernabeu, C. (2012) The splicing factor SRSF1 as a marker for endothelial senescence. *Frontiers in Physiology*. 3 (54), 1–6.

Blanco, F.J., Grande, M.T., Langa, C., Oujo, B., et al. (2008) S-endoglin expression is induced in senescent endothelial cells and contributes to vascular pathology. *Circulation Research*. 103 (12), 1383–1392.

Bodnar, A.G., Ouellette, M., Frolkis, M., Holt, S.E., et al. (1998) Extension of life-span by introduction of telomerase into normal human cells. *Science*. 279 (5349), 349–352.

Bose, T., Cieślar-Pobuda, A. & Wiechec, E. (2015) Role of ion channels in regulating Ca^{2+} homeostasis during the interplay between immune and cancer cells. *Cell Death & Disease*. 6e1648.

Boutz, P. & Chawla, G. (2007) MicroRNAs regulate the expression of the alternative splicing factor nPTB during muscle development. *Genes & Development*. 21 (1), 71–84.

Boutz, P.L., Stoilov, P., Li, Q., Lin, C.H., et al. (2007) A post-transcriptional regulatory switch in polypyrimidine tract-binding proteins reprograms alternative splicing in developing neurons. *Genes & Development*. 21 (13), 1636–1652.

Braumüller, H., Wieder, T., Brenner, E., Aßmann, S., et al. (2013) T-helper-1-cell cytokines drive cancer into senescence. *Nature*. 494 (7437), 361–365.

Burd, C.E., Sorrentino, J.A., Clark, K.S., Darr, D.B., et al. (2013) Resource Monitoring Tumorigenesis and Senescence In Vivo with a p16 INK4a -Luciferase Model. *Cell*. 152 (1–2), 340–351.

Busslinger, M., Moschonas, N., Flavell, R. a, Hill, M., et al. (1981) Aberrant Splicing Results from a Single Point Mutation in an Intron. *Cell*. 27 (Part 1), 289–298.

Campisi, J. (2005) Senescent cells, tumor suppression, and organismal aging: Good citizens, bad neighbors. *Cell*. 120 (4), 513–522.

Campisi, J., Andersen, J.K., Kapahi, P. & Melov, S. (2011) Cellular senescence: A link between cancer and age-related degenerative disease? *Seminars in Cancer Biology*. 21 (6), 354–359.

Camps, J., Pitt, J.J., Emons, G., Hummon, A.B., et al. (2013) Genetic amplification of the NOTCH modulator LNX2 upregulates the WNT/β-catenin pathway in colorectal cancer. *Cancer Research*. 73 (6), 2003–2013.

Capell, B.C., Drake, A.M., Zhu, J., Shah, P.P., et al. (2016) MLL1 is essential for the senescence-associated secretory phenotype. *Genes & Development*. 30 (3), 321–336.

Chan, R.C. & Black, D.L. (1997) The polypyrimidine tract binding protein binds upstream of neural cell-specific c-src exon N1 to repress the splicing of the intron downstream. *Molecular and Cellular Biology*. 17 (8), 4667–4676.

Chandra, T., Ewels, P.A., Schoenfelder, S., Furlan-Magaril, M., et al. (2015) Global reorganization of the nuclear landscape in senescent cells. *Cell Reports*. 10 (4), 471–484.

Chang, J., Wang, Y., Shao, L., Laberge, R.M., et al. (2016) Clearance of senescent cells by ABT263 rejuvenates aged hematopoietic stem cells in mice. *Nature Medicine*. 22 (1), 78–83.

Chen, H., Ruiz, P.D., McKimpson, W.M., Novikov, L., et al. (2015) MacroH2A1 and ATM Play Opposing Roles in Paracrine Senescence and the Senescence-Associated Secretory Phenotype. *Molecular Cell*. 59 (5), 719–731.

Chen, Z., Trotman, L.C., Shaffer, D., Lin, H.-K., et al. (2005) Crucial role of p53-dependent cellular senescence in suppression of Pten-deficient tumorigenesis. *Nature*. 436 (7051), 725–730.

Cheung, H.C., Hai, T., Zhu, W., Baggerly, K.A., et al. (2009) Splicing factors PTBP1 and PTBP2 promote proliferation and migration of glioma cell lines. *Brain*. 132 (8), 2277–2288.

Chien, Y., Scuoppo, C., Wang, X., Fang, X., et al. (2011) Control of the senescence-associated secretory phenotype by NF-kappaB promotes senescence and enhances chemosensitivity. *Genes & Development*. 25 (20), 2125–2136.

Childs, B.G., Durik, M., Baker, D.J. & van Deursen, J.M. (2015) Cellular senescence in aging and age-related disease: from mechanisms to therapy. *Nature Medicine*. 21 (12), 1424–1435.

Clower, C. V, Chatterjee, D., Wang, Z., Cantley, L.C., et al. (2010) The alternative splicing repressors hnRNP A1/A2 and PTB influence pyruvate kinase isoform expression and cell metabolism. *Proceedings of the National Academy of Sciences*. 107 (5), 1894–1899.

Cohen-Eliav, M., Golan-Gerstl, R., Siegfried, Z., Andersen, C.L., et al. (2013) The splicing factor SRSF6 is amplified and is an oncoprotein in lung and colon cancers. *Journal of Pathology*. 229 (4), 630–639.

Coles, L.S., Bartley, M.A., Bert, A., Hunter, J., et al. (2004) A multi-protein complex containing cold shock domain (Y-box) and polypyrimidine tract binding proteins forms on the vascular endothelial growth factor mRNA: Potential role in mRNA stabilization. *European Journal of Biochemistry*. 271 (3), 648–660.

Collado, M., Gil, J., Efeyan, A., Guerra, C., et al. (2005) Tumour biology: senescence in premalignant tumours. *Nature*. 436 (7051), 642.

Collado, M. & Serrano, M. (2010) Senescence in tumours: evidence from mice and humans. *Nature Reviews Cancer*. 10 (1), 51–57.

Coppé, J.-P., Desprez, P.-Y., Krtolica, A. & Campisi, J. (2010) The senescence-associated secretory phenotype: the dark side of tumor suppression. *Annual review of pathology*. 599–118.

Coppé, J.-P., Patil, C.K., Rodier, F., Sun, Y., et al. (2008) Senescence-associated secretory phenotypes reveal cell-nonautonomous functions of oncogenic RAS and the p53 tumor suppressor. *PLoS Biology*. 6 (12), 2853–2868.

Coppé, J.P., Patil, C.K., Rodier, F., Krtolica, A., et al. (2010) A human-like senescence-associated secretory phenotype is conserved in mouse cells dependent on physiological oxygen. *PLoS ONE*. 5 (2), e9188.

Coppé, J.P., Rodier, F., Patil, C.K., Freund, A., et al. (2011) Tumor suppressor and aging biomarker p16 INK4a induces cellular senescence without the associated inflammatory secretory phenotype. *Journal of Biological Chemistry*. 286 (42), 36396–36403.

Corrionero, A., Miñana, B. & Valcárcel, J. (2011) Reduced fidelity of branch point recognition and alternative splicing induced by the anti-tumor drug spliceostatin A. *Genes & Development*. 25 (5), 445–459.

Courtois-Cox, S., Genther Williams, S.M., Reczek, E.E., Johnson, B.W., et al. (2006) A negative feedback signaling network underlies oncogene-induced senescence. *Cancer Cell*. 10 (6), 459–472.

d'Adda di Fagagna, F., Reaper, P.M., Clay-Farrace, L., Fiegler, H., et al. (2003) A DNA damage

checkpoint response in telomere-initiated senescence. *Nature*. 426 (6963), 194–198.

Dankort, D., Filenova, E., Collado, M., Serrano, M., et al. (2007) A new mouse model to explore the initiation, progression, and therapy tumors. *Genes & Development*. 21 (415), 379–384.

Dannenberg, J.H., van Rossum, A., Schuijff, L. & te Riele, H. (2000) Ablation of the retinoblastoma gene family deregulates G(1) control causing immortalization and increased cell turnover under growth-restricting conditions. *Genes & Development*. 14 (23), 3051–3064.

Davalos, A.R., Kawahara, M., Malhotra, G.K., Schaum, N., et al. (2013) p53-dependent release of Alarmin HMGB1 is a central mediator of senescent phenotypes. *Journal of Cell Biology*. 201 (4), 613–629.

David, C.J., Chen, M., Assanah, M., Canoll, P., et al. (2010) HnRNP proteins controlled by c-Myc deregulate pyruvate kinase mRNA splicing in cancer. *Nature*. 463 (7279), 364–368.

Deisseroth, A., Ko, C.W., Nie, L., Zirkelbach, J.F., et al. (2015) FDA approval: Siltuximab for the treatment of patients with multicentric castleman disease. *Clinical Cancer Research*. 21 (5), 950–954.

Demaria, M., Ohtani, N., Youssef, S.A., Rodier, F., et al. (2014) An essential role for senescent cells in optimal wound healing through secretion of PDGF-AA. *Developmental Cell*. 31 (6), 722–733.

Deng, Q., Liao, R., Wu, B.L. & Sun, P. (2004) High intensity ras signaling induces premature senescence by activating p38 pathway in primary human fibroblasts. *The Journal of Biological Chemistry*. 279 (2), 1050–1059.

Dinarello, C.A. (2010) Anti-inflammatory Agents: Present and Future. *Cell*. 140 (6), 935–950.

DiRocco, D.P., Bisi, J., Roberts, P., Strum, J., et al. (2014) CDK4/6 inhibition induces epithelial cell cycle arrest and ameliorates acute kidney injury. *American journal of physiology. Renal physiology*. 306 (4), F379-88.

Dörr, J.R., Yu, Y., Milanovic, M., Beuster, G., et al. (2013) Synthetic lethal metabolic targeting of cellular senescence in cancer therapy. *Nature*. 501 (7467), 421–425.

Dvinge, H., Kim, E., Abdel-Wahab, O. & Bradley, R.K. (2016) RNA splicing factors as oncoproteins and tumour suppressors. *Nature Reviews Cancer*. 16 (7), 413–430.

Efeyan, A., Murga, M., Martinez-Pastor, B., Ortega-Molina, A., et al. (2009) Limited role of murine ATM in oncogene-induced senescence and p53-dependent tumor suppression. *PLoS ONE*. 4 (5), e5475.

Elyada, E., Pribluda, A., Goldstein, R.E., Morgenstern, Y., et al. (2011) CKIα ablation highlights a critical role for p53 in invasiveness control. *Nature*. 470 (7334), 409–413.

Eskens, F. a L.M., Ramos, F.J., Burger, H., O'Brien, J.P., et al. (2013) Phase I pharmacokinetic and pharmacodynamic study of the first-in-class spliceosome inhibitor E7107 in patients with advanced solid tumors. *Clinical Cancer Research*. 19 (22), 6296–6304.

Ewald, J.A., Desotelle, J.A., Wilding, G. & Jarrard, D.F. (2010) Therapy-induced senescence in cancer. *Journal of the National Cancer Institute*. 102 (20), 1536–1546.

Ewald, J.A., Peters, N., Desotelle, J.A., Hoffmann, F.M., et al. (2009) A High-Throughput Method to Identify Novel Senescene-Inducing Compounds. *Journal of Biomolecular Screening*. 14 (7), 853–858.

Fellmann, C., Hoffmann, T., Sridhar, V., Hopfgartner, B., et al. (2013) An optimized microRNA backbone for effective single-copy RNAi. *Cell Reports*. 5 (6), 1704–1713.

Finn, R.S., Crown, J.P., Lang, I., Boer, K., et al. (2015) The cyclin-dependent kinase 4/6 inhibitor palbociclib in combination with letrozole versus letrozole alone as first-line treatment of oestrogen receptor-positive, HER2-negative, advanced breast cancer (PALOMA-1/TRIO-18): A randomised phase 2 study. *The Lancet*. 16 (1), 25–35.

Fleischmann, R. (2006) Anakinra in the treatment of rheumatic disease. *Expert Review of Clinical Immunology*. 2 (3), 331–340.

Franceschi, C. & Campisi, J. (2014) Chronic inflammation (Inflammaging) and its potential contribution to age-associated diseases. *Journals of Gerontology - Series A Biological Sciences and Medical Sciences*. 69 (S1), S4–S9.

Fregoso, O.I., Das, S., Akerman, M. & Krainer, A.R. (2013) Splicing-Factor Oncoprotein SRSF1 Stabilizes p53 via RPL5 and Induces Cellular Senescence. *Molecular Cell*. 50 (1), 56–66.

Freund, A., Orjalo, A. V, Desprez, P.-Y. & Campisi, J. (2010) Inflammatory networks during cellular senescence: causes and consequences. *Trends in Molecular Medicine*. 16 (5), 238–246.

Freund, A., Patil, C.K. & Campisi, J. (2011) p38MAPK is a novel DNA damage response-independent regulator of the senescence-associated secretory phenotype. *The EMBO Journal*. 30 (8), 1536–1548.

Fu, X.-D. & Ares, M. (2014) Context-dependent control of alternative splicing by RNA-binding proteins. *Nature Reviews Genetics*. 15 (10), 689–701.

Galluzzo, M., D'Adamio, S., Servoli, S., Bianchi, L., et al. (2016) Tofacitinib for the treatment of psoriasis. *Expert Opinion on Pharmacotherapy*. 17 (10), 1421–1433.

Gama-Carvalho, M., Barbosa-Morais, N.L., Brodsky, A.S., Silver, P. a, et al. (2006) Genome-wide identification of functionally distinct subsets of cellular mRNAs associated with two nucleocytoplasmic-shuttling mammalian splicing factors. *Genome Biology*. 7 (11), R113.

Garfinkel, S., Brown, S., Wessendorf, J.H.M. & Maciag, T. (1994) Post-Transcriptional Regulation of Interleukin 1α in Various Strains of Young and Senescent Human Umbilical Vein Endothelial Cells. *Proceedings of the National Academy of Sciences*. 91 (4), 1559–1563.

Ge, Z., Quek, B.L., Beemon, K.L. & Hogg, J.R. (2016) Polypyrimidine tract binding protein 1 protects mRNAs from recognition by the nonsense-mediated mRNA decay pathway. *eLife*. 5 (e11155), 1–25.

Gewirtz, D.A. (2013) Autophagy and senescence: A partnership in search of definition. *Autophagy*. 9 (5), 808–812.

Gewirtz, D.A., Holt, S.E. & Elmore, L.W. (2008) Accelerated senescence: An emerging role in tumor cell response to chemotherapy and radiation. *Biochemical Pharmacology*. 76 (8), 947–

957.

Gil, J. & Peters, G. (2006) Regulation of the INK4b–ARF–INK4a tumour suppressor locus: all for one or one for all. *Nature Reviews Molecular Cell Biology*. 7 (9), 667–677.

Gilbert, L.A. & Hemann, M.T. (2010) DNA damage-mediated induction of a chemoresistant niche. *Cell*. 143 (3), 355–366.

Glick, A.B., Lee, M.M., Darwiche, N., Kulkarni, A.B., et al. (1994) Targeted deletion of the TGF-βi gene causes rapid progression to squamous cell carcinoma. *Genes & Development*. 8 (20), 2429–2440.

Goemans, N.M., Tulinius, M., Akker, J.T. Van Den, Ph, D., et al. (2011) Systemic Administration of PRO051 in Duchenne's Muscular Dystrophy. *The New England Journal of Medicine*. 364 (16), 1513–1522.

Gorgoulis, V.G. & Halazonetis, T.D. (2010) Oncogene-induced senescence: The bright and dark side of the response. *Current Opinion in Cell Biology*. 22 (6), 816–827.

Granovsky, M., Fata, J., Pawling, J., Muller, W.J., et al. (2000) Suppression of tumor growth and metastasis in Mgat5-deficient mice. *Nature Medicine*. 6 (3), 306–312.

Gray-Schopfer, V.C., Cheong, S.C., Chong, H., Chow, J., et al. (2006) Cellular senescence in naevi and immortalisation in melanoma: a role for p16? *British Journal of Cancer*. 95 (4), 496–505.

Grivennikov, S.I., Greten, F.R. & Karin, M. (2010) Immunity, Inflammation, and Cancer. *Cell*. 140 (6), 883–899.

Gudmundsdottir, T., F. Winther, J., De Fine Licht, S., G. Bonnesen, T., et al. (2015) Cardiovascular disease in Adult Life after Childhood Cancer in Scandinavia: A population-based cohort study of 32,308 one-year survivors. *International Journal of Cancer*. 137 (5), 1176–1186.

Guo, H., Nagy, T. & Pierce, M. (2014) Post-translational glycoprotein modifications regulate colon cancer stem cells and colon adenoma progression in Apcmin/+ mice through altered Wnt receptor signaling. *Journal of Biological Chemistry*. 289 (45), 31534–31549.

Guo, J., Jia, J. & Jia, R. (2015) PTBP1 and PTBP2 impaired autoregulation of SRSF3 in cancer cells. *Scientific Reports*. 5 (14548), 1–11.

Haines, N. & Irvine, K.D. (2003) Glycosylation regulates Notch signalling. *Nature Reviews Molecular Cell Biology*. 4 (10), 786–797.

Hanahan, D. & Weinberg, R.A. (2011) Hallmarks of cancer: The next generation. *Cell*. 144 (5), 646–674.

Harley, C.B., Futcher, A.B. & Greider, C.W. (1990) Telomeres shorten during ageing of human fibroblasts. *Nature*.345 (6274) pp.458–460.

Harrison, D.E., Strong, R., Sharp, Z.D., Nelson, J.F., et al. (2009) Rapamycin fed late in life extends lifespan in genetically heterogeneous mice. *Nature*. 460 (7253), 392–395.

Hayakawa, T., Iwai, M., Aoki, S., Takimoto, K., et al. (2015) SIRT1 suppresses the senescence-associated secretory phenotype through epigenetic gene regulation. *PLoS ONE*. 10 (1),

e0116480.

Hayflick, L. (1965) The limited in vitro lifetime of human diploid cell strains. *Experimental Cell Research*. 37 (3), 614–636.

Hayflick, L. & Moorhead, P.S. (1961) The serial cultivation of human diploid cell strains. *Experimental Cell Research*. 25 (3), 585–621.

He, X., Ee, P.L.R., Coon, J.S. & Beck, W.T. (2004) Alternative Splicing of the Multidrug Resistance Protein 1 / ATP Binding Cassette Transporter Subfamily Gene in Ovarian Cancer Creates Functional Splice Variants and Is Associated with Increased Expression of the Splicing Factors PTB and SRp20. *Clinical Cancer Research*. 10 (14), 4652–4660.

He, X., Pool, M., Darcy, K.M., Lim, S.B., et al. (2007) Knockdown of polypyrimidine tract-binding protein suppresses ovarian tumor cell growth and invasiveness in vitro. *Oncogene*. 26 (34), 4961–4968.

Hegele, A., Kamburov, A., Grossmann, A., Sourlis, C., et al. (2012) Dynamic Protein-Protein Interaction Wiring of the Human Spliceosome. *Molecular Cell*. 45 (4), 567–580.

Helman, A., Klochendler, A., Azazmeh, N., Gabai, Y., et al. (2016) p16(Ink4a)-induced senescence of pancreatic beta cells enhances insulin secretion. *Nature Medicine*. 22 (4), 412–420.

Herranz, N., Gallage, S., Mellone, M., Wuestefeld, T., et al. (2015) mTOR regulates MAPKAPK2 translation to control the senescence-associated secretory phenotype. *Nature Cell Biology*. 17 (9), 1205–1217.

Hirao, A., Kong, Y.Y., Matsuoka, S., Wakeham, A., et al. (2000) DNA damage-induced activation of p53 by the checkpoint kinase Chk2. *Science*. 287 (5459), 1824–1827.

Hoare, M., Ito, Y., Kang, T.-W., Weekes, M.P., et al. (2016) NOTCH1 mediates a switch between two distinct secretomes during senescence. *Nature Cell Biology*. 18 (9), 979–992.

Hong, D.S., Kurzrock, R., Naing, A., Wheler, J.J., et al. (2014) A phase I, open-label, single-arm, dose-escalation study of E7107, a precursor messenger ribonucleic acid (pre-mRNA) splicesome inhibitor administered intravenously on days 1 and 8 every 21 days to patients with solid tumors. *Investigational New Drugs*. 32 (3), 436–444.

Hsu, J., Hsu, M., Sorger, T., Herlyn, M., et al. (1999) Heparin/endothelial cell growth supplement regulates matrix gene expression and prolongs life span of vascular smooth muscle cells through modulation of Interleukin-1. *In Vitro Cellular & Developmental Biology*. 35 (10), 647–654.

Hsu, T.Y.-T., Simon, L.M., Neill, N.J., Marcotte, R., et al. (2015) The spliceosome is a therapeutic vulnerability in MYC-driven cancer. *Nature*. 525 (7569), 384–388.

Hubackova, S., Krejcikova, K., Bartek, J. & Hodny, Z. (2012) IL1-and TGFβ -Nox4 signaling, oxidative stress and DNA damage response are shared features of replicative, oncogene-induced, and drug-induced paracrine 'Bystander senescence'. *Aging*. 4 (12), 932–951.

Iannello, A., Thompson, T.W., Ardolino, M., Lowe, S.W., et al. (2013) p53-dependent chemokine production by senescent tumor cells supports NKG2D-dependent tumor elimination by natural

killer cells. *The Journal of Experimental Medicine*. 210 (10), 2057–2069.

Im, S.-H. & Rao, A. (2004) Activation and deactivation of gene expression by Ca2+/calcineurin-NFAT-mediated signaling. *Molecules and Cells*. 18 (1), 1–9.

Itahana, K., Dimri, G. & Campisi, J. (2001) Regulation of cellular senescence by p53. *European Journal of Biochemistry*. 268 (10), 2784–2791.

Iwasa, H., Han, J. & Ishikawa, F. (2003) Mitogen-activated protein kinase p38 defines the common senescence-signalling pathway. *Genes to Cells*. 8 (2), 131–144.

Izaguirre, D.I., Zhu, W., Hai, T., Cheung, H.C., et al. (2012) PTBP1-dependent regulation of USP5 alternative RNA splicing plays a role in glioblastoma tumorigenesis. *Molecular Carcinogenesis*. 51 (11), 895–906.

Izquierdo, J.M., Majós, N., Bonnal, S., Martínez, C., et al. (2005) Regulation of fas alternative splicing by antagonistic effects of TIA-1 and PTB on exon definition. *Molecular Cell*. 19 (4), 475–484.

Jamieson, T., Clarke, M., Steele, C.W., Samuel, M.S., et al. (2012) Inhibition of CXCR2 profoundly suppresses inflammation-driven and spontaneous tumorigenesis. *Journal of Clinical Investigation*. 122 (9), 3127–3144.

Janzen, V., Forkert, R., Fleming, H.E., Saito, Y., et al. (2006) Stem-cell ageing modified by the cyclin-dependent kinase inhibitor p16INK4a. *Nature*. 443 (7110), 421–426.

Jensen, M.A., Wilkinson, J.E. & Krainer, A.R. (2014) Splicing factor SRSF6 promotes hyperplasia of sensitized skin. *Nature Structural & Molecular Biology*. 21 (2), 189–197.

Jia, R., Li, C., McCoy, J.P., Deng, C.X., et al. (2010) SRp20 is a proto-oncogene critical for cell proliferation and tumor induction and maintenance. *International Journal of Biological Sciences*. 6 (7), 806–826.

Jiang, C., Hu, X., Wang, L., Cheng, H., et al. (2015) Excessive proliferation and impaired function of primitive hematopoietic cells in bone marrow due to senescence post chemotherapy in a T cell acute lymphoblastic leukemia model. *Journal of Translational Medicine*. 13234.

Jin, W., Bruno, I.G., Xie, T., Sanger, L.J., et al. (2003) Polypyrimidine Tract-Binding Protein Down-Regulates Fibroblast Growth Factor. *Cancer Research*. 63 (19), 6154–6157.

Jing, H., Kase, J., Dörr, J.R., Milanovic, M., et al. (2011) Opposing roles of NF- k B in anti-cancer treatment outcome unveiled by cross-species investigations. *Genes & Development*. 25 (20), 2137–2146.

Jun, J.-I. & Lau, L.F. (2010) The matricellular protein CCN1 induces fibroblast senescence and restricts fibrosis in cutaneous wound healing. *Nature Cell Biology*. 12 (7), 676–685.

Jung, H., Lee, D., Lee, J., Park, D., et al. (2015) Intron retention is a widespread mechanism of tumor-suppressor inactivation. *Nature Genetics*. 47 (11), 1242–1248.

Kaida, D., Motoyoshi, H., Tashiro, E., Nojima, T., et al. (2007) Spliceostatin A targets SF3b and inhibits both splicing and nuclear retention of pre-mRNA. *Nature Chemical Biology*. 3 (9), 576–583.

Kalathur, M., Toso, A., Chen, J., Revandkar, A., et al. (2015) A chemogenomic screening identifies CK2 as a target for pro-senescence therapy in PTEN-deficient tumours. *Nature Communications*. 67227.

Kang, C., Xu, Q., Martin, T.D., Li, M.Z., et al. (2015) The DNA damage response induces inflammation and senescence by inhibiting autophagy of GATA4. *Science*. 349 (6255), aaa5612.

Kang, T.-W., Yevsa, T., Woller, N., Hoenicke, L., et al. (2011) Senescence surveillance of pre-malignant hepatocytes limits liver cancer development. *Nature*. 479 (7374), 547–551.

Kansara, M., Leong, H.S., Lin, D.M., Popkiss, S., et al. (2013) Immune response to rb1-Regulated senescence limits radiation-Induced osteosarcoma formation. *Journal of Clinical Investigation*. 123 (12), 5351–5360.

Karni, R., de Stanchina, E., Lowe, S.W., Sinha, R., et al. (2007) The gene encoding the splicing factor SF2/ASF is a proto-oncogene. *Nature Structural & Molecular Biology*. 14 (3), 185–193.

Kendall, G.C., Mokhonova, E.I., Moran, M., Sejbuk, N.E., et al. (2012) Dantrolene enhances antisense-mediated exon skipping in human and mouse models of Duchenne muscular dystrophy. *Science Translational Medicine*. 4 (164), 164ra160.

Kim, E., Ilagan, J.O., Liang, Y., Daubner, G.M., et al. (2015) SRSF2 Mutations Contribute to Myelodysplasia by Mutant-Specific Effects on Exon Recognition. *Cancer Cell*. 27 (5), 617–630.

Kim, K.-H., Chen, C.-C., Monzon, R.I. & Lau, L.F. (2013) Matricellular protein CCN1 promotes regression of liver fibrosis through induction of cellular senescence in hepatic myofibroblasts. *Molecular and Cellular Biology*. 33 (10), 2078–2090.

Kim, K.S., Kim, M.-S., Seu, Y.B., Chung, H.Y., et al. (2007) Regulation of replicative senescence by insulin-like growth factor-binding protein 3 in human umbilical vein endothelial cells. *Aging Cell*. 6 (4), 535–545.

King, H.A., Cobbold, L.C. & Willis, A.E. (2010) The role of IRES trans-acting factors in regulating translation initiation. *Biochemical Society Transactions*. 38 (6), 1581–1586.

Klune, J.R., Dhupar, R., Cardinal, J., Billiar, T.R., et al. (2008) HMGB1: Endogenous Danger Signaling. *Molecular Medicine*. 14 (7–8), 476–484.

Knoch, K.P., Meisterfeld, R., Kersting, S., Bergert, H., et al. (2006) cAMP-dependent phosphorylation of PTB1 promotes the expression of insulin secretory granule proteins in β cells. *Cell Metabolism*. 3 (2), 123–134.

Koh, C.M., Bezzi, M., Low, D.H.P., Ang, W.X., et al. (2015) MYC regulates the core pre-mRNA splicing machinery as an essential step in lymphomagenesis. *Nature*. 523 (7558), 96–100.

Kojima, H., Kunimoto, H., Inoue, T. & Nakajima, K. (2012) The STAT3-IGFBP5 axis is critical for IL-6/gp130-induced premature senescence in human fibroblasts. *Cell Cycle*. 11 (4), 730–739.

Kong, X., Feng, D., Wang, H., Hong, F., et al. (2012) Interleukin-22 induces hepatic stellate cell senescence and restricts liver fibrosis in mice. *Hepatology*. 56 (3), 1150–1159.

Kortlever, R.M., Higgins, P.J. & Bernards, R. (2006) Plasminogen activator inhibitor-1 is a critical downstream target of p53 in the induction of replicative senescence. *Nature Cell Biology*. 8 (8), 877–884.

Krimpenfort, P., Quon, K.C., Mooi, W.J., Loonstra, A., et al. (2001) Loss of p16Ink4a confers susceptibility to metastatic melanoma in mice. *Nature*. 413 (6851), 83–86.

Krishnamurthy, J., Ramsey, M.R., Ligon, K.L., Torrice, C., et al. (2006) p16INK4a induces an age-dependent decline in islet regenerative potential. *Nature*. 443 (7110), 453–457.

Krishnamurthy, J., Torrice, C., Ramsey, M.R., Kovalev, G.I., et al. (2004) Ink4a/Arf expression is a biomarker of aging. *The Journal of Clinical Investigation*. 114 (9), 1299–1307.

Krizhanovsky, V., Yon, M., Dickins, R.A., Hearn, S., et al. (2008) Senescence of activated stellate cells limits liver fibrosis. *Cell*. 134 (4), 657–667.

Krtolica, A., Parrinello, S., Lockett, S., Desprez, P.Y., et al. (2001) Senescent fibroblasts promote epithelial cell growth and tumorigenesis: a link between cancer and aging. *Proceedings of the National Academy of Sciences*. 98 (21), 12072–12077.

Ksiazek, K., Jörres, A. & Witowski, J. (2008) Senescence induces a proangiogenic switch in human peritoneal mesothelial cells. *Rejuvenation Research*. 11 (3), 681–683.

Kuilman, T., Michaloglou, C., Mooi, W.J. & Peeper, D.S. (2010) The essence of senescence. *Genes & Development*. 24 (22), 2463–2479.

Kuilman, T., Michaloglou, C., Vredeveld, L.C.W., Douma, S., et al. (2008) Oncogene-induced senescence relayed by an interleukin-dependent inflammatory network. *Cell*. 133 (6), 1019–1031.

Kuilman, T. & Peeper, D.S. (2009) Senescence-messaging secretome: SMS-ing cellular stress. *Nature Reviews Cancer*. 9 (2), 81–94.

Kumar, S., Millis, A.J. & Baglioni, C. (1992) Expression of interleukin 1-inducible genes and production of interleukin 1 by aging human fibroblasts. *Proceedings of the National Academy of Sciences*. 89 (10), 4683–4687.

Laberge, R.-M., Sun, Y., Orjalo, A. V, Patil, C.K., et al. (2015) MTOR regulates the pro-tumorigenic senescence-associated secretory phenotype by promoting IL1A translation. *Nature Cell Biology*. 17 (8), 1049–1061.

Laberge, R.M., Zhou, L., Sarantos, M.R., Rodier, F., et al. (2012) Glucocorticoids suppress selected components of the senescence-associated secretory phenotype. *Aging Cell*. 11 (4), 569–578.

Lahtela, J., Corson, L.B., Hemmes, A., Brauer, M.J., et al. (2013) A high-content cellular senescence screen identifies candidate tumor suppressors, including EPHA3. *Cell Cycle*. 12 (4), 625–634.

Latz, E., Xiao, T.S. & Stutz, A. (2013) Activation and regulation of the inflammasomes. *Nature Reviews Immunology*. 13 (6), 397–411.

Di Leonardo, A., Linke, S.P., Clarkin, K. & Wahl, G.M. (1994) DNA damage triggers a prolonged

p53- dependent G arrest ana long-term induction of Cipl in normal human fibroblasts. *Genes & Development*. 8 (21), 2540–2551.

Lesina, M., Wörmann, S.M., Morton, J., Diakopoulos, K.N., et al. (2016) RelA regulates CXCL1 / CXCR2-dependent oncogene-induced senescence in murine Kras -driven pancreatic carcinogenesis. *The Journal of Clinical Investigation*. 126 (8), 2919–2932.

Li, H., Collado, M., Villasante, A., Strati, K., et al. (2009) The Ink4/Arf locus is a barrier for iPS cell reprogramming. *Nature*. 460 (7259), 1136–1139.

Lin, A.W., Barradas, M., Stone, J.C., van Aelst, L., et al. (1998) Premature senescence involving p53 and p16 is activated in response to constitutive MEK/MAPK mitogenic signaling. *Genes & Development*. 12 (19), 3008–3019.

Liu, D. & Hornsby, P.J. (2007) Senescent human fibroblasts increase the early growth of xenograft tumors via matrix metalloproteinase secretion. *Cancer research*. 67 (7), 3117–3126.

Liu, R., Loraine, A.E. & Dickerson, J.A. (2014) Comparisons of computational methods for differential alternative splicing detection using RNA-seq in plant systems. *BMC bioinformatics*. 15 (1), 364.

Liu, S. & Cheng, C. (2015) Alternative RNA splicing and cancer. *Wiley Interdisciplinary Reviews: RNA*. 4 (5), 547–566.

Loo, D.T., Fuquay, J.I., Rawson, C.L. & Barnes, D.W. (1987) Extended culture of mouse embryo cells without senescence: inhibition by serum. *Science*. 236 (4798), 200–202.

Lu, C., Sheehan, C., Rak, J.W., Chambers, C. a, et al. (1996) Endogenous interleukin 6 can function as an in vivo growth- stimulatory factor for advanced-stage human melanoma cells. *Clinical Cancer Research*. 2 (8), 1417–1425.

Lu, C., Vickers, M.F. & Kerbel, R.S. (1992) Interleukin 6: a fibroblast-derived growth inhibitor of human melanoma cells from early but not advanced stages of tumor progression. *Proceedings of the National Academy of Sciences*. 89 (19), 9215–9219.

Lu, Y.C., Yeh, W.C. & Ohashi, P.S. (2008) LPS/TLR4 signal transduction pathway. *Cytokine*. 42 (2), 145–151.

Lujambio, A., Akkari, L., Simon, J., Grace, D., et al. (2013) Non-cell-autonomous tumor suppression by p53. *Cell*. 153 (2), 449–460.

Lv, X. xi, Wang, X. xing, Li, K., Wang, Z. yan, et al. (2013) Rupatadine Protects against Pulmonary Fibrosis by Attenuating PAF-Mediated Senescence in Rodents. *PLoS ONE*. 8 (7), 1–15.

Lynch, T.P., Ferrer, C.M., Jackson, S.R., Shahriari, K.S., et al. (2012) Critical role of O-linked β-N-acetylglucosamine transferase in prostate cancer invasion, angiogenesis, and metastasis. *Journal of Biological Chemistry*. 287 (14), 11070–11081.

Ma, S., Liu, G., Sun, Y. & Xie, J. (2007) Relocalization of the polypyrimidine tract-binding protein during PKA-induced neurite growth. *Biochimica et Biophysica Acta - Molecular Cell Research*. 1773 (6), 912–923.

Maier, J. a, Voulalas, P., Roeder, D. & Maciag, T. (1990) Extension of the life-span of human

endothelial cells by an interleukin-1 alpha antisense oligomer. *Science*. 249 (4976), 1570–1574.

Makeyev, E. V., Zhang, J., Carrasco, M.A. & Maniatis, T. (2007) The MicroRNA miR-124 Promotes Neuronal Differentiation by Triggering Brain-Specific Alternative Pre-mRNA Splicing. *Molecular Cell*. 27 (3), 435–448.

Mallette, F.A., Gaumont-Leclerc, M.F. & Ferbeyre, G. (2007) The DNA damage signaling pathway is a critical mediator of oncogene-induced senescence. *Genes & Development*. 21 (1), 43–48.

Malo, N., Hanley, J.A., Cerquozzi, S., Pelletier, J., et al. (2006) Statistical practice in high-throughput screening data analysis. *Nature Biotechnology*. 24 (2), 167–175.

Mantovani, A., Allavena, P., Sica, A. & Balkwill, F. (2008) Cancer-related inflammation. *Nature*. 454 (7203), 436–444.

Maquat, L.E., Kinniburgh, A.J., Beach, L.R., Honig, G.R., et al. (1980) Processing of human beta-globin mRNA precursor to mRNA is defective in three patients with beta+-thalassemia. *Proceedings of the National Academy of Sciences*. 77 (7), 4287–4291.

Marcoux, S., Le, O.N.L., Langlois-Pelletier, C., Laverdière, C., et al. (2013) Expression of the senescence marker p16INK4a in skin biopsies of acute lymphoblastic leukemia survivors: a pilot study. *Radiation Oncology*. 8252.

Martin, N., Popov, N., Aguilo, F., Loghlen, A.O.R., et al. (2013) Interplay between Homeobox proteins and Polycomb repressive complexes in p16INK4a regulation. *The EMBO Journal*. 32 (7), 982–995.

Massagué, J. (2008) TGFβ in Cancer. *Cell*. 134 (2), 215–230.

McClorey, G. & Wood, M.J. (2015) An overview of the clinical application of antisense oligonucleotides for RNA-targeting therapies. *Current Opinion in Pharmacology*. 2452–58.

Mendell, J.R., Rodino-Klapac, L.R., Sahenk, Z., Roush, K., et al. (2013) Eteplirsen for the treatment of Duchenne muscular dystrophy. *Annals of Neurology*. 74 (5), 637–647.

Di Micco, R., Fumagalli, M., Cicalese, A., Piccinin, S., et al. (2006) Oncogene-induced senescence is a DNA damage response triggered by DNA hyper-replication. *Nature*. 444 (7119), 638–642.

Michaloglou, C., Vredeveld, L.C.W., Soengas, M.S., Denoyelle, C., et al. (2005) BRAFE600-associated senescence-like cell cycle arrest of human naevi. *Nature*. 436 (7051), 720–724.

Michaud, K., Solomon, D.A., Oermann, E., Kim, J.S., et al. (2010) Pharmacologic inhibition of cyclin-dependent kinases 4 and 6 arrests the growth of glioblastoma multiforme intracranial xenografts. *Cancer Research*. 70 (8), 3228–3238.

Minagawa, S., Araya, J., Numata, T., Nojiri, S., et al. (2011) Accelerated epithelial cell senescence in IPF and the inhibitory role of SIRT6 in TGF-β-induced senescence of human bronchial epithelial cells. *American Journal of Physiology-Lung Cellular and Molecular Physiology*. 300 (3), L391–L401.

Minamino, T., Orimo, M., Shimizu, I., Kunieda, T., et al. (2009) A crucial role for adipose tissue p53 in the regulation of insulin resistance. *Nature Medicine*. 15 (9), 1082–1087.

Mitchell, S.A., Spriggs, K.A., Bushell, M., Evans, J.R., et al. (2005) Identification of a motif that mediates polypyrimidine tract-binding protein-dependent internal ribosome entry. *Genes & Development*. 19 (13), 1556–1571.

Mitchell, S.A., Spriggs, K.A., Coldwell, M.J., Jackson, R.J., et al. (2003) The Apaf-1 internal ribosome entry segment attains the correct structural conformation for function via interactions with PTB and unr. *Molecular Cell*. 11 (3), 757–771.

Di Mitri, D., Toso, A., Chen, J.J., Sarti, M., et al. (2014) Tumour-infiltrating Gr-1+ myeloid cells antagonize senescence in cancer. *Nature*. 515 (7525), 134–137.

Mitsuhashi, S., Shima, H., Li, Y., Tanuma, N., et al. (2008) Tautomycetin suppresses the TNFα/NF-κB pathway via inhibition of IKK activation. *Internation Journal of Oncology*. 33 (5), 1027–1035.

Moiseeva, O., Deschênes-Simard, X., St-Germain, E., Igelmann, S., et al. (2013) Metformin inhibits the senescence-associated secretory phenotype by interfering with IKK/NF-κB activation. *Aging Cell*. 12 (3), 489–498.

Morancho, B., Martínez-Barriocanal, Á., Villanueva, J. & Arribas, J. (2015) Role of ADAM17 in the non-cell autonomous effects of oncogene-induced senescence. *Breast cancer research : BCR*. 17106.

Muñoz-Espín, D., Cañamero, M., Maraver, A., Gómez-López, G., et al. (2013) Programmed cell senescence during mammalian embryonic development. *Cell*. 155 (5), 1104–1118.

Muñoz-Espín, D. & Serrano, M. (2014) Cellular senescence: from physiology to pathology. *Nature Reviews Molecular Cell Biology*. 15 (7), 482–496.

Nakajima, H., Hori, Y., Terano, H., Okuhara, M., et al. (1996) New antitumor substances, FR901463, FR901464 and FR901465. II. Activities against experimental tumors in mice and mechanism of action. *The Journal of Antibiotics*. 49 (12), 1204–1211.

Narita, M. & Lowe, S.W. (2005) Senescence comes of age. *Nature Medicine*. 11 (9), 920–922.

Narita, M., Nuñez, S., Heard, E., Narita, M., et al. (2003) Rb-mediated heterochromatin formation and silencing of E2F target genes during cellular senescence. *Cell*. 113 (6), 703–716.

Narita, M., Young, A.R., Arakawa, S., Samarajiwa, S.A., et al. (2011) Spatial coupling of mTOR and autophagy augments secretory phenotypes. *Science*. 332 (6032), 966–970.

Natarajan, V., Komarov, A.P., Ippolito, T., Bonneau, K., et al. (2014) Peptides genetically selected for NF-κB activation cooperate with oncogene Ras and model carcinogenic role of inflammation. *Proceedings of the National Academy of Sciences*. 111 (4), E474–E483.

Nawrocki, S.T., Griffin, P., Kelly, K.R. & Carew, J.S. (2012) MLN4924: a novel first-in-class inhibitor of NEDD8-activating enzyme for cancer therapy. *Expert Opinion on Investigational Drugs*. 21 (10), 1563–1573.

Nelson, C.E., Hakim, C.H., Ousterout, D.G., Thakore, P.I., et al. (2016) In vivo genome editing improves muscle function in a mouse model of Duchenne muscular dystrophy. *Science*. 351 (6271), 403–407.

Nelson, G., Wordsworth, J., Wang, C., Jurk, D., et al. (2012) A senescent cell bystander effect: Senescence-induced senescence. *Aging Cell*. 11 (2), 345–349.

Ness, K.K., Armstrong, G.T., Kundu, M., Wilson, C.L., et al. (2015) Frailty in childhood cancer survivors. *Cancer*. 121 (10), 1540–1547.

Obenauf, A.C., Zou, Y., Ji, A.L., Vanharanta, S., et al. (2015) Therapy-induced tumour secretomes promote resistance and tumour progression. *Nature*. 520 (7547), 368–372.

Oeffinger, K., Mertens, A. & Sklar, C. (2006) Chronic health conditions in adult survivors of childhood cancer. *The New England Journal of Medicine*. 355 (15), 1572–1582.

Okumura, N., Yoshida, H., Kitagishi, Y., Nishimura, Y., et al. (2011) Alternative splicings on p53, BRCA1 and PTEN genes involved in breast cancer. *Biochemical and Biophysical Research Communications*. 413 (3), 395–399.

Olovnikov, A.M. (1973) A theory of marginotomy. *Journal of Theoretical Biology*. 201 (41), 181–190.

Oltean, S. & Bates, D.O. (2014) Hallmarks of alternative splicing in cancer. *Oncogene*. 33 (46), 5311–5318.

Orjalo, A. V, Bhaumik, D., Gengler, B.K., Scott, G.K., et al. (2009) Cell surface-bound IL-1alpha is an upstream regulator of the senescence-associated IL-6/IL-8 cytokine network. *Proceedings of the National Academy of Sciences*. 106 (40), 17031–17036.

Parrinello, S., Coppe, J.P., Krtolica, A. & Campisi, J. (2005) Stromal-epithelial interactions in aging and cancer: senescent fibroblasts alter epithelial cell differentiation. *Journal of Cell Science*. 118 (Pt 3), 485–496.

Parrinello, S., Samper, E., Krtolica, A., Goldstein, J., et al. (2003) Oxygen sensitivity severely limits the replicative lifespan of murine fibroblasts. *Nature Cell Biology*. 5 (8), 741–747.

Partridge, E.A. (2004) Regulation of Cytokine Receptors by Golgi N-Glycan Processing and Endocytosis. *Science*. 306 (5693), 120–124.

Passos, J.F., Nelson, G., Wang, C., Richter, T., et al. (2010) Feedback between p21 and reactive oxygen production is necessary for cell senescence. *Molecular Systems Biology*. 6 (347), 1–14.

Pattabiraman, D.R., Bierie, B., Kober, K.I., Thiru, P., et al. (2016) Activation of PKA leads to mesenchymal-to-epithelial transition and loss of tumor-initiating ability. *Science*. 351 (6277), aad3680.

Pazolli, E., Alspach, E., Milczarek, A., Prior, J., et al. (2012) Chromatin remodeling underlies the senescence- associated secretory phenotype of tumor stromal fibroblasts that supports cancer progression. *Cancer Research*. 72 (9), 2251–2261.

Pelz, O., Gilsdorf, M. & Boutros, M. (2010) web cellHTS2: a web-application for the analysis of high-throughput screening data. *BMC Bioinformatics*. 11 (185), 1–6.

Pérez-Mancera, P.A., Young, A.R.J. & Narita, M. (2014) Inside and out: the activities of senescence in cancer. *Nature Reviews Cancer*. 14 (8), 547–558.

Perrigue, P.M., Silva, M.E., Warden, C.D., Feng, N.L., et al. (2015) The Histone Demethylase Jumonji Coordinates Cellular Senescence Including Secretion of Neural Stem Cell-Attracting Cytokines. *Molecular Cancer Research*. 13 (4), 636–650.

Picelli, S., Faridani, O.R., Björklund, A.K., Winberg, G., et al. (2014) Full-length RNA-seq from single cells using Smart-seq2. *Nature Protocols*. 9 (1), 171–181.

Pinho, S.S. & Reis, C.A. (2015) Glycosylation in cancer: mechanisms and clinical implications. *Nature Reviews Cancer*. 15 (9), 540–555.

te Poele, R.H., Okorokov, A.L., Jardine, L., Cummings, J., et al. (2002) DNA Damage Is Able to Induce Senescence in Tumor Cells in Vitro and in Vivo DNA Damage Is Able to Induce Senescence in Tumor Cells in Vitro and in Vivo. *Cancer Research*. 62 (6), 1876–1883.

Poulikakos, P.I., Persaud, Y., Janakiraman, M., Kong, X., et al. (2011) RAF inhibitor resistance is mediated by dimerization of aberrantly spliced BRAF(V600E). *Nature*. 480 (7377), 387–390.

Pramono, Z.A.D., Wee, K.B., Wang, J.L., Chen, Y.J., et al. (2012) A Prospective Study in the Rational Design of Efficient Antisense Oligonucleotides for Exon Skipping in the DMD Gene. *Human Gene Therapy*. 23 (7), 781–790.

Pribluda, A., Elyada, E., Wiener, Z., Hamza, H., et al. (2013) A senescence-inflammatory switch from cancer-inhibitory to cancer-promoting mechanism. *Cancer cell*. 24 (2), 242–256.

Qiu, L., Joazeiro, C., Fang, N., Wang, H.Y., et al. (2000) Recognition and ubiquitination of Notch by Itch, a Hect-type E3 ubiquitin ligase. *Journal of Biological Chemistry*. 275 (46), 35734–35737.

Rader, J., Russell, M.R., Hart, L.S., Nakazawa, M.S., et al. (2013) Dual CDK4/CDK6 inhibition induces cell-cycle arrest and senescence in neuroblastoma. *Clinical Cancer Research*. 19 (22), 6173–6182.

Ramakrishnan, P., Clark, P.M., Mason, D.E., Peters, E.C., et al. (2013) Activation of the transcriptional function of the NF-kappaB protein c-Rel by O-GlcNAc glycosylation. *Science Signaling*. 6 (290), ra75.

Rao, D.D., Vorhies, J.S., Senzer, N. & Nemunaitis, J. (2009) siRNA vs. shRNA: Similarities and differences. *Advanced Drug Delivery Reviews*. 61 (9), 746–759.

Ressler, S., Bartkova, J., Niederegger, H., Bartek, J., et al. (2006) p16INK4A is a robust in vivo biomarker of cellular aging in human skin. *Aging Cell*. 5 (5), 379–389.

Roberson, R.S., Kussick, S.J., Vallieres, E., Cells, L.C., et al. (2005) Escape from Therapy-Induced Accelerated Cellular Senescence in p53-Null Lung Cancer Cells and in Human Lung Cancers. *Cancer research*. 65 (7), 2795–2803.

Robles, S.J. & Adami, G.R. (1998) Agents that cause DNA double strand breaks lead to p16INK4a enrichment and the premature senescence of normal fibroblasts. *Oncogene*. 16 (9), 1113–1123.

Rodier, F., Coppé, J.-P., Patil, C.K., Hoeijmakers, W.A.M., et al. (2009) Persistent DNA damage signalling triggers senescence-associated inflammatory cytokine secretion. *Nature Cell*

Biology. 11 (8), 973–979.

Rodier, F., Muñoz, D.P., Teachenor, R., Chu, V., et al. (2011) DNA-SCARS: distinct nuclear structures that sustain damage-induced senescence growth arrest and inflammatory cytokine secretion. *Journal of Cell Science*. 124 (Pt 1), 68–81.

Rothwell, P.M., Fowkes, F.G.R., Belch, J.F., Ogawa, H., et al. (2011) Effect of daily aspirin on long-term risk of death due to cancer: Analysis of individual patient data from randomised trials. *The Lancet*. 377 (9759), 31–41.

Ruhland, M.K., Loza, A.J., Capietto, A.-H., Luo, X., et al. (2016) Stromal senescence establishes an immunosuppressive microenvironment that drives tumorigenesis. *Nature Communications*. 711762.

Sadaie, M., Dillon, C., Narita, M., Young, A.R.J., et al. (2015) Cell-based screen for altered nuclear phenotypes reveals senescence progression in polyploid cells after Aurora kinase B inhibition. *Molecular Biology of the Cell*. 26 (17), 2971–2985.

Sage, J., Mulligan, G.J., Attardi, L.D., Miller, A., et al. (2000) Targeted disruption of the three Rb-related genes leads to loss of G(1) control and immortalization. *Genes & Development*. 14 (23), 3037–3050.

Salama, R., Sadaie, M., Hoare, M. & Narita, M. (2014) Cellular senescence and its effector programs. *Genes & Development*. 28 (2), 99–114.

Salton, M. & Misteli, T. (2016) Small Molecule Modulators of Pre-mRNA Splicing in Cancer Therapy. *Trends in Molecular Medicine*. 22 (1), 28–37.

Sarkisian, C.J., Keister, B.A., Stairs, D.B., Boxer, R.B., et al. (2007) Dose-dependent oncogene-induced senescence in vivo and its evasion during mammary tumorigenesis. *Nature Cell Biology*. 9 (5), 493–505.

Sarrazin, S., Lamanna, W.C. & Esko, J.D. (2011) Heparan Sulfate Proteoglycans. *Cold Spring Harbor Perspectives in Biology*. 3 (7), 1–33.

Schmitt, C.A., Fridman, J.S., Yang, M., Lee, S., et al. (2002) A Senescence Program Controlled by p53 and p16< sup> INK4a</sup> Contributes to the Outcome of Cancer Therapy. *Cell*. 109 (3), 335–346.

Schroder, K. & Tschopp, J. (2010) The Inflammasomes. *Cell*. 140 (6), 821–832.

Scotti, M.M. & Swanson, M.S. (2015) RNA mis-splicing in disease. *Nature Reviews Genetics*. 17 (1), 19–32.

Sebestyen, E., Zawisza, M. & Eyras, E. (2015) Detection of recurrent alternative splicing switches in tumor samples reveals novel signatures of cancer. *Nucleic Acids Research*. 43 (3), 1345–1356.

Seitz, C.S., Lin, Q., Deng, H. & Khavari, P.A. (1998) Alterations in NF-kappaB function in transgenic epithelial tissue demonstrate a growth inhibitory role for NF-kappaB. *Proceedings of the National Academy of Sciences*. 95 (5), 2307–2312.

Serrano, M. & Blasco, M.A. (2001) Putting the stress on senescence. *Current Opinion in Cell*

Biology. 13 (6), 748–753.

Serrano, M., Lin, A.W., McCurrach, M.E., Beach, D., et al. (1997) Oncogenic ras Provokes Premature Cell Senescence Associated with Accumulation of p53 and p16 INK4a. *Cell*. 88 (5), 593–602.

Shah, P.P., Donahue, G., Otte, G.L., Capell, B.C., et al. (2013) Lamin B1 depletion in senescent cells triggers large-scale changes in gene expression and the chromatin landscape. *Genes & Development*. 27 (16), 1787–1799.

Sharpless, N.E. & Sherr, C.J. (2015) Forging a signature of in vivo senescence. *Nature Reviews Cancer*. 15 (7), 397–408.

Shaw, P.J., McDermott, M.F. & Kanneganti, T.-D. (2011) Inflammasomes and autoimmunity. *Trends in Molecular Medicine*. 17 (2), 57–64.

Shay, J.W., Pereira-Smith, O.M. & Wright, W.E. (1991) A role for both RB and p53 in the regulation of human cellular senescence. *Experimental Cell Research*. 196 (1), 33–39.

Shelton, D.N., Chang, E., Whittier, P.S., Choi, D., et al. (1999) Microarray analysis of replicative senescence. *Current Biology*. 9 (17), 939–945.

Shirai, C.L., Ley, J.N., White, B.S., Kim, S., et al. (2015) Mutant U2AF1 Expression Alters Hematopoiesis and Pre-mRNA Splicing In Vivo. *Cancer Cell*. 27 (5), 631–643.

Shivshankar, P., Brampton, C., Miyasato, S., Kasper, M., et al. (2012) Caveolin-1 deficiency protects from pulmonary fibrosis by modulating epithelial cell senescence in mice. *American Journal of Respiratory Cell and Molecular Biology*. 47 (1), 28–36.

Sone, H. & Kagawa, Y. (2005) Pancreatic beta cell senescence contributes to the pathogenesis of type 2 diabetes in high-fat diet-induced diabetic mice. *Diabetologia*. 48 (1), 58–67.

Sousa-Victor, P., Gutarra, S., García-Prat, L., Rodriguez-Ubreva, J., et al. (2014) Geriatric muscle stem cells switch reversible quiescence into senescence. *Nature*. 506 (7488), 316–321.

Sparmann, A. & Bar-Sagi, D. (2004) Ras-induced interleukin-8 expression plays a critical role in tumor growth and angiogenesis. *Cancer cell*. 6 (5), 447–458.

Spellman, R., Llorian, M. & Smith, C.W.J. (2007) Crossregulation and Functional Redundancy between the Splicing Regulator PTB and Its Paralogs nPTB and ROD1. *Molecular Cell*. 27 (3), 420–434.

Spellman, R. & Smith, C.W.J. (2006) Novel modes of splicing repression by PTB. *Trends in Biochemical Sciences*. 31 (2), 73–76.

Storer, M., Mas, A., Robert-Moreno, A., Pecoraro, M., et al. (2013) Senescence is a developmental mechanism that contributes to embryonic growth and patterning. *Cell*. 155 (5), 1119–1130.

Sun, Y., Campisi, J., Higano, C., Beer, T.M., et al. (2012) Treatment-induced damage to the tumor microenvironment promotes prostate cancer therapy resistance through WNT16B. *Nature Medicine*. 18 (9), 1359–1368.

Supek, F., Miñana, B., Valcárcel, J., Gabaldón, T., et al. (2014) Synonymous mutations frequently act as driver mutations in human cancers. *Cell*. 156 (6), 1324–1335.

Tabebordbar, M., Zhu, K., Cheng, J.K.W., Chew, W.L., et al. (2016) In vivo gene editing in dystrophic mouse muscle and muscle stem cells. *Science*. 351 (6271), 407–411.

Takahashi, S., Kubo, K., Waguri, S., Yabashi, A., et al. (2012) Rab11 regulates exocytosis of recycling vesicles at the plasma membrane. *Journal of Cell Science*. 125 (17), 4049–4057.

Takeuchi, H. & Haltiwanger, R.S. (2014) Significance of glycosylation in Notch signaling. *Biochemical and Biophysical Research Communications*. 453 (2), 235–242.

Tamura, F., Sato, Y., Hirakawa, M., Yoshida, M., et al. (2016) RNAi-mediated gene silencing of ST6GalNAc I suppresses the metastatic potential in gastric cancer cells. *Gastric Cancer*. 19 (1), 85–97.

Tanaka, T., Ogata, A. & Narazaki, M. (2010) Tocilizumab for the treatment of rheumatoid arthritis. *Expert Review of Clinical Immunology*. 6 (6), 843–854.

Tang, Y., Horikawa, I., Ajiro, M., Robles, a I., et al. (2012) Downregulation of splicing factor SRSF3 induces p53β, an alternatively spliced isoform of p53 that promotes cellular senescence. *Oncogene*. 32 (22 2011), 2792–2798.

Tarutani, M., Cai, T., Dajee, M. & Khavari, P.A. (2003) Inducible activation of Ras and Raf in adult epidermis. *Cancer Research*. 63 (2), 319–323.

Tasdemir, N., Banito, A., Roe, J.-S., Alonso-Curbelo, D., et al. (2016) BRD4 connects enhancer remodeling to senescence immune surveillance. *Cancer Discovery*. 6 (6), 612–629.

Tchkonia, T., Morbeck, D.E., Von Zglinicki, T., Van Deursen, J., et al. (2010) Fat tissue, aging, and cellular senescence. *Aging Cell*. 9 (5), 667–684.

Tefferi, A. (2013) JAK inhibitors for myeloproliferative neoplasms : clarifying facts from JAK inhibitors for myeloproliferative neoplasms : clarifying facts from myths. *Blood*. 119 (12), 2721–2730.

Tominaga-Yamanaka, K., Abdelmohsen, K., Martindale, J.L., Yang, X., et al. (2012) Nf90 coordinately represses the senescence-associated secretory phenotype. *Aging*. 4 (10), 695–708.

Toso, A., Revandkar, A., DiMitri, D., Guccini, I., et al. (2014) Enhancing chemotherapy efficacy in pten-deficient prostate tumors by activating the senescence-associated antitumor immunity. *Cell Reports*. 9 (1), 75–89.

Tremain, R., Marko, M., Kinnimulki, V., Ueno, H., et al. (2000) Defects in TGFβ signaling overcome senescence of mouse keratinocytes expressing v-ras Ha. *Oncogene*. 19 (13), 1698–1709.

Turner, N.C., Ro, J., André, F., Loi, S., et al. (2015) Palbociclib in Hormone-Receptor-Positive Advanced Breast Cancer. *The New England Journal of Medicine*. 373 (3), 209–219.

Tuveson, D.A., Shaw, A.T., Willis, N.A., Silver, D.P., et al. (2004) Endogenous oncogenic K-rasG12D stimulates proliferation and widespread neoplastic and developmental defects. *Cancer Cell*. 5 (4), 375–387.

Utikal, J., Polo, J.M., Stadtfeld, M., Maherali, N., et al. (2009) Immortalization eliminates a roadblock during cellular reprogramming into iPS cells. *Nature*. 460 (7259), 1145–1148.

Vaziri, H. & Benchimol, S. (1998) Reconstitution of telomerase activity in normal human cells leads to elongation of telomeres and extended replicative life span. *Current Biology*. 8 (5), 279–282.

Vijayachandra, K., Lee, J. & Glick, A.B. (2003) Smad3 regulates senescence and malignant conversion in a mouse multistage skin carcinogenesis model. *Cancer Research*. 63 (13), 3447–3452.

Visser, K.E. De, Eichten, A. & Coussens, L.M. (2006) Paradoxical roles of the immune system during cancer development. *Nature Reviews Cancer*. 6 (1), 24–37.

Vossler, M.R., Yao, H., York, R.D., Pan, M.G., et al. (1997) cAMP activates MAP kinase and Elk-1 through a B-Raf- and Rap1-dependent pathway. *Cell*. 89 (1), 73–82.

Wahl, M.C. & Lührmann, R. (2015) SnapShot: Spliceosome Dynamics III. *Cell*. 162 (3), 690–690.

Wajapeyee, N., Serra, R.W., Zhu, X., Mahalingam, M., et al. (2008) Oncogenic BRAF induces senescence and apoptosis through pathways mediated by the secreted protein IGFBP7. *Cell*. 132 (3), 363–374.

Wang, C., Norton, J.T., Ghosh, S., Kim, J., et al. (2008) Polypyrimidine Tract-binding Protein (PTB) differentially affects malignancy in a cell line-dependent manner. *Journal of Biological Chemistry*. 283 (29), 20277–20287.

Wang, E.T., Sandberg, R., Luo, S., Khrebtukova, I., et al. (2008) Alternative isoform regulation in human tissue transcriptomes. *Nature*. 456 (7221), 470–476.

Wang, S., Moerman, E.J., Jones, R.A., Thweatt, R., et al. (1996) Characterization of IGFBP-3, PAI-1 and SPARC mRNA expression in senescent fibroblasts. *Mechanisms of Ageing and Development*. 92 (2–3), 121–132.

Wang, W., Chen, J.X., Liao, R., Deng, Q., et al. (2002) Sequential activation of the MEK-extracellular signal-regulated kinase and MKK3/6-p38 mitogen-activated protein kinase pathways mediates oncogenic ras-induced premature senescence. *Molecular and Cellular Biology*. 22 (10), 3389–3403.

Watson, J.D. (1972) Origin of concatemeric T7 DNA. *Nature: New biology*. 239 (94), 197–201.

Wculek, S.K. & Malanchi, I. (2015) Neutrophils support lung colonization of metastasis-initiating breast cancer cells. *Nature*. 528 (7582), 413–417.

Weber, K.S., Hildner, K., Murphy, K.M. & Allen, P.M. (2010) Trpm4 Differentially Regulates Th1 and Th2 Function by Altering Calcium Signaling and NFAT Localization. *The Journal of Immunology*. 185 (5), 2836–2846.

Wee, K.B., Pramono, Z.A.D., Wang, J.L., MacDorman, K.F., et al. (2008) Dynamics of co-transcriptional pre-mRNA folding influences the induction of dystrophin exon skipping by antisense oligonucleotides. *PLoS ONE*. 3 (3), e1844.

Wei, W., Hemmer, R.M. & Sedivy, J.M. (2001) Role of p14(ARF) in replicative and induced senescence of human fibroblasts. *Molecular and Cellular Biology*. 21 (20), 6748–6757.

Wojciechowski, D. & Vincenti, F. (2013) Tofacitinib in kidney transplantation. *Expert Opinion on Investigational Drugs*. 22 (9), 1193–1199.

Wu, B. & Guo, W. (2015) The Exocyst at a Glance. *Journal of Cell Science*. 128 (16), 2957–2964.

Xie, J., Lee, J.-A., Kress, T.L., Mowry, K.L., et al. (2003) Protein kinase A phosphorylation modulates transport of the polypyrimidine tract-binding protein. *Proceedings of the National Academy of Sciences*. 100 (15), 8776–8781.

Xu, L., Park, K.H., Zhao, L., Xu, J., et al. (2016) CRISPR-mediated Genome Editing Restores Dystrophin Expression and Function in mdx Mice. *Molecular Therapy*. 24 (3), 564–569.

Xu, M., Tchkonia, T., Ding, H., Ogrodnik, M., et al. (2015) JAK inhibition alleviates the cellular senescence-associated secretory phenotype and frailty in old age. *Proceedings of the National Academy of Sciences*. 112 (46), E6301–E6310.

Xue, W., Zender, L., Miething, C., Dickins, R.A., et al. (2007) Senescence and tumour clearance is triggered by p53 restoration in murine liver carcinomas. *Nature*. 445 (7128), 656–660.

Xue, Y., Zhou, Y., Wu, T., Zhu, T., et al. (2009) Genome-wide Analysis of PTB-RNA Interactions Reveals a Strategy Used by the General Splicing Repressor to Modulate Exon Inclusion or Skipping. *Molecular Cell*. 36 (6), 996–1006.

Yamamoto, S., Shimizu, S., Kiyonaka, S., Takahashi, N., et al. (2008) TRPM2-mediated Ca2+influx induces chemokine production in monocytes that aggravates inflammatory neutrophil infiltration. *Nature Medicine*. 14 (7), 738–747.

Yamaoka, K. & Tanaka, Y. (2014) Targeting the Janus kinases in rheumatoid arthritis: focus on tofacitinib. *Expert Opinion on Pharmacotherapy*. 15 (1), 103–113.

Yang, G., Rosen, D.G., Zhang, Z., Bast, R.C., et al. (2006) The chemokine growth-regulated oncogene 1 (Gro-1) links RAS signaling to the senescence of stromal fibroblasts and ovarian tumorigenesis. *Proceedings of the National Academy of Sciences*. 103 (44), 16472–16477.

Yosef, R., Pilpel, N., Tokarsky-Amiel, R., Biran, A., et al. (2016) Directed elimination of senescent cells by inhibition of BCL-W and BCL-XL. *Nature Communications*. 711190.

Yoshimoto, S., Loo, T.M., Atarashi, K., Kanda, H., et al. (2013) Obesity-induced gut microbial metabolite promotes liver cancer through senescence secretome. *Nature*. 499 (7456), 97–101.

Youm, Y.H., Kanneganti, T.D., Vandanmagsar, B., Zhu, X., et al. (2012) The NLRP3 Inflammasome Promotes Age-Related Thymic Demise and Immunosenescence. *Cell Reports*. 1 (1), 56–68.

Zhou, J., Fujiwara, T., Ye, S., Li, X., et al. (2015) Ubiquitin E3 Ligase LNX2 is Critical for Osteoclastogenesis In Vitro by Regulating M-CSF/RANKL Signaling and Notch2. *Calcified Tissue International*. 96 (5), 465–475.

Zhu, J., Woods, D., McMahon, M. & Bishop, J.M. (1998) Senescence of human fibroblasts induced by oncogenic Raf. *Genes & Development*. 12 (19), 2997–3007.

Zhu, Y., Tchkonia, T., Pirtskhalava, T., Gower, A.C., et al. (2015) The Achilles' heel of senescent cells: From transcriptome to senolytic drugs. *Aging Cell*. 14 (4), 644–658.

Appendix

Table A1. Plasmids.

Vector	Insert	Antibiotic resistance	
		Mammalian	Bacterial
LXSN	empty vector	Neomycin	Ampicillin
pLNC	ER:RAS	Neomycin	Ampicillin
pGIPZ	empty vector/shRNA	Puromycin	Ampicillin & Zeocin™
pRRL (LT3GEPIR)	empty vector/shRNA	Puromycin	Ampicillin
CMV-tight	empty vector/PTBP1	Puromycin	Ampicillin
CMV-rtTA3	vector	Hygromycin	Ampicillin

Table A2. Antibiotics.

Antibiotic	Company	Working concentration
Neomycin (Geneticin®)	gibco	400 µg/ml
Puromycin	InvivoGen	0.8 µg/ml
Hygromycin	InvivoGen	25 µg/ml
Ampicillin	Sigma	100 mg/ml
Zeocin™	InvivoGen	25 mg/ml

Table A3. shRNA sequences.

Target		shRNA sequence	Target		shRNA sequence
AKR1C1	1	CAGAAAGGAAAGACAATAA	*SACM1L*	1	CATCTGGTGGCAGGTAATT
	2	ATATTGATTCTGCTCATTT		2	CATGCATTCATGTTCTATT
	3	AGAAAGGAAAGACAATAAT		3	TGGAACTCAATGATACGAT
	4	TTGGATTATGTTGACCTCT		4	GGGATCGACTAAGTATTTT
BRD8	1	AGCCTGTTACAGATGACAT	*SKP1A*	1	GCAAGACCTTCAATATCAA
	2	CGGAGAGAGAACCTAGTGA		2	CAGAAAGCATCCATCATGA
	3	AGGAAGAGGATCAAGGAGA		3	CAAACAATCTGTGACTATT
	4	AGGAGAGATATAGACGGCT		4	CAGCAGCAAGTCAATTGTA
PLCB1	1	GTCATCGGACTCTCTCTTA	*TMEM219*	1	CCTTGGCTCTGAGTTGGAA
	2	CCCTCGACCTGAAATTGAT		2	AAGGATCTTCTGCAGGACA
	3	AGAGATAGAATAAAGTTGA		3	AGGACAACTGGTCCTTATC
	4	TGTTTGAGAATAGCAGTTT		4	GGAGACGGTCCAGACAGGA
PP1A	1	GCATCTATGGTTTCTACGA	*UBE2V2*	1	CTGGAGTACTCGAAATAGA
	2	ACGACCTTCTGCGACTATT		2	GACAAGGAGTCCTAGGTAT
	3	GCGGCCATAGTGGACGAAA		3	GTCTAATGATGTCCAAAGA
	4	GGCTACGAGTTCTTTGCCA		4	GTCAGTTAGATTTGTAACA
PTBP1	52	CGGCACAGTGTTGAAGATC	*UNG*	1	CTGTGAGCTTTATCAGATA
	53	AGACCAGAGATTTTATTTT		2	AAGAGTTGTCTACAGACAT
	86	GGATTCAAGTTCTTCCAGA		3	TGGGATTTGTTGCAGAAGA
	87	CGCGTGAAGATCCTGTTCA		4	TGCAGTTGTGTCCTGGCTA
PTPN14	1	GCCACAAGATATCAGTATT	*p53*	1	TCTCTTCCTCTGTGCGCCG
	2	CCTGGACTTAAATTATTTA	*mTOR*	2	AGGCCTATGGTCGAGATTT
	3	AAGTTCAAGGTCACCACGA			
	4	AGTACAAGTTTGTCTACCA			

Table A4. PCR conditions.

	shRNA mir-30 to mir-E			pBabe-PTBP1 to CMVtight			Splicing validation		
Step	°C	Time	Cycles	°C	Time	Cycles	°C	Time	Cycles
Initial Denaturation	94	2 min	1	94	5 min	1	94	5 min	1
Denaturation	94	15 s		94	30 s		94	30 s	
Annealing	54	30 s	33	72	105 s	31	56	30 s	33
Extension	68	25 s					70	25 s	
Final extension	68	5 min	1	72	5 min	1	70	5 min	1
Storage	4	∞	-	4	∞	-	4	∞	-

All PCR reactions were performed in a Bio-Rad Dyad Peltier Thermal cycler

Table A5. Primer sequences.

a. PCR

Primer Name	Sequence
miRE-Xho-short-fw	AGAAGGCTCGAGAAGGTATATTGC
miRE-EcoPlasmid-rev	GCTCGAATTCTAGCCCCTTGAAGTCCGAGG
CMVptbp1F	CGTTCGAAGCCACCATGGACGGCATTGTCCCA
CMVptbp1R	CCGGTTTAAACCTAGATGGTGGACTTGGAGAAG
ATP2B4 F	GATCCTCTGGTTCCGGGG
ATP2B4 R	GCTGTGGATGGACTTTTGGT
Exoc7 F	TACTCCCCTGCTATCCCCAA
Exoc7 R	ATGTAGGCATCGGTCTCCAC
Mark3 F	CTGTCCCATGAAGCCACAC
Mark3 R	TTTCATGCTCCAGGTGAAGC
Med23 F	GTTGAGATATGTATTGGAGCAGC
Med23 R	TCAGATCGCTCCATGGCATA
NAV1 F	CCACGGACGATGTTCACG
NAV1 R	ATTCACCAGGCTCTGCTCAA
PPP3CB F	AGGAGAGTGAAAGTGTGCTGA
PPP3CB R	TGTACAGCATCTTTCCGAGGT
RAPGEF2 F	ATGGCTTCAGTGAACATGGA
RAPGEF2 R	GCTTCACTTTTCGAGCCATTTG
R3HDM1 F	TGGAAGCAGCAAAAGCATAGG
R3HDM1 R	TGGTTGTTGAGTCATAGGAGGA
SNX14 F	GCAGAATCACCAACACGCAA
SNX14 R	GCAACATAGCTCCCTCCATTG
STX3 F	GAAGGCACGAGATGAAACGA
STX3 R	CATCTGAAGACAAGGGTGGC

b. Sequencing

Target vector	Sequence
pGIPZ	GCATTAAAGCAGCGTATC
pRRL	TGTTTGAATGAGGCTTCAGTAC
iCMV Forward	AGCTCGTTTAGTGAACCGTCAGATC
iCMV Reverse	ACCACTTTGTACAAGAAAGCTGGGT

Table A6. siRNA sequences.

NCBI symbol	siRNA Target Sequence	Product Id	Product Name
ABCD4	CCCTACCTTAACCCAAATGAA	SI00289646	Hs_ABCD4_2
ABCD4	CCCGTTCACCCTCGTCTACTA	SI00289639	Hs_ABCD4_1
AKR1C1	CTTGGTGATTTCAGCAAGCTA	SI00025781	Hs_AKR1C1_1
AKR1C1	CAGCCAGGCTAGTGACAGAAA	SI03066196	Hs_AKR1C1_8
ALOX5	ACCGACGTAAAGAACTGGAAA	SI00294714	Hs_ALOX5_2
ALOX5	GAGATTCACCATTGCAATCAA	SI00294728	Hs_ALOX5_4
ASB15	CAAGTTATGATATTCAGCTAA	SI00149527	Hs_ASB15_1
ASB15	TAAGACACTCTGGGAATTCAA	SI00149534	Hs_ASB15_2
BPIFB2	CTGCACATTGGGAGCCTTATA	SI00138614	Hs_BPIL1_2
BPIFB2	CTGGTGCAGAAGCACATTAAA	SI00138628	Hs_BPIL1_4
BRD8	AAGGCGATGAGACTCCACTTA	SI03035424	Hs_BRD8_12
BRD8	AAGGTAGATGATCATCCTGAA	SI00091147	Hs_BRD8_3
C10orf2	CTGGCAGGCTAGTGTAGATAA	SI00131250	Hs_PEO1_2
C10orf2	CAGGATCGCAGCTCAAGACTA	SI00131257	Hs_PEO1_3
CCL23	CAGGAAGAATTGAACTTGTCA	SI00339724	Hs_CCL23_2
CCL23	TTAGAGCAATTCATCTAATAA	SI03021312	Hs_CCL23_5
CDKN2A	TACCGTAAATGTCCATTTATA	SI02664403	Hs_CDKN2A_15
CEBPB	CGGGCCCTGAGTAATCGCTTA	SI02777292	Hs_CEBPB_5
CTDSPL	CCAGTGCAACGTCAGCTTAAA	SI00081431	Hs_CTDSPL_2
CTDSPL	CTGAGTGTTCCAAACCAGTAA	SI03093685	Hs_CTDSPL_8
DCLK3	CAGGCAGGCCTATGCGATGAA	SI03070249	Hs_DCAMKL3_5
DCLK3	CAGGGTCGTGACCGTAGTGAA	SI03071558	Hs_DCAMKL3_6
DUSP11	CCCTTATGTATTCAAGCTTAA	SI02658845	Hs_DUSP11_5
DUSP11	AAGAAGGTGGTATCCTTATAA	SI04437636	Hs_DUSP11_10
EMR4P	CAGCAACGGTTCTTACACCAA	SI00379568	Hs_EMR4_2
EMR4P	CAGCACGGGCAGATTCAAGAA	SI04904298	Hs_EMR4P_3
ERCC3	CCGGGAATATGTGGCAATCAA	SI00002422	Hs_ERCC3_1
ERCC3	ACCCATGTGCATGAGTACAAA	SI00002443	Hs_ERCC3_4
FBXW4	CAGCACCTTCACTGTCAAGTA	SI00132097	Hs_SHFM3_1
FBXW4	TGGGAAGATTGGCATTCATAA	SI00132104	Hs_SHFM3_2
GPRC5D	ATCATCGAGCTCAATCAACAA	SI03047184	Hs_GPRC5D_6
GPRC5D	CAGAGGTATGATGTTTGTGAA	SI02643389	Hs_GPRC5D_5
IFNA17	TTGTGGTGAATGTAACAATAT	SI03025869	Hs_IFNA17_6
IFNA17	CAAGGTTACCCATCTCAAGTA	SI03054814	Hs_IFNA17_9
IL15	TTGTTTAAGGGTGATAGTCAA	SI00157430	Hs_IL15_2
IL15	TCCGGAGATGCAAGTATTCAT	SI00157437	Hs_IL15_3
IL17RE	CACAAGGGACTTCGCTCTAAA	SI00152411	Hs_IL17RE_1
IL17RE	CCGGGCTATTCGGGTGACCAT	SI03082625	Hs_IL17RE_9
ITCH	CAAGAGCTATGAGCAACTGAA	SI00141085	Hs_ITCH_3
ITCH	ATGGGTAGCCTCACCATGAAA	SI03051839	Hs_ITCH_5
KCNA5	CGCGGACGAGATACGCTTCTA	SI03085124	Hs_KCNA5_5
KCNA5	CTCGGTCTTGGTTATCCTCAT	SI03091900	Hs_KCNA5_6
KCNQ4	CGGGCATCTCTGAGACTCAAA	SI00067186	Hs_KCNQ4_1
KCNQ4	CTGGTACTACTATGACAGTAT	SI00067207	Hs_KCNQ4_4
LNX2	CAGCCACTTAGTTTACCAGAA	SI02779476	Hs_LNX2_5

LNX2	AGCCGAGTACTTTCAGCGAAA	SI03043369	Hs_LNX2_6
MAP3K6	CACCATCCAAATGCTGTTGAA	SI00288218	Hs_MAP3K6_5
MAP3K6	CCACAAGAACATAGTGCGCTA	SI04438049	Hs_MAP3K6_11
MAPK14	CTCCGAGGTCTAAAGTATATA	SI03089989	Hs_MAPK14_12
METTL10	CAGCGATACATGCACAAAGAT	SI00541527	Hs_LOC399818_2
METTL10	TTCCGAGAATATGGAGATACA	SI03022229	Hs_LOC399818_5
NRG1	TCGGCTGCAGGTTCCAAACTA	SI03116974	Hs_NRG1_10
NRG1	TATCACCATCGTGGAATCAAA	SI03112487	Hs_NRG1_9
PLCB1	CAGAGATGATCCGGTCATATA	SI02781184	Hs_PLCB1_6
PLCB1	CACACTACCAAGTATAATGAA	SI00109984	Hs_PLCB1_4
PPP1CB	CACTATTGGATGTGATTCTAA	SI02759204	Hs_PPP1CB_6
PPP1CB	AACAGCTAATCCGCCGAAGAA	SI03027724	Hs_PPP1CB_7
PROK2	TCGCTCTGGAGTAGAAACCAA	SI00131523	Hs_PROK2_2
PROK2	TACGGACTTCATTTAACCGAT	SI03109708	Hs_PROK2_6
PTBP1	GCGCGTGAAGATCCTGTTCAA	SI02649206	Hs_PTBP1_18
PTBP1	CACGCACATTCCGTTGCCTTA	SI00141638	Hs_PTBP1_5
PTBP1	ATGGTATGAGTGTAATCTAAA	SI00043631	Hs_PTBP1_2
PTPN14	CGGTGTGGCATTTACAATATA	SI02225916	Hs_PTPN14_5
PTPN14	AAGGGCGATTACGATGTACAT	SI02225923	Hs_PTPN14_6
RBCK1	GAGGATTACCAGCGATTTCTA	SI00088732	Hs_C20orf18_1
RBCK1	GTGCCAGATCGTGGTACAGAA	SI03106649	Hs_C20orf18_5
RELA	CCGGATTGAGGAGAAACGTAA	SI02663094	Hs_RELA_7
RNF6	AACCTTACCTCAAGACCATAA	SI03029173	Hs_RNF6_6
RNF6	TCGGCTTATGAGAGACCATAA	SI03116988	Hs_RNF6_8
RNFT1	ACAGGTAACTGCAGTGTTAAA	SI00113659	Hs_LOC51136_4
RNFT1	CAGAATCTGGAGATCATGGTA	SI03063298	Hs_LOC51136_7
SKP1	AACACTGTAAGGATTGTTCCA	SI00301819	Hs_SKP1A_5
SKP1	TCGCAAGACCTTCAATATCAA	SI02758700	Hs_SKP1A_9
SLC25A40	AACCTGGATTATAATGAAGAA	SI02778237	Hs_MCFP_6
SLC25A40	CAGGGTTATTCCCGCCTTCTA	SI00123095	Hs_MCFP_3
SSU72	ACGCCAGATGAAAGCAATCAA	SI00103502	Hs_HSPC182_4
SSU72	ACGGTAGCATTACCCAAATAA	SI00103488	Hs_HSPC182_2
TMEM219	AGCCCTAGAATGGGTGAGGAA	SI00473249	Hs_LOC124446_4
TMEM219	TGGCCTAGTTCCCGACTTGTT	SI05034169	Hs_TMEM219_1
TP53	CAGAGTGCATTGTGAGGGTTA	SI00011655	Hs_TP53_3
UBE2V2	CAGAAGCTCCTCCGTCAGTTA	SI02665103	Hs_UBE2V2_5
UBE2V2	AAGACGTCTAATGATGTCCAA	SI03031518	Hs_UBE2V2_6

Table A7. Chemical compounds.

Compound Name	CAS Number	MDL or Catalogue number	Supplier
(+)-JQ1	1268524-70-4	4499	Tocris
6-Methyl-2-(phenylethynyl)pyridine hydrochloride	219911-35-0	MFCD02262119	Sigma
Acetylsalicylic acid	50-78-2	MFCD00002430	Sigma
AKR1C1 inhibitor	4906-68-7	123850	Calbiochem
Amitriptyline hydrochloride	549-18-8	MFCD00012537	Sigma
Amoxapine	14028-44-5	MFCD00069210	Sigma
Beclomethasone	4419-39-0	MFCD00135614	Sigma
BF-170 hydrochloride	22191-97-5	MFCD08705340	Sigma
BW-B 70C	134470-38-5	1304	Tocris
Clemastine fumarate	-	MFCD00137486	Sigma
Desipramine hydrochloride	58-28-6	MFCD00058108	Sigma
Edelfosime	77286-66-9	3022	Tocris
Enoximone	77671-31-9	MFCD00867130	Sigma
ET-18-OCH3	-	MFCD00135190	Sigma
FIPI	939055-18-2	3600	Tocris
Forskolin	66575-29-9	MFCD00082317	Sigma
Hydrocortisone	50-23-7	MFCD00011654	Sigma
Ibudilast	50847-11-5	MFCD00864808	Sigma
Imipramine hydrochloride	113-52-0	MFCD00012669	Sigma
Indomethacin	53-86-1	MFCD00057095	Sigma
N-Desmethylclozapine	6104-71-8	MFCD00210189	Sigma
NU2058	161058-83-9	MFCD05664734	Sigma
PHA 767491 hydrochloride	845538-12-7	MFCD11519962	Sigma
Propionylpromazine hydrochloride	7681-67-6	MFCD01941563	Sigma
Tautomycetin	119757-73-2	2305	Tocris
Trequinsin hydrochloride	78416-81-6	MFCD01076563	Sigma
Triamcinolone	124-94-7	MFCD00010477	Sigma
Triflupromazine hydrochloride	-	MFCD00058103	Sigma
XE 991 dihydrochloride	122955-13-9	2000	Tocris
YM 976	191219-80-4	MFCD04113219	Sigma
Zileuton	111406-87-2	MFCD00866097	Sigma

Table A8. Antibodies.

Target	Clone	Company	Catalogue number	Application	Dilution
53BP1	Polyclonal	Novus Biologicals	NB100-304	IF	1/1000
BrdU	3D4	BD Biosciences	555627	IF	1/1000
C/EBP β	H-7	Santa Cruz	sc-7962	IF	1/200
CCL2/MP-1	24822	R&D	MAB279	IF	1/100
CCL20/MIP-3α	67310	R&D	MAB360	IF	1/100
E-Cadherin	36	BD Biosciences	61081	IF	1/1000
GAPDH	Polyclonal	Abcam	ab22555	WB	1/10000
Gro-α/CXCL1	Polyclonal	R&D	AF-275	IF	1/100
IL-6	Polyclonal	R&D	AB-206-NA	IF	1/100
IL-8/CXCL8	6217	R&D	MAB208	IF	1/100
IL1α	4414	R&D	MAB200	IF	1/100
IL1β	8516	R&D	MAB201	IF	1/100
MAPKAPK2	E341	Abcam	ab32567	WB	1/1000
NF-κB p65	A	Santa Cruz	s-109	IF	1/100
p-(Ser/Thr) ATM/ATR	Polyclonal	Cell Signaling	2851	IF	1/100
p-MAPKAPK2	Polyclonal	Santa Cruz	sc-31675	WB	1/200
$p16^{INK4a}$	JC-8	CRUK	–	IF	1/500
$p21^{Cip1}$	M-19	Santa Cruz	sc-471	IF	1/100
p38 MAPK	Polyclonal	Cell Signaling	9212	WB	1/500
p53	DO-1	Santa Cruz	sc-126	IF	1/100
PTBP1	Polyclonal	Abcam	ab5642	IF/WB	1/1000
VEGFc	23410	R&D	MAB2931	IF	1/100
ZFP36L1	A-21	Santa Cruz	sc-134091	WB	1/200
γ-H2AX	JBW301	Millipore	05-636	IF	1/100
Goat IgG	AlexaFluor® 594	Invitrogen	A11058	IF	1/1000
Mouse IgG	AlexaFluor® 488	Invitrogen	A11029	IF	1/1000
Mouse IgG	AlexaFluor® 488	Invitrogen	A11059	IF	1/1000
Mouse IgG	AlexaFluor® 594	Invitrogen	A11032	IF	1/1000
Rabbit IgG	AlexaFluor® 594	Invitrogen	A11037	IF	1/1000
Rat IgG	AlexaFluor® 488	Invitrogen	A11006	IF	1/1000
Goat IgG	HRP	Santa Cruz	sc-2020	WB	1/5000
Mouse IgG	HRP	Santa Cruz	sc-2005	WB	1/5000
Rabbit IgG	HRP	Santa Cruz	sc-2004	WB	1/5000

Table A9. RT-qPCR primer sequences.

Target	Forward primer	Reverse primer
AKR1C1	TTCATGCCTGTCCTGGGATTT	CTGGCTTTACAGACACTGGAAAA
BRD8	TTGGGTATCAGTTAGCAGAGCA	TCAACAGTTTCCACCACTTCTC
C/EBPβ	ACCCACGTGTAACTGTCAGCC	TCAACAGCAACAAGCCCGT
CCL2	AGCTCGCACTCTCGCCTCCAG	GGCATTGATTGCATCTGGCTGAGC
CCL20	GGCGAATCAGAAGCAGCAAGCAAC	ATTGGCCAGCTGCCGTGTGAA
CDKN1a	CCTGTCACTGTCTTGTACCCT	GCGTTTGGAGTGGTAGAAATCT
IL1a	AGTGCTGCTGAAGGAGATGCCTGA	CCCCTGCCAAGCACACCCAGTA
IL1b	TGCACGCTCCGGGACTCACA	CATGGAGAACACCACTTGTTGCTCC
IL6	CCAGGAGCCCAGCTATGAAC	CCCAGGGAGAAGGCAACTG
IL8	GAGTGGACCACACTGCGCCA	TCCACAACCCTCTGCACCCAGT
INHBA	CGGCGCTTCTGAACGCGATC	GCTGTTCCTGACTCGGCAAACGT
INK4a	CGGTCGGAGGCCGATCCAG	GCGCCGTGGAGCAGCAGCAGCT
MMP1	TGTGGTGTCTCACAGCTTCC	CGCTTTTCAACTTGCCTCCC
MMP3	TGTTCGTTTTCTCCTGCCTGT	CAGCAGCCCATTTGAATGCC
p38	ATGCATAATGGCCGAGCTGT	TTTCTTGCCTCATGGCTTGG
p65	TTGAGGTGTATTTCACGGGACC	GCACATCAGCTTGCGAAAAGG
PLCB1	GGAAGCGGCAAAAAGAAGCTC	CGTCGTCGTCACTTTCCGT
PP1A	ACTACGACCTTCTGCGACTAT	AGTTCTCGGGGTACTTGATCTT
PTBP1	AGCGCGTGAAGATCCTGTTC	CAGGGGTGAGTTGCCGTAG
PTPN14	GGACAAATTCGCTAATGAGCCT	TAATCGCCCTTCAAGCACATC
RPS14	CTGCGAGTGCTGTCAGAGG	TCACCGCCCTACACATCAAACT
SACM1L	GCTGAAGCTGCATATCACACC	ACGGTCAATGGTAAGTACGTCA
SKP1A	GACCATGTTGGAAGATTTGGGA	TGCACCACTGAATGACCTTTT
TMEM219	ACGGTCCAGACAGGAACAAGA	CTGAGCAGGATATGGGTGGC
UBE2V2	AGTTCCTCGTAATTTTCGCTTGT	CCCCAGCTAACTGTACCGT
UNG	ATTGATAGGAAGCGGCACCA	TGCAGCAGCTCATTGGTCTT
VEGFC	AGAGAACAGGCCAACCTCAA	TGGCATGCATTGAGTCTTTC